Impacts of land-cover change on the regional climate of Northern Germany

Dissertation

zur Erlangung des Doktorgrades

der Naturwissenschaften im Fachbereich

Geowissenschaften

der Universität Hamburg

vorgelegt von

Anja Hermans

aus Hamburg

Hamburg

2016

Als Dissertation angenommen vom Fachbereich Geowissenschaften
der Universität Hamburg
auf Grund der Gutachten von Prof. Dr. Hans von Storch
und Dr. Burkhardt Rockel

Datum der Disputation: 2. Dezember 2016

Abstract

Land-cover is continuously modified both by natural as well as anthropogenic processes. These modifications show impacts on climate especially on the regional scale. The scope of this thesis is to investigate impacts of land-cover changes on the regional climate of Northern Germany with special focus on Hamburg and Berlin. For this purpose, the regional climate model COSMO-CLM (CCLM) is used in a convection permitting mode at a horizontal grid mesh size of 2.8 km.

A broad spectrum of land-cover changes from anthropogenic impacts -so far- across large-scale impacts caused by one-way land-cover changes up to possible land-cover changes in terms of ongoing urbanization are addressed.

In the first step, the maximum range of regional climate impacts due to extreme land-cover changes is investigated. Four extreme land-cover scenarios are implemented in CCLM: mixed forest only, non-irrigated arable land only and continuous urban fabric only with either sealed or porous ground. For these scenarios 2-year simulations for 2002 and the year of a strong heat wave, 2003 are conducted. Clear effects on near surface temperature caused by a different portioning of surface fluxes and changes in the hydrological cycle become visible. It is shown, that the current land-cover of Northern Germany has already led to an effect on the regional climate compared to the potential natural land cover, namely mixed forest.

Strongest impacts are caused by the most extreme scenario: sealed urban land. This scenario causes for example increased summer mean 2 m temperatures up to 4 K higher than in the control run due to diminished evaporative cooling. In general, changes in the degree of sealing and the amount of vegetation show strongest effects in this sensitivity study.

In the second step, combined effects of land-cover and greenhouse-gas changes on the climate of Northern Germany are analyzed for the end of the 21st century (2090-2099) compared to the land cover status for the time slice 1998-2007. Herein, two urban scenarios are applied and evaluated: the urban sprawl and the compact city scenario. Both scenarios are based on the assumption of a growing urban population and an increasing demand on living space. In the "urban sprawl" scenario, the currently as "growing" declared urban areas of Northern Germany are enlarged horizontally. Their urban characteristics are kept constant. In the "compact city" scenario, urban growth happens next to low horizontal growth, especially in the vertical with clearly higher buildings and the building of new housing on vacant plots. Simulations results suggest that the two land-cover change scenarios play a minor role for the regional climate of Northern Germany with respect to urban growth. Nevertheless, on the local scale land-cover changes play an important role in the surface energy budget and the hydrological cycle. In general, changes in the degree of sealing and the amount of vegetation lead again to strongest effects on the surface climate. This becomes especially evident in the "compact city" scenario with sealed ground. The fast run-off of precipitation at the surface due to the sealed and vegetation free surfaces prevents the storage of water. Whereas temperatures in both land-cover change scenarios are increased particularly in summer, due to the decreased cooling effect of evaporation. The increased turbulence above the cities caused by the increased heating and a higher roughness length leads to impacts on the local wind field and therefore influences the precipitation pattern around the modified cities.

Zusammenfassung

Die Landbedeckung wird kontinuierlich sowohl durch natürliche als auch durch anthropogene Einflüsse verändert. Diese Änderungen wirken sich auf das Klima insbesondere auf der regionalen Skala aus. Das Ziel dieser Doktorarbeit ist es den Einfluss von Landnutzungsänderungen auf das regionale Klima von Norddeutschland und insbesondere von Hamburg und Berlin zu untersuchen. Dafür wird das regionale Klimamodell COSMO-CLM (CCLM) in konvektionsauflösendem Modus bei einer horizontalen Gitterweite von 2.8 km verwendet. Ein breites Sprektrum an Landnutzungsänderungen von bisherigen anthropogenen Einflüssen über grossflächigen Änderungen mit einseitigen Landnutzungsänderungen über mögliche Landnutzungsänderungen in Bezug auf fortschreitender Urbanisierung werden betrachtet. Zunächst wird der maximale Effekt auf das regionale Klima, den extreme Landnutzungsänderungen hervorrufen können, abgeschätzt. Dazu werden vier extreme Landnutzungsänderungsszenarien in das CCLM implementiert: nur Mischwald, nur nicht bewässerte Landwirtschaft und nur durchgängig städtische Bebauung mit einmal versiegeltem und einmal durchlässigem Boden. Für diese Szenarien werden 2-jahres Simulationen für die Jahre 2002 und 2003, dem Jahr mit einer starken Hitzeperiode, durchgefürt. Es zeigen sich deutliche Effekte auf die bodennahe Temperatur durch eine veränderte Aufteilung der bodennahen Flüsse und den hydrologischen Kreislauf. Die heutige Landbedeckung scheint bereits jetzt deutliche Effekte auf das regionale Klima von Norddeutschland bewirkt zu haben wie der Vergleich zur potentiellen natürlichen Landbedeckung, nämlich Mischwald, zeigt. Insgesamt führt die durchgängig städtische Bebauung mit versiegeltem Boden zu den stärksten Effekten. Dieses Szenario verursacht bis zu 4 K höhere mittlere Sommertemperaturen in 2 m Höhe als im Kontrolllauf aufgrund verringerter Kühlung durch Verdunstung. Insgesamt rufen Veränderungen des Versiegelungsgrads und der Vegetation die stärksten Effekte im Rahmen dieser Sensititivitätsstudie hervor.

Im zweiten Schritt werden kombinierte Effekte von Landnutzungsänderungen und erhöhter Treibhausgaskonzentration auf das Klima von Norddeutschland am Ende des 21. Jahrhunderts (2090-2099) im Vergleich zum Zeitraum 1998 bis 2007 mit heutiger Landnutzung untersucht. Dabei werden zwei Stadtszenarien, die "gestreute Stadt" und die "kompakte Stadt", angewendet und evaluiert. In beiden Szenarien wird davon ausgegangen, dass sowohl die städtische Bevölkerung als auch der Wohnflächenbedarf pro Person weiter zunimmt. Bei der "gestreuten Stadt" wird die Stadtfläche Norddeutschlands, orientiert an als wachsend geltenden Städten, horizontal vergrößert. Die städtischen Eigenschaften bleiben dabei unverändert. Im Szenario "kompakte Stadt" wachsen die Stadtflächen etwas horizontal doch insbesondere vertikal durch deutlich höhere Gebäude und durch Neubauten auf Freiflächen innerhalb der Stadt. Die Simulationsergebnisse zeigen, dass die durchgeführten Landnutzungsänderungen in Hinblick auf Stadtwachstum eine untergeornete Rolle für das Klima von Norddeutschland spielen. Jedoch haben sie auf der lokalen Skala einen wichtigen Einfluss auf den Bodenenergiehaushalt und den hydrologischen Kreislauf. Auch hier rufen Änderungen des Versiegelungsgrades und der Vegetation die stärksten Effekte hervor. Vor allem in der kompakten Stadt mit versiegeltem Boden wird das deutlich. Der versiegelte Boden führt einerseits zu einem schnellen Abfluss von Niederschlag und andererseits kombiniert mit fehlender Vegetation, zu fehlendem Wasserresorvoir am Boden. Beide Szenarien bewirken vor allem höhere Sommertemperaturen aufgrund des fehlenden kühlenden Effekts durch Verdunstung. Die vergrößerte Turbulenz über der Stadt und die höhere Rauhigkeitslänge beeinflussen das

lokale Windfeld was wiederum zu Veränderungen im Niederschlagsfeld um die veränderten Städte herum führt.

Contents

1. Introduction

1.1. Motivation

Mankind impacts on its environment in various ways. Mostly visible are changes in the land-cover. As people settled in one place they changed the land-cover around them leading finally to nearly no wilderness around them (Luyssaert et al., 2014). Farmland or cities were founded and roads were constructed, for instance, in former forest areas. In Germany, there are only few areas with low anthropogenic influences which have a comparable character as the original wilderness.
The way how people modify their surrounding depends on numerous factors which differ considerably not only over the world and the different climate zones, but even from one place to another: even in the same country, city or village.

Land-cover changes in turn, impact on the climate system. Next to greenhouse-gases, land-cover changes have the largest anthropogenic impact on climate. These climate impacts are again strongly dependent on the degree of change, the spatial extend and the geographical location of the land-cover changes. Anthropogenic land-cover change is even one of the few climate forcings for which the net direction of the climate response over the last two centuries is still not known (Myhre et al., 2013). This uncertainty is a result of the often counteracting temperature responses to the many biogeophysical effects and the biogeochemical versus biogeophysical effects (e.g Gaillard et al., 2015).

The present thesis aims to quantify the impacts of land-cover changes on the regional and local climate of Northern Germany (Fig. 1.1). Often, more attention is put on regions which play a more important role for the global climate, as e.g. the tropical rainforest. Here in contrast, the focus is on a comparable small domain with rather low significance for the world's climate. This domain is characterized by a nearly complete modified land-cover with hardly any wilderness, low orographic variations framed in the North by the North Sea and the Baltic Sea. Nevertheless, it is the home of a large number of people who are also confronted with climate change. With only the metropolitan areas of Hamburg and Berlin, more than 11 million inhabitants are addressed in this domain. Information about the regional characteristics of climate change is essential in order to quantify its impacts on human societies. Furthermore, political decisions about adaptation strategies have to be developed to be prepared for a change in climate characteristics in the future.

To decide about future land-cover modifications, it is of great importance to understand the feedback of land-cover changes on the climate system. This thesis approaches in a first step the range of impacts due to already performed land-cover changes. The maximum range of climate impacts due to land-cover change scenarios in terms of sensitivity studies is addressed in the following steps in order to make statements about:

- To what extent has the current land-cover of Northern Germany already contributed to climate modifications?
- What effects have extreme land-cover changes on the regional climate under extreme climate conditions?
- Which spectrum of meteorological variables is affected due to land-cover changes?

- What might be the maximum range of climate impacts due to land-cover changes in Northern Germany?
- How far do land-cover changes influence the surroundings?
- Which land-cover modifications have the strongest impacts on the regional climate?

The tool to deal with these questions in the frame of this thesis is the regional climate model COSMO-CLM (CCLM). To use the CCLM, firstly, the mechanisms of land-cover changes in the CCLM have to be understood and shortcomings have to be identified. Therefore, the following questions have to be clarified:

- Is the regional climate model CCLM an appropriate tool to deal with the impacts of land-cover changes on the regional climate?
- Which uncertainties have to be taken into account?

Northern Germany (Fig. 1.1) is characterized by heterogeneous land-cover and experiences maritime in the north to continental influenced climate in the east. Here, cities represent especially the impacts of anthropogenic land-cover changes. In Northern Germany, Berlin and Hamburg are the largest cities with the highest populations followed by Bremen and Hannover. To capture the physical effects of these cities and the specific land-cover characteristics of Northern Germany, the very high, convection permitting horizontal resolution of about 2.8 km (0.025°) is applied for the CCLM. As there were few experiences with this high resolution climate simulations, it was a challenge to determine an appropriate model set-up in terms of nesting strategies to use CCLM in the convection permitting horizontal resolution of 2.8 km.

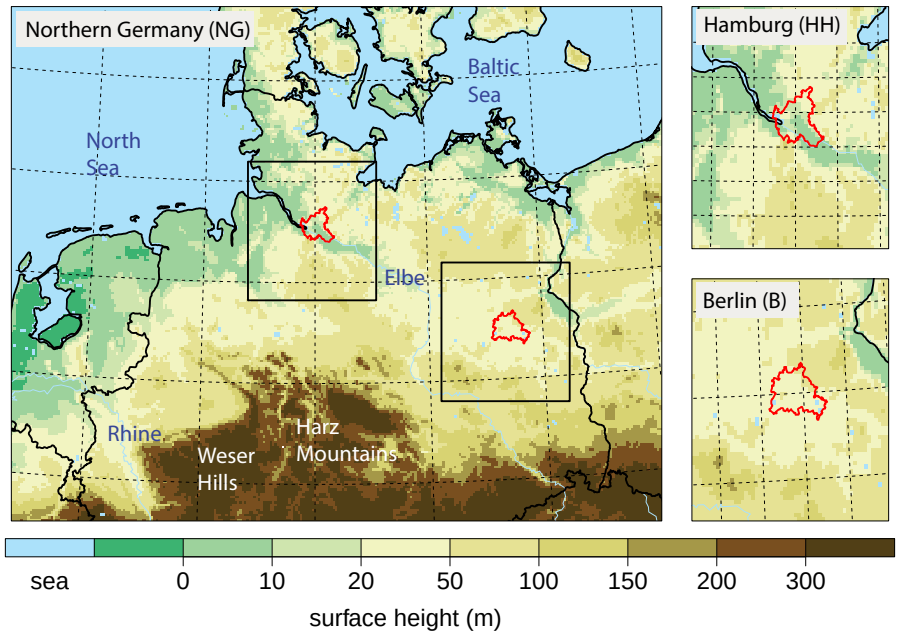

Figure 1.1.: Orography map of the simulation domain. Later referred to "Northern Germany" (NG), Hamburg (HH, topright) and Berlin (B, bottomright). The political borders of Hamburg and Berlin are drawn in red.

Land-cover changes over time. Various drivers alter the shape of the physical land surface. An important factor plays the climate and its changes. Both aspects will change continuously in future times. Therefore people will be subjected to both effects. So the following question arises:

- How could or should future land-cover of Northern Germany look like?

Mankind is especially vulnerable to extreme climate events such as heat waves or intense rainfall. The high resolution of the climate simulations with the CCLM allows to address the following additional questions:

- Where do we see the fingerprint of urban growth?
- What are the hot-spots of climate impacts due to combined effects of land-cover and GHG changes in Northern Germany at the end of the 21st century?

In summary, the objective of this thesis is to address a broad spectrum of climate impacts due to land-cover changes for Northern Germany to study both, the physical mechanisms and the meaning for inhabitants in or nearby the area of modified surfaces. The following section will give an overview of recent related research activities before the strategy of this thesis will be outlined in the last section of this chapter.

1.2. Current state of knowledge

In this section, the frame of already performed research is summarized. The focus is on problems and uncertainties concerning impacts of land-cover changes on climate. The physical interaction of land-use and land-cover (LULC) and weather and climate will be discussed in Chapter 2 in more detail.

Explanation of terms

The atmosphere and the underlying land-cover are in constant dialogue resulting from diverse interactions. Similar to the oceans, land areas provide the lower boundary for the atmosphere, with which they exchange energy, momentum, water and chemical components. The term "land-cover" denotes "the observed physical and biological cover of the earth's land, as vegetation or man-made features" (Gregorio and Jansen, 2000). In contrast, "land-use" is "the total of arrangements, activities, and inputs that people undertake in a certain land-cover type" (Gregorio and Jansen, 2000). Both, land-cover and land-use are determined by anthropogenic as well as natural factors. Natural factors such as the geographical situation, soil type and soil characteristics, or the relief favor, avoid or at least make specific land-use forms difficult. Next to the natural conditions, anthropogenic factors play an important role mainly in terms of politics.

Interactions between the atmosphere and the land-cover can be distinguished from biogeochemical and biogeophysical interactions (e.g Findell et al., 2007). Biogeochemical processes summarize the influence of vegetation on the atmospheric gas composition, as for example the concentrations of CO_2 or CH_4. Plants interact, e.g., with the carbon cycle via the emissions of biogenic volatile compounds, reactive carbon compounds that affect aerosol formation and atmospheric chemistry, influencing e.g. ozone concentration. Biogeochemical processes affect the atmosphere by non-linear interactions both in anthropogenic dominated regions as well as in "natural" landscapes (Denman et al., 2007). Here, the focus is on modifications of physical characteristics of the land surface like the albedo, the roughness length, the vegetation density or the water conductivity

influenced by vegetation, namely biogeophysical interactions. At the regional scale, biogeophysical effects exert a direct, measurable effect, while biogeochemical effects are more relevant in the context of global climate change since the timescale of carbon dioxide (CO_2) mixing in the atmosphere is very short (Gaillard et al., 2015). Consequently, regional changes in the carbon balance affect regional climate only indirectly by affecting the global CO_2 concentration (Gaillard et al., 2015). Depending on the region, biogeophysical and biogeochemical feedback of land-cover on climate can amplify or dampen each other (Arora and Montenegro, 2011). Following Claußen et al. (2001), biogeophysical interactions play a more important role in temperate to high latitudes than biogeochemical processes.

The meaning of land-cover change for weather and climate

Next to changes in the emission of greenhouse gases - land-use changes are the most important anthropogenic influences on climate (Pielke et al., 2002). One important characteristic of the land surface is the pronounced spatial heterogeneity that spans a wide range of scales (Giorgi and Avissar, 1997). This heterogeneity affects the surface energy and water budget, as well as the land-atmosphere exchanges of momentum, heat, water and other constituents through a number of highly non-linear processes (Giorgi and Avissar, 1997; Pitman, 2003). Therefore, land-cover conversions have important effects on the regional climate (e.g. Bounoua et al., 2002).

Land-atmosphere interactions have been shown to be relevant for several regions and time scales. Observational and modeling studies clearly demonstrate that land-use and land-cover changes (LULCC) play an important biogeophysical and biogeochemical role in the climate system from the local landscape to regional and even continental scales (Foley et al., 2005; Pielke et al., 2011; Brovkin et al., 2013; Luyssaert et al., 2014; Mahmood et al., 2014). Regional land-cover changes can affect the global climate by teleconnections (Pielke, 2001; Avissar and Werth, 2005). Simulations by Bonan (1997, 1999) show that perturbations of the land surface are able to extend into the middle troposphere and alter the atmospheric circulation (Feddema et al., 2005). Therefore, land-cover changes are important for climate simulations of the future (Feddema et al., 2005). The Global Land-Atmosphere Climate Experiment (GLACE, Koster et al., 2004, 2006) pinpointed that land-atmosphere interactions tend to be particularly important in transitional zones between dry and wet climates. Moreover, these "hot spots" of land-atmosphere coupling are also inherently modified with shifts in climate regimes, for instance due to climate change (Seneviratne et al., 2006). They can thus be displaced on longer time-scales. Finally, long-term vegetation dynamics and human-induced land-use changes can also interact with the rest of the climate system on decadal-to-centennial time scales (Cramer et al., 2001; Claußen et al., 2004; Pielke, 2005).

It has been difficult to summarize the effects of land-cover change on climate because different biogeophysical effects offset each other in terms of climate impacts (Pielke et al., 2002). On global and annual scales, regional impacts are often of opposite sign and are therefore not well represented in annual global average statistics (Pielke et al., 2002; Feddema et al., 2005).

The climatic effect of land-cover change, whether at local or global scales, is still not well understood and quantified. A striking example is given by the recent largest model study focusing on the impacts of anthropogenic land-cover changes on the climate of the northern hemisphere: the Land Use and Climate, IDentification of robust impacts (LUCID) intercomparison project (Pitman et al., 2009; de Noblet-Ducoudré et al., 2012) where different climate models show different sensitivity to historical land-cover change (both in terms of change in surface fluxes and consequently of climate response), thus highlighting the uncertainties in the description of the underlying biogeophysical processes.

Further progress was made by the Coupled Model Intercomparison Project phase 5 (CMIP5, Brovkin et al., 2013) and planned Coupled Model Intercomparison Project phase 6 (CMIP6, Meehl

et al., 2014) . Lubowski et al. (2008) concluded that without adequately considering the biogeophysical impacts of LULCC on climate, an appropriate response to the threats posed by human intervention into the climate system will not be sufficiently addressed.

There is already a huge amount of investigations on vegetation-climate interactions. In parts they present different results which implies additional uncertainty for climate projections (Pitman et al., 2009). Projected land-cover changes cause in some regions a temperature increase, but in other regions temperature decreases (Lamptey et al., 2005). Also, DeFries et al. (2002) conclude that the effects of land-use changes depend on the geographic position and can lead either to an amplification of climate change or a reduction. These processes, however, are not well constrained with observations in current climate models, which leads to large uncertainties in the assessment of the overall land-cover change impact. The deployment of flux-tower measurements will certainly play a key role in future research in this field, allowing modelers to evaluate and improve climate models in terms of their ability to realistically represent surface fluxes under different land-cover conditions.

Koster and Suarez (1995) stated that land surface processes contribute significantly to the variance of annual precipitation over continents. In particular, the role of soil moisture for precipitation in midlatitudes and transitional climate zones was highlighted in several investigations (e.g. Betts et al., 1996). The precipitation variability again reflects local evaporation variability (Koster and Suarez, 1995). These responds are strongest to the land surface during summer, when moist convection dominates (Koster and Suarez, 1995). It has been established that vegetation growth enhances evapotranspiration (Crucifix et al., 2005). Increases in vegetation density result in cooler and moister near-surface conditions (e.g Bounoua et al., 2002). Koster et al. (2000) conclude that in continental mid-latitudes, oceanic impacts on precipitation are relatively small to soil moisture impacts, during summer time. For northern hemispheric summers, Koster et al. (2004) found regions of strong coupling between soil moisture and precipitation and Seneviratne et al. (2006) showed, that soil-moisture plays an important role in terms of summer climate variability.

Land-cover changes in Northern Germany

Land-cover changes are very diverse. In Germany especially political decisions play an important role. New questions followed in regional planning due to the accelerated turnaround of energy policy in 2011 after the amendment of the German Atomic Energy Act (Hoymann and Goetzke, 2014). The question was, how to use available land to meet the needs of the society in terms of the environmental policy. Especially climate protection gained a growing importance, since 10% of emitted GHG in Germany can be led back to land-use: forestry, agriculture as well as settlement and transportation and changes therein (Strogies and Gniffke, 2011). On average, there is a daily increase in settlement and transport areas of 69 ha per day in Germany (2010 to 2013, Statistisches Bundesamt, 2015) leading especially to surface sealing and a reductions of vegetated areas. Following structural calculations of the Federal Institute for Construction, Urban and Regional Research in the Federal Office for Construction and Regional Planning (Bundesinstitut für Bau-, Stadt und Raumforschung im Bundesamt für Bauwesen und Raumordnung, BBSR), a change of the land-cover from 2010 to 2030 in terms of a reduction of arable land by 2% and an increase in forest land (+0.9%) and settlement and transportation areas (+1.1%) is expected (BBSR, 2012). To deal with these interactions between climate change and land-use in Germany, the project "CC-Land-StraD" was founded (Hoymann and Goetzke, 2014). Results of their simulations with the "Land Use Scanner" showed that several regions in Germany will further be faced to settlement pressure, regardless of demographic change.

Method: Dealing with the impacts of land-cover/ land-use changes on weather and climate

In this thesis, the regional climate model CCLM is used in its standard version with the multi-layer soil-vegetation-atmosphere transfer (SVAT) scheme TERRA_ML (Schrodin and Heise, 2001; Graßelt, 2010; Doms et al., 2011).

Other common methodologies to deal with comparable surface-atmosphere interactions are observations eddy covariance flux towers (e.g. FLUXNET[1], Ray et al., 2001 or Bonan et al., 2008), satellite sensors or experimental measurements (e.g Bosch and Hewlett, 1982). Nevertheless, these experiments are usually short-term, limited to special areas or only few variables are addressed. Furthermore, it is difficult to investigate impacts of land-cover changes on the possible future climate.

Numerical models allow to represent both, land-cover (changes) and weather or climate at the same time over a variety of variables and dimensions as well as time ranges. It is a known issue that taking vegetation cover into account significantly impact model performance (Grimmond, 2007). Various different land-cover changes are possible to investigate without changing the "real world". There are numerous different approaches in terms of land surface models (LSM) to describe the impacts of the earth surface on weather and climate in numerical or meteorological models respectively. The most limiting factor concerning the complexity of the LSM is usually the associated computational time. Nevertheless, the introduction of land-surface processes is also very difficult in atmospheric models because of the complicated interactions between atmosphere, vegetation and soil (Beljaars, 1995). Beljaars (1995) summarize that current LSM are mainly physically based and use Monin-Obukow similarity for the atmosphere-surface interactions. The complexity of these models ranges from simple bucket models to sophisticated land-surface parameterization (LSP) with multiple vegetation, soil and snow layers (e.g. Koster et al., 2000; Slater et al., 2001).

Already at an early stage of regional model development, the key role of land-atmosphere interactions has been recognized (see e.g., Pielke et al. (1998) for a review). For example, Avissar and Pielke (1989) implemented a parametrization of sub-grid scale surface heterogeneity in a mesoscale model and found an impact on local circulations where contrasts in sensible heating were generated by surface heterogeneity (Davin et al., 2011). Avissar (1998) divides the LSPs in three types: (i) the "bucket" type, introduced by (Manabe and Bryan, 1969); (ii) the "Soil-Vegetation-Atmosphere Transfer (SVAT) schemes" type, introduced by (Deardorff, 1978); and (iii) the "mosaic-of-tiles" type, introduced by (Avissar and Pielke, 1989). Especially in the numerical weather prediction the interface between the atmosphere, soil and vegetation is usually described by LSPs based on SVAT schemes, which mainly focus on a correct representation of the energy and mass fluxes between atmosphere, soil and vegetation (Chen et al., 1996; Warrach et al., 2002).

Davin et al. (2011) coupled the CCLM with the more sophisticated Community Land Model version 3.5 (CLM, Oleson et al., 2004 and 2008) and compared the new COSMO-CLM[2] and the standard CCLM with TERRA_ML against observations for the domain of Europe at a horizontal resolution of 0.44° ($\sim 50\,\mathrm{km}$).

The representation of land processes differ considerably between CLM3.5 and TERRA_ML. A summary of these differences is presented in (Davin et al., 2011).

Urban impacts on weather and climate are investigated with special attention. Focusing on the parameterization of urban land, there were recently several developments in the CLM-Community. Since 2010, three parameterizations for urban land-use were incorporated into CCLM (Trusilova et al., 2016). These parameterizations vary in their complexity, required city parameters and their computational cost (Trusilova and Riecke, 2015): The urban canopy model (UCM) of high com-

[1] http://fluxnet.ornl.gov/

plexity with the Double Canyon Effect Parameterization (DCEP), CCLM-DCEP (Schubert et al., 2012) is based on the Building Effect Parameterization, BEP (Martilli et al., 2002). Herein, parameters that describe buildings must be specified for each grid cell based on available urban building data sets or urban land-use classes as described in the work of Schubert and Grossman-Clarke (2013).

Regional climate models are an appropriate tool to analyse interactions between the biosphere and climate, as effects of land surface processes are highly related to regional scales. In addition, the effects of land surface descriptions on the simulated climate were investigated using regional models (Seneviratne and Stöckli, 2007; Maynard and Royer, 2004; Pitman et al., 2004).

The strength of regional climate models (RCMs) lies in a better representation of features as the orography, lakes, complex coastlines, and heterogeneous land-use than by general circulation models (GCMs). Therefore, RCMs provide better description and lead to a better understanding of regional climatic processes (Giorgi, 1990; Frei et al., 2003; Leung and Qian, 2003).

The higher resolution of convection permitting climate simulations (CPCS) allows additionally a better representation of orography and surface fields. Deep convection can be explicitly resolved in place of uncertain parametrizations. Hence, convection parametrizations are a known source of major uncertainties and errors in the simulation of present-day and future climates (e.g. Molinari and Dudek, 1992; Dai et al., 1999; Brockhaus et al., 2008). Both, Hohenegger et al. (2008) and Prein et al. (2013), found the most important added value of convection permitting climate simulations in the diurnal cycle, improved timing of summer convective precipitation, the intensity of most extreme precipitation, and the size and shape of precipitation. Prein et al. (2013) could attribute these improvements to the explicit treatment of deep convection and the more realistic model dynamics. Besides, they stated that improvements in the summer temperature fields can be fully attributed to the higher resolved orography. Finally, Prein et al. (2013) summarize, that the added value of CPCSs is predominantly found in summer, in complex terrain, on small spatial and temporal scales, and for high precipitation intensities.

Next to the above explained advantages of RCMs, there are several issues which have to be kept in mind if working with RCMs: Due to the limitation of the domain, numerical errors are induced by the unrealistic boundaries that do not occur in the real atmosphere. The jump in resolution between the driving data and the RCM or between the different RCM nests causes uncertainties. The spin up time, that means the time until the soil-temperature has reached a state of balance starting from the coarse initial field, has to be long enough. The update frequency of the lateral boundary conditions has to be adopted to the model experiment. The physical parametrisations can cause inconsistencies. As well as the horizontal and vertical interpolation can introduce errors. The quality of the results also depends on the domain size and location and last but not least on the quality of the driving data. More details on this issue can be found e.g. in Rummukainen (2010), Laprise (2008) or Giorgi and Mearns (1999).

Land-cover change scenarios

Information about the regional characteristics of climate change is essential in order to quantify its impacts on human societies and ecosystems (Davin and Seneviratne, 2012). Several investigations have been carried out focusing on the sensitivity of RCMs to changes in vegetation and/or land-use (e.g. Sanchez et al., 2007; Pielke, 2001; Pielke et al., 1999). However, in spite of progress in integrating biophysical and socio-economic drivers of land-use change (Veldkamp and Verburg, 2004), prediction of future land-use remains difficult. It is exceedingly difficult, and probably not even possible, to predict the complex interplay of social, economic, and demographic factors and how they will alter land-cover in future (DeFries et al., 2002). Scenario analysis provides an alternative tool to assist this extrapolation. Scenarios are consistent and possible future devel-

opment paths which are subject to specific overall conditions (Alcamo et al., 2006). Although, scenarios are no forecasts, they are able to show options for actions, visualize alternative future development pathways and identify domains with particular pressure on land-use (Verburg et al., 2004; Couclelis, 2005; Lambin et al., 2006). Land-use change modeling, especially if done in a spatially explicit, integrated and multi-scale manner, is an important technique for the projection of alternative pathways into the future, for conducting experiments that test our understanding of key processes, and for describing the latter in quantitative terms (Lambin et al., 2001). Projections can be used as an early warning system for the effects of future land-use changes and pin-point hot-spots that are priority areas of in-depth analysis or policy intervention.

Focus of analyses

Increasing greenhouse gas concentrations are expected to further alter temperature and precipitation patterns in the mean as well as in the variability (Christensen et al., 2007). Associated with the simulated changes in variability, climate scenarios project major changes in extreme values of temperature (e.g. Schär and Jendritzky, 2004; Seneviratne et al., 2006; Vidale et al., 2007; Kjellström et al., 2007; Lenderink et al., 2007), or precipitation (e.g. Christensen and Christensen, 2003; Nikulin et al., 2010). Also the inter-annual variability of summer climate in Europe (e.g. Schär and Jendritzky, 2004; Giorgi et al., 2004; Vidale et al., 2007) is expected to increase, potentially causing more frequent heat waves. The underlying mechanisms for changes in extremes are linked to changes in the large-scale circulation (e.g. Meehl and Tebaldi, 2004) and/or to changes in small-scale physical processes such as soil moisture-atmosphere interactions (e.g. Seneviratne et al., 2006) or effects of clouds on the surface radiative forcing (e.g. Lenderink et al., 2007). However, several investigations have shown that land-climate interactions play a key role for these projections (Seneviratne et al., 2010; Teuling et al., 2010; Zampieri et al., 2009; Vidale et al., 2007; Gálos et al., 2013), particularly during extreme years (Jaeger and Seneviratne, 2011).

1.3. Strategy

The review of literature presented in the last section has shown the frame of scientific knowledge in which this thesis is embedded. There are still several gaps to close in the area of land-cover change and climate feedbacks. Chapter 2 will present the theory beyond land-cover changes. In Chapter 3 the methods which are used in this study are described. In Chapter 4, a sensitivity study of extreme land-cover changes for NG is presented. Chapter 5 deals with the analyses of combined effects of land-cover and GHG changes on the regional and local climate of Northern Germany.

2. Land-use and land-cover changes- observed and simulated

This chapter presents an overview of the theoretical background regarding physical impacts of land-cover changes on weather and climate with a special focus on Northern Germany, Hamburg and Berlin. It is shown 1. why land-cover changes, 2. which changes have been observed so far, and 3. how changes could look like in future.

2.1. Main physical interactions between the surface and the atmosphere

Surface energy balance

The surface energy balance equation (e.g. Stull, 1988) describes the interaction of many processes occurring at the land-atmosphere interface. At the surface, the energy fluxes of net radiation (R_n), latent heat (λE, latent heat of vaporization λ times the evaporation E), sensible heat (H), and the ground heat flux (G) are in balance (e.g. Pielke et al., 2002) with the rate of change of energy stored in the layer, $\delta R_n/\delta t$ (Eq. 2.1).

$$R_n + H + \lambda E + G = \delta R_n/\delta t \tag{2.1}$$

For an active layer of infinitesimal small thickness, $\delta R_n/\delta t$ is equal zero and can be neglected. In other situations, the active layer has a measurable thickness. In this case the rate of change of energy stored in the layer, $\delta R_n/\delta t$, must be included in the equation. In many instances, also lateral fluxes (advection) have to be taken into account. This situation is, for instance, the case for vegetation or snow.

The net radiation is the sum of net shortwave (S_n) and net longwave radiation (L_n):

$$R_n = S\downarrow - S\uparrow + L\downarrow - L\uparrow, \tag{2.2}$$

where, $S\downarrow$ is the incoming and $S\uparrow$ is the outgoing shortwave radiation. $L\downarrow$ is the atmospheric counter-radiation and $L\uparrow$ is the emitted terrestrial emission which depends on the surface emissivity ε times the Stefan Boltzmann constant ($\sigma = 5.67 \cdot 10^{-8}$ $\mathrm{Wm^{-2}K^{-4}}$) times the surface temperature T_s raised to the power of four:

$$L\uparrow = \varepsilon\ \sigma\ T_s^4 \tag{2.3}$$

Eq. 2.3 illustrates, above all, the connections of the surface radiation components to T_s. $S\downarrow$ and $S\uparrow$ are linked in the following way:

$$S\uparrow = \alpha\ S\downarrow \tag{2.4}$$

The difference of these two terms

$$S\downarrow - S\uparrow = S\downarrow (1-\alpha) \tag{2.5}$$

is the net solar radiation at the surface. The albedo (α) is the ratio of incoming to outgoing solar radiation for a given surface. Fluxes are considered positive when directed towards the surface (energy source) and negative when directed away from the surface (energy sinks). Exceptions are $L\uparrow$ and $S\uparrow$ (outgoing radiation fluxes), for which a minus sign is explicitly used in the energy balance equation.

Biogeophysical effects influence the above described energy balance (Eq. 2.1) between the surface and the atmosphere. The main biogeophysical feedbacks arise from (i) land-surface characteristics such as albedo and roughness, and (ii) evapotranspiration (Levis, 2010). Modelling experiments have shown that the albedo effect on the surface temperature can be significant (Bala et al., 2007; Liang et al., 2010). Nevertheless, it is difficult to confidently quantify the climate impact due to changes in the surface albedo (Spangmyr, 2010). The albedo not only varies between substances and surfaces, it also varies for the same surface over the course of a day or a year. The collective albedo of a forest can be as low as 0.05 (Oke, 1987) while the albedo of single parts of vegetation themselves, such as individual leaves (usually around 0.3), may be larger. The multitude of layers and surfaces enable multiple reflections within the forest canopy, because each surface that is hit by the radiation absorbs a part of it. In the IPCC AR5 report, this impact of the albedo is classified as scientifically challenging with medium to low level of scientific understanding.

The hydrological cycle over land

The hydrological cycle can be described by the water balance equation. The main source is precipitation (P); the sinks are evapotranspiration (E), runoff (Q), infiltration (I) and water storage ΔS:

$$P - E - Q - I = \Delta S \tag{2.6}$$

The equation of water balance (Eq. 2.6) and energy balance (Eq. 2.1) are closely connected with either evapotranspiration or latent heat flux. If soil moisture is lacking, no evapotranspiration can take place and most of the incoming energy (net radiation) goes into sensible heat flux, thus strongly increase the air temperature. Reversely, if water is almost infinitely available, then a large amount of energy will be used for evapo(transpi)ration, thus leading to a net cooling compared to dry surfaces. These effects are, however, only important in regions where soil moisture is the main controlling factor for evapotranspiration (Seneviratne et al., 2010).

Levis (2010) pointed out that surface-atmosphere feedbacks can be modified or eliminated by anthropogenic land-cover changes. Moreover, it is rare that a single feedback dominates or is the only one being active (e.g. Gaillard et al., 2015). They further conclude that often several feedbacks occur together which increases the difficulty of interpreting the results.

2.2. Observations of land-use and land-cover changes

Over the last centuries to millennia human land-use has altered one third to one half of the Earth's land surface, with the most notable change being the transformation of natural vegetation to arable land (Vitousek et al., 1997). Climate impacts due to human activities have been found in local, regional and global trends in modern atmospheric temperature records and other relevant climatic indicators (Mahmood et al., 2010). In the last 300 years, arable land and grasslands have been expanded by 460% or 560% respectively (Goldewijk, 2001). A temperature decrease of about 1

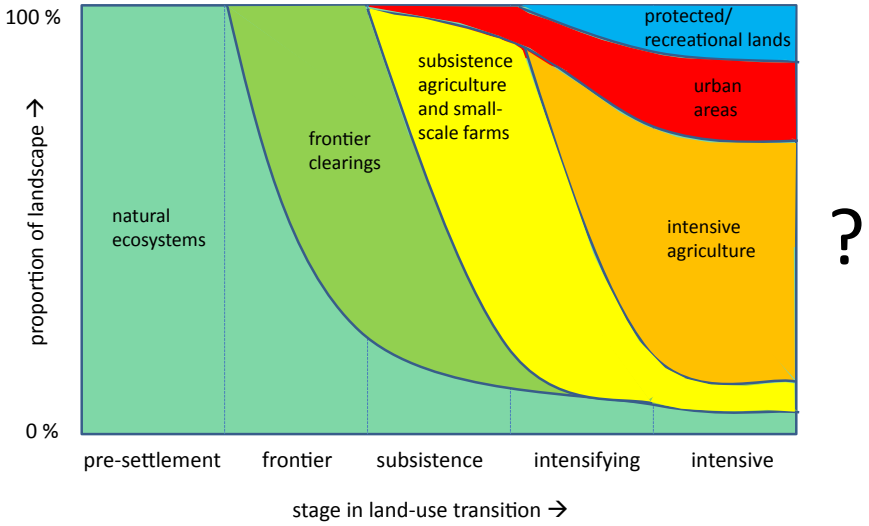

Figure 2.1.: Schematic description of typical pattern of the transition in land-use activities that a region might experience over time after Foley et al. (2005); DeFries et al. (2004).

to 2 K resulting from anthropogenic induced historical land-cover changes in mid-latitude agricultural regions is estimated by several studies (Betts, 2001; Bounoua et al., 2002; Chase et al., 2000; Feddema et al., 2005; Hansen et al., 1998; Matthews et al., 2004).

Following DeFries et al. (2004), conversions and modifications of land typically happen in a transition that follows a sequence of different land-use regimes as shown in Fig. 2.1: From pre-settlement natural vegetation to frontier clearing, then to subsistence agriculture and small-scale farms, and finally to intensive agriculture, urban areas, and protected recreational lands. Different parts of the world are in different transition stages, depending on their history, social and economic conditions, and ecological context. Furthermore, not all parts of the world move linearly through these transitions. Rather, some places remain in one stage for a long period of time, while others move rapidly between stages (Foley et al., 2005; DeFries et al., 2004).

Gibbard et al. (2005) summarized that previous studies on the effects of land-cover change (Betts, 2000; Bonan, 2001; Govindasamy et al., 2001; Hansen et al., 1998; Brovkin et al., 1999; Bonan, 1997; Oleson et al., 2004) have indicated that the historical mid-latitude land-cover change has increased surface albedo, leading to cooling of the atmosphere. These studies suggested that human-induced land-cover change from forest to crop lands could lead to a cooling of 0.25 K on a global scale (Govindasamy et al., 2001). This may have contributed to the millennial cooling before the 20th century, and that northern mid-latitude agricultural regions are about 1-2 K cooler in winter and spring compared to the pre-industrial state. This can be explained by the replacement of forest by crop lands (Betts, 2005).

2.2.1. Effects of urbanization

The global population has become concentrated in cities (UN, 2012). As of 2011, more than 52% of the global population lives in urban areas. In 2006, urban areas accounted for 67-76% of the total energy use and for 71-76% of the energy-related CO_2 emissions. By 2050, the urban population is expected to increase to 5.6-7.1 billion, meaning 64-69% of the world population (Seto and Dhakal, 2014). In Europe, it is projected that 82% of all people will live in cities by

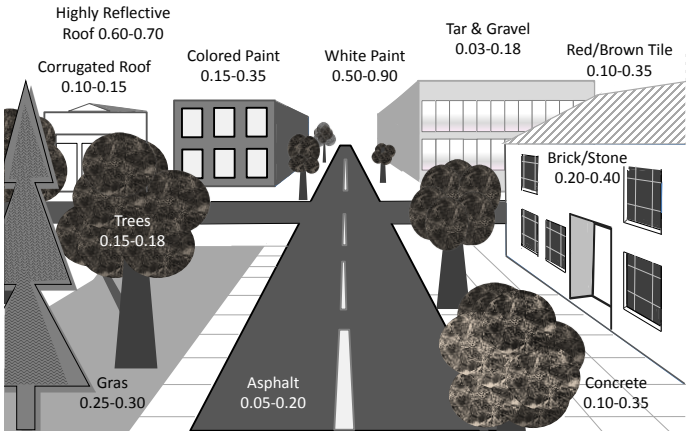

Figure 2.2.: Different albedos in the urban environment after Goodman (1999).

2050. Urban areas are among the most modified environments on earth. Cities are at the same time directly affected by climate change and main driver of climate change. Urban climate is the result of overlapping global and local impacts. A considerable number of observational studies show that urban areas cause changes in temperature, wind, humidity, and rainfall, produce peculiar circulations, and affect local or even regional weather and climate (Landsberg, 1970; Oke, 1987; Cotton and Pielke Sr, 2007).

The "urban heat island (UHI) effect" (Oke, 1982) is probably the most thoroughly investigated aspect of the urban climate. The UHI effect describes the relative warmth of a city compared with surrounding rural areas. UHIs are an extreme case of how land-use modifies regional climate (Fan and Sailor, 2005). The reduced vegetation cover, impervious surface area, and morphology of buildings in cityscapes lead to lower evaporative cooling and increased heat storage and finally to local heating (Kueppers et al., 2007). The UHI varies from city to city and reaches up to 12 K (Memon et al., 2011).

While human energy production is relatively small globally compared with the radiation received by the sun, it is locally important in cities, where it can reach 20 to 70 Wm^{-2} (Crutzen, 2004). Urban areas generally have higher ratios of sensible to latent heat transfer (Bowen ratio) due to reduced vegetation and the high fraction of impervious surfaces and drains, which lead to reduced evapotranspiration and increased sensible heat transfer (Jin et al., 2005; Taha, 1997). Here, the maximum sensible energy flux can be several orders of magnitude higher than the latent energy flux (e.g Grimmond and Oke, 1995; Grossman-Clarke et al., 2010; Hanna et al., 2011). Finally, the relative magnitude of partitioning into sensible energy flux varies with season, geographical location of the urban area, and within urban land-use variations (Mahmood et al., 2014).

The urban climate depends essentially on the size of the city, on the building density, the amount of sealed area, and the natural exposition. Horizontal temperature gradients between urban and suburban areas alter wind patterns and turbulence. Generally, the urban canopy increases surface roughness and exerts a frictional drag, reducing wind speeds (Oke, 1987). How changed wind patterns affect energy transfer by advection depends on the characteristics of each city. As for air pollution, in addition to providing condensation nuclei for cloud formation, Arnfield (2003) reports that recent studies largely confirm early assessments, showing up to 10% reduction in incoming short-wave radiation. Cities usually have lower albedo values than rural surfaces (e.g Spangmyr, 2010). Two to five percent lower albedo values of cities in comparison to crop-lands, at the same latitude, are common.

Urban areas can impact natural precipitation pattern in various ways, see e.g. Shepherd (2005) for a review. Mechanisms for urban-induced rainfall include: (1) creating, enhancing or modifying mesoscale circulations and thus destabilizing the atmosphere (e.g. Shepherd et al., 2002; Shepherd and Burian, 2003), (2) promoting convergence of air near the surface due to increases in surface roughness (e.g. Bornstein and Lin, 2000; Thielen et al., 2000), (3) increasing the amount of condensation nuclei due to enhanced aerosols in the urban environment (e.g Diem and Brown, 2003; Mölders and Olson, 2004); or adding moisture to the air from industrial sources. The UHI produces updrafts on the leeward or downwind side of cities. This initiates moist convection under favourable thermodynamic conditions and can lead to surface precipitation (Han et al., 2014). Shepherd et al. (2002) found in their study an average increase in rainfall of 5.8% for the cities examined, and an increase of 28.4% over downwind areas, compared to upwind control areas. Cities can even affect the route of thunderstorms as stated by Changnon (2001). Already Changnon and Stanley (1981) found similar precipitation increases during summer months within and 50 to 75 km downwind of the city. Trusilova et al. (2008) showed in numerical experiments with the PSU-NCAR Mesoscale Model (MM5) in combination with the TEB (Town Energy Balance) model that near-surface temperature and precipitation are effected by urbanization on local and even regional scales.

2.2.2. Land-use and land-cover changes in Northern Germany

Germany is densely populated and characterized by a peripheral concentrated settlement structure, in comparison to other European countries (Dosch and Beckmann, 2011). Furthermore, large-scale differences in the distribution of urban areas are typical (Fig. 2.3). Cities in Germany and Europe have a long lasting history of growing thereby each city has its own characteristics. Despite of a stagnating population, urban and transportation areas are still increasing and even declared as a central issue of the spatial development in Germany since several decades (Dosch and Beckmann, 2011). In 2011, 13% of the cadastral land register is described as "settlement and transportation areas" (Dosch and Beckmann, 2011). An analysis of the "Bundesamt für Bau-, Stadt- und Raumforschung" (Federal Institute for Building, Urban Affairs and Spatial Research, BBSR) of land-use and land-cover changes for the period of 1993 to 2008 shows beside an apparent increase in settlement and transportation areas, a moderate increase in forest areas and a slight increase in water bodies, whereas arable land experiences decrease (Dosch and Beckmann, 2011). The potential vegetation, namely vegetation that would most likely exist in the absence of human land-use, is characterized by (with few exceptions) temperate deciduous and mixed forest for Northern Germany (Geist et al., 2006). Although, the population growth has virtually stagnated of Germany, settlement areas are still growing (Fig. 2.4). Nevertheless, recently the rate of immigration has increased rapidly. This situation will very probably lead to an additional increase in settlement areas in the future.

Hamburg

Hamburg is the second largest city in Germany with a population size of roughly 1.8 million. The city spans over an area of 40 km north-east to south-west and 42 km southeast-nortwest with an overall size of 755,3 km^2. Hamburg is characterized by a growing population status (Fig. 2.4, Dosch and Beckmann, 2011). As a city-state, in 2009, a high proportion of 60% of the city are settlement and transportation areas (Dosch and Beckmann, 2011). "Arable land" covers 186 km^2 of the city state, whereas forest covers 6% (48 km^2). Water bodies take up 8% (61 km^2) of the city area.

Hamburg is a very green city with many parks and street canyon trees. Only a small part of

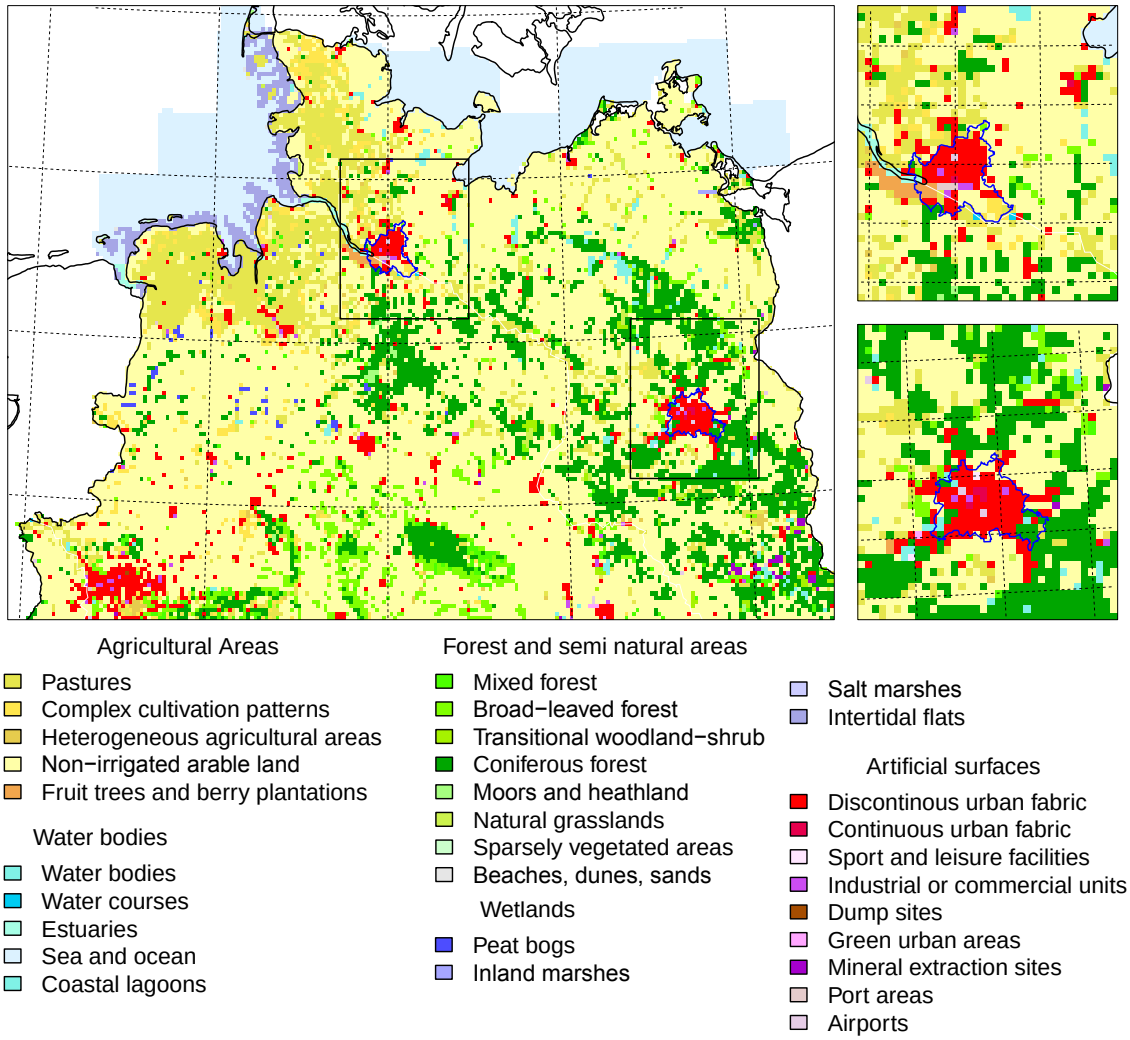

Figure 2.3.: CORINE (CoORdination of INformation on the Environment, Keil et al., 2011) land-cover maps interpolated from (Δx=1 km) to the model domain (Δx=2.8 km): Northern Germany, Hamburg and Berlin.

Hamburg is covered by buildings higher than 20 m. This is important because Carraca and Collier (2007) report that high-rise buildings are particularly important for the initiation of convection by urban areas. Currently, the settlement development is characterized by a beginning trend of re-urbanisation and thus a concentration of development in the center.

Berlin

Berlin is the capital and the largest city of Germany. Same as Hamburg, Berlin is a state city with a large proportion of settlement and transportation areas of 70% (Dosch and Beckmann, 2011). Water bodies take up about 7%, arable land 4%, and forest roughly 18% of the domain. Berlin is located in eastern Germany with a population of around 3.4 million people in 2012. The city spans over an area of 30 km in north-south direction and between 20 and 45 km in east-west direction with an overall size of 892 km^2. Also for Berlin ongoing growing is expected (Fig. 2.4).

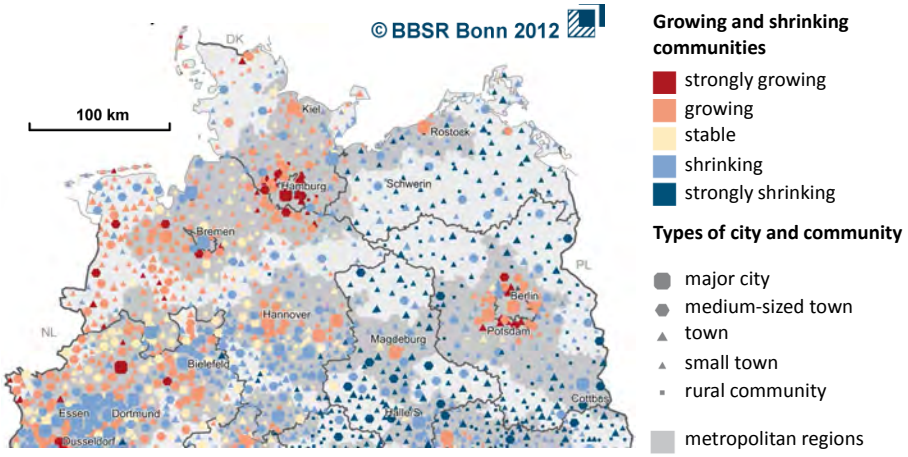

Figure 2.4.: Growing and shrinking cities in Northern Germany (Dosch and Beckmann, 2011). Data resource: Ongoing spatial monitoring system of the Bundesamt für Bau-, Stadt- und Raumforschung (BBSR). Geometric base: Federal Agency for Cartography and Geodesy (BKG, Bundesamt für Kartographie und Geodaesie), municipality associations, 31.12.2010. Considered structural indicators: population development (2005-2010); total migratory balance (2008/09/10); workplace developments (2005-2010); rate of unemployment (2009/10); actual taxable capacity (2009/10) and purchasing power (2009).

2.3. Land-cover and land-use change drivers and scenarios

2.3.1. Drivers of land-use and land-cover changes

Land-cover is not static; it is changing through either conversion or modification. Human activities have modified the environment for thousands of years. Significant population increase, migration, and accelerated socio-economic activities have intensified these environmental changes over the last centuries (Mahmood et al., 2010).

There are numerous drivers of LULCC which interact in a complex way (Lambin et al., 2006). Fig. 2.5 gives a schematic overview of selected drivers. The typical drivers included in regional and local scenarios are similar to those used in global scenarios but are, of course, described in much greater detail. The higher the horizontal resolution of the investigated domain the more factors can be or rather should be taken into account for the development of land-cover scenarios. The location of change is determined by a range of factors including biophysical (for example topography, soil, and/or precipitation), demographic (population, accessibility), and socio-economic (land tenure, education level) (Alcamo et al., 2006). Local characteristics finally determine the mix of factors. For European scenarios, e.g. the effects of the Common Agricultural Policy (CAP) needs to be taken into account, while other studies single out soil characteristics as the main determinant of land-use (e.g. Bakker et al., 2005).

As explained above, there are various drivers which might influence the development of LULC change. LULC scenarios are an appropriate tool to face this situation. Scenarios are plausible views of the future based on “if, then” assertions - If the specified conditions are met, then future LULC will be realized in a particular way (Alcamo et al., 2006). Scenario analysis does not eliminate the uncertainties about the future, but it does provide a means to represent current knowledge in the form of consistent, conditional statements about the future (Lambin et al., 2006). Projections

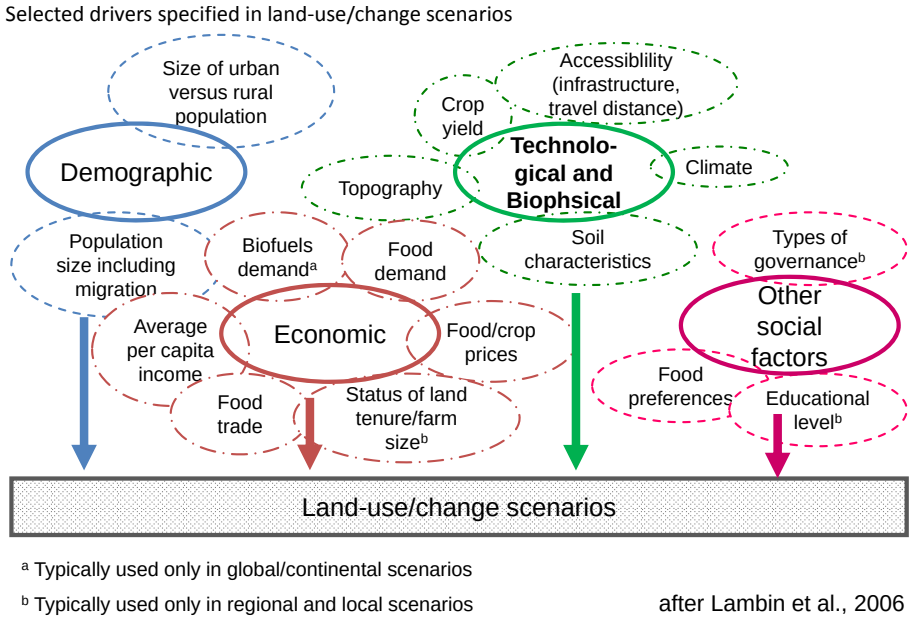

Figure 2.5.: Schematic diagram of main drivers of land-use and land-cover change after Lambin et al. (2006).

of LULC change require assumptions about future global vegetation as well as assumptions of society's countless decisions on where to settle, where to build, where to grow crops, and what lands to protect (Alcamo et al., 2006). Therefore, LULC change scenarios are basically determined by demography, economy, technology and biophysical characteristics as well as other social factors (Alcamo et al., 2006; Lambin et al., 2006). These characteristics are a result of various other factors as illustrated in Fig. 2.5.

2.3.2. Land-use and land-cover change scenarios in the IPCC reports

In the frame of the IPCC reports[1], land-use and land-cover scenarios are implemented only indirectly. No explicit, region dependent features are taken into account. Rather assumption about future LULC modifications are included in terms of anthropogenic GHG emissions (Special Report on Emission Scenarios, SRES, Nakicenovic et al., 2000 and more recently, in Representative Concentration Pathways, RCP, Moss et al., 2008). The latter are mainly driven by anthropogenic GHG emissions, by population size, economic activity, lifestyle, energy use, land-use patterns, technology and climate policy (Moss et al., 2008).

In many SRES scenarios CO_2 emissions from loss of forest cover peak after several decades and than gradually decline. (In the scenarios no feedback effect of future climate change on emissions from the biosphere has been assumed). This pattern is consistent with scenarios in the literature and can be associated with a slowing of population growth, followed be a decline in some scenarios, increasing agriculture productivity, and increasing scarcity of forest land. These factors allow for a reversal of the current trend of loss of forest cover in many cases. Emissions decline fastest in the B1 family. Only in the A2 family do net anthropogenic CO_2 emissions from land-use change remain positive through 2100. As was the case for energy-related emissions,

[1] www.ipcc.ch

CO_2 emission related to land use change in the A1 family cover the widest range. The diversity across these scenarios is amplified through the high economic growth, increasing the range of alternatives, and through the different modelling approaches and their treatment of technology. RCP scenarios are four greenhouse gas concentration (not emissions) trajectories adopted by the IPCC for its 5th Assessment Report (AR5) (Moss et al., 2008).

2.3.3. Land-use and land-cover change scenarios for Northern Germany

It is difficult to identify general LULC scenarios for Northern Germany as each municipal administration of the numerous communities in Northern Germany is primarily responsible for their own community. Land-cover changes are therefore mainly correlated to the demand in particular areas. If communities are growing, new settlement areas are determined. However, usually each community wants to be attractive to citizens and new citizens and employers. With increasing level of prosperity the demand for conditions for living change. As shown in Fig. 2.5 many drivers determine the development of land-use or land-cover. Generally, all communities are asked to adopt to climate change by mitigation strategies and to contribute to reduced GHG emissions. The BBSR recently summarized a framework "adaption to climate change for city and region" and a "cross-evaluation of joint projects of the Federation regarding climate adaption" based on the results of twelve research and development programs with 55 individual projects (BBSR, 2016b,a).

Land-use and land-cover change scenarios for Hamburg

In the frame of the research project KLIMZUG-NORD[2], regional strategies concerning climate changes in the metropolitan area of Hamburg until 2050 have been developed. Three socio-economic scenarios for urban development are developed. The first scenario "Dismanteling and Conversion" assumes a decreasing population size and ageing population with reduced public funds. The second scenario "Flourishing Commercial Location" is based on the assumption of a stagnant number of inhabitants with sufficient public funds. In the third scenario "Compact City" could be the result of a growing city with good public funds. More details about these scenarios can be found in Kruse et al. (2014). The impacts of these KLIMZUG scenarios on the atmospheric conditions of Hamburg have been investigated in several studies e.g. with the mesoscale meteorological model METRAS (e.g. Schoetter et al., 2013 or Boettcher et al., under review) or the use of a cellular automata (Daneke, 2012).

Land-use change scenarios for Berlin

To deal with spatial and urban planing aspects of climate in Berlin, the city climate development plan StEP Klima[3] was established in 2011. This adaption process is based on the strategy of conversion, improvement and conservation of existing structures in terms of the built city and open spaces. The goal of StEP is to preserve the quality of life in the city in the face of climate change and to improve it wherever possible. The policy of urban development of Berlin has followed the guidelines of the "compact city" and the "city of short distances" for many years. In the context of StEP it has been shown that these guidelines and the idea of inner development underlying them are still the best suited to ensure an urban environment worth living in under the conditions of climate change. The fields of activity include for instance the unsealing of sealed urban areas, increasing the vegetation cover within the city, increasing the albedo of urban surfaces or to minimize the anthropogenic heat amount transferred to the atmosphere.

[2] www.klimzug-nord.de

[3] www.stadtentwicklung.berlin.de/planen/stadtentwicklungsplanung/de/klima/

3. Set up of model experiments

After a short introduction of the model domain (Section 3.1), the regional climate model COSMO-CLM (CCLM) is introduced (Section 3.2). Important features of the model for this study with focus on the land-cover and land-use description are discussed (Section 3.2.1). Finally, sensitivity studies concerning the nesting strategy for the applied model experiments are shown (Section 3.3).

3.1. The model domain: Northern Germany

The region of interest, called Northern Germany (NG) in the following, covers a domain of 770x560 km^2 (Fig. 1.1). In the north, the North Sea and the Baltic Sea are located. Both shelf seas do not only moderate the annual temperature cycle and moisten the air in general, but also directly contribute to mesoscale circulations like sea breezes. However, impacts of these mesoscale phenomena are more connected to the coastal areas. Depending on tide, the influence of the seas can reach about 40 km inland (Schlünzen, 1990). In the south, the North German Plain is bounded by a low mountain range (german: Mittelgebirge). Weather and climate in this domain is mainly characterized by transitions of high and low pressure systems (e.g. Riediger and Gratzki, 2014). Spatially, Northern Germany is faced by the transitions from oceanic (north) to continental climate (south-east).

Hamburg

Hamburg is located next to the river Elbe between the North Sea (about 100 km north-west of the city) and the Baltic Sea (about 80 km north east of the city, Fig. 1.1). This position of Hamburg leads to a particularly oceanic characterized climate with dominant maritime impacts. Nevertheless, during easterly winds, also continental impacts are present. Summers in Hamburg are usually moderately warm but rainy and winters are normally mild due to the moderating influence of the Gulf Stream. The soil textures of Hamburg are clay-loam, sandy-loam and sand (Fig. 3.2).

The dense building structure, the high heat capacity of buildings, the high degree of surface sealing, a low fraction of vegetation and increased emissions lead to a modified urban climate of Hamburg compared to the rural surrounding. Although, Hamburg is characterized by a good air ventilation due to the short distance to the sea and a comparable high amount of green- and water bodies compared to other European cities. A particular urban UHI effect can be observed (e.g. Hoffmann, 2009; Schlünzen et al., 2010; Bechtel and Schmidt, 2011). In mean, the temperature of the urban city core of Hamburg is more than 1 K higher than in the surrounding. As the high density of buildings in Hamburg stores heat during daytime, the UHI is more pronounced at night than at daytime. The UHI effect of Hamburg varies also throughout the annual cycle: The strongest effect occurs between May and October with up to 3 K higher temperatures in the city core compared to the rural surrounding (Hoffmann, 2009; Schlünzen et al., 2010). Furthermore, Hamburg impacts on the precipitation distribution. Same as for other large cities, an increase in precipitation in the range of 5 up to 20% can be observed in the downwind area of the city in a distance of about 30 km (Hoffmann, 2009; Schlünzen et al., 2010). More details about the climate of Hamburg can be e.g. found in Riecke and Rosenhagen (2010) or von Storch and Claußen (2011).

Berlin

Berlin is located in north-eastern Germany next to the river Spree in an area of low-lying marshy woodlands with a mainly flat topography. It is part of the vast Northern European Plain that stretches from northern France to western Russia. The predominant soil texture of Berlin and the near surrounding is loam (Fig. 3.2). Summers are warm and sometimes humid and winters are relatively cold. In winter, the climate of Berlin is more continental influenced in terms of east European high-pressure areas which lead to the formation of temperature inversions. Spring and autumn are generally chilly to mild. Berlin is faced by moderate rainfall throughout the year. The geographically area of Berlin and around is located in a so called "priority region" which is especially vulnerable to climate change, as announced by the "Deutsche Anpassungsstrategien an den Klimawandel" (DAS, Bundes-Ministerium für Umwelt, 2008) as this region is already confronted by a low water availability. Also for Berlin, an UHI evolves especially during night and in the densely built-up areas with decadal mean of ΔT_{2m} up to 6 K during summer nights (Fenner et al., 2014). More information about the climate of Berlin can be e.g. found in Fehrmann (2009).

3.2. The regional climate model COSMO-CLM

The COSMO model in CLimate Mode (COSMO-CLM, or CCLM, e.g. Früh et al., 2016, Rockel et al., 2008, Baldauf et al., 2011 ore Steppeler et al., 2003) is used to study the impact of land-cover changes on the climate of Northern Germany. CCLM is the climate version of the non-hydrostatic COSMO model (COnsortium for SMall scale MOdelling) employed by several weather services for numerical prediction. It is jointly used and developed by the COSMO and the Climate Limited-area Modelling Community (CLM-Community[1]). In this thesis, CCLM is used in the version 4.8.

The CCLM dynamical core is based on the primitive thermodynamical equations describing atmospheric motions. A non-hydrostatic and fully compressible form of these equations is used, allowing applications on a wide range of spatial scales. The model equations are discretized on a three-dimensional grid based on a rotated geographical coordinate system. In the vertical, a generalized terrain-following height coordinate is used.

CCLM comprises a set of physical parametrizations representing various processes. The vertical radiative transfer within the atmosphere is calculated based on a so-called δ-two-stream radiation scheme (Ritter and Geleyn, 1992) for short- and long-wave fluxes in a plane parallel and horizontally homogeneous atmosphere. In this parametrization, three spectral intervals in the solar part and five spectral intervals in the thermal part of the spectrum are used. The radiative active constituents are water vapor, cloud water, cloud ice, ozone, aerosols, carbon dioxide and other minor trace gases. Vertical mixing is parametrized according to a level 2.5 closure using TKE as a prognostic variable (Mellor and Yamada, 1982). The formation of grid-scale clouds and subsequent precipitation is parametrized by a bulk micro-physics scheme including water vapor, cloud water, cloud ice, rain and snow. Subgrid-scale cloudiness is interpreted by an empirical function depending on relative humidity and height. A corresponding cloud water content is also interpreted.

More details on the model dynamics and physics are available in Steppeler et al. (2003) or in the detailed documentation of the model [2].

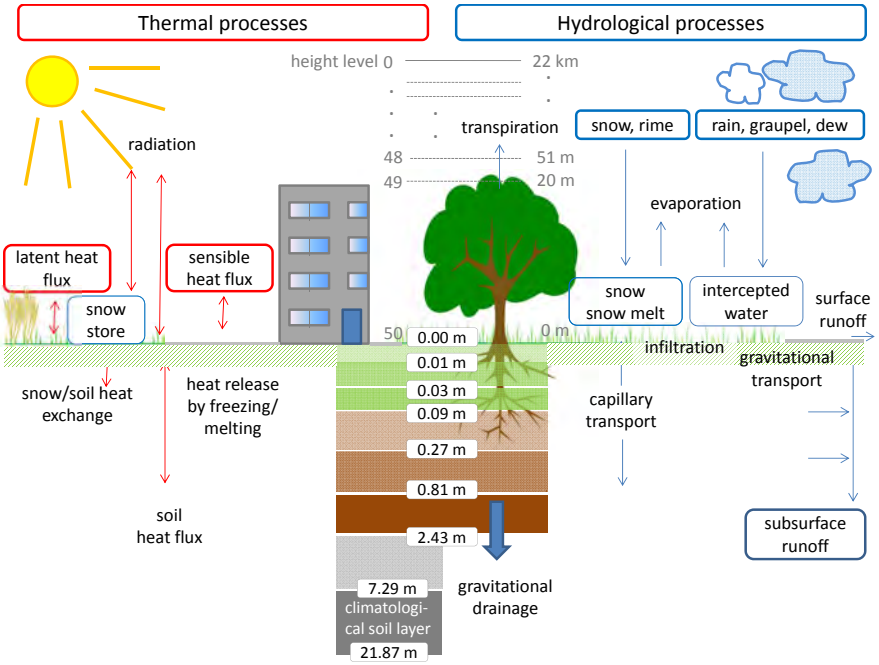

Figure 3.1.: Energetic and hydrological processes considered in TERRA_ML. Illustrated are on the left hand side the processes relevant for the energy budget, and on the right hand side, the corresponding processes relevant for the water budget. Indicated are the ten soil level and the atmospheric level.

3.2.1. Land-atmosphere interactions in COSMO-CLM: TERRA_ML

Soil-Vegetation-Atmosphere-Transfer (SVAT) processes are modelled in the standard CCLM by the multi-layer (ML) version of TERRA (Schrodin and Heise, 2001; Graßelt, 2010; Doms et al., 2011, TERRA_ML). TERRA_ML provides the lower boundary conditions for the atmospheric circulation model and gives information about surface and soil conditions by solving simultaneously the thermal and hydrological budgets of the soil. The coupling is modelled by a stability and roughness-length dependent surface flux formulation. TERRA_ML consists of two parts which describe various thermal and hydrological processes in the soil (Fig. 3.1): In the first part the computation of hydrological processes (Section 2.1) such as bare soil evaporation and plant transpiration is performed. In the second part the thermal processes (Section 2.1) are described by solving the equation of heat conduction and the Richards equation.

Description of the land surface

TERRA_ML does not include an explicit vegetation layer. The status of the earth's surface is described in terms of so called external parameters. The surface input data-sets of external data used in CCLM is described by Smiatek et al. (2008). Time invariant or slowly varying external data are necessary as boundary conditions. Two different types of external parameters are distinguished: (a) directly available "primary data" from datasets offered by specialized institutions and (b) from the primary data derived "secondary data" (Doms et al., 2011).

[1] http://www.clm-community.eu
[2] http://www.cosmo-model.org

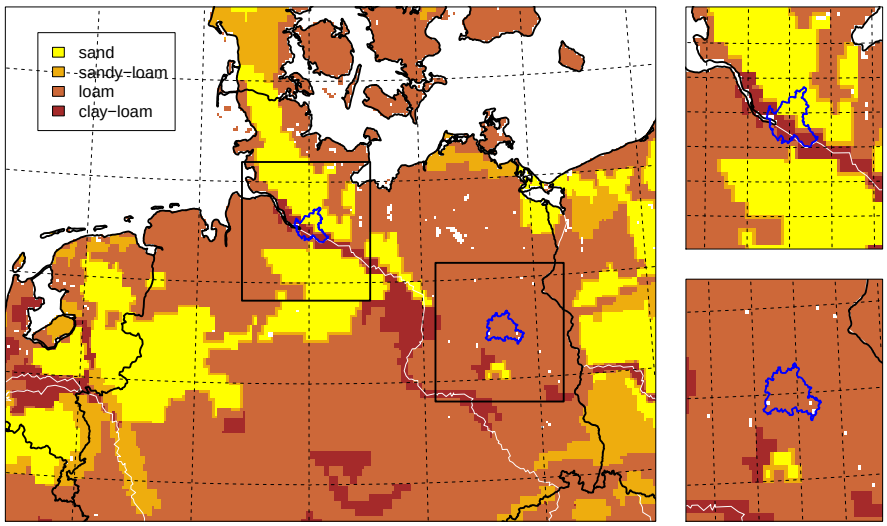

Figure 3.2.: FAO (FAO/UNESCO, 1997) soil texture map of the model domain: Northern Germany, Hamburg (topright) and Berlin (bottomright).

The primary data include time-invariant parameters such as orography, dominant land-use, dominant soil texture, and the annual mean near surface temperature. Land-surface orography is provided by the GLOBE[3] data-set of the National Geophysical Data Center with 30 arc seconds resolution.

The applied soil map is based on the Food and Agriculture Organization (FAO) of the United Nations (FAO-Unesco, 1974) digital soil map of the world. The FAO soil map provides soil texture information for the top soil layer (0-30 cm) and the bottom soil layer (30-100 cm). The data set has a resolution of 5 arc minutes ($\sim$ 10 km).

TERRA_ML uses only the top layer information across all model layers. Parameters of the soil model (heat capacity, water storage capacity, etc.) strongly depend on soil texture. Between five different soil textures (sand, sandy loam, loam, loamy clay and clay) and ice, rock and peat is distinguished in TERRA_ML. Whereas, hydrological processes in the ground are not taken into account for ice and rock.

At the lower boundary of the active soil layers a temperature field has to be prescribed for TERRA_ML. Here, the climatological mean is used. Deep soil temperatures are used from the Climate Research Unit (CRU) of the University of East Anglia. They provide global data-sets of mean monthly surface climate over land areas, excluding Antarctica, interpolated from station data to 0.5 degree lat/lon for a range of variables (e.g., mean temperature[4])

To assess the secondary data, association tables are mostly used to relate the variables required for the model. The roughness length over land depends on the subgrid-scale variance of orography and the land-use. Plant characteristics are determined by the dominant land-cover. The parameters required by TERRA_ML are the fractional area covered by plants (PLCOV), the leaf area index (LAI), and the root depth (ROOTDP). Apparently, these parameters depend on the time of the year. Normally, in order to simulate an annual course of the data, maximum and minimum values for PLCOV and LAI are used. A simple analytical annual course depending on latitude and height is prescribed to interpolate between maximum and minimum values. Wooded areas are described

[3] http://www.ngdc.noaa.gob/mgg/topo/globe.html
[4] http://www.cru.uea.ac.uk/cru/data/hrg.thm

in terms of fractions of the grid element covered by deciduous forest (FOR_D) and by evergreen forest (FOR_E). Wooded areas have two different important effects (in the model). Firstly, the influence on snow albedo of forests (Eq. 3.5). For a given value of snow water equivalent the snow albedo for wooded areas is much lower than for areas covered by low vegetation. Secondly, the transpiration rate of wooded areas is treated. As shown by different field campaigns, irrespective of the dense vegetation cover, the high LAI values and sometimes large ROOTDPs, for similar values of soil water content, forests show lower transpiration rates compared to other vegetation types. This can be accounted for by increasing the minimum stomata resistance of forests. To provide the inclusion of these effects, the fields of fractional forest cover, separated into deciduous and evergreen forest was introduced.

Hydrological processes

The hydrological part of the soil model, illustrated in the right part of Fig. 3.1, predicts the liquid water contents of various reservoirs of water at the surface and in the soil by solving the Richard's equation. In addition to the different soil layers, the soil model consists of the interception reservoir (which contains all surface water including dew on plants and on the soil) and the snow reservoir (containing snow but also frozen surface water and rime).

The coupling of soil and atmosphere is by precipitation and by the formation of dew and rime as a source of water as well as by evaporation and transpiration as a sink of water. As an additional sink the loss of soil water by runoff is taken into account. Exchange and transport of water between the reservoirs is assumed to occur via infiltration, percolation and capillary movement as well as melting of snow and by freezing of water in the interception reservoir. Vertical soil water transport and runoff from soil layers are not considered for soil textures ice and rock as mentioned before. For the other soil textures, the water budget of the soil layers depends on the boundary values of the upper and the lower boundary of the soil model, on the water extraction by evaporation, on gravitational and capillary transports and on the runoff formation. The evapotranspiration of plants (E_{trans}) is parametrized based on the Biosphere-Atmosphere-Transfer Scheme (BATS) developed by Dickinson (1984). Net evapotranspiration E is the sum of bare soil evaporation E_{bare}, plant transpiration E_{trans}, sublimation from the snow E_s and evaporation from the interception storage E_I weighted by their respective areal coverages:

$$E = (1 - f_I - f_{snow})[(1 - f_{veg})E_{bare} + f_{veg}E_{trans}] + f_I E_I + f_s E_s, \tag{3.1}$$

where f_I is the areal fraction covered by interception water, f_s is the areal fraction covered by snow, and f_{veg} is the areal fraction covered by plants. The parametrization of bare soil evaporation follows as well Dickinson (1984). Therein, it is assumed that bare soil evaporates at a potential rate E_p as long as the upward diffusion of soil moisture can supply enough water:

$$E_{bare} = min(E_p, E_{bare}^{max}), \tag{3.2}$$

where the maximum bare soil evaporation rate E_{bare}^{max} can be sustained by soil moisture diffusion, is parametrized in terms of the soil moisture of the upper layer and the average soil moisture of all layers and of the soil texture. Soil moisture is initialized at the beginning of the simulation by the forcing data and evolves freely in the course of the simulation.

Structural changes in vegetation, such as changes in the leaf area index (LAI), the roughness length (Z_0), and the root depth (ROOTDP) modify the evapotranspiration of water from the land surface. While the LAI influences the amount of intercepted water and the partitioning of energy fluxes into sensible (H) and latent heat (λE), the roughness length (Z_0) affects the turbulent mixing

of heat into the atmosphere (e.g. Adrian, 1996). The rooting depth determines the amount of water extracted from the soils by the vegetation.

Thermal processes

The thermal processes parameterized in TERRA_ML are illustrated in the left part of Fig. 3.1: The vertical distribution of the soil temperature is calculated by solving the heat conduction equation (Fourier's law). The upper boundary condition is obtained by computing the energy balance at the surface, while the lower boundary condition is given by a prescribed climatological temperature.

The surface albedo α for diffuse solar radiation is a mixture of soil albedo α_{soil}, vegetation albedo α_{plant} and eventually snow albedo α_{snow} depending on the fraction of each according to Eq. 3.3:

$$\alpha = SNOWC\,\alpha_{snow} + (1 - SNOWC)(PLCOV\,\alpha_{plant} + (1 - PLCOV \cdot \alpha_{soil}), \tag{3.3}$$

where, SNOWC is the snow cover fraction and $\alpha_{plant} = 0.15$ is the prescribed constant plant albedo. α_{soil} is determined in CCLM by using a coefficient depending on the soil texture, which is multiplied by the soil water content in the upper soil layer:

$$\alpha_{soil} = \alpha_{drysoil} - (\Delta\alpha_{wetsoil} \cdot \frac{1}{depth\_of\_first\_half\_layer} \cdot W_{SO}), \tag{3.4}$$

whereby, $\alpha_{drysoil}$ the albedo of dry soil, $\Delta\alpha_{wetsoil}$ is the slope of solar albedo with respect to soil water content, the depth of the first half layer is given in meter and W_{SO} is the multi-layer soil moisture content in meter. The solar albedo of dry soil depends on the soil texture. The snow albedo α_{snow} is computed by Eq. 3.5.

$$\alpha_{snow} = \alpha_{snow_{min}} + freshsnow \cdot (\alpha_{snow_{max}} - \alpha_{snow_{min}}) \cdot (1 - FOR_E - FOR_D) \cdot \alpha_{snow_{fe}} \cdot FOR_E + \alpha_{snow_{fd}} \cdot FOR_D, \tag{3.5}$$

herein, $\alpha_{snow_{min}}$ is the minimum and $\alpha_{snow_{max}}$ is the maximum solar albedo of snow for forest free surfaces, "freshsnow" is a weighting function indicating the "freshness" of snow, $\alpha_{snow_{fe}}$ is the solar albedo of snow for surfaces with deciduous forest (FOR_D) and $\alpha_{snow_{fe}}$ is respectively the solar albedo for surfaces with evergreen forest (FOR_E).

The albedo for direct short-wave radiation over land surfaces is calculated following Hou et al. (2002) by multiplying the surface albedo with a zenith angle dependency function. There are two zenith angle dependency functions for strong (bare soil) and weak (vegetation) dependencies, which are combined on the fraction of each. Over sea, the albedo for direct short-wave radiation is determined by an empirical equation following Taylor et al. (1996).

The solar radiation budget (S_n) is determined by:

$$S_n = S_{dir\downarrow} + S_{dif\downarrow} - S_{dif\uparrow}, \tag{3.6}$$

where $S_{dir\downarrow}$ is the direct and $S_{dif\downarrow}$ is the diffuse downward shortwave radiation. The diffuse upward shortwave radiation $S_{dif\uparrow}$ is defined by $S_{dif\uparrow} = \alpha S_{dif\downarrow} + \alpha_{dir} S_{dir\downarrow}$. The surface albedo α_{dir} for direct solar radiation is almost similar to α but takes additionally the incident angle into account.

3.2.2. Potentials and limitations of TERRA_ML

TERRA_ML is based on a non-dynamic grid architecture of surface characteristics. Therefore external parameters are given for whole grid boxes. The subgrid-scale heterogeneity of the land surface is not explicitly taken into account (besides considering the partial coverage of the soil surface by vegetation and snow for albedo and evapotranspiration calculations). Only one soil column can exist in each grid cell. If the grid cell is not ice or rock, vegetation can be present and is characterized by a grid averaged LAI, PLCOV and ROOTDP, without further distinction between different plant types. Furthermore, biogeochemistry and vegetation dynamics are not included.

The inaccuracy representation of short- and long-wave radiation is a known issue of TERRA_ML. For example Davin et al. (2011) found a substantial underestimation of the surface net shortwave radiation while Jaeger et al. (2008) found significant errors in both, the net short- and long-wave radiation which they attributed to the simulated cloud cover.

CCLM 4.8 does not contain urban physio-graphic parameters, anthropogenic heat sources, an urban parametrization, nor is their performance validated for urban areas (Neunhäuserer et al., 2007). The assumption of a flat urban geometry introduces two significant errors in the resulting energy balance (Sailor and Fan, 2002): Firstly, some urban surfaces will be partially shaded by structures. This depends on the urban geometry, the solar angle and the relative contributions of direct and diffuse radiation. Additionally, short-wave radiation reflected by any urban surface may be partially intercepted and absorbed by other urban surfaces.
TERRA_ML is a so-called 2nd generation land surface scheme. Nowadays, these schemes have been superseded by more advanced 3rd generation schemes which include in particular a more process-based representation of evapotranspiration by explicitly resolving the process of photosynthesis and its control on stomata conductance (e.g., Sellers et al., 1997 or Pitman, 2003, for an historical overview of LSM development).

However, the overall advantage of TERRA_ML is that it is fast and efficiently coupled and therefore, well integrated into the COSMO and CCLM model respectively. TERRA_ML is running stable at all scales, from coarse - COSMO-EU (Δx=7 km) to fine scales- COSMO-DE (Δx= 2.8 km) and therefore good experiences with this model exist. For these reasons it is used in this thesis.

3.2.3. Implementation of land-cover change in COSMO-CLM

Land-use change can be implemented in CCLM 4.8 by manipulating the external data. As described above, land-cover in CCLM is characterized by ROOTDP, LAI, PLCOV, Z_0, $Z_{0(veg)}$, PLCOV, and FOR_D and FOR_E. There are no explicit land-use classes used. In this thesis, two approaches of land-cover change are applied. In Section 3.3 land-cover is changed in accordance to the CORINE-Lookup table (Doms et al., 2011). As described in more detail in Chapter 4 new land-cover characteristics are applied for the whole domain. The second approach is applied in Chapter 5. Since, the land-cover in CCLM is described by the external parameters and not by land-cover classes, explicit land-cover classes need to be defined. For this purpose, the CORINE land-cover map (Fig. 2.3) is interpolated to the rotated CCLM grid. Thus, external parameters can be linked to land-cover classes as defined in the CORINE land-cover map.

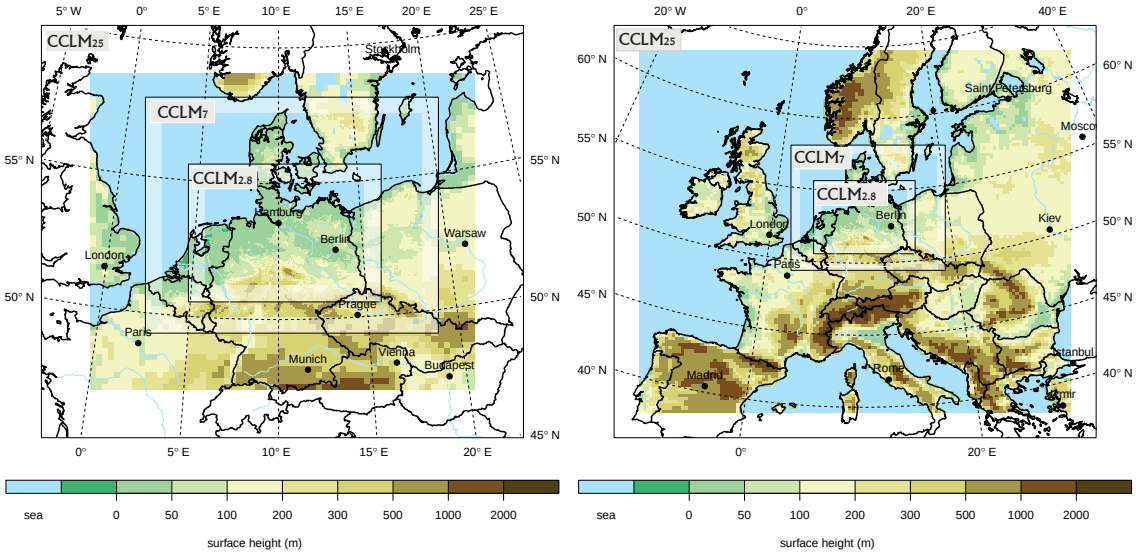

Figure 3.3.: Nesting domains applied in this thesis: Model domains as used by a) the evaluation of CCLM simulations driven by NCEP I and b) later-on used in Chapter 4 by CCLM simulations driven by ERAinterim (left) and model domains with a larger domain of the $CCLM_{25}$ simulation as used in Chapter 5 (right).

3.3. Nesting strategies for convection permitting COSMO-CLM simulations

There were few experiences in the application of CCLM on the convection permitting scale of 2.8 km and no experiences with this high-resolution for Northern Germany at the beginning of this PhD thesis for climate simulations. The DWD uses the numerical weather prediction model COSMO-DE with a horizontal resolution of 2.8 km nested in the COSMO-EU (7 km horizontal resolution).

Due to the high computational effort for such kind of CCLM simulations, it had to be considered, if the nested CCLM simulation with 7 km resolution is really necessary. Hence, two convection permitting CCLM simulations with different nesting strategies were performed over Northern Germany for 2007 and 2008: On the one hand dynamically downscaled from ERAinterim (Dee et al., 2011) as well as from NCEP I (Kalnay et al., 1996) reanalyses data to 25 km and then directly downscaled to the convection permitting scale of 2.8 km. On the other hand, dynamically downscaled with an additional nest of 7 km between the 25 km and the 2.8 km simulation (Tab. 3.1). In the following, the specific configurations of the CCLM simulations of the sensitivity studies are shortly introduced.

3.3.1. Specific configurations for sensitivity studies

$CCLM_{25}$

In all simulations at the horizontal resolution of 25 km (0.22°, $CCLM_{25}$), 5 years spin up time are left to the model. Experiences have shown, that after five years the soil-moisture has gained a status of balance (Geyer, 2013). Meteorological initial and boundary conditions are taken 6 hourly. At the lateral boundaries the relaxation scheme by Davies (1976) is applied. Spectral nudging (von Storch et al., 2000) is employed for the large scale wind above 850 hPa for this simulation

to avoid the large scale circulation differing considerably from the forcing data. The domain for the $CCLM_{25}$ simulations in this chapter and for Chapter 4 encompasses 75 times 65 grid points (about 1875x1625 km^2) and for Chapter 5 150 times 130 grid points (about 3750x3250 km^2). All $CCLM_{25}$ simulations are performed with 32 vertical atmospheric layers.

Table 3.1.: Overview of nesting characteristics of each performed CCLM simulation in the frame of this chapter.

Configuration	$CCLM_{25}$	$CCLM_{2.8\_I}$	$CCLM_7$	$CCLM_{2.8\_II}$
Domain size	75 x 65; 150 x 130	275 x 200	140 x 170	275 x 200
Grid spacing [°]	0.22	0.025	0.0625	0.025
No. of vert. layers	32	50	40	50
Time step [s]	150	25	60	25
Spin up	5 yrs	1 month	3 months	1 month
Forcing	NCEPI/ERAinterim	$CCLM_{25}$	$CCLM_{25}$	$CCLM_7$

$CCLM_7$

Taking climate information (e.g., soil temperature and moisture) from the $CCLM_{25}$ simulation, just two month for the 7 km (0.0625°, $CCLM_7$) simulation are chosen as spin up time. The applied configuration for $CCLM_7$ is adopted from the operational weather forecast model COSMO-EU from the DWD. $CCLM_7$ is forced 3-hourly in this study. The domain for this nest encompasses 140 times 170 grid points (about 980x1190 km^2) and 40 vertical atmospheric layers.

$CCLM_{2.8}$

The applied configuration for the CCLM 2.8 km run ($CCLM_{2.8}$) was adopted from the operational weather forecast model COSMO-DE from the DWD (Baldauf et al., 2011). A rotated longitude-latitude grid of 200 times 274 grid points (about 770x560 km^2) with 0.025° ($\sim$ 2.8 km) grid mesh size and an integration time step of 25 s is used. The model domain covers Northern Germany. 50 model layers with a stretched vertical grid are used. The lowest level is placed 20 m above ground, and the model top lies at 22 km above mean sea level. Deep convection parametrization is switched off completely, small-scale shallow convection is still parametrized by the appropriate part of the Tiedtke scheme (Tiedtke, 1989). $CCLM_{2.8}$ is forced hourly.

3.3.2. Evaluation of simulated model data against observations

This section does not substitute a comprehensive evaluation of the application of CCLM in the convection permitting mode. This was the focus of other studies such as of Hohenegger et al. (2008) or Prein et al. (2013). The intention of this section is to determine whether the results of the $CCLM_{2.8}$ simulations are comparable to well established configurations of regional climate models in general and which nesting option towards the convection permitting mode leads to best results regarding the 2 m temperature and total precipitation.

In the course of this thesis, the domain of the $CCLM_{25}$ was altered. Therefore, both nesting configurations with the different domain sizes of the $CCLM_{25}$ simulations are regarded (Fig. 3.3) in the following evaluation to properly assess the best nesting strategy out of the two nesting approaches (triple nesting: $CCLM_{25}$-$CCLM_7$-$CCLM_{2.8}$ versus double nesting: $CCLM_{25}$-$CCLM_{2.8}$).

The main climate parameters, namely 2 m temperature and total precipitation are evaluated for 2007 and 2008. This period was chosen because of the availability of gridded observation data at that time.

Temperature

To evaluate the simulated 2 m temperature data of the $CCLM_{2.8}$ simulations, two gridded observation data sets are applied. Firstly, the ECA&D data (Haylock et al., 2008) from the ENSEMBLES project with a horizontal resolution of approximately 25 km and additionally the interpolated station data of the DWD (downloaded from WebWerdis, TAMM), with a horizontal resolution of 1 km are taken. Both observation data sets are interpolated to the $CCLM_{2.8}$-grid.

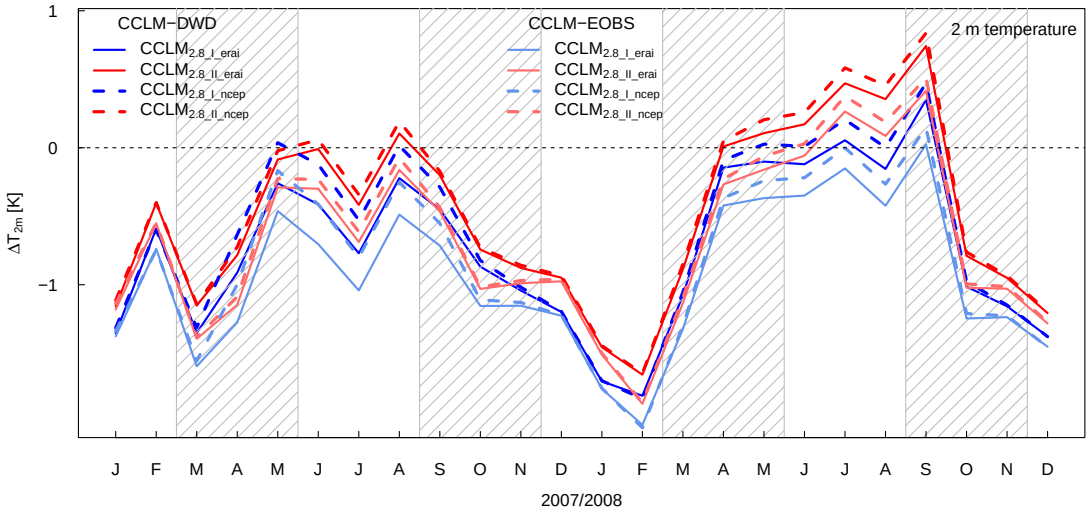

Figure 3.4.: Spatially averaged monthly mean differences in the 2 m temperature for different nesting strategies for the years 2007 and 2008.

Fig. 3.4 shows the spatially averaged monthly mean differences between the $CCLM_{2.8}$ simulations and both, the DWD observations and the ECA&D observations for the land areas of Northern Germany without water bodies. Reddish colours represent triple nested $CCLM_{2.8II}$ simulations and bluish colors double nested $CCLM_{2.8I}$ simulations respectively. The subscripts "erai" and "ncep" indicated the applied reanalyses (ERAinterim and NCEP I) for the $CCLM_{25}$ simulations.

The NCEP I driven $CCLM_{25}$ simulation is conducted with the original land-cover description with minimum and maximum values of LAI and PLCOV, on the small domain (75x65 grid boxes, Fig. 3.3, left). For the "erai" simulations the ECOCLIMAP2 land-cover map, with monthly values of LAI and PLCOV is used on the large domain (150x130 grid boxes, Fig. 3.3, right).

In general, Fig. 3.4 shows a cold bias in mean for the evaluated CCLM simulations. The graph in Fig. 3.4 illustrates a lower bias for the triple nested $CCLM_{2.8II}$ simulations in general. Only in the summer month of 2008, the double nested $CCLM_{2.8I}$ simulations have a lower bias. All $CCLM_{2.8}$ simulations show a particularly high bias in winter in terms of underestimations up to 2 K. Best results or low bias values respectively are shown from May to September in 2007 and from April to September in 2008.

These results drawn from Fig. 3.4 indicate firstly, that the performance of $CCLM_{2.8}$ simulations considerably vary but in a comparable range as well established configurations of regional climate

Table 3.2.: Spatially averaged bias values of nesting evaluation for the 2 m temperature and total precipitation.

Gridded obs.	CCLM data	2 m temperature bias in K					Total precipitation bias in mm				
		MAM	JJA	SON	DJF	year	MAM	JJA	SON	DJF	year
DWD	$CCLM_{2.8\_I\_erai}$	-0.6	-0.3	-0.7	-1.3	-0.7	1.5	-9.0	-6.8	-2.1	-16.5
	$CCLM_{2.8\_I\_ncep}$	-0.5	-0.1	-0.6	-1.3	-0.6	-1.4	-15.0	-9.9	-5.4	-31.6
EOBS	$CCLM_{2.8\_I\_erai}$	-0.9	-0.5	-0.9	-1.4	-0.9	7.3	-5.7	-3.9	-1.8	-4.0
	$CCLM_{2.8\_I\_ncep}$	-0.8	-0.3	-0.8	-1.4	-0.8	4.5	-11.6	-7.0	-5.1	-19.2
mean of double nest.		**-0.7**	**-0.3**	**-0.8**	**-1.4**	**-0.8**	**3.0**	**-10.3**	**-6.9**	**-3.6**	**-17.8**
DWD	$CCLM_{2.8\_II\_erai}$	-0.5	0.1	-0.5	-1.1	-0.5	0.3	-12.9	-6.3	-1.0	-19.9
	$CCLM_{2.8\_II\_ncep}$	-0.4	0.2	-0.4	-1.1	-0.4	-1.8	-16.6	-8.4	-4.0	-30.8
EOBS	$CCLM_{2.8\_II\_erai}$	-0.7	-0.1	-0.7	-1.2	-0.7	6.1	-16.6	-3.4	-0.7	-7.5
	$CCLM_{2.8\_II\_ncep}$	-0.7	-0.1	-0.7	-1.2	-0.7	4.0	-13.2	-5.4	-3.7	-18.4
mean of triple nest.		**-0.6**	**0.0**	**-0.6**	**-1.2**	**-0.6**	**2.2**	**-14.8**	**-5.9**	**-2.4**	**-19.2**

models. Finally, these results indicate a better performance of the $CCLM_{2.8II}$ nesting configuration compared to the $CCLM_{2.8I}$ configuration.

Precipitation

Same as for the 2 m temperature, simulation results of total precipitation of double and triple nested $CCLM_{2.8}$ simulations are compared to two gridded observations data sets. On the one hand the corresponding precipitation values of the ECA&D data set and on the other hand the REGNIE[5] data set with a horizontal resolution of 1 km provided by the DWD. As it can be seen from Fig. 3.5, the bias range in terms of total precipitation as simulated by $CCLM_{2.8}$ simulations lies in a range between -28 to 20 mm per month. Whereas, underestimations of the monthly total precipitation sum dominate.

3.3.3. Conclusions for convection permitting CCLM simulations for Northern Germany

The aim of this short nesting-evaluation with observations was on the one hand to check which nesting strategy leads to the best results and on the other hand, to figure out, if the convection permitting simulations perform similar or even better than other simulations with lower horizontal resolutions. Especially at the beginning of this thesis but also still, the literature pool in the field of convection-permitting climate simulations was and is comparable low (Suklitsch et al., 2011). Most studies related to convection-permitting scales were developed in the framework of numerical prediction so far. Therefore the used configurations of the CCLM simulations were also adopted from the numerical weather model COSMO where good experiences with the applied configurations are made.

Indeed, the time span of the applied evaluation of two year is very short. This is one reason, why this short evaluation does not replace a detailed added value study. Nevertheless, even-though computational resources are continuously increased, the computational cost still remains a limiting factor. The intention of further studies with $CCLM_{2.8}$ simulations in the following is mainly to asses impacts due to land-cover changes. Spatial plots of $CCLM_{2.8}$ simulation results in this study

[5] http://www.dwd.de/DE/leistungen/regnie/regnie.html

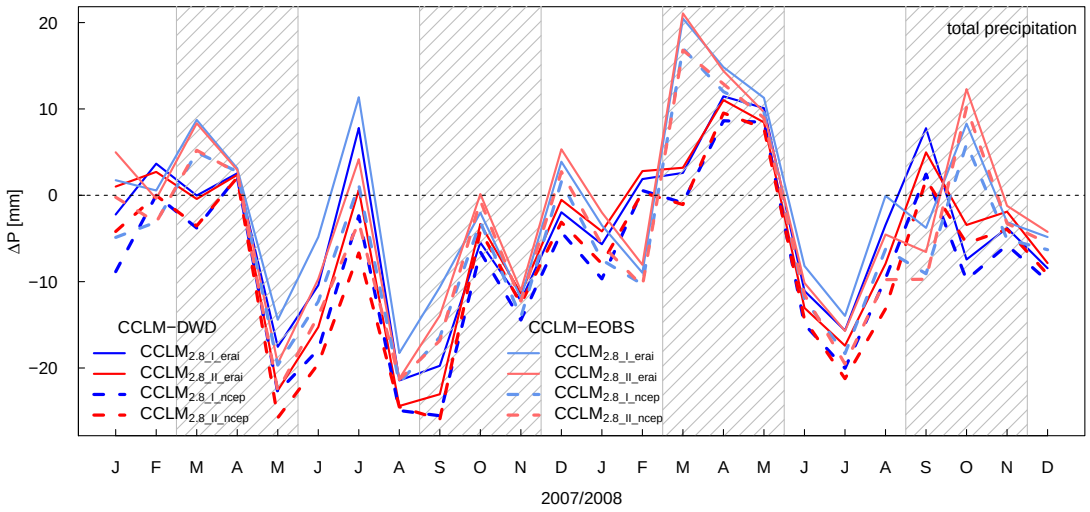

Figure 3.5.: Same as Fig. 3.4 but for total precipitation.

showed a large spin-up domain along the border of the simulated domain. To exclude this disturbed area, on each side of the domain, 25 grid boxes (∼70 km) were cut. Also Brisson et al. (2016) came meanwhile to the same conclusion that the model domain must be large enough for the same reason. They concluded that a domain size of 180 x 180 grid-points is found in their test to be necessary. Here, it can be shown, that bias values of the $CCLM_{2.8}$ simulations lie in a comparable range as other RCMs (e.g. Kotlarski et al., 2014). Especially, the improved results for summer temperatures in the triple nested 2.8 km resolution simulation, but also the less intense sponge zone, lead to the conclusion that a nest of 7 km between the 25 km and the 2.8 km resolution simulation should be taken to aim at best possible simulation results. In contrast, Brisson et al. (2016) found double nesting ($CCLM_{25}$ to $CCLM_{2.8}$) to be appropriate for $CCLM_{2.8}$ simulations. However, in their study they focused exclusively on total precipitation.

4. Effects of extreme land-cover change scenarios on regional climate

4.1. Purpose of this sensitivity study

The purpose of this chapter is to study the interaction between the land surface and the atmosphere in CCLM, improving the understanding of land-cover change effects on the regional climate system and to investigate the maximum range of impacts due to extreme land-cover change scenarios. For this reason a simplified set of climate model simulations based on extreme land-cover changes is performed.

In Section 2 the methodology and the simulation set up are described. In Section 3, the effects due to the land-cover scenarios on the atmospheric conditions of Northern Germany are analysed and explanations for impacts are delivered. Finally, the results of this study are summarized and put in context to other published findings in Section 4.

4.2. Simulations set-up

CCLM is triple-nested down as described in Section 3.3 to a horizontal grid resolution of 2.8 km grid mesh size (Fig. 3.3, left). Initial and lateral boundary conditions are derived from the ERAinterim reanalysis data (Dee et al., 2011). A sensitivity study is performed for the period of 2002 and the year of the European heat wave 2003 (e.g. Beniston, 2004). To test the reliability of the CCLM simulations in terms of internal variability, two control runs are performed. The first run is started at the 1st of December 2001 giving one month spin up time to the model. The second control run is started one month earlier at the 1st of November 2001 giving two month spin up time to the model. The differences between these two control runs are negligible. Therefore just one control run with original land-cover description is shown in the following analyses. For the control run, external parameters are given by the CCLMs preprocessor PEP (Smiatek et al., 2008), meteorological forcing data is provided by CCLM simulation output. Extreme land-cover change scenarios are implemented into the model set up by changing the external data (see Section 3.2.1). Following the CORINE[1] (CoORdination of INformation on the Environment) lookup table of the European Topic Centre on Land Cover (ETC/LC) for characteristic parameters for plants (Doms et al., 2011), the translation from land-cover class to external parameters was performed for each simulation domain (25 km, 7 km and 2.8 km, Tab. 4.1). All changes are conducted on the whole domain. That means only one land-cover is applied in the model domain. This is done without regard to whether specific vegetation types could realistically grow in a given grid cell.

Forest

The first land-cover change scenario of this study is supposed to be close to a land-cover state as it could have looked like before anthropogenic settlement. Potential vegetation of Northern Germany is mixed forest (e.g. Foley et al., 2005). Mixed forest - later referred as ”forest“ - is described

[1] http://sia.eionet.europa.eu/CLC200/classes/index_html

in the CORINE Land Cover classes as follows: "Vegetation formation composed principally of trees, including shrub and bush under storey, where neither broad-lived nor coniferous species predominate." In fact, the mean vegetation roughness length is increased to 1 m and the root depth to 0.8 m. The plant cover (PLCOV) is defined by a range of 0.5 and 1.0, the leaf area index (LAI) by a range of 4.0 and 7 as depicted in Tab. 4.1.

Table 4.1.: External data definition in dependence on the land-cover class after Doms et al. (2011).

Land-cover	Z_0 [m]	ROOTDP [m]	PLCOV (max/min)	LAI (max/min)
Forest	1.00	0.80	1.00/0.50	7.00/4.00
Arable	0.10	1.00	0.90/0.45	5.00/0.20
Urban	1.00	0.60	0.05/0.05	4.70/0.10
Urban sealed	1.00	0.00	0.00	0.00
Mean original	0.45	1.55	0.86/0.53	3.35/0.85

Arable

The second land-cover scenario of this study includes the lowest range of land-cover changes applied on Northern Germany, since it is already covered by about 60% of arable land (CORINE). Therefore, the parameter changes apparent in this scenario are smaller than in others. "Non-irrigated arable land" is chosen for all landmasses in the model domain - later referred as "arable". This land-cover class is described by the CORINE land-cover classes in the following way: "Cereals, legumes, fodder crops, root crops and fallow land. Includes flowers and tree (nurseries cultivation) and vegetables, whether open field or under plastic or glass (including market gardening). Includes aromatic, medicinal and culinary plants. Does not include permanent pasture." Here, arable land is characterized by a low roughness length (Z_0) of 0.1 m and a rootdepth (ROOTDP) of 1 m (Tab. 4.1).

Urban porous

"Continuous urban fabric" (later referred as "urban porous") is referred in the CORINE description as follows: "Most of the land is covered by structures and the transport network. Buildings, roads and artificially surfaced areas cover more than 80% of the total surface. Non-linear areas of vegetation and bare soils are exceptional." A very simplified urban description is used in this chapter. Urban land-cover is rendered by another roughness length (Z_0) of 1 m compared to the mean Z_0 of 0.45 m. The strongly reduced vegetation is reflected in low plant cover fractions (PLCOV, 0.05) with no variation over the annual cycle and low LAI (0.1 to 4.7 in maximum) over the year (Tab. 4.1). No building structures with their shading effects are taken into account. Nevertheless, this is the way how cities are included in the CCLM simulations for the IPCC reports - so far.

Urban sealed

The fourth and most extreme scenario is a combination of the urban land-cover as described above, and an extreme change of the soil textures - meaning the surface was completely sealed (the whole land surface was put to rock). Therefore, ROOTDP, PLCOV and LAI are set to zero. This scenario

will be referred to as "urban sealed" in the following analyses. In the CCLM model formulation, the surface albedo is described depending on the soil texture, the soil moisture, and plant cover (Chapter 3.2.1). Therefore, in this simulation a higher surface albedo than in the control run and the other scenarios will occur: the albedo of dry rock is defined as $\alpha = 0.3$. In a typical urban environment in the midlatitudes a lower surface albedo due to, e.g., dark asphalt streets, shading effects by buildings or dark roofs is typical (see Fig. 2.2). However, Cotton and Pielke Sr (2007) point out that cities have a higher albedo than plowed fields and crop-land because the concrete and buildings are more reflective.

4.3. Changes in the atmospheric conditions of 2002 and 2003

In this section, on the one hand the effects on the regional climate, which occur due to the land-cover change, are presented. The effects which would have a direct impact on our life are highlighted. Effects on the heat wave summer 2003 are discussed in particular detail. On the other hand, it is shed light on the processes leading to the simulated climate change through a detailed analysis of selected model parameters. All evaluations are performed for the grid boxes of the domain covered with at least 50% land.

It is focused on averaged regional changes taking a closer look on Hamburg and Berlin. Impacts by different land-cover change scenarios on regional climate are analysed via their annual cycles, spatial distribution of seasonal mean values and mean diurnal cycles of the whole domain of interest (Fig. 1.1). Several parameters concerning the energy budget and the hydrological cycle are taken into account. The near surface temperature is taken as a first indicator for changes. From this point of view, observed changes can be a feedback due to a changed partitioning of sensible and latent surface heat fluxes. Latent heat flux also links the surface energy balance to the hydrological cycle. A changed amount of evaporation alters the atmospheric humidity, especially in the boundary layer thereby changing also the intensity of moist convection and the degree of cloudiness. A changed cloud cover at different altitudes might feedback differently on the shortwave downward flux. Changes in atmospheric water content are finally linked to the occurrence of precipitation. The year 2002, which is characterized by temperatures about 1 K higher and a total precipitation, which is about 25% higher than for the measurement standard (Müller-Westermeier and Riecke, 2003) and the year 2003, in contrast, was particularly dry and warmer than the long-time mean (Müller-Westermeier and Riecke, 2004). Especially, the European heat wave in June, July and August stand out in this year. In January of both years and partly in February of 2003, noticeable snow events occurred. They led to peaks in the albedo of arable, urban and urban-sealed land-cover scenarios.

In the following, surface energy parameters with a positive sign indicate the direction towards the surface and negative surface parameters the energy flux from the surface towards the atmosphere. For an easier interpretation of changes in the surface fluxes, the differences to the control run were calculated such that positive values stand for an increase, and negative values for a decrease of the parameters.

4.3.1. Land-cover induced temperature changes

The land-cover changes clearly imprint on the mean temperatures of all land pixels of the domain of interest (Fig. 4.1). The surface temperature (T_s) follows the same annual cycle as the 2 m temperature (T_{2m}) albeit an offset.

The urban sealed scenario results in the largest changes in the regional averaged near surface temperatures. T_s and T_{2m} are clearly increased by this land-cover scenario, most pronounced in

the warm season from May to August by values between 2 and 4.5 K compared to the control run. The same qualitative behaviour holds for T_{2m}, T_s, the minimum ($T_{min(2m)}$) and the maximum ($T_{max(2m)}$) temperatures in 2 m height of the urban sealed scenario. $T_{max(2m)}$ is even increased by 5.3 K in May 2002. In contrast, all other scenarios show stronger impacts in summer/autumn of 2003 compared to 2002. Likewise for the urban porous and the forest scenario, T_s is always a bit lower than T_{2m} for urban sealed land-cover. This is caused by the increased roughness length (Tab. 4.1) and the reduced wind speed in 10 m height (Fig. 4.4). In contrast, arable land shows slightly higher T_s than T_{2m} values. Here, a lower roughness length and increased wind speeds in 10 m height are responsible.

Also, urban porous scenario leads to increased summer temperatures, but of a lower degree than for urban sealed scenario. The range of temperature increase for the urban porous scenario is between 0.5 and 2.5 K. In the rest of the year, the urban porous simulation shows different impacts compared to the urban sealed simulation: Firstly, there is a temperature decrease in May and April in the range of -0.2 to -0.3 K. Similarly, there are lower T_{2m} and T_s values of up to -0.9 K in

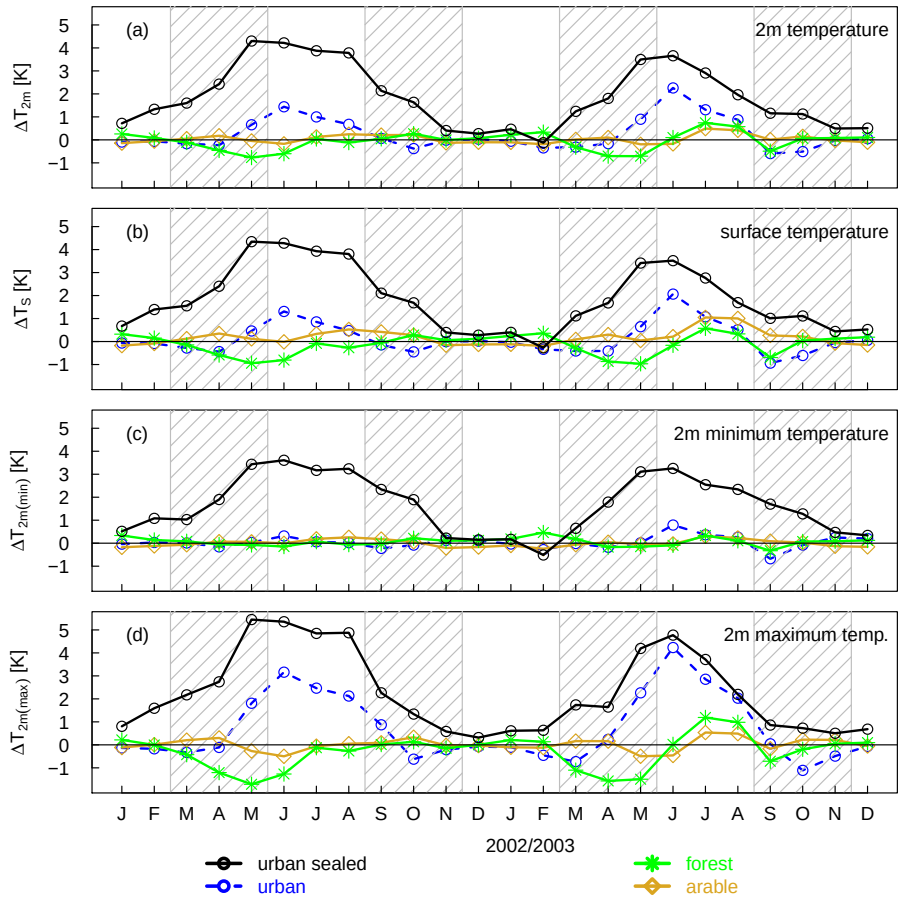

Figure 4.1.: Mean monthly (a) 2 m temperature (T_{2m}), (b) surface temperature (T_S), (c) 2 m minimum temperature ($T_{2m(min)}$) and (d) 2 m maximum temperature ($T_{2m(max)}$) differences to the control run with original land-cover. Shown are the simulation results of the urban sealed scenario (black line), the urban porous scenario (blue line), the mixed forest scenario (green line) and the arable scenario (ochre yellow line). Area means for all land pixels of the simulation domain are shown.

autumn. Particularly strong impacts by urban porous land are visible for $T_{max(2m)}$. From May to August an increase in the range of 2 K up to 4 K is simulated. In contrast to urban sealed land, $T_{min(2m)}$ in the urban porous scenario is only slightly affected by a low increase in June by less than 1 K. Therefore, the spread of temperatures is most enlarged in the urban porous scenario.

The forest scenario causes lower mean T_{2m} of -0.1 to -0.8 K in spring. This cooling effect is even stronger for T_s leading to a decrease of more than -0.9 K. $T_{max(2m)}$ is most reduced in May (-1.7 K). A temperature decrease is also visible following the 2003 heat wave (September). T_{2m}, T_s, $T_{min(2m)}$ and $T_{max(2m)}$ decrease by about -0.3 to -0.7 K compared to the control run in this month. Different impacts are shown for the summer seasons of both years. Whereas in summer 2002, slight cooling effects can be seen, the summer 2003 is characterised by a temperature increase caused by the forest land-cover. $T_{max(2m)}$ increases by more than 1 K in comparison to the control run in July and August. T_{2m} shows an increase of about 0.5 K during that time. Changes in $T_{min(2m)}$ are very small throughout the year.
In comparison to the other extreme scenarios, arable land shows low impacts on the regional temperatures of Northern Germany. This could be the fact because most of Northern Germany's land-cover is currently used as arable land (Fig. 2.3), resulting in smaller changes in this scenario compared to the control run with respect to the changes simulated for the other scenarios. Only for arable land, the T_s difference is higher than the T_{2m} throughout the two years. For July to September, T_{2m} is slightly increased by 0.1 to 0.2 K in 2002 and 0.4 to 0.5 K in 2003. For T_s, slightly more pronounced increases in July and August between 0.3 to 1.0 K occur. Also, $T_{max(2m)}$ is increased by about 0.5 K in July and August 2003.

Temperature extremes due to land-cover changes

There are no changes in the domain mean number of summer days (SD, days with $T_{max(2m)}$ greater-equal 25 °C) in the arable and forest land scenarios (Tab. 4.2). In contrast, arable and forest land clearly lead to a reduction of SD for Hamburg (HH) and Berlin (B). In HH, the number of SD is reduced by 7 and in B by 8 days in the arable land scenario. Forest land causes a reduction of 10 days for HH and of 9 days for B. Both urban scenarios, in contrast, lead to a substantial increase of SDs for the whole model domain of Northern Germany (NG) and a still strong, increase in HH and B (urban porous: +16% for B and up about +50% for NG, urban sealed: +28% for B up to about 73% for NG). The number of hot days (HDs), that means days with $T_{max(2m)}$ greater-equal 30°C is considerably decreased by the arable scenario (HH: -38%, B: -44%) and by the forest scenario (HH: -38%, B: -37%, Tab. 4.2). However, the arable scenario leads to no impacts on the mean number of HDs of NG. The forest scenario causes even an increase in HDs for NG (+20%). In terms of HDs, the urban scenarios show extremely high impacts: the urban porous scenario causes an increase of 200% and the urban sealed scenario of even 280% compared to the control run.

The number of tropical nights (TNs), meaning days with $T_{min(2m)}$ greater-equal 20°C is substantially increased by the urban sealed scenario (Tab. 4.2). This increase is most pronounced for NG (+20 days instead of 3 days) and HH (+18 days and instead of 2 days) a weaker form for B (+32 days instead of 7 days). Hot periods (HPs, consecutive HDs of more than 5 days) last considerably longer due to the urban scenarios (greater +100%) for all three domains. Both, the arable and the forest scenario lead to a decrease in the duration of HPs for HH, and in contrast, to an increase in the duration of HPs for NG. Here, only one HP is considered as shown in (Tab. 4.2, last three rows) which emerged in HH and B, but not for the whole domain of NG. Only arable or only forest land-cover of NG would prevent this HP in B. Whereas the two urban scenarios would double and even triple the number of HPs per year.

Table 4.2.: Total number of daily temperature extremes for summer (JJA) in the investigated 2-year time period per year for Northern Germany (NG), Hamburg (HH) and Berlin (B). Corresponding reference values (REF) from the control run and the impacts due to the land-cover scenarios compared to REF are given.

Extreme index	**Definition [unit]**	**Region**	**Number of days**	**Change of the number of days**			
			REF	**arable-REF**	**forest-REF**	**urban-REF**	**urb. seal.-REF**
SD	when	**NG**	41	0	0	20	30
Number of summer	Tmax $\geq 25°C$	**HH**	43	-7	-10	10	23
days	[day]	**B**	63	-8	-9	10	18
HD	when	**NG**	10	0	2	20	28
Number of hot	Tmax $\geq 30°C$	**HH**	13	-5	-5	12	23
days	[day]	**B**	27	-12	-10	16	21
TN	when	**NG**	3	1	1	2	20
Number of tropical	Tmin $\geq 20°C$	**HH**	2	2	0	2	18
nights	[day]	**B**	7	3	0	3	32
HP	when	**NG**	3	1	2	4	6
Duration of	Tmax $\geq 30°C$	**HH**	3	0	0	3	5
hot periods	[day]	**B**	5	-3	-3	6	8
no. HP	when	**NG**	0	0	0	1	2
Number of	Tmax $\geq 30°C$	**HH**	1	0	0	0	1
hot periods	[day] for >5 days	**B**	1	-1	-1	1	2

4.3.2. Explanations for temperature changes

In the following, the mechanisms behind the temperature changes simulated in the different extreme land-cover scenarios are discussed.

Partitioning of sensible and latent heat flux

For all types of land-cover change, the partitioning of sensible and latent heat flux explain most of the temperature changes. This effect is most pronounced for urban sealed land. The strong temperature increase in the urban sealed scenario is mainly caused by an increase of the sensible and a decrease of the latent heat flux shown in .

The summer temperature increase in the urban porous scenario can also be explained by a pronounced reduction of latent heat flux by about 20 to 60 W/m^2 and an increase of sensible heat flux by 10 to 40 W/m^2 (Fig. 4.2). In contrast, in spring and autumn, the latent heat flux of the urban porous scenario is increased and the sensible heat flux is decreased. This results in the simulated slight decrease of the e.g. 2 m temperature by less than 1 K (Fig. 4.1).

The simulated temperature decrease in spring for the forest scenario, is caused by an increase of the latent heat flux of up to about 20 W/m^2 and a decrease of the sensible heat flux by up to 10 W/m^2. Significant changes appear again during the heat wave 2003. The sensible heat flux increases notably - in August 2003 even stronger than the sensible heat flux of urban sealed land. However, the latent heat flux of forest does not decrease as strong as the one of urban sealed land. Therefore, the temperature increase in the forest scenario is not as pronounced as the temperature increase due to urban sealed land (Fig. 4.1).

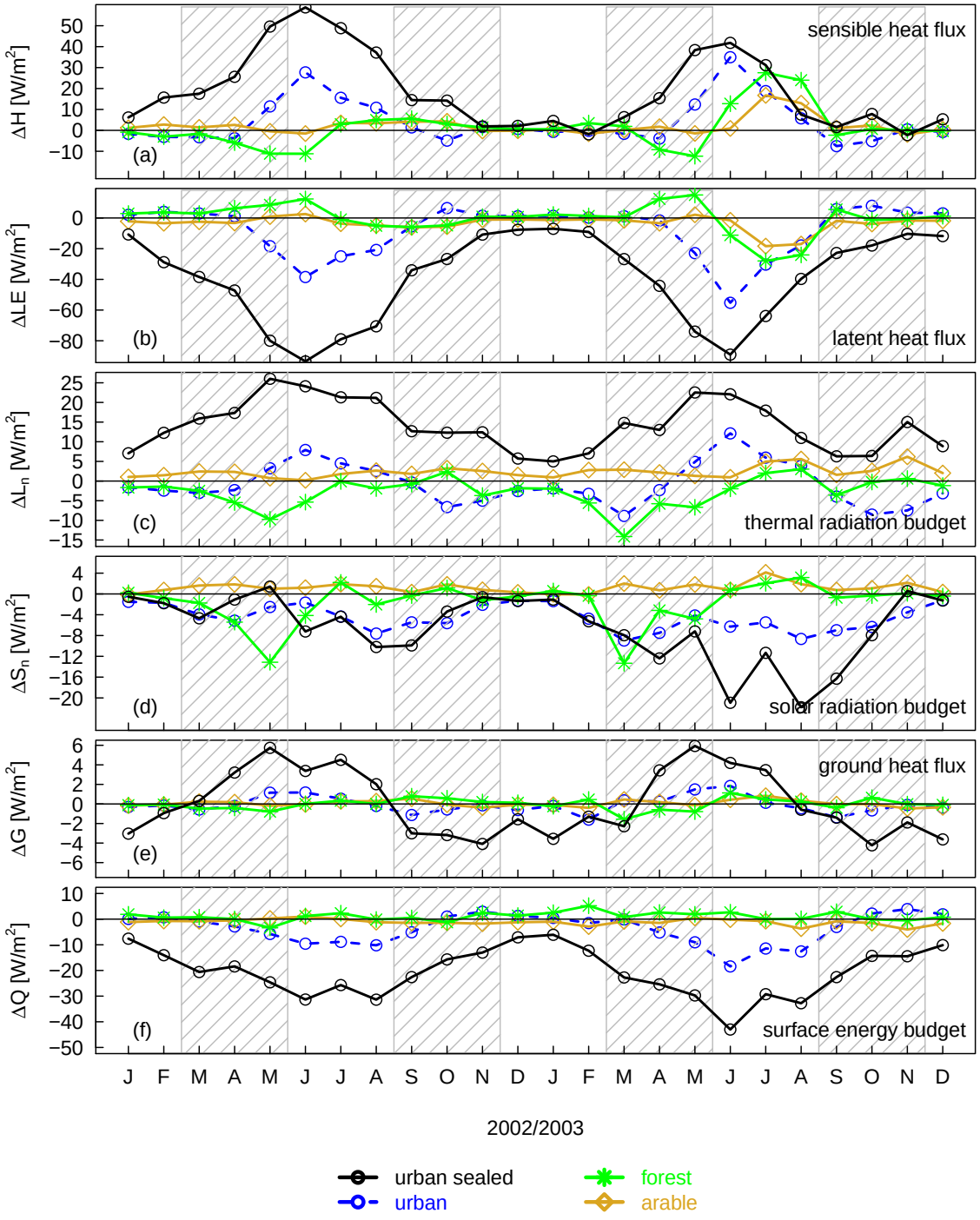

Figure 4.2.: Mean monthly changes in surface fluxes due to different land-cover change scenarios (same as in Fig. 4.1) compared to the control run with original land-cover description. Depicted are the (a) sensible heat flux (H), (b) latent heat flux (LE), (c) thermal radiation budget (L_n), (d) the solar radiation budget (S_n), (e) the ground heat flux (G) and (f) the surface energy budget (R_n). Positive values stand for an increase, and negative values for a decrease of the parameters (differences were calculated accordingly).

For arable land, the slight temperature increase in late summer 2002 and the more intense increase in summer 2003 is caused by increased sensible and decreased latent heat fluxes.

Correlation of 2 m temperature and sensible heat flux

Usually, an increase/decrease in sensible heat flux is associated with an increase/decrease of the 2 m temperature. In this study, it can be seen that pronounced increases in the 2 m temperature result in pronounced increase sensible heat flux for the two urban scenarios (Fig. 4.1 and Fig. 4.2). This relation is also visible for the forest scenario in May and June. The decrease of sensible heat flux at that time appears in combination with a temperature reduction. But for summer 2003, it looks different for the arable and more pronounced for the forest scenario: Clear increases in sensible heat flux in summer 2003 do not result in a comparable temperature increase as can be seen likewise for the urban sealed scenario. In August 2003, the sensible heat flux is even higher for the forest scenario than for the urban sealed scenario. Nevertheless, larger temperatures can be seen for the urban sealed scenario than for the forest scenario. A possible explanation could be a colder status of forest before the heat wave leading to a weaker heating.

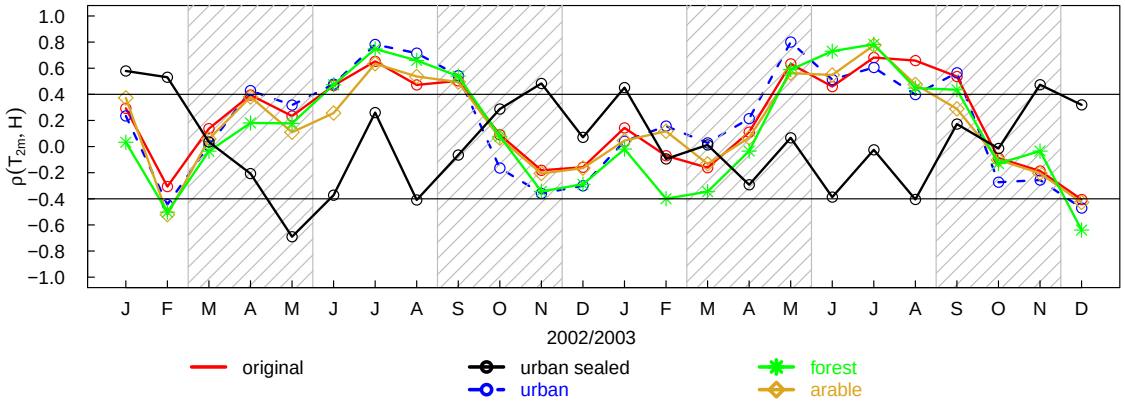

Figure 4.3.: Mean field correlation of 2 m temperature (T_{2m}) with the sensible heat flux (H).

Simulations with original, forest, arable and urban porous land-cover show similar variations of their field correlation between 2 m temperature and sensible heat flux in Fig. 4.3. Strongest correlations appear in the summer month of mostly more than 0.4. The correlations weaken during the transient seasons and winter. During some periods, the urban sealed scenario displays considerably different sensible heat flux - temperature relationships compared to the other scenarios. Especially in July 2002 and 2003, lower correlations than for the other scenarios can be found. At the same time, all scenarios but the urban sealed one displays the highest correlations of all considered time periods.

Further changes in the surface energy budget

The urban sealed scenario results in the largest changes in the thermal radiation budget (Fig. 4.2, c) and strongest impacts of the applied scenarios. The maximum increase of the monthly mean temperature in May in Fig. 4.1, is reflected by an increased thermal radiation budget. The solar radiation budget is reduced in the urban sealed scenario throughout the whole time period. This seems to be in contradiction with a decrease of total cloud cover (Fig. 4.5, d) for both years. However, the increased albedo (Fig. 4.4, a) of the urban sealed scenario leads to increased diffuse upward shortwave radiation and therefore reduces the net solar radiation budget at the surface.

The urban sealed scenario shows strongest impacts on the ground heat flux compared to the other scenarios (Fig. 4.2, e). In spring and summer, the ground heat flux is increased by mostly 3 to 6 W/m^2 and in autumn and winter, it is decreased by mostly 3 to 5 W/m^2 in the urban sealed scenario.

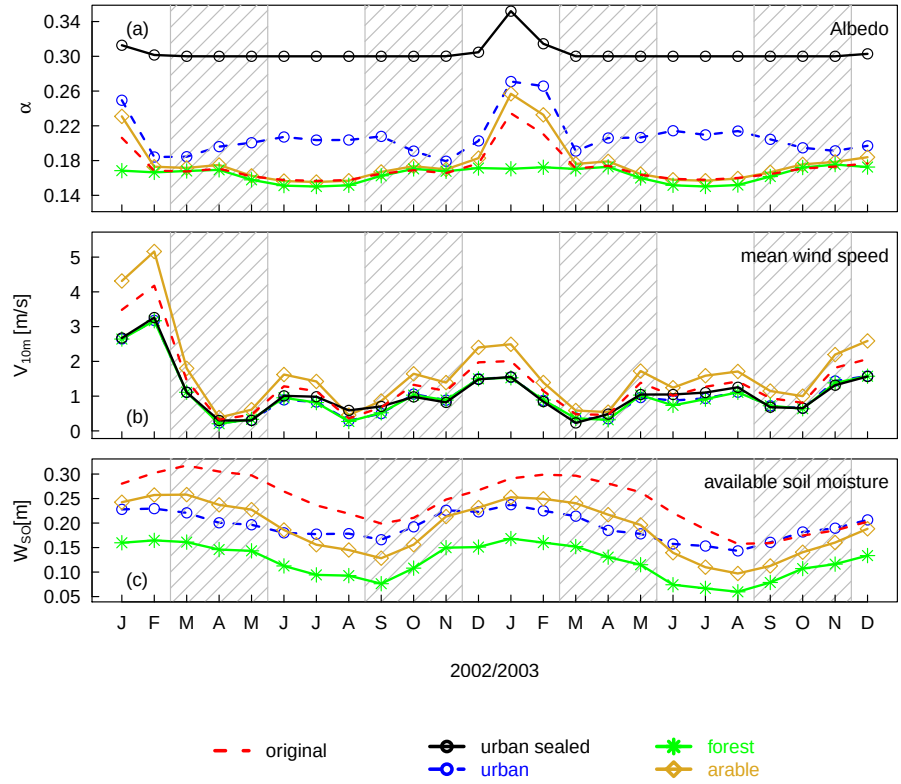

Figure 4.4.: Absolut values of the (a) albedo at the surface (α), (b) the mean wind speed (V_{10m}) and (c) the available soil moisture (W_{SO}) of each scenario (depicted as in Fig. 4.1 and for the control run with the original land-cover description (dashed red line). The soil moisture for the urban sealed scenario is zero (not plotted).

In the urban sealed scenario, both, the thermal conductivity of rock is higher and the pore volume is lower than for other soil textures. Therefore, heat is conducted faster compared to the other applied scenarios and the control run. In summary, a clear reduction of the surface energy budget by up to 45 W/m^2 in June 2003 is shown due to the substantial reduction of latent heat flux compared to the increase of sensible heat and ground heat fluxes.
While the change in thermal radiation of the urban porous scenario also partly contributes to the temperature increases in summer, stronger influence on temperature reduction can be seen in spring and autumn. For monthly mean temperature increases of 1 to 2 K in summer, the thermal radiation contributes by 7 to 10 W/m^2. For lower temperature decreases in spring and autumn of no more than 0.5 K the thermal radiation contributes 3 to 10 W/m^2. Therefore, especially the thermal radiation plays an important role for temperature reductions during spring and autumn in the urban porous scenario. Similarly, the urban porous land-cover scenario displays a reduction of the solar radiation budget during both years due to an increased albedo for this scenario (Fig. 4.4, a). Impacts on the ground heat flux by the urban porous scenario are low compared to the urban sealed scenario. A slight increase can be seen for May and June only, therewith contributing slightly to

the temperature increase in Fig. 4.1. In general, the surface energy budget is reduced during 2002 and 2003 in the extreme urban scenarios - especially during summer.

For 2002 and 2003, a decrease of the thermal radiation budget due to the forest scenario occurs with few exceptions. The higher amount of PLCOV and a higher LAI in the forest scenario leads to a slightly lower albedo compared to the control run (Fig. 4.4, a). Therefore, forest is able to absorb more incident solar radiation. For October 2002, July and August 2003, the thermal radiation budget increases slightly. This increase is caused by an increase of the solar radiation budget which leads finally to the described increase of the surface and 2 m temperature in Fig. 4.1. For the solar radiation budget of forest, two negative peaks become visible. One in May 2002 and the other in March 2003. This is in line with an increase of total cloud cover (Fig. 4.5, d). Nearly no effects on the ground heat flux occur. In summary, the simulated changes in the thermal and solar radiation cancel each other, so that almost no effects on the surface energy budget are shown for forest.

Arable land shows a slightly increased thermal radiation budget throughout 2002 and 2003 together with negligible changes in the ground heat flux for arable land this leads to no impacts on the surface energy budget.

Except for forest, all scenarios clearly reflect the snow occurrences in January and February 2002 and 2003 by an increase of the albedo (Fig. 4.4). During these snow events, also the albedo of arable land rises higher than in the control run. The reason for this is probably the homogeneity in the arable scenario compared to the mixed land-cover in the control run.

4.3.3. Impacts on the hydrological cycle

The hydrological cycle is most significantly affected by a change of the surface evaporation as shown in Fig. 4.5 (a). Changes in the surface evaporation correspond to the simulated changes in latent heat flux as seen in Fig. 4.2 (b) but accordingly in the unit "mm". Also the change in integrated water vapor (IWV) shows similar impacts throughout the annual cycle.

The urban porous scenario and the forest scenario lead to an increase of total precipitation during some periods in the two years simulated. Urban sealed and arable land are characterized by a mean decrease of total precipitation during 2002 and 2003 by about 9 mm and 3.4 mm respectively per month.

The latent heat flux and thus the surface evaporation are reduced for the urban sealed scenario with a negative peak in June of each year of roughly 100 mm less evaporation (Fig. 4.5, a). This lack of evaporative cooling leads on one hand to the pronounced heating of the urban sealed simulation as seen in Fig. 4.1 and on the other hand to less IWV (Fig. 4.5, c) and finally to less total precipitation (Fig. 4.5, b). Most pronounced reductions of total precipitation due to the urban sealed scenario appear in May, July and August 2002 and April to July 2003. In June 2002, a lower reduction of the precipitation amount can be seen. In agreement with less IWV and higher temperatures (Fig. 4.1), also the total cloud cover amount is reduced throughout both years (Fig. 4.5, d). Finally, the surface water budget (Fig. 4.5, e) provides information on what changes in total precipitation and surface evaporation in combination with run-off and changes in water storage actually mean for the domain (Section 2.1). For the urban sealed scenario, the run-off term is very high due to large surface run-off amounts (not shown). This leads to the diminishing season dependent variation of the hydrological cycle. No water is stored in the urban sealed scenario.

The urban porous scenario shows a comparable variability of the annual cycle of the change in total precipitation throughout the two years as seen for the urban sealed scenario but on a higher level with a higher range. Also here a strong relationship between changes in atmospheric

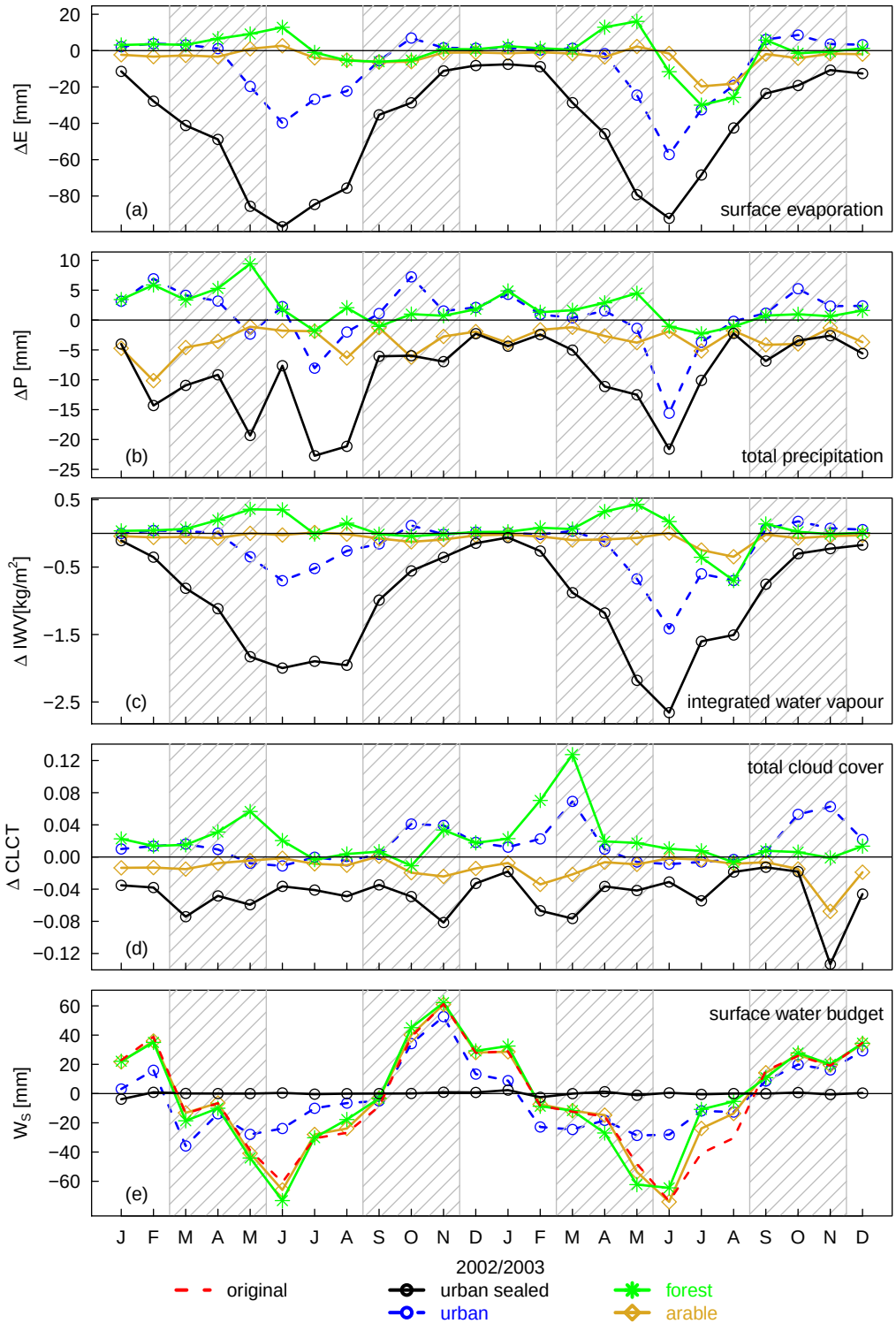

Figure 4.5.: Differences of monthly sums of (a) surface evaporation (E), (b) total precipitation (P), (c) integrated water vapor (IWV) and (d) total cloud cover (CLCT) due to the different land-cover scenarios as described in Fig. 4.1. (e) Absolute values of the net surface water budget for each scenario and the control run with original land-cover.

moisture and total precipitation can be seen. Although, there are several comparable impacts in the urban porous and urban sealed scenarios- the change of total cloud cover in the urban porous scenario shows an opposite change compared to the urban sealed scenario. The surface water budget of urban porous shows an annual cycle similar to the other non-urban scenarios but with a lower amplitude in summer. Therefore, less water is transported to the atmosphere. In early spring in contrast, more water is transported to the atmosphere in the urban porous scenario than the other land-cover scenarios. This contributes to an increase of total cloud cover and a higher total precipitation amount in early spring.

Lower spring temperatures seen for the forest scenario are accompanied by increased moisture in the atmosphere in terms of surface evaporation, IWV, total cloud cover and finally increased total precipitation amounts. Strongest impacts by the forest scenario can be seen in summer 2003: Surface evaporation and IWV are clearly reduced by up to 30 mm and up to 0.6 kg/m^2 respectively. Same can be seen for the arable scenario. While there are just small variations in the mean monthly change of surface evaporation throughout the annual cycle, summer 2003 is characterized by a pronounced decrease of surface evaporation and a decrease of IWV. In the arable scenario, total precipitation and total cloud cover are reduced during both years. Concerning changes in the surface evaporation and IWV, summer 2003 shows strong impacts: both parameters are clearly reduced in that time leading to a reduced surface water budget. This lower evaporative cooling contributes to the temperature increase seen in Fig. 4.1.

Hydrological extremes due to land-cover changes

Hydrological extremes in terms of consecutive dry days (CDD) that is the number of days with daily precipitation of less than 1 mm, the number of dry periods (no.CDD) defined by CDD lasting for at least 5 days, the number of intense precipitation days (RR10, daily P$\geq$10 mm) and heavy precipitation days (RR20, daily P$\geq$ 20 mm) are shown in Tab. 4.3. Here, also the number of precipitation days (PD) is presented for a reference value to RR10 and RR20. All land-cover scenarios seem to increase the CDDs for NG. Whereas the urban sealed scenario shows the strongest effect by additional 4 days. The urban porous and the urban sealed scenario cause also a considerable increase of CDDs for B, the impacts on HH are lower. As already seen in Fig. 4.5 (b) also the forest scenario contributes to less total precipitation which is presented by an increase of CDDs in all domains. The number of dry periods (at least 5 consecutive dry days, no.CDD) is only in B affected by a slight increase due to the urban sealed scenario. PDs are decreased due to the arable scenario for NG and HH, the urban porous scenario for B and for the urban sealed scenario for all domains in JJA. Only the forest scenario shows for HH and B and the urban porous scenario for HH a slight increase in the number of precipitation days. For the urban sealed scenario also the number of RR10 and RR20 decreases. The forest scenario seems to induce more RR10 for B and more RR20 for HH and B. The arable scenario shows an increase of RR20 for HH.

Nevertheless, this analysis can only indicate directions of impacts due to the land-cover change scenarios. The "dry climate" in the urban sealed scenario is underlined for JJA. Whereas, the forest scenario causes a slightly more "humid" climate during JJA.

Cloud radiation feedback

Clouds are fundamental parameters of the climate system, owing to their strong impact on surface radiation. The latter feeds back into clouds by exerting a strong control on surface heat and moisture fluxes which induces changes in the atmospheric stratification and convection. Here, the interactions between the radiation fluxes and total cloud cover (CLCT), which take place in the model simulations, are explored.

Table 4.3.: Scenarios and regions abbreviations as in Tab. 4.2 but for daily precipitation extremes per year.

Extreme index	Definition [unit]	Region	Number of days	Change of the number of days			
			REF	arable-REF	forest-REF	urban-REF	urb. seal.-REF
CDD	when	**NG**	13	1	1	1	4
Number of consec.	Rday $\leq$ 1 mm	**HH**	14	0	1	1	0
dry days	[day]	**B**	13	0	1	3	3
no.CDD	when	**NG**	5	0	0	0	0
Number of	Rday $\leq$ 1 mm	**HH**	4	0	0	0	0
dry periods	[day] for $\geq$5 days	**B**	4	0	0	0	1
PD	when	**NG**	27	-1	0	0	-3
Number of	Rday $\geq$ 1 mm	**HH**	32	-2	1	1	-4
precipitation days	[day]	**B**	26	0	1	-1	-4
RR10	when	**NG**	4	0	0	0	-1
Number of intense	Rday $\geq$ 10 mm	**HH**	6	0	0	0	-2
precipitation days	[day]	**B**	3	0	1	0	-1
RR20	when	**NG**	2	0	0	0	-1
Number of heavy	Rday $\geq$ 20 mm	**HH**	2	1	1	0	-1
precipitation days	[day]	**B**	1	0	1	0	0

As mentioned before, the CLCT of the urban sealed and arable scenario is reduced during the whole simulation period (Fig. 4.5). In contrast, the urban porous and forest scenario show mainly increases and unchanged conditions for CLCT throughout the simulation period. All these changes in CLCT are mainly manifested in a reduction of low clouds (not shown).

The urban sealed scenario leads to a reduction in CLCT due to negligible surface evaporation and reduced IWV (Fig. 4.5).

For the arable scenario, less CLCT is simulated than in the original simulation due to less IWV (Fig. 4.5). As expected, the forest scenario leads to a higher CLCT through a combination of increased latent heat flux (λE, Fig. 4.2) and IWV (Fig. 4.5, c). A strong relation could be seen for the thermal and solar radiation budget in May 2002 and March 2003 (Fig. 4.5 and Fig. 4.2).

Less pronounced than for the forest scenario, also the urban porous scenario shows an increase in CLCT throughout the year. This increase in CLCT can be partly explained by reduced temperatures leading to increased lower tropospheric stability, thereby increasing low cloud cover.

4.3.4. Soil moisture limitation

The role of soil moisture for the described impacts by the applied land-cover change scenarios is investigated in this section. The land-atmosphere coupling involves numerous complex interactions and feedbacks linked to e.g. local soil moisture. Soil moisture is often the main quantity limiting surface evaporation and, hence, controlling the partitioning of incoming energy into latent and sensible heat flux.

A simple diagnostic proposed by Seneviratne et al. (2006) is applied for analysing soil moisture-temperature interactions in all scenarios but the urban sealed scenario as evaporation is by definition zero in that scenario. Following Seneviratne et al. (2006), the sensitivity of evaporation

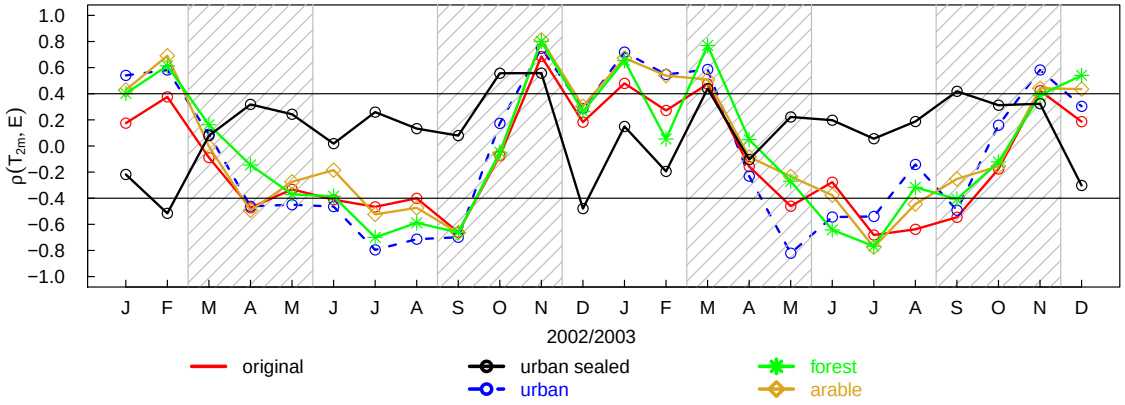

Figure 4.6.: Mean field correlation of 2 m temperature (T_{2m}) with the surface evaporation (E).

on soil moisture can be expressed by the correlation of evaporation and 2 m temperature. This can be seen as a reverse measure of soil-moisture-temperature coupling, as negative correlations point to a strong control of soil moisture upon evapotranspiration and temperature (while positive correlations generally point to strong atmospheric control on evapotranspiration). Looking at the correlations between 2 m temperature and surface evaporation for the simulations (Fig. 4.6), it becomes apparent that during the vegetation period (April to October) negative correlations dominate and during the rest of the time positive correlations. Therefore, it can be concluded that all except urban sealed scenarios show strong relations between soil moisture upon evapotranspiration and temperature in summer, and strong atmospheric control on evaporation in winter.

4.3.5. Regional distribution of atmospheric impacts by land-cover changes

The regional distribution of impacts by land-cover changes are discussed in terms of seasonal (DJF, MAM, JJA, and SON) mean changes in the following.

2 m Temperature

In Fig. 4.7 the regional distribution of land-cover induced changes in T_{2m} are shown for 2002 and 2003 respectively. The strong heating by the urban sealed scenario from May to August seen in Fig. 4.1 is increased with growing distance from the coasts. Temperature increases further inland of Northern Germany are up to 2 K higher than along the coasts. Nevertheless, the urban sealed scenario even impacts on the Baltic Sea and the German Bight in MAM and SON, and most pronounced again in JJA by a T_{2m} increase of 0.2 to 0.8 K. The strongest impacts over water are located along the coastlines. Regions with originally forest land-cover in the control run (indicated in Fig. 2.3) are particularly affected by T_{2m} increases due to the urban sealed scenario. This is primarily visible in SON. For instance, T_{2m} increases in the region of the Teutoburg Forest (in 2002) are up to 1 K larger compared to regions with arable land-cover in the control run.

The slight mean decrease in T_{2m} due to the urban porous scenario in MAM (Fig. 4.1) is irregular distributed throughout the domain. Showing regions with no or nearly no T_{2m} changes and regions with T_{2m} decreases mainly between 0.2 to 0.4 K. In 2003, also larger domains with T_{2m} decreases between 0.4 and 0.8 K can particularly be seen along the German-Polish border in the center-east of the domain and on the left border of the domain. However, the temperature increase in May (Fig. 4.1) dominates the regional distribution of temperature changes for MAM. Similar to

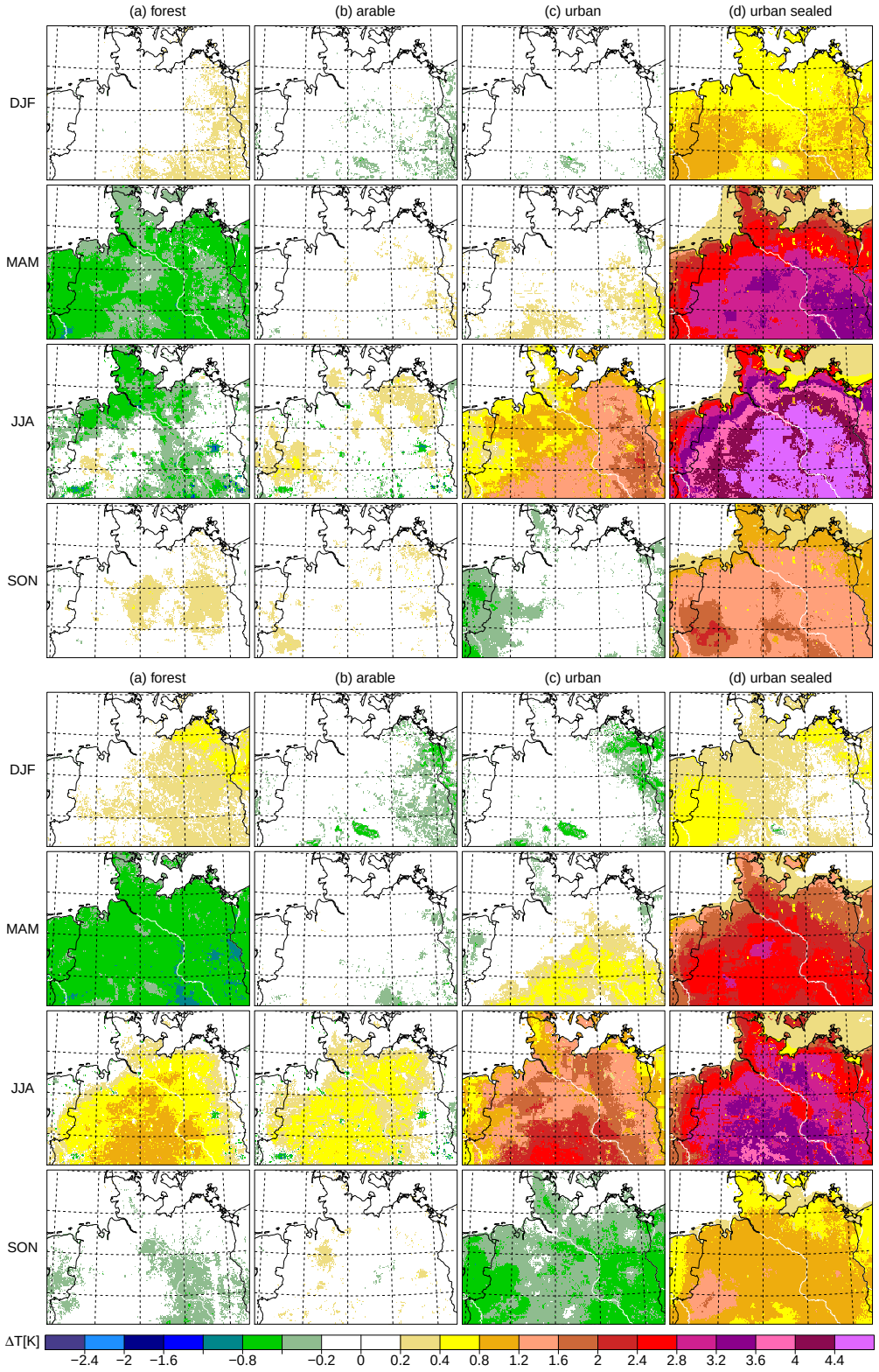

Figure 4.7.: 2002 (upper panel) and 2003 (lower panel) seasonal mean 2 m temperature differences to the control run with original land-cover for (a) the mixed forest, (b) the arable land, (c) the urban (porous) and (d) the urban sealed scenario. The results for each season are shown in row I-IV: (I) DJF, (II) MAM, (III) JJA and (IV) SON.

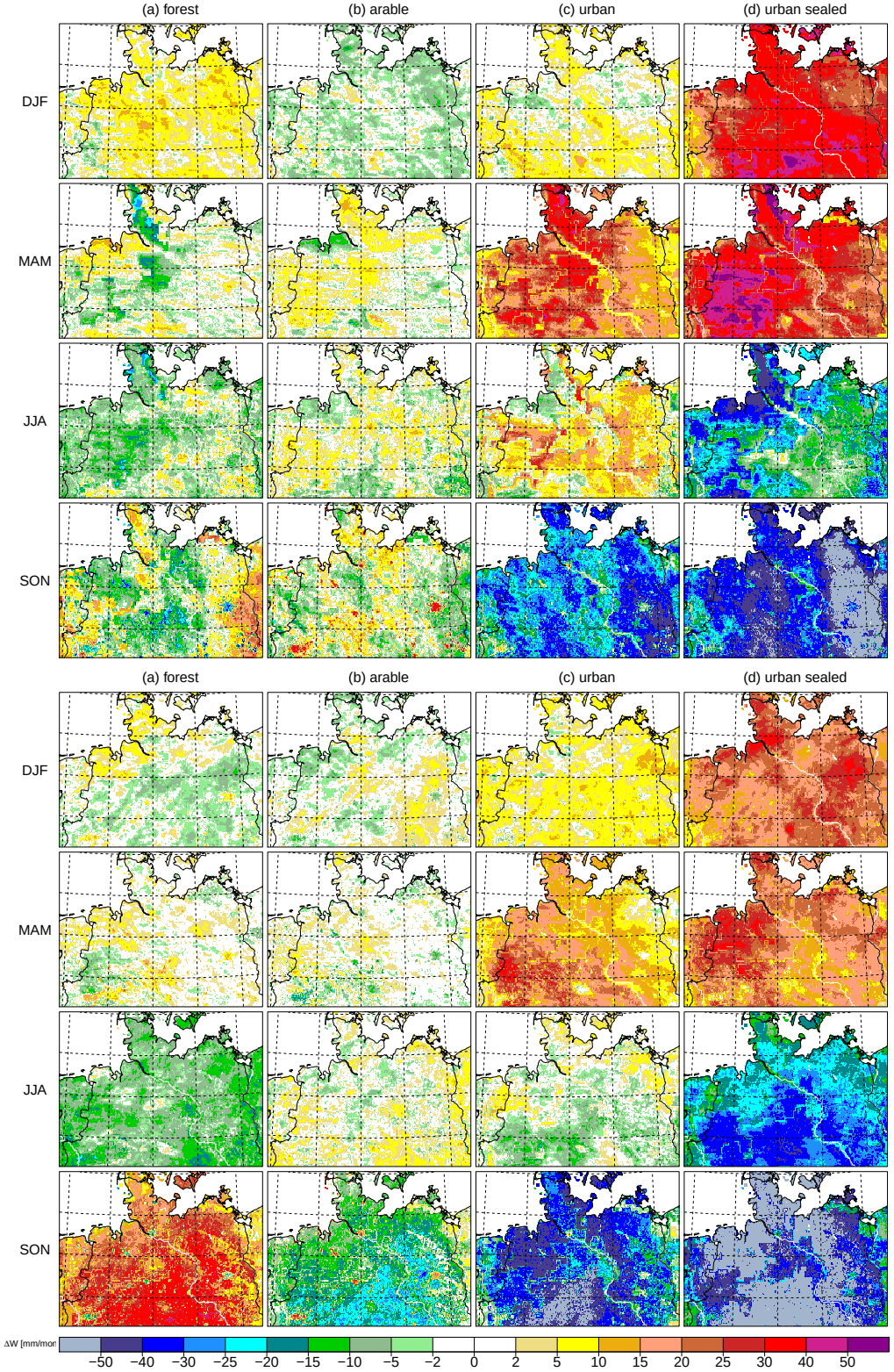

Figure 4.8.: Differences in the surface water budget as denoted in Fig. 4.7.

the urban sealed scenario, the urban porous scenario shows a pronounced increase in T_{2m} with distance to the coasts in JJA of both years. In JJA 2003, there are mainly T_{2m} increases of 0.4 to 1.6 K along the coasts. T_{2m} increases of more than 2 K are simulated in the south-center of the domain. In JJA 2002, this discrepancy is not as strong but the differences in T_{2m} changes between the coastal and the central regions are in the range of 1 K. The most pronounced T_{2m} decreases in SON 2002 due to the urban porous scenario (Fig. 4.1) are visible in the western part of the domain. In SON 2003, there are T_{2m} decreases over nearly the entire land surfaces of the domain.

It is clearly shown that forest acts to cool on T_{2m} in contrast to urban land-cover, especially in MAM (in 2002 also for JJA). For Berlin and Hamburg, this cooling effect is particularly evident. In Berlin considerable lower temperatures of more than 0.8 K less than in the control run are simulated due to the replacement of urban land-cover by mixed forest in JJA of both years. The T_{2m} decrease in JJA 2002 is particularly located in areas adjacent to the North Sea coast and the Baltic Sea. But also along the river Elbe areas of lower T_{2m} are visible reaching their maximum extend in the south-center to eastern part of the model domain. In JJA 2003, the spatial distribution of the temperature changes appears completely different. Increases of the 2 m temperature are most focused in the centre to south of the model domain with maximum values of about 1 K in the forest scenario. By increasing distance from the coasts the T_{2m} differences increase. For the arable scenario, few changes in T_{2m} of low extend and low amplitude are simulated in the eastern part of the model domain. Same as for the forest scenario, the replacement of the largest cities of Northern Germany (Berlin, Hamburg, Hannover) by the arable scenario would lead to lower T_{2m} in JJA than the urban environment generates now. A slight temperature increase in 2002 is visible in the north-east and south-west of Northern Germany. In 2003, by contrast, the temperature increase is clearly extended throughout the model domain, covering nearly the whole land surface. Just along the coastline no temperature change is visible nor along the east and west border of the model domain. Interestingly, the replacement of the large cities Berlin, Hamburg, Hannover, or Bremen by the arable scenario would even lead to a stronger cooling effect of -0.4 to -1.2 K in 2003 than for forest. For JJA 2002, the forest scenario leads to stronger cooling effects than the arable scenario at the same places.

Surface water budget

To capture changes in the regional distribution of the hydrological cycle - the surface water budget delivers most informative values. Especially during the heat wave in 2003, the surface water budget plays an important role concerning the drying-out of the model domain (Fig. 4.5). The regional distribution of the change in the surface water budget shows again the most prominent impact in the urban sealed scenario for both years (Fig. 4.8). As mentioned before it is apparent that there is no annual variation of the surface water budget of the urban sealed scenario. Therefore, the maps of changes in Fig. 4.8 reflect where the strongest impacts - due to the sealing - occur. Not just the urban sealed but also urban porous simulation reflects impacts by the soil textures (Fig. 3.2). Especially for the run-off term in Eq. 2.6 the soil textures and the existence and extent of vegetation play an important role. In summer of both years, pronounced effects appear for regions with the former soil textures loam - a soil texture with a good storage of surface water. As described above, 2002 and 2003 were climatologically very different. This is depicted once more for the surface water budget.

In the change of the surface water budget due to the urban porous scenario, some structures caused by the different soil textures are shown. In this scenario, the soil textures are not changed and therefore the impact is not as strong as for urban sealed scenario. In DJF a reduction of the surface water budget is depicted- although there is an increase of total precipitation during that time. However, the subsurface runoff of the urban porous scenario is clearly increased and leads

to the decrease in the surface water budget following Eq. 2.6. Changes in the surface water budget at the locations of the currently large cities in Northern Germany are visible in the forest, arable, urban porous and urban sealed scenarios. Therefore, even if there is no change in the soil texture in the model formulation of a city clear urban impacts occur due to the sparse or even eliminated vegetation in cities.

4.3.6. Changes in the diurnal cycle

To explore the occurrence of impacts due to the above discussed land-cover changes in more detail, the diurnal cycles of 2 m temperature (T_{2m}) changes and of changes in the total precipitation amount (P) are analyzed for each season in the following.

2 m temperature

Fig. 4.9 shows that changes in T_{2m} due to the land-cover scenarios are hardly daytime dependent in SON and DJF. Only due to the urban scenarios slight effects on the diurnal cycle of T_{2m} occur. In DJF, the urban sealed simulation shows a small increase in the degree of change in T_{2m} in the morning until noon followed by a decrease in the afternoon. In SON 2003, the urban porous scenario leads to strongest temperature decreases of about 0.8 K at 15 UTC in the afternoon.

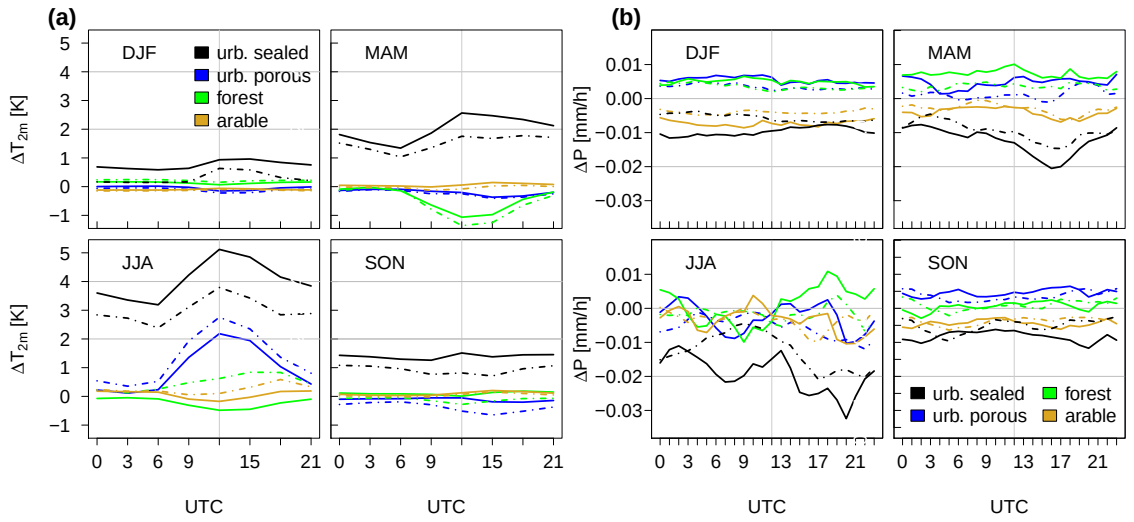

Figure 4.9.: Mean diurnal cycle of a) 2 m temperature and b) total precipitation differences for 2002 (solid line) and 2003 (dashed line) for each season.

In MAM and JJA, significant daytime dependent effects on T_{2m} due to the applied land-cover changes appear. In MAM, mainly the urban sealed and the forest scenario show effects on the diurnal cycle. The urban sealed simulation shows for both years an increased T_{2m}-level throughout the day with a maximum at 12 UTC and a minimum at 6 UTC, respectively. In 2002, the changes are smaller and feature a less pronounced maximum against noon compared to 2003. In total, T_{2m} is increased between 1.8 K up to 2.5 K at noon in MAM. The T_{2m} decrease by forest seen in Fig. 4.1 is manifested in a decrease of the diurnal variation compared to the control run. Starting with sunrise, the T_{2m} decrease deepens until noon to 15 UTC by more than 1 K and than approaches again the status of the control run. Therefore, forest clearly dampens the diurnal variation of T_{2m} in MAM. The T_{2m} decrease in MAM due to the urban porous scenario shown in Fig. 4.1 is especially

shown during the afternoon between 15 and 18 UTC, with T_{2m} about 0.5 K lower than in the control run. The urban sealed scenario leads to a clear increase in T_{2m} throughout the day in JJA. Starting with sunrise, changes in T_{2m} increase sharply until noon showing their highest value of more than 5 K in 2002 compared to the control run. After this maximum, T_{2m} differences decrease over night to a minimum - still more than at least 2.2 K higher than the control run - before sunrise. In JJA 2002, the diurnal cycle of urban sealed simulation leads to larger differences to the control run than in 2003 and as already seen in Fig. 4.1. All other scenarios show stronger effects in 2003 than in 2002 for the diurnal temperature cycle. Urban land with porous ground shows the strongest variation of impacts on the diurnal cycle of T_{2m}. While there is only a slight increase of T_{2m} during night time in 2003, there is a rapid increase starting from sunrise going up to more than 2 K higher than in the control run at noon. In the forest scenario, changes in the diurnal cycle of T_{2m} are also different between the two years (similar to the annual cycle characteristics). T_{2m} increases and decreases over the daytime are simulated for 2002 and 2003 respectively. In contrast to the urban scenarios, the forest scenario clearly features the largest T_{2m} increases in the late afternoon around 15 UTC. The arable scenario leads to rather similar effects in both JJAs, with slightly higher values simulated for 2003. The temperature increase due to the arable scenario is most pronounced in the evening.

Total precipitation

Regarding the changes in the diurnal cycle of total precipitation (P) due to land-cover changes, the urban sealed simulation shows most pronounced impacts in all seasons (Fig. 4.9, b). Overall, there are roughly no daytime dependent effects on the diurnal cycle of P changes in SON and DJF in all considered scenarios.

In MAM and JJA of both years, the urban sealed scenario causes the most pronounced decrease in P in the late afternoon to early evening. Strongest variations in the change of P due to the urban sealed scenario take place during daytime. At night, the P decrease by the urban sealed scenario is quite evenly. Particular different effects by the urban sealed scenario are visible in the morning between 6 and 14 UTC for JJA of 2002 and 2003: Starting at 4 UTC the changes in the diurnal cycles of P even have different signs. In 2002, the change in P rises to a maximum decrease in the morning between 7 and 8 UTC. By contrast, in 2003, P changes attain their smallest values at about 10 UTC. In the forest simulation, the increase in P in JJA of 2002 arises especially in the evening at 19 UTC. At the same time of the day also a slight increase in P can be seen in JJA of 2003. Nevertheless, this increase in P is accompanied by decreased P during the rest of the day.

4.4. Impacts of anthropogenic land-cover changes on Northern Germany

In Section 4.2 it was already mentioned that "mixed forest" is also the declared potential vegetation of Northern Germany. If the results above are analyzed from the point of view that the control run stands for the anthropogenic land-cover changes so far and the "forest"-simulation is the original land-cover- it is possible to identify some additional findings out of the performed CCLM simulations in the frame of this chapter.

Of course, the following results have to be viewed carefully since only two years are simulated and mixed forest is only close to the vegetation which might have been the originally wilderness of Northern Germany.

Furthermore, it has to be kept in mind that the forcing data of ERAinterim introduce anthropogenic impacts. The assumption is- that only the simulations domains of this study are not

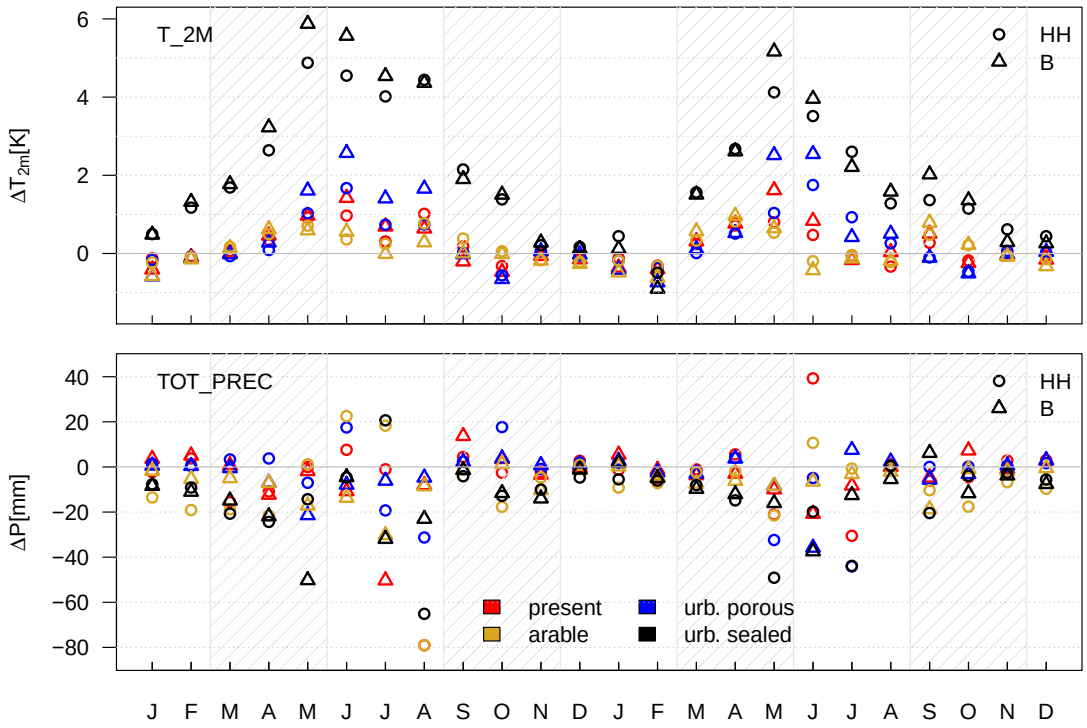

Figure 4.10.: Impacts of extreme land-cover changes (only arable land, only urban porous and only urban sealed land) and the present ("present") land-cover of Hamburg and Berlin compared to the potential vegetation, mixed forest. Only grid boxes within the political borders are taken into account.

settled (see Fig. 3.3, left).

Fig. 4.10 shows changes in the 2 m temperature (T_{2m}, top) and changes in the total precipitation amount (P, bottom) due to land-cover changes compared to the forest simulations with the so called potential vegetation. To capture the largest range of impacts, only present-day urban pixel (from the control run) of Hamburg and Berlin are investigated (see Fig. 5.24, "urban city core").

Especially from this point of view the strong impact of the urban sealed scenario is highlighted. Compared to forest, the urban sealed scenario leads to a mean monthly T_{2m} increase of up to 6 K in May 2002 for Berlin. In May 2003, the increases (+ 4 K for Hamburg and + 5 K for Berlin) are lower but show still the highest values of this year. This maximum in the rate of change in T_{2m} in May can be linked to the highest degree of land-cover change in this month.

The present-day urban areas have increased the monthly mean T_{2m} in May and June of both years. Here, not in May but in June (2002) and July (2003) the clear maxima of increase occur because the current urban-areas have also certain green spaces.

The urban porous land-cover acts in a similar way as the present-day urban areas on T_{2m}, nevertheless much stronger pronounced.

Referring to both years, 2002 and 2003, it is shown that arable land-cover tends to act cooling outside of the vegetation period in DJF and partly also in other months (2002: November, 2003: June, July and August) compared to mixed forest.

Shown impacts on T_{2m} are mainly more pronounced for Berlin than for Hamburg. This effect could be attributed to the dampening effect of the Baltic and North Sea on Hamburg and the

stronger continental climate influence on Berlin.

Impacts on P due to the arable scenario and the urban sealed scenario contribute to a decrease of the monthly mean of P nearly throughout the year compared to mixed forest (Fig. 4.10, bottom). Due to a complete sealing in the urban sealed scenario there are particularly decreases of P during warm month which experience in parallel a strong increase in T_{2m} (e.g. May (2002, Berlin): -50 mm or August (2002, Hamburg): -65 mm (2002) and May (2003, Hamburg): -50 mm or July (2003, Hamburg): -45 mm). The urban porous scenario seems to cause a decrease of P in May as shown for both years, 2002 and 2003. Nevertheless, these two month allow no overall conclusion on the impact especially since the rest of the year no clear trend towards increases or decreases of P is visible due to the present land-cover compared to the mixed-forest land-cover. The present land-cover has also lead to no clear impact on the monthly mean P of Hamburg and Berlin. However, especially P pattern could be modified due to the anthropogenic impacts in terms of land-cover changes (here: present, arable, urban porous and urban sealed land-cover) which are not captured in this analysis.

4.5. Discussions and Conclusions

The scope of this chapter is to address the maximum range of regional climate impacts due to extreme land-cover changes in a regional climate model. Four extreme scenarios with uniform land-cover are integrated for the years of 2002 and 2003: mixed forest only, non-irrigated arable land only and continuous urban fabric only with either sealed or porous ground. The regional climate model COSMO-CLM is applied with these scenarios for the temperate climate domain of Northern Germany.

The changed land-cover of the scenarios show effects on the surface energy and water budget, as well as the land-atmosphere exchanges of momentum, heat, and water. It turns out that especially a changed degree of sealing leads to most pronounced impacts on the regional atmospheric conditions in this study. This becomes especially evident in the urban sealed scenario. The sealing has strong effects on the hydrological cycle and prevents a storage of precipitation water. Therefore, especially in summer, evaporative cooling is missing. Also, the amount of plant cover shows clear effects on the regional atmospheric conditions. Sharp transitions of temperature change between winter and summer are visible for the applied urban scenarios with low and no plant cover.

The effects of land-cover change appear to be strongest in the vegetation period from April to October, indicating that land surface processes have a prominent influence on the atmosphere during this time, which is in line with previous modelling studies (e.g. Koster and Suarez, 1995; Davin et al., 2011). During the vegetation period surface fluxes are stronger and have a larger potential to affect atmospheric conditions, whereas during the cold season the atmospheric circulation is expected to have more influence on surface conditions (Davin et al., 2011).

For the forest scenario, temperature decreases occur due to increased evaporative cooling in spring. During the heat wave in summer 2003, the forest land-cover even leads to higher temperatures than in the control run, due to missing surface evaporation and hence reduced evaporative cooling. Additionally, the lower forest albedo absorbs more shortwave radiation.

A total change of Northern Germany's land-cover to non-irrigated arable land shows slight impacts due to the rather small changes in land-cover since most parts of Northern Germany are used in terms of arable land. In total, arable land leads to a drier climate with partly increased surface temperatures. In Fig. 4.7 was shown, that a replacement of the current cities like Berlin and Hamburg by arable land or forest would lead to cooler conditions in summer in those regions. This would imply that an increase of plant cover in cities could reduce the heat stress in urban areas during the warm season.

Both urban scenarios show pronounced temperature increases in summer caused by a reduction in latent heat fluxes and therewith a lack of evaporative cooling. The urban scenario with porous ground leads to slightly lower temperatures in spring and autumn. Monthly mean maximum temperatures ($T_{max(2m)}$) clearly increase in summer by values up to 3.2 K in 2002 and 4.2 K in 2003 compared to the control run. Also Wiesner et al. (2014) found in their field data for Hamburg slightly higher maximum temperatures in the city center compared to suburban areas. Due to less evaporation, the IWV decreases and finally, less total precipitation is simulated in the urban scenarios. However, most pronounced impacts appear in the urban sealed scenario. The complete sealing of the surface leads to a fast runoff of precipitation water and nearly inhibits surface evaporation. Less total cloud cover and less latent heat flux enhance the drying out of the atmosphere in that scenario and result in temperatures increases of more than 5.5 K in 2002 and 4.7 K in 2003 in terms of the 2 m mean maximum temperature ($T_{max(2m)}$) in the summer months.

The urban scenarios show most pronounced impacts on the hydrological cycle and the energy budget in June: For total precipitation, surface evaporation, IWV (Fig. 4.5, a-c), and latent heat flux (Fig. 4.2, b) strongest reductions are visible.

Heat wave 2003 under changed land-cover conditions

All scenarios in this study showed even higher mean temperatures for the heat wave of 2003 than actually occurred for the control run. At a first glance, one could have expected that the current land-cover in Northern Germany which is included in the control run is somehow a mixture of the applied land-cover change scenarios and should therefore result in a mean climate among all of the results of the applied scenarios. But, not all land-cover forms of the actual land-cover of Northern Germany are addressed in this study. Northern Germany's land-cover is highly differentiated into a multiplicity of land-cover forms with different characteristics. Here, e.g. non-irrigated arable land was taken into account while there are also areas covered by irrigated instead of non-irrigated arable land. Grassland was also not addressed in the applied scenarios. It comes along, that heterogeneity affects the surface energy and water budgets, as well as the land-atmosphere exchanges of momentum, heat, water, and other constituents, through a number of highly non-linear processes (Giorgi and Avissar, 1997). These effects are not considered as the applied land-cover scenarios are homogeneously distributed in the model domain.

Forests usually lead to cooler and moister conditions during summer in most parts of temperate zones (e.g. Gálos et al., 2013) - as long as sufficient soil moisture is available (Teuling et al., 2010). For the special case of summer 2003, the soil already dried out in spring, thus limiting tree transpiration during summer. In that year, large scale damage to trees also occurred due to drying out of tree roots.

One particular question which comes into mind is: Why were mean temperature increases for the urban sealed scenario in summer 2003 simulated to be lower than in 2002? The urban sealed scenario and the control run are not that different in summer 2003 compared to summer 2002. This is a result of the dryness in the control run approaching that of the urban sealed scenario.

Differences between a real city and the applied simplified urban land-cover scheme

Although, the "urban" scenarios in this study include few features of real urban land, some typical urban heat characteristics are represented, like e.g. a modified roughness length, less vegetation and for the urban sealed scenario - drastic sealing. Urban climate often lacks of evaporation, and faces a warmer and drier climate in summer - this becomes apparent in this study. For the urban sealed scenario, this effect is clearly more pronounced than for the urban porous scenario.

Conversions of vegetated to urban land usually leads to a reduction of the diurnal temperature range, and changes in precipitation (e.g. Oke, 1987). Here, an increased diurnal temperature range is illustrated. Usually, the anthropogenic heating in urban areas can affect the near surface air temperature and potentially play a role in creating urban heat islands (e.g. Taha, 1997). In this study, the anthropogenic heating is not taken into account. Thus, a more detailed description of urban areas could lead to e.g. higher surface temperatures than shown in this study.

The urban scenario with sealed ground shows a clear higher surface albedo than the control run and the other scenarios. In the CCLM model formulation, the surface albedo is described in dependency of the soil textures, the soil moisture, and plant cover. Therefore, the drying-out of the urban surface results in the described higher albedo. In a real urban environment a lower surface albedo due to e.g. dark asphalt streets, shading effects by buildings or dark roofs is typical. This lower albedo would have again impacts on the surface energy balance. The diffuse shortwave upward radiation flux would be decreased due to a lower albedo. Finally, the solar radiation budget at the surface would be increased in a typical urban environment.

This study gives a first glance at interactions between land-cover change and its feedbacks on Northern Germany's atmospheric conditions in a regional climate model. It becomes apparent, that substantial land-cover changes show also strong impacts on the regional atmospheric conditions. Here, it is only accounted for changes in the physical characteristics of the land surface. An idea how strong such dramatic land-cover changes could impact the present atmospheric conditions is presented. The climate at the end of the 21^{st} century is likely to be warmer than today. And in fact, e.g. land-cover sealing is rapidly increasing. This in combination with an increase in the CO_2 concentration could even lead to much more pronounced changes for the future local climate than already discussed. This underlines the importance of land-cover change scenarios for the future climate. However, significant uncertainties remain. On the one hand, land-cover change impacts could even be stronger, accounting for e.g. anthropogenic heat fluxes or defining another albedo for urban areas. On the other hand, impacts could also be smoother taking into account e.g. a more realistic description of vegetation in the model system. Nevertheless, it has to be kept in mind that this study reflects very simplified changes in the land-cover for a relative short time period.

5. Combined effects of land-cover and greenhouse-gas changes on the climate of Northern Germany

5.1. Purpose of this study

As shown in Chapter 4, pronounced land-cover changes have an impact on the regional climate of Northern Germany. Especially (model-)urban land-cover showed strong effects.

This leads to the question how physical land-cover changes combined with changes in the greenhouse gas (GHG) concentration might impact the regional climate of Northern Germany in future.

Current developments indicate especially a transformation of cityscapes (Dosch and Beckmann, 2011). Additionally, the urban population is expected to further increase. For Europe, 82% of the population is expected to live in cities in 2050 (United Nations, 2011). In this chapter, two different future urban structure scenarios combined with increased greenhouse-gases are analyzed for the end of the 21st century. The land-cover scenarios with different approaches of urban growth are implemented into the CCLM. Motivated by the convection permitting horizontal resolution of 2.8 km grid mesh size the focus of the following evaluations is on local impacts on the surface climate.

The results are discussed from two points of view. On the one hand, Northern Germany and in particular Hamburg and Berlin are analyzed as a whole. Impacts on the radiation budget, the hydrological cycle and the near surface wind field are evaluated. On the other hand, changed climate conditions are evaluated from the view of the citizen of modified land-cover districts and adjacent areas.

5.2. Set-up of land-cover change simulations for Northern Germany

Firstly, the applied greenhouse gas-scenario is introduced. This is followed by the description of the two land-cover scenarios for Northern Germany which have been implemented into CCLM. Finally, the set up of the CCLM-simulations for this study is summarized.

5.2.1. Description of the applied greenhouse gas scenario

Data of the general circulation model (GCM) ECHAM5 (Roeckner et al., 2003) are used as forcing data for the CCLM simulations. Due to the limitation of computational time, only one emission scenario could be applied. The IPCC/SRES scenario "A1B" (Nakicenovic et al., 2000) was selected. The A1B storyline emphasis "a future world of very rapid economic growth, global population that peaks in mid-century and declines thereafter, and the rapid introduction of new and more efficient technologies. Major underlying themes are convergence among regions, capacity building and increased cultural and social interactions, with a substantial reduction in regional differences in per capita income" (Nakicenovic et al., 2000). In the A1B scenario a balanced development relying not too heavily on one particular energy source and moderate land-use changes

are assumed. Whereas at the beginning of this study, the A1B scenario mirrored a kind of mid-level development path, the GHG emissions have meanwhile risen at the rate projected for more extreme scenarios.

The A1B scenario is related to the recently introduced RCP6.0 scenario (Moss et al., 2010) where a stabilization of the radiative forcing in 2100 of about 850 ppm $C0_2$ equivalent is expected, followed by a reduced radiative forcing until 2300.

Overall, it is assumed that no major volcanic eruption or changes in some natural sources (e.g. CH_4 and N_2O), or unexpected changes in total solar irradiance occur. By the mid-21st century, the magnitude of the projected climate change is substantially affected by the choice of emissions scenario in the applied GCMs (Hartmann et al., 2013).

5.2.2. 1st land-cover scenario: urban sprawl

Motivation for this scenario

In this first applied land-cover scenario, "urban sprawl" illustrated in Fig. 5.1, it is assumed that the demand of living space in urban areas of Northern Germany is going to further increase. Also, immigration of war refugees, economic migrants or climate refugees stays or becomes an important aspect in terms of additional urban citizens. Another issue which is addressed by this scenario is the trend that even for decreasing urban population densities, the amount of built-up area per person is increasing (Seto et al., 2010; Angel et al., 2011). That means that citizens have a higher demand for living space per person. Good or improved public transportation bridges large distances around the city core leading to a sprawling of the cities. Affordable housing in suburban areas leads to an additional scattering of the city. The wish of families with children to live in greenfield areas but still close to the city core is another motivation, that might contribute to an expansion of urban areas in the future.

Technical realization

The urban sprawl (A1Bspr) scenario, stands for a clear enlargement of the urban areas of Northern Germany. This is done by enlarging the cities which have currently a growing status (Fig. 2.4) by the expense of arable land. All model grid boxes of the evaluation domain declared by the CORINE-data as continuous urban and urban fabric land are summed up (Fig. 2.3) and afterwards the urban area is increased by 50%. That means, the originally urban-grid boxes with an area of about 7150 km^2 are increased to an area of about 10725 km^2.

Especially Berlin (B) and Hamburg (HH) but also Bremen, Hannover, Kiel and Lübeck are modified. The direction of the growing of these cities is orientated according to Fig. 2.4.

The ECOCLIMAP II dataset (Faroux et al., 2007) is used for the definition of the necessary external data for the TERRA_ML. The ECOCLIMAP II dataset offers monthly instead of annual maximum and minimum values of LAI, $Z_{0(veg)}$ and PLCOV. Since there is no land-cover classification in the CCLM model system, the corresponding external data (Chapter 3.2.1) have to be declared. In contrast to Chapter 4, not the CORINE-table is used. In order to implement the new land-cover characteristics, the land-use class "continuous urban land" in the CORINE land-cover map had been assigned to the external data of the ECOCLIMAP II database. Since not all "continuous urban land" grid boxes have the same characteristics in terms of external data, monthly mean values of all "continuous urban land" grid boxes are used to define the corresponding external data values (Tab. 5.1). Therefore, all new urban grid boxes got the characteristics from Tab. 5.1. Former "continuous urban land" grid boxes were not modified.

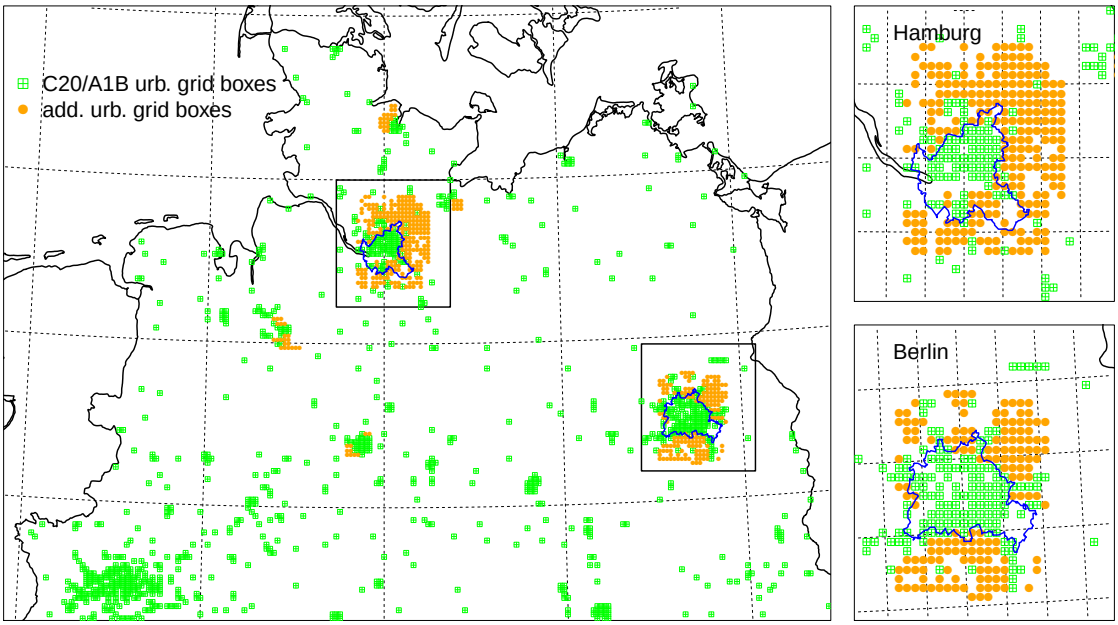

Figure 5.1.: The urban sprawl scenario: green boxes indicate urban grid boxes in the C20 and the A1B simulation. Orange dots show the additional urban grid boxes added in the urban sprawl scenario with the characteristics presented in Tab. 5.1.

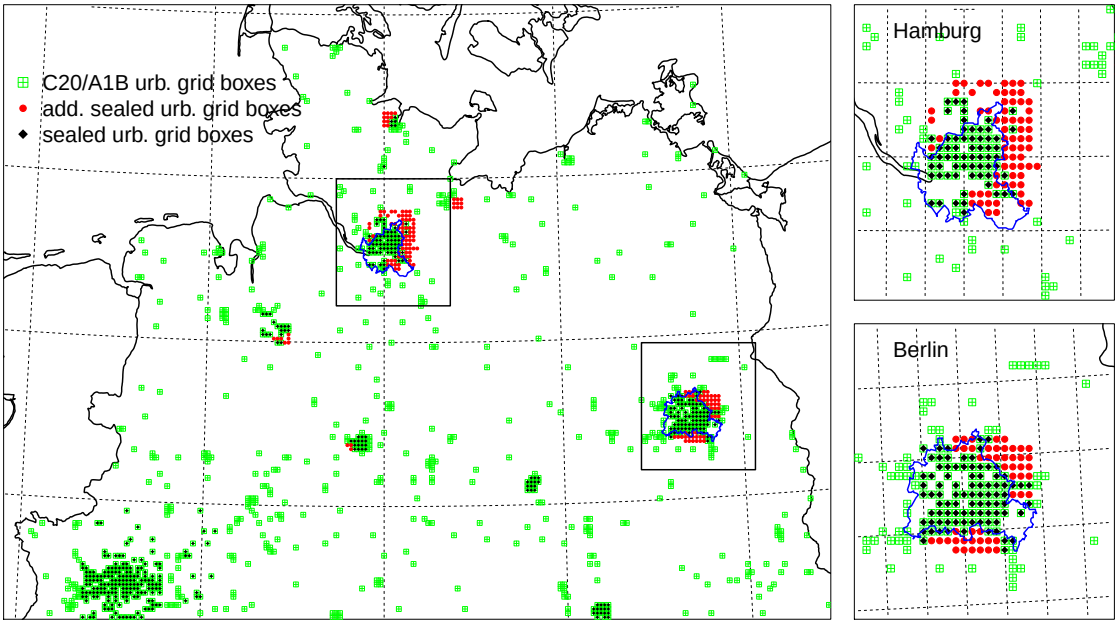

Figure 5.2.: The compact city scenario: same as for Fig. 5.1, green boxes indicate urban places in the C20 and the A1B simulation. Red dots show the additional sealed urban grid boxes added in the compact city scenario and black diamonds declare former urban grid boxes which become sealed due to the compact city scenario.

Table 5.1.: Overview of land-cover characteristics included in the applied land-cover scenarios. Shown are the monthly values of the mean grid boxes (mgb) of the whole model domain, Northern Germany, the added urban grid boxes in the urban sprawl scenario (spr) and of the sealed grid boxes of the compact city scenario (com).

	Month	Jan	Feb	Mar	Apr	May	Jun	Jul	Aug	Sep	Oct	Nov	Dec
Grid box	Parameter												
mgb		0.34	0.35	0.36	0.37	0.42	0.42	0.42	0.39	0.38	0.37	0.35	0.34
spr	$\mathbf{Z}_0$	0.81	0.82	0.82	0.83	0.84	0.84	0.84	0.83	0.83	0.83	0.82	0.81
com		1.5											
mgb		0.34	0.35	0.36	0.37	0.42	0.42	0.42	0.39	0.38	0.37	0.35	0.34
spr	$\mathbf{Z}_{0(veg)}$	0.41	0.43	0.44	0.45	0.47	0.47	0.46	0.46	0.46	0.45	0.44	0.42
com		0											
mgb		0.53	0.65	0.73	0.80	0.88	0.88	0.87	0.84	0.83	0.80	0.71	0.56
spr	**PLCOV**	0.41	0.43	0.44	0.45	0.47	0.47	0.46	0.46	0.46	0.45	0.44	0.42
com		0											
mgb		0.83	1.4	1.78	2.4	3.5	3.66	3.37	2.99	2.78	2.5	1.73	0.94
spr	**LAI**	0.41	0.43	0.44	0.45	0.47	0.47	0.46	0.46	0.46	0.45	0.44	0.42
com		0											
mgb		1.2											
spr	**ROOTDP**	0.41											
com		0											

5.2.3. 2nd land-cover scenario: compact city

Motivation for this scenario

The compact city illustrated in Fig. 5.2 shall mirror a city where both, working place and residence are located in closer distances to minimize the volume of traffic- a so called "city of short distances". Urban growth happens in terms of densification of the city. New skyscrapers are built as they offer the opportunity to create a large amount of new living space on a comparatively small area.

Technical realization

The second scenario, "compact city", later referred to as A1Bcom, describes a dense built-up area with very high buildings and large proportions of sealed ground. Same as for the urban sprawl scenario, it is assumed that only cities continue to grow which have currently a growing status in Northern Germany (Fig. 2.4). Large parts of already built-up areas are changed to sealed urban grid boxes. The number of urban grid boxes in the model domain is raised by 25% to an area of about 9000 km^2. 50% of all urban grid boxes, that means 4500 km^2 become sealed and their surface roughness is considerably increased to 1.5 m (Tab. 5.1).

The same method to define the new land-cover characteristics in terms of external parameters as described for the urban sprawl scenario is applied (Tab. 5.1).
The dates 16./17.7.2099 are missing in the A1Bcom data set for the 2 m temperature due to inconsistencies during the computing process. Therefore, these dates are excluded from the analyses dealing with the 2 m temperature. Nevertheless, since 10 years have been simulated, these two missing dates have no impacts on the results at all.

Table 5.2.: Overview of long-term simulations with 2.8 km grid mesh size that are evaluated in this chapter.

Acronym	Meaning	Period
C20	CCLM simulation under C20 GHG conditions	1998-2007
A1B	CCLM simulation under the A1B GHG emission scenario	2090-2099
A1B**spr**	CCLM simulation under the A1B GHG emission scenario and the urban **spr**awled land-cover scenario	2090-2099
A1B**com**	CCLM simulation under the A1B GHG emission scenario and the **com**pact city land-cover scenario	2090-2099

5.2.4. Setup of long-term simulations

To study regional and local climate impacts resulting from both GHG effects and land-cover changes time slices of ten years are simulated: 1998 to 2007 and 2090 to 2099. ECHAM5-MPIOM simulations (Roeckner et al., 2003) for the 4th IPCC Assessment Report are used as forcing data for the CCLM simulations. The applied ECHAM5 data have a horizontal resolution of 1.875° (∼200 km), 31 vertical levels and four soil layers. The same model set-up as described in Section 3.3.1 is used. As described in Chapter 4, all land-cover changes were applied in all CCLM domains (Fig. 3.3, right). Tab. 5.2 presents an overview of the simulations which are evaluated in this chapter.

To quantify the impact of climate change alone, one simulation for a control time period (1998 to 2007, C20) and one projection (2090 to 2099, A1B) with the reference land-cover are conducted as well.

5.3. Changed climate conditions for Northern Germany at the end of the 21st century

A similar strategy to evaluate the impacts of the applied scenarios as in Section 4.3 is applied:

Firstly, the focus is put on averaged regional changes of the whole domain of Northern Germany (NG), Hamburg (HH) and Berlin (B). This is followed by analyses of their annual cycles, spatial distribution of seasonal mean values and mean diurnal cycles of NG, HH and B. Also here, several parameters concerning the energy budget and the hydrological cycle are taken into account. But furthermore, more attention is put on changes in the wind field in the model domain.

5.3.1. Scenario induced temperature changes

Fig. 5.3, left, shows the mean annual cycle of (a) T_{2m}, (b) T_s, (c) $T_{2m(min)}$ and (d) $T_{2m(max)}$ temperature of the C20 simulation representing the "current" climate (1998-2007) of Northern Germany (NG), Hamburg (HH) and Berlin (B). It is visible that B is less maritime and more continental climate influenced than the whole domain of NG or HH respectively. This is marked by higher summer and lower winter temperatures for B. Most pronounced temperature differences between B and HH and NG are visible for $T_{2m(max)}$ in summer: the monthly mean temperature maximum in B is about 2 K higher than for HH and NG in that time.

The increase of GHGs in the A1B simulation leads to larger impacts on the monthly mean temperatures of all three domains (NG, HH, B, Fig. 5.3, right) than that induced by the land-cover changes.

The A1B scenario leads to a regional mean increase of T_{2m} ranging from 1.5 K in February and May to about 4.8 K in December for the end of the 21st century (2090-2099) (Fig. 5.3, a). For HH, T_{2m} increases are slightly higher in the first half of the year and partly slightly lower in the second half of the year as shown in the A1B simulation. For B, the T_{2m} increases simulated in the A1B simulation are lower in March, April and May and larger in July, August and September. In August, the highest differences between the T_{2m} increases due to the A1B scenario are present between HH and B.

Both, T_s (Fig. 5.3, b) and $T_{min(2m)}$ (Fig. 5.3, c) of the A1B simulation follow a comparable annual variation of differences as shown for T_{2m} of each simulation (Fig. 5.3). It becomes apparent that the strongest impacts are shown for $T_{min(2m)}$ due to the A1B simulation compared to the C20 simulation (+1.7 to about +5 K).

For the large domain of NG, impacts due to the land-cover scenarios A1Bspr and A1Bcom are not detectable. For HH and B, the A1Bspr scenario leads to a slight additional increase in T_{2m}, T_s, $T_{max(2m)}$ from May to August (not more than 0.2 K for T_{2m} and T_s, $\leq$0.5 for $T_{2m(max)}$). No impacts due to the A1Bspr scenario are visible on the monthly mean $T_{2m(min)}$ of HH and B.
The A1Bcom scenario leads to a clear additional increase in T_{2m}, T_s, $T_{min(2m)}$ and $T_{max(2m)}$ throughout the year with the highest values in the warm season from April to September (up to +1 K). In the course of the year, B experiences a slightly higher increase in T_{2m} abd T_s than HH due to the A1Bcom scenario. The largest temperature increase in $T_{max(2m)}$ due to the A1Bcom scenario is shown in May.

To conclude, all scenarios, A1B, A1Bspr and A1Bcom contribute to a warmer climate at the end of the 21st century. A1Bspr and A1Bcom show strongest increases during the summer month and the A1B scenario increases particularly winter temperatures.

Extreme temperature events

As seen above, all applied scenarios (A1B, A1Bspr and A1Bcom) induce changes in the near surface temperature. Nevertheless, mankind and particularly citizens of cities are especially vulnerable to extreme climate events. To account for extreme temperature events, different climate indicators are calculated from the simulations outputs for JJA and presented in Tab. 5.3 as numbers for the domains of NG, HH and B.

Summer days (SD), defined as the number of days with $T_{2m(max)}$ greater/equal 25°C are increased in the period of 2090 to 2099 due to the A1B, the A1Bspr and the A1Bcom scenario compared to the period from 1998 to 2007 (Tab. 5.3). For NG, the number of SDs in JJA is roughly doubled in the A1B simulation compared to the C20 simulation (9 versus 19 days). For HH and B, the land-cover changes lead to marked additional increases in the number of SDs: Compared to the A1B scenario, the A1Bspr scenario increases the number of SDs additionally by roughly 3 days for HH and 2 days for B. Similarly, the A1Bcom scenario leads to the highest number of SDs in JJA (HH: + 5.3 days per year, B: +3.8 days per year).

The A1B simulation alone leads to a particular increase in the number of hot days (HD), i.e. days with a daily $T_{max(2m)}$ above or equal to 30°C,. HDs occur for NG (+ 3.5 days) and HH (+4 days), more than three times often and for B (+ 6.8 days), nearly double as often as in the C20 simulation. It is interesting to note, that the number of HDs increases more in the A1Bspr simulation compared to the A1Bcom simulation for both, HH (A1Bspr: +2.3, A1Bcom: + 1.9 days) and B (A1Bspr: +2.2, A1Bcom: + 1.4 days, Tab. 5.3).

The number of days where the daily $T_{min(2m)}$ is above the threshold of 20°C indicates "tropical

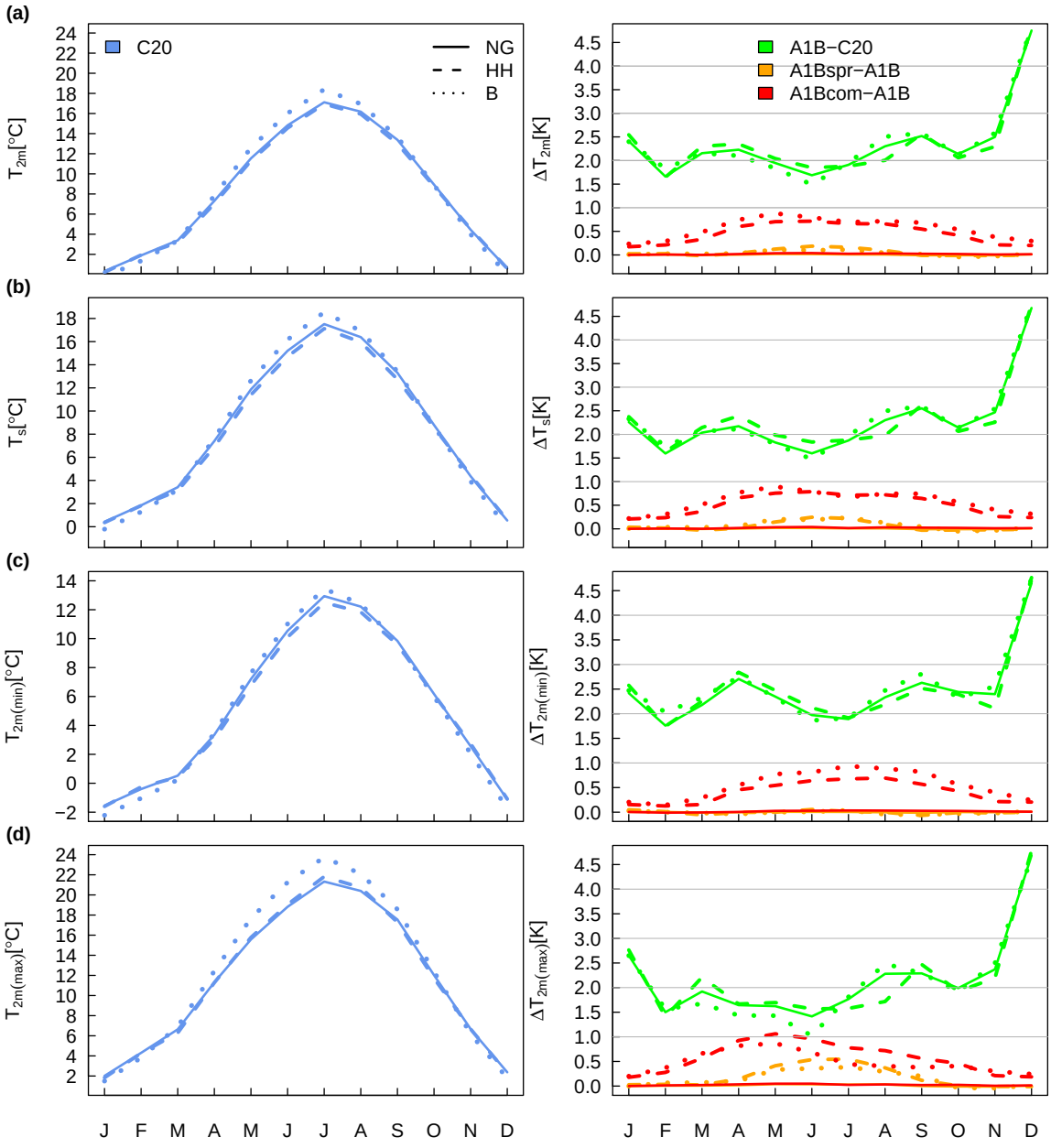

Figure 5.3.: On the left panel, the absolute temperatures for Northern Germany, Hamburg and Berlin from the C20 simulation are shown. On the right panel, the differences between the future scenario A1B compared to the C20 simulation (A1B-C20) and the changes due to the land-cover change scenarios compared to the A1B simulation (A1Bspr-A1B and A1Bcom-A1B) are drawn for each domain (NG, HH and B) for (a) the 2 m temperature (T_{2m}), (b) the surface temperature (T_s), (c) the 2 m minimum temperature ($T_{2m(min)}$) and (d) the 2 m maximum temperature ($T_{2m(max)}$). Herein, only land-data are taken into account.

Table 5.3.: Total number of daily temperature extremes for summer (JJA) in the investigated 10-year time periods per year.

Extreme index	Definition [unit]	Region	Number of days	Change of the number of days		
			C20	A1B vs. C20	A1Bspr vs. A1B	A1Bcom vs. A1B
SD	when	**NG**	9.1	10.4	0.3	0.2
Number of summer days	Tmax $\geq$25°C [day/a]	**HH**	12.7	9.6	3.3	5.3
		B	23.3	13.6	2.2	3.8
HD	when	**NG**	1.0	3.5	0.1	0.1
Number of hot days	Tmax $\geq$ 30°C [day]	**HH**	1.3	4.0	2.3	1.9
		B	3.8	6.8	2.2	1.4
TN	when	**NG**	0.2	2.0	0.0	0.1
Number of tropical nights	Tmin $\geq$ 20°C [day]	**HH**	0.2	0.9	0.2	1.0
		B	0.6	2.5	0.0	2.6
HP	when	**NG**	0.3	0.2	0.0	0.0
Duration of hot periods	Tmax $\geq$ 30°C [day]	**HH**	0.3	0.4	0.1	0.1
		B	0.5	0.3	0.1	0.0
no. HP	when	**NG**	0.0	0.1	0.0	0.0
Number of hot periods	Tmax $\geq$ 30°C [day]	**HH**	0.0	0.1	0.0	0.0
	for >5 days	**B**	0.1	0.2	0.0	0.1

nights" (TN). For NG, this index occurs in the reference period most often in B (0.6 days per JJA-season), only roughly 0.2 days per JJA in HH and the mean domain of NG. Also here, the A1B scenario leads to considerable increases in the number of TNs with regard to the corresponding values in the C20 simulation. Equally, hot periods (no. HP) occur more frequently in A1Bspr than in A1Bcom for HH (MAM and SON) and B (MAM and JJA) shown in Tab. 5.3 but still very rarely.

Although, there are more HDs in the A1Bspr simulation, the thermal stress is higher in the A1Bcom scenario. That is because high daytime temperatures cool down much slower. Indeed, the data in Tab. 5.3 show that the number of TNs in the A1Bcom simulation is approximately twice as high for HH and B compared to the A1B simulation.

5.3.2. Explanations for temperature changes

In Section 5.3.1 the impacts on the near surface temperature due to the A1B, the A1Bspr and the A1Bcom scenario are discussed. At this point, the reasons for the temperature changes are examined by inspecting the surface energy budget.

Partitioning of sensible and latent heat flux

As described in Eq. 2.1 to 2.3 the surface temperature is strongly connected to the surface fluxes.

Fig. 5.4 shows the annual cycles of the surface energy budget of each CCLM simulation of this chapter. In a) the mean annual cycle of the energy budget components is shown for the period from 1998 to 2007 as represented by the C20 simulation. During summer, HH and B show lower latent heat flux (λE) than the NG domain because vegetation amount is less implying less surface evaporation (E). At the same time, the higher temperatures (Fig. 5.3) explain the higher sensible heat fluxes (H) in B.

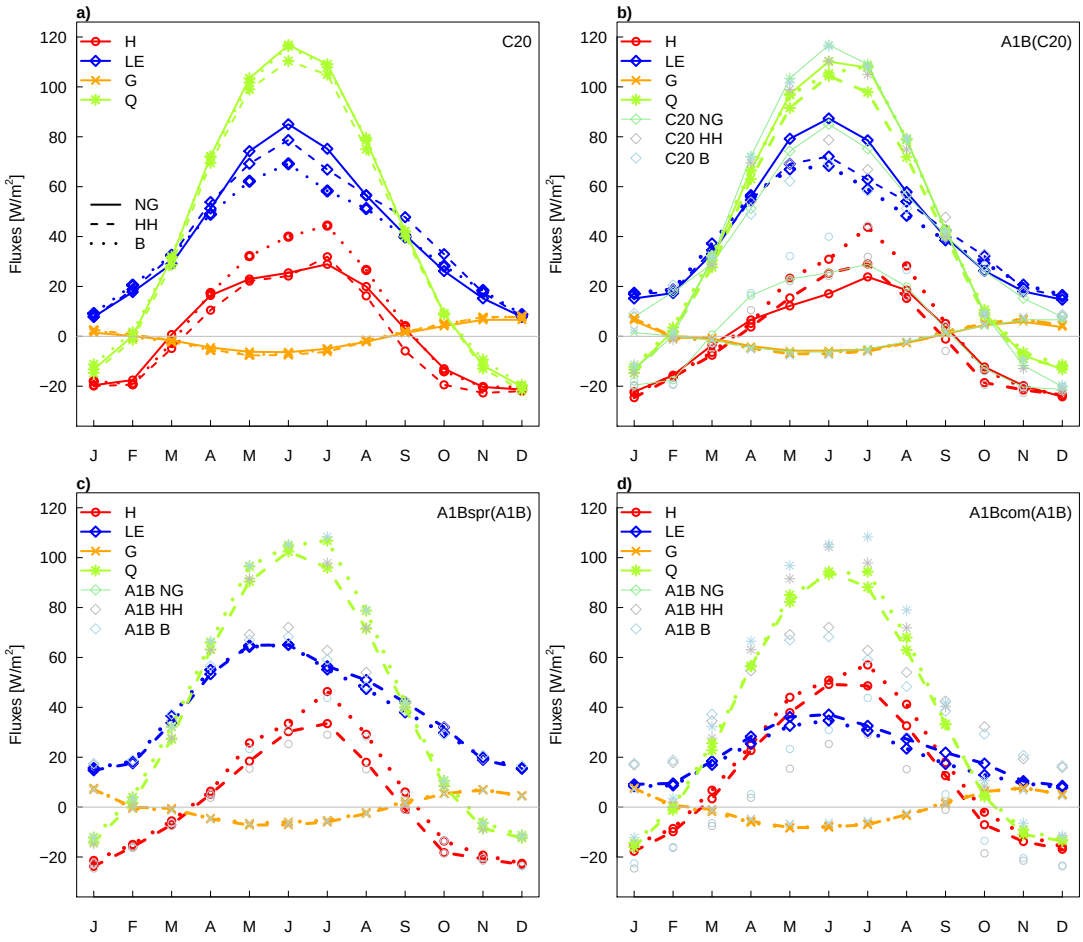

Figure 5.4.: Annual cycle of the surface energy budget (sensible heat flux (H), latent heat flux (λE), ground heat flux (G) and the net radiation budget (Q) for a) the C20, b) the A1B, c) the A1Bspr and d) the A1Bcom simulation. For b) the corresponding fluxes of the C20 simulation are indicated by lightgrey,-blue and -green for HH, B and NG, respectively. For c) and d), the corresponding fluxes of the A1B simulation are indicated by lightgrey and -blue for HH and B.

Although, the monthly mean temperature (T_s and T_{2m}) is increased by the A1B scenario, H and Q decrease for NG in the A1B simulation (Fig. 5.4, b). λE is increased by the A1B scenario compared to the C20 simulation. This increase in λE in the atmosphere could increase the amount of clouds, in the case of ice clouds, helping to retain more heat, which again leads to more evaporation of water and the addition of more water vapor into the atmosphere, which leads to more heat in the atmosphere, in a positive feedback cycle. G is increased in December - therefore more solar heat is transferred to the ground. This can partly explain the strong temperature increase in that month.

The A1Bspr and the A1Bcom scenarios lead to no impacts on the surface energy budget of NG in terms of monthly mean values, therefore only the corresponding values for HH and B are shown in Fig 5.4, c) and d). Nevertheless, for the domains of HH and B, there are impacts detectable due to the A1Bspr and the A1Bcom scenario.

The A1Bspr scenario (Fig. 5.4, c) increases the urban effect which was already visible for the

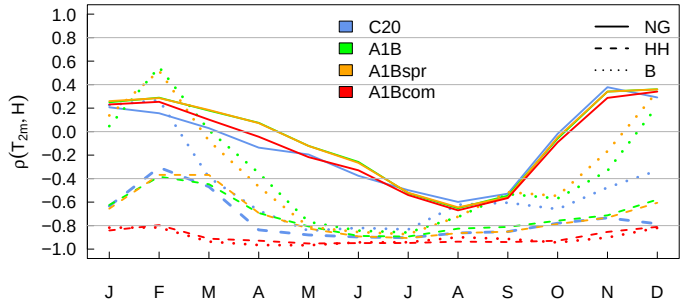

Figure 5.5.: Correlation of 2 m temperature (T_{2m}) and sensible heat flux (H).

period from 1998 to 2007 in the results of the C20 simulation: The reduction in λE fluxes leads to an increase in temperature (Fig. 5.3) which then increases H fluxes.

The A1Bcom scenario leads to the strongest impacts on the radiation budget components in Fig. 5.4, d, compared to the A1B and the A1Bspr scenario. λE fluxes are roughly halved throughout the annual cycle compared to the outcome of the A1B simulation. Therewith, H fluxes are approximately doubled compared to the results of the A1B simulation. These described impacts on λE and H can explain the temperature increases seen in Fig. 5.3 caused by the A1Bcom scenario to a great extent.

Correlation of 2 m temperature and sensible heat flux

The field correlations between 2 m temperature and sensible heat flux in Fig. 5.5 demonstrate that especially the cities, HH and B, show strong correlations particularly in summer. For HH and B, strongest correlations appear earlier (May, June, July) in the annual cycle than for NG (July, August, September).

Impacts due to the applied scenarios are especially visible for B. A1Bspr follows nearly the same curve of correlation as shown for the A1B simulation.

The A1Bcom scenario leads to the strongest correlation between T_{2m} and H lasting the whole annual cycle at a value of 0.8 to roughly 1 for both, HH and B. On NG, A1Bcom impacts only by slightly higher correlations in summer.

Further changes in the surface energy budget

Fig. 5.6, a and b, clearly shows that the temperature increases due to the A1B scenario cannot be explained by changes in the net thermal radiation (L_n) nor by changes in the net solar radiation (S_n). Because both fluxes are reduced in the A1B simulation compared to the C20 simulation. This would normally lead to lower temperatures. The A1Bspr scenario causes slight increases in the thermal radiation flux for HH and B from May to August what contributes to the temperature increase at the same time. The impact on the solar radiation due to the A1Bspr scenario is indifferent. However, the A1Bcom scenario shows clear impacts on both fluxes: the thermal radiation flux is increased and the solar radiation flux is decreased throughout the annual cycle for HH and B. For B, there are in each case higher increases and decreases visible. The increased thermal radiation contributes also here to the observed increase in the temperature as discussed above. Nevertheless, the decrease in the solar radiation counteracts to the temperature increases.

Changes in the surface albedo (α, Fig. 5.6, c) play a fundamental role for the simulated temperature changes in the A1B simulation. The large temperature changes in December and January

can be partly attributed to clear decreases in α at the same time. But also in November, February and March, α is reduced in the A1B simulation compared to the C20 simulation. These decreases in α are caused by reduced snow cover (Fig. A.2, c) during this time of the year at the end of the 21st century compared to 1998-2007.

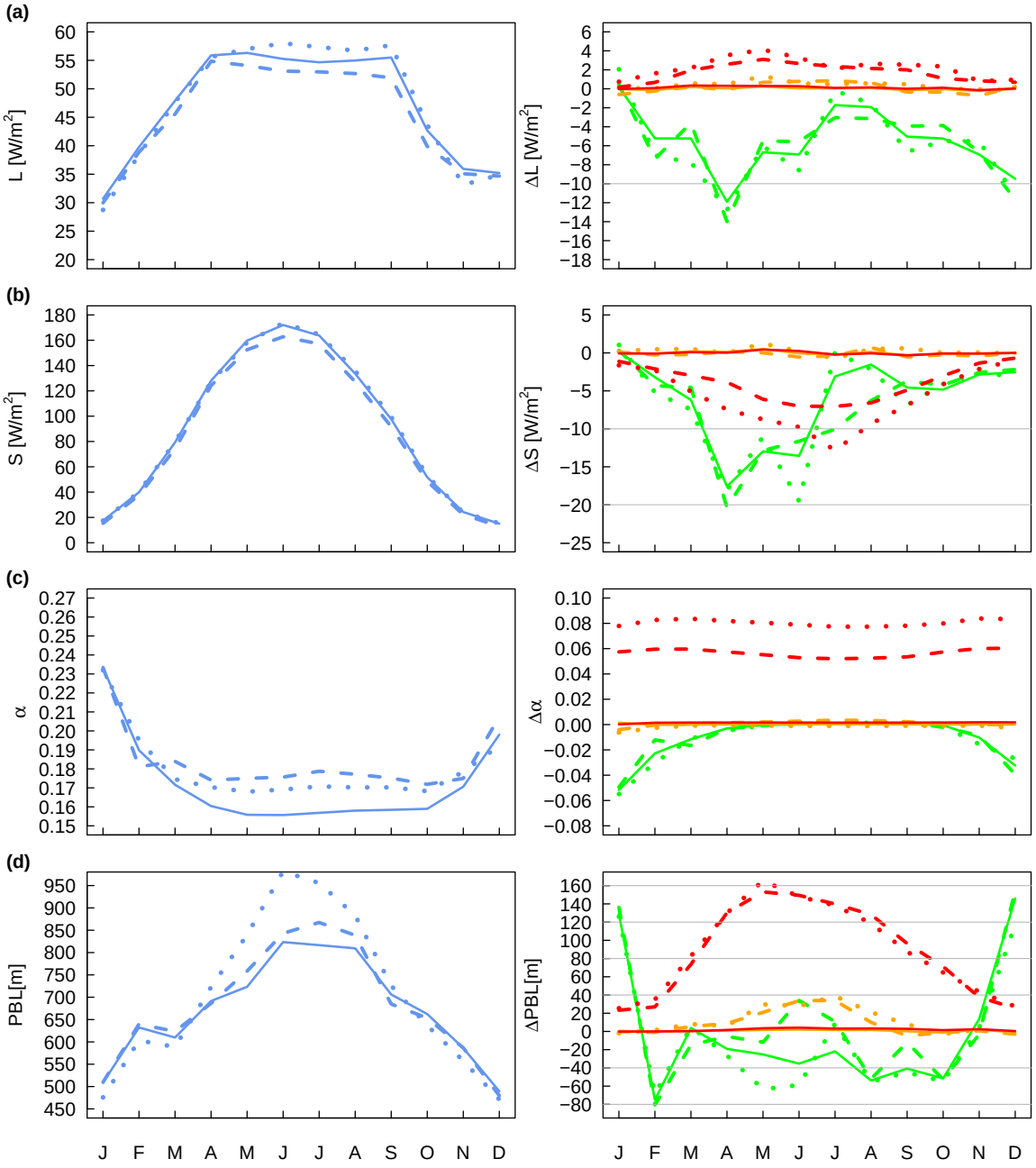

Figure 5.6.: Same as Fig. 5.3 but for (a) the thermal radiation budget (L), (b) the solar radiation budget (S), (c) the surface albedo and (d) the mean boundary layer height.

Changes in α of NG, HH and B are hardly detectable due to the A1Bspr scenario in terms of monthly mean values. Whereas, A1Bcom shows clear impacts on α for HH and even more pronounced for B. In both cities, α is considerably increased (+0.06 for HH and +0.08 for B) in the A1Bcom simulation. This explains the reduced solar radiation flux in Fig. 5.6, b). This phenomenon occurred also in Chapter 4 for the urban sealed scenario. The reason for the increased

α is on one hand the reduced vegetation in the domain of HH and B but especially on the other hand the change of the soil texture to rock for sealed grid boxes.

In terms of the planetary boundary layer (PBL) height, NG, HH and B show considerable differences in the C20 simulation (Fig. 5.6, d). For B, a particular high PBL (+150 m compared to NG) is shown for May to August. The PBL of HH is only slightly higher as the PBL height of NG. The A1B scenario leads to considerable increases (about +140 m) in the PBL height in January and February for HH, B and NG, respectively. However, for the rest of the year the PBL height of NG and B is reduced due to the A1B scenario. Also for HH, reductions in the PBL height due to the A1B scenario dominate in the rest of the year aside from June, where the PBL height is increased in HH. The A1Bspr scenario leads to an increase in the PBL height of HH and B from May to August by up to 40 m. The A1Bcom scenario shows again impacts on the whole annual cycle in terms of an increased PBL height (+20 up to 160 m) of HH and B. Whereby, maximum increases in the PBL height occur in combination with the highest monthly mean temperatures from May to August.

Impacts on the wind speed

Changes in the wind field impact clearly on mankind. Wind can e.g. both, help to tolerate high temperatures but also -in contrast- strengthen heat waves by the presence of calm days. Fig. 5.7 (a, left) illustrates that there is a low variation of the mean monthly wind speed in 10 m height (V_{10m}) throughout the annual cycle during the mean period from 1998 to 2007 as represented by the C20 simulation. V_{10m} follows for the domains of NG, HH and B the same annual variation with a slight peak in February and a slight minimum in December. Differences between NG, HH and B, appear only for the amplitude: V_{10m} for NG is highest, followed by HH and B with the lowest V_{10m}. These differences in V_{10m} indicate the proximity to the coastlines.

Following the A1B scenario, V_{10m} will be increased in May, June, July, November and particularly in January and December for the period 2090-2099 (Fig. 5.7, a, right). Whereas, in February, March, August to October, decreases in V_{10m} are shown. V_{10m} above HH increases slightly stronger from April to June and decreases lower in August and September than NG.

In the A1Bspr simulation, increases in V_{10m} above B throughout the annual cycle by 0.2 m/s are shown. Also for HH slightly higher V_{10m} occur in the A1Bspr simulation but of a clear lower degree ($\leq$ 0.1 m/s). Strongest increases in V_{10m} for HH due to the A1Bspr scenario are visible from May to August.

The A1Bcom scenario decreases V_{10m} especially for HH (-0.3 to 0.45 m/s) but also for B (-0.15 to -0.28 m/s). For both cities, the decreases of V_{10m} due to the A1Bcom scenario are most pronounced in winter.

The different impacts due to the A1Bspr and the A1Bcom scenario seem to be partly a result of the different urban shapes and roughness lengths in the two land-cover scenarios. In the A1Bspr scenario HH and B are large homogeneous areas whereas in the A1Bcom scenario, HH and B, are pronounced spatial barriers due to the high roughness length.

Higher values of $V_{10m(max)}$ are shown for NG than for HH and B for 1998 to 2007 in the C20 simulation (Fig. 5.7, b, left). $V_{10m(max)}$ is lowest in January and December ($\sim$10.3 m/s) and highest in February and June ($\sim$11.4 m/s) for NG. For HH the $V_{10m(max)}$ minima in January and February ($\sim$9.7 m/s) are lower than for NG and the maxima appear in June, July and August ($\sim$ 11.2 m/s). For B, the lowest values in January and February with roughly 8.8 m/s are clearly lower than for NG and HH. However, a strong pronounced maximum is shown for B in June (roughly 10 m/s).

The changes of $V_{10m(max)}$ due to the A1B scenario are similar to the changes in V_{10m} (Fig. 5.7, b, right). The A1Bspr scenario leads again to smaller increases in $V_{10m(max)}$ slightly more pronounced for B than for HH. For HH, impacts due to the A1Bspr scenario are again lower and even

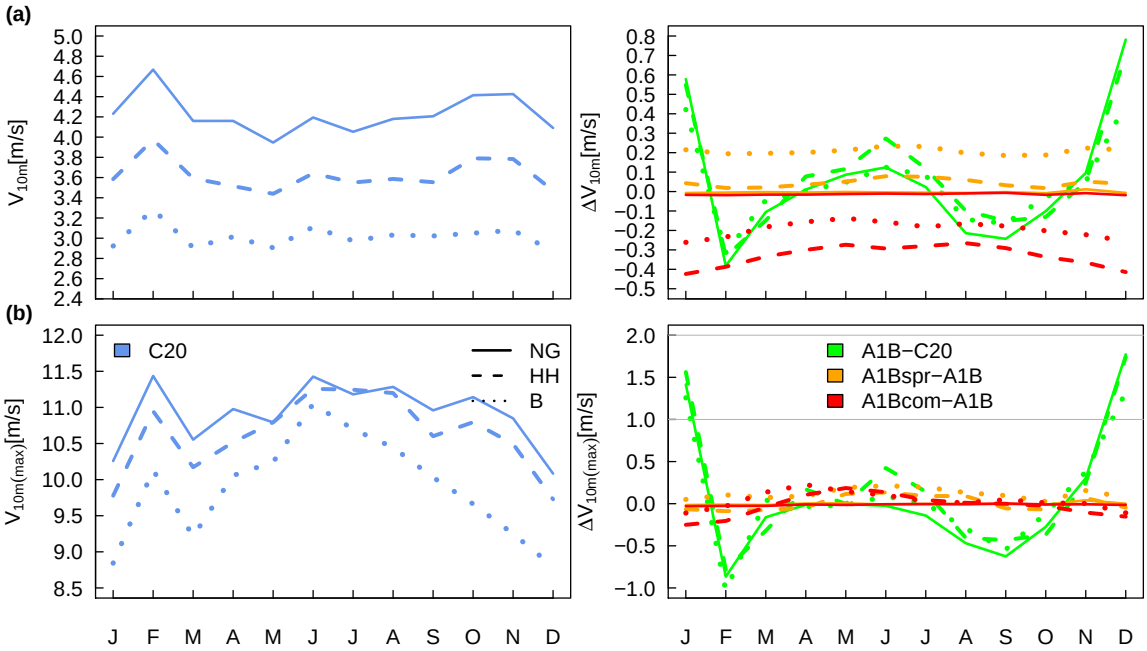

Figure 5.7.: Same as Fig. 5.3 but for (a) the mean wind speed in 10 m height (V_{10m}) and (b) the mean maximum wind speed in 10 m height ($V_{10m(max)}$).

slight decreases appear from January to March.

The A1Bcom scenario leads to to reduced $V_{10m(max)}$ in winter and to slightly increased $V_{10m(max)}$ during the rest of the year, most pronounced in May and June.

5.3.3. Impacts on the hydrological cycle

The monthly surface evaporation (E), simulated in the C20 run, shows a close connection to the near surface temperature (T_s, T_{2m}): low E is connected with low T_s and T_{2m} and vice versa (Fig. 5.8, a, left). There is less E in the domains of HH and B than for NG in summer. The difference in E between HH and NG is less pronounced than between B and NG. For B, differences are roughly twice as strong. In September and October, the highest E is shown for HH. The A1B scenario impacts E from November to January in terms of increases in all domains, NG, HH and B (Fig. 5.8, a, right). This is in line with the observed temperature increases. For NG, the A1B scenario leads also to increased E from March to July. In contrast, impacts on HH and B are very different in the same period: For B, a slightly more pronounced increase in E compared to NG is visible from March to May. Whereas in August and September, a slightly reduced E is shown for B. For HH, a less pronounced increase (than for B or NG) in E in March is followed by reduced E for June to September (-3 to -6 mm/month). The A1Bspr scenario increases this reduction of E due to the A1B scenario for HH from May to August by nearly doubling the decrease. Also for B, the A1Bspr causes a reduced E but less pronounced and only from May to July. The A1Bcom scenario leads to decreased E for both, HH and B, throughout the year ranging from lowest values from December to February by roughly 10 mm less E to about 35 mm less E in May and June. Effects on the monthly E of HH and B due to the A1Bspr scenario are nearly in the same range as the effects due to the A1B scenario. However, effects due to the A1Bcom scenario are even clearly more pronounced than due to the A1B scenario for HH and B.

The total monthly precipitation amount P varies for 1998-2007 between 45 and 70 mm for NG,

45 mm and 85 mm for HH and 45 and 65 mm for B (Fig. 5.8, b, left). Highest P appear for NG in January, October and November, lowest amounts occur in April in terms of the C20 simulation. For HH, three P peaks are visible: in January, June and November. Also for HH, lowest P occur in April. P shows lower variations for B than for HH or NG. Highest P's occur in summer and November and January.

In terms of P, impacts due to the A1B scenario are mostly stronger than impacts due to the land-cover scenarios A1Bspr and A1Bcom as illustrated in Fig. 5.8 (b, right). In general, the A1B scenario leads to an increase in P from January to May and September to December and a decrease in June, July and August. Also for P, the most considerable impact due to the A1B scenario is shown in December by an increase of 35 mm in all three domains. In January and February, B and HH experience a slightly stronger increase in P than NG. During the rest of the year, changes in P due to the A1B scenario are comparable for HH and B to NG. Nevertheless, the smaller domains of HH and B show more variations.

As seen for the near surface temperature, the land-cover change scenarios A1Bspr and A1Bcom show insignificant impacts on P for NG throughout the year (Fig. 5.8, b, right). Land-cover changes in the A1Bspr simulation lead to a increase in P in May, June, July and August to October for HH and for B. In the summer months, the A1Bspr scenario leads therefore to a reduction of the climate change signal seen in the A1B simulation. But in May, the already considerable increase in P due to the A1B scenario is strengthened due to the A1Bspr scenario.
The A1Bcom scenario shows comparable impacts as the A1Bspr scenario for HH and B. The land-cover changes in the A1Bcom scenario cause an increase in P in May, June, August, September and October in HH, and from May to July and September in B. From December to March, P is slightly higher in HH due to the A1Bcom scenario and therefore A1Bcom contributes to a strengthening of the climate change signal of the A1B scenario in these month. In contrast, there is a slight decrease in P in April for B due to the A1Bcom scenario, which dampens the climate change signal of the A1B scenario for this month.

The higher P from October to May as well as the higher temperatures throughout the year are linked to an increase in E. This leads again to an increased integrated water vapor amount (IWV) of 2 to about 5.5 mm/m^2 compared to the C20 simulation for the whole year (Fig. 5.8, c, left and right). No impacts due to the land-cover change scenarios A1Bspr and A1Bcom are visible in terms of changes in the monthly mean IWV amount.

Impacts due to the A1B scenario on the total cloud cover (CLCT) are comparable to the impacts on P but slightly shifted by one month (Fig. 5.8, d). An increase in CLCT is shown from September to June and a decrease in July and August due to the A1B scenario. In December and April the most pronounced increases in CLCT are present. Impacts due to the land-cover changes in the A1Bspr and the A1Bcom simulation are very low with no trend. Same as for IWV, impacts due to the land-cover change scenarios show low to no impacts in the vertical distribution of water.

Finally, the surface water budget W is marked by a pronounced annual cycle due to the A1B scenario which impacts strengthening especially in June to August (-10 to -15 mm/month) and October to December (+10 to 21 mm/month (Fig. 5.9). These changes in W are mainly mirrored by the changes in P due to the A1B scenario. For HH, impacts due to the A1B scenario differ mainly in July (instead of a reduced W a slightly increased W can be seen) and November (a lower increase) from the curve for NG. Effects due to the A1B scenario on the domain of B are close to the effects for NG, only in April a decrease instead of a slight increase in the W is shown. The A1Bspr scenario shows to be counteracting to the A1B scenario on W. From May to July, the reduction of the W would be lower following the A1Bspr scenario since the A1Bspr scenario impacts increasing of the W at that time for both, HH and B. Likewise, but only for HH, the increase in the surface water budget due to the A1B scenario in November and December would

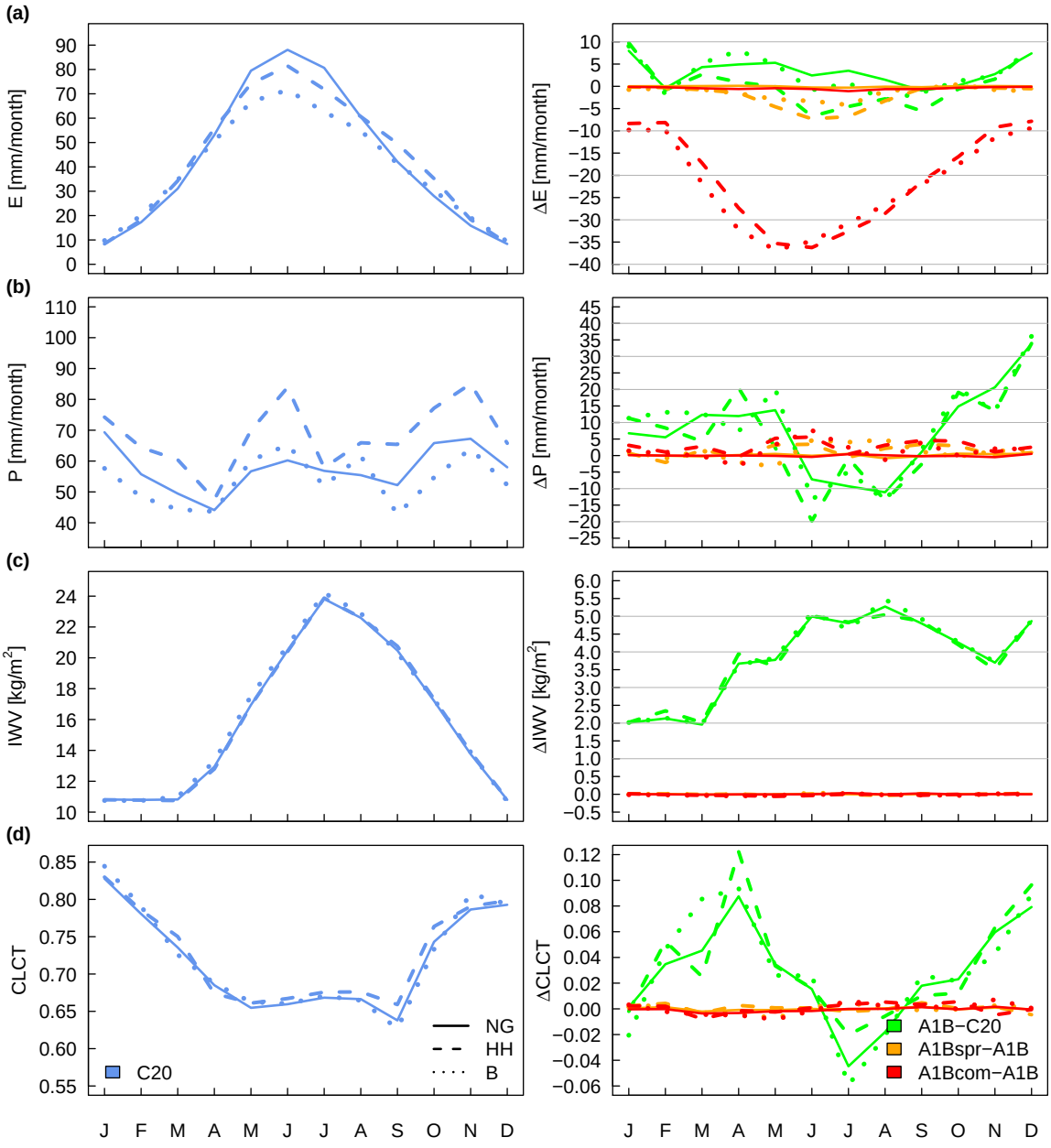

Figure 5.8.: Same as Fig. 5.3 but for (a) the surface evaporation (E), (b) the total precipitation (P), (c) the integrated water vapor (IWV) and (d) the total cloud cover amount (CLCT) for Northern Germany (solid line), Hamburg (broken line) and Berlin (dotted line).

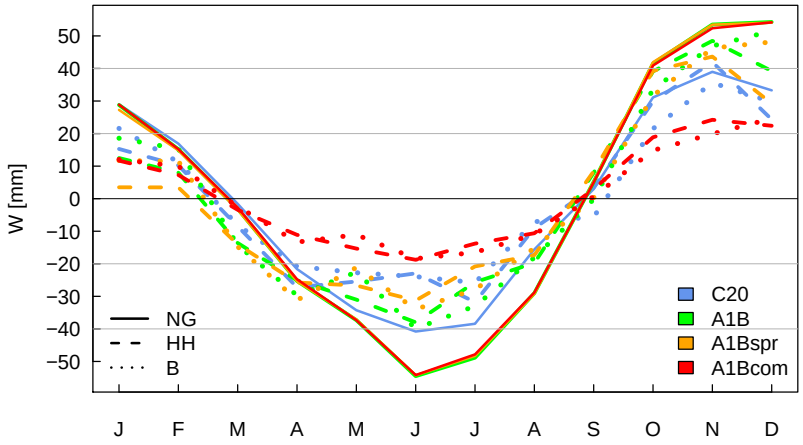

Figure 5.9.: Annual cycle of the surface water budget (W) for NG (solid line), HH (broken line) and B (dotted line) of the C20, the A1B, the A1Bspr and the A1Bcom simulation.

be lower following the A1Bspr scenario. The most significant effect due to the A1Bspr scenario is shown in January by a reduction of about 15 mm of the surface water budget for HH and B in that month while the A1B scenario shows only low effects. This decrease in January and the decrease in December due to the A1Bspr scenario is caused by clearly increased monthly mean subsurface run-off (shown in the appendix Fig. A.2) especially for HH at this time.

The A1Bcom scenario has a stronger impact on the surface water budget of HH and B, than the A1B scenario. The A1Bcom scenario even compensates the effects of the A1B scenario on the surface water budget. The rock surface with no vegetation throughout large parts of HH and B leads to a particularly reduced subsurface runoff and a prominent increase of the surface runoff. Finally, the A1Bcom leads to a considerable decrease in the water input from October to February and also to a considerable decrease of the water output from the surface from May to August. Therefore, the A1Bcom scenario causes a lower surface water budget throughout the annual cycle.

Extreme hydrological events

Similar to the analyzis of thermal extreme climate events several extreme hydrological indices are computed (Tab. 5.4) to capture the impacts of the A1B, A1Bspr and A1Bcom scenario with respect to the vulnerability of citizens of NG, HH and B.

Dry periods play an important role, for example, in terms of arable land because management cost increase due to irrigation or in terms of air pollution or pollen count. All applied scenarios for the future climate of NG indicate changes in the duration of dryperiods and the likelihood of occurrence for the end of the century (Tab. 5.4). Due to the A1B scenario, the number of consecutive dry days (CDD) will be nearly similar for NG, HH and B (3.3, 3.2 and 3.2 days per JJA season) whereas CDD differs in the C20 simulation clearly more pronounced (NG: 2.6, HH: 1.7 and B: 2.7 days). The A1Bspr and the A1Bcom scenario tend to reduce CDD for HH (A1Bspr: -0.2 and A1Bcom: -0.3). For B, A1Bspr tends to reduce CDDs, while the A1Bcom scenario shows no impact.

Although, CDD is nearly equal for NG, HH and B due to the A1B scenario, the number of dry periods (no.CDD) will be more different due to the A1B scenario: For NG and HH, the number of dry periods will be slightly increased due to the A1B scenario (+0.4 and 0.1), whereas for B a clear increase of 1 day is shown. Both land-cover scenarios counteract to this increase of the

Table 5.4.: Total number of the daily precipitation extremes in JJA per year for the investigated 10-year time periods.

Extreme index	Definition [unit]	Region	Number of days C20	Change of the number of days A1B-C20	A1Bspr-A1B	A1Bcom-A1B
CDD	when	**NG**	2.6	0.7	0	0.1
No. of consec.	$P < 1$ mm [day]	**HH**	1.7	1.5	-0.2	-0.3
dry days		**B**	2.7	0.5	-0.1	0
No.CDD	when	**NG**	3.7	0.4	0	0
No. of dry periods	$P < 1$ mm [day]	**HH**	3.6	0.1	0	0.1
	for > 5 days	**B**	3.4	1.0	-0.6	-0.4
PD	when	**NG**	43.1	-7.8	0	0.1
No. of precip days	$P > 1$ mm [day]	**HH**	47.7	-7.8	-0.7	0.1
		B	45.8	-7.4	0.5	1.2
No.WP	when	**NG**	0.3	-0.2	0	0
No. of wet periods	$P > 1$ mm [day]	**HH**	0.7	-0.5	0	0
	for > 5 days	**B**	0.2	-0.1	0	0
RR10	when	**NG**	4.4	-0.7	0	0
No. of intense	$P \geq 10$ mm [day]	**HH**	5.4	-0.5	-0.2	0
precipitation days		**B**	4.6	-1	-0.3	0.2
RR20	when	**NG**	1.1	0.1	0.0	0
Number of very heavy	$P \geq 20$ mm [day]	**HH**	1.2	0	0.3	0.3
precipitation days		**B**	1	0.5	0.1	0

number of dry periods in B (A1Bspr: -0.6, A1Bcom: -0.4). For HH, A1Bcom seems to contribute to an increased number of dry periods.

Tab. 5.4 illustrates that there are more precipitation days (PD) in DJF and MAM and less PDs in JJA at the end of the century following the A1B, the A1Bspr and the A1Bcom scenario for NG. On the local scale of HH and B, differences in the effects pm PD of A1Bspr and A1Bcom become visible. A1Bspr impacts in different ways on the number of PDs of two cities. In HH, the number of PDs is increased by the A1Bspr scenario in DJF and SON, and decreased in JJA. Therefore, the additional decrease of PDs in JJA intensify the climate change signal. In contrast, A1Bspr dampens the climate change signal in B at the same time (Tab. 5.4). For both, HH and B, A1Bcom increases the number of PDs in DJF and decreases the number of PDs in MAM (Tab. 5.4).

In line with the number of PDs also the number of wet periods (no.WP) decreases, most pronounced for HH, due to the A1B scenario for all three domains. The A1Bspr and the A1Bcom scenario show no impacts on the number of wet periods.

The number of intense precipitation days (RR20) is reduced in the A1B simulation for NG (-0.7 days), HH (-0.5 days) as well as B (-1 day). The A1Bspr scenario would additionally reduce the number of wet periods for HH and B. In contrast, the A1Bcom scenario would lead to a lower decrease of the number of intense precipitation days for B. However, the A1B scenario supports the occurrence of very heavy precipitation events (RR20) with daily precipitation sums greater/equal 20 mm per for NG and B. The strongest increase in RR20 due to the A1B scenario by 0.5 days is shown in B. The A1Bspr scenario contributes to an additional increase of RR20 for HH (+0.3 days) and B (+0.1 days) and the A1Bcom scenario only for HH (+0.3 days).

Cloud radiation feedback

Cloud cover plays an essential role in the radiation budget or the hydrological cycle. Here, the total cloud cover amount (CLCT) is discussed with respect to impacts due to the A1B, A1Bspr and A1Bcom scenario (Fig. 5.8, d). The C20 simulation in Fig. 5.8 (d, left) shows that there is an annual cycle in CLCT in all domains: it is highest in the cold season (maximum in January) and lowest in the warm season (minimum in September).

HH has slightly higher CLCT than NG or B during most of the month. Only in November, December, January and February, a higher CLCT amount occurs for B. Nevertheless, the monthly mean values show only minor differences. The CLCT is lowest in September for all three domains and highest in January respectively.

The A1B scenario leads to an increase in CLCT from February to May and November and December. Largest changes can be seen in April and December. This could be an attributing factor of the observed increases in the near surface temperature. CLCT is increased nearly throughout the year for NG due to the A1B scenario. Only in January, July and August, reductions of CLCT appear. The land-cover changes in the A1Bspr and A1Bcom simulations show no clear picture with respect to impacts for the region of NG.

Soil temperature

For land-use and land-cover interactions with the atmosphere, the soil plays an important role in terms of water and heat storage. Also in Chapter 4 it was shown that the soil conditions considerably impact the atmosphere.

The A1B scenario leads to changes in T_{so} throughout all soil layers (Fig. 5.10, left). Changes up to a depth of 1.42 m are linked to changes of the surface temperature, changes in 2.86 m depth show weak seasonal variations and from 5.74 m and deeper impacts on T_{so} are independent of the season. Especially in the soil layer, the pronounced temperature increases in December and January are mirrored. The temperature increases in the upper soil layers (0.005-0.16 m) are in the range (+1.5 to +5 K) of temperature increases at the surface.

Increases in T_{so} due to the A1Bspr scenario are visible throughout all soil layers for B and only up to a depth of 0.7 m for HH.

Soil water content

For NG, the A1B scenario leads to an increase in the soil water content (W_{SO}) from October to May, and to a decrease from July to September in the first six soil layers up to a depth of about 0.7 m (Fig. 5.10, b). Strongest increases in W_{SO} can be seen in April and December. This is also reflected in the annual cycle of total precipitation seen in Fig. 5.8, b. Interestingly, the domain of B shows higher soil moisture contents than HH and NG in the upper five soil layers throughout the year. This can be attributed to the different soil textures throughout NG. While the HH domain has three different soil textures: sand, sandy-loam and clay-loam (Fig. 3.2). The B domain has only loam soil texture following the soil-map used for the simulations of this study. Loam is able to store more water than sand or sandy-loam. This explains the differences in the soil moisture contents.

As seen for other parameters, the impacts on W_{SO} for NG due to the A1Bspr scenario are small. But for HH and B there are clear impacts detectable: From June to January there is a clear increase in W_{SO} throughout all modelled soil layers due to the A1Bspr scenario in both domains. In the depth of 0.7 m and lower, the increase is visible in all month. Changes in W_{SO} in the A1Bspr

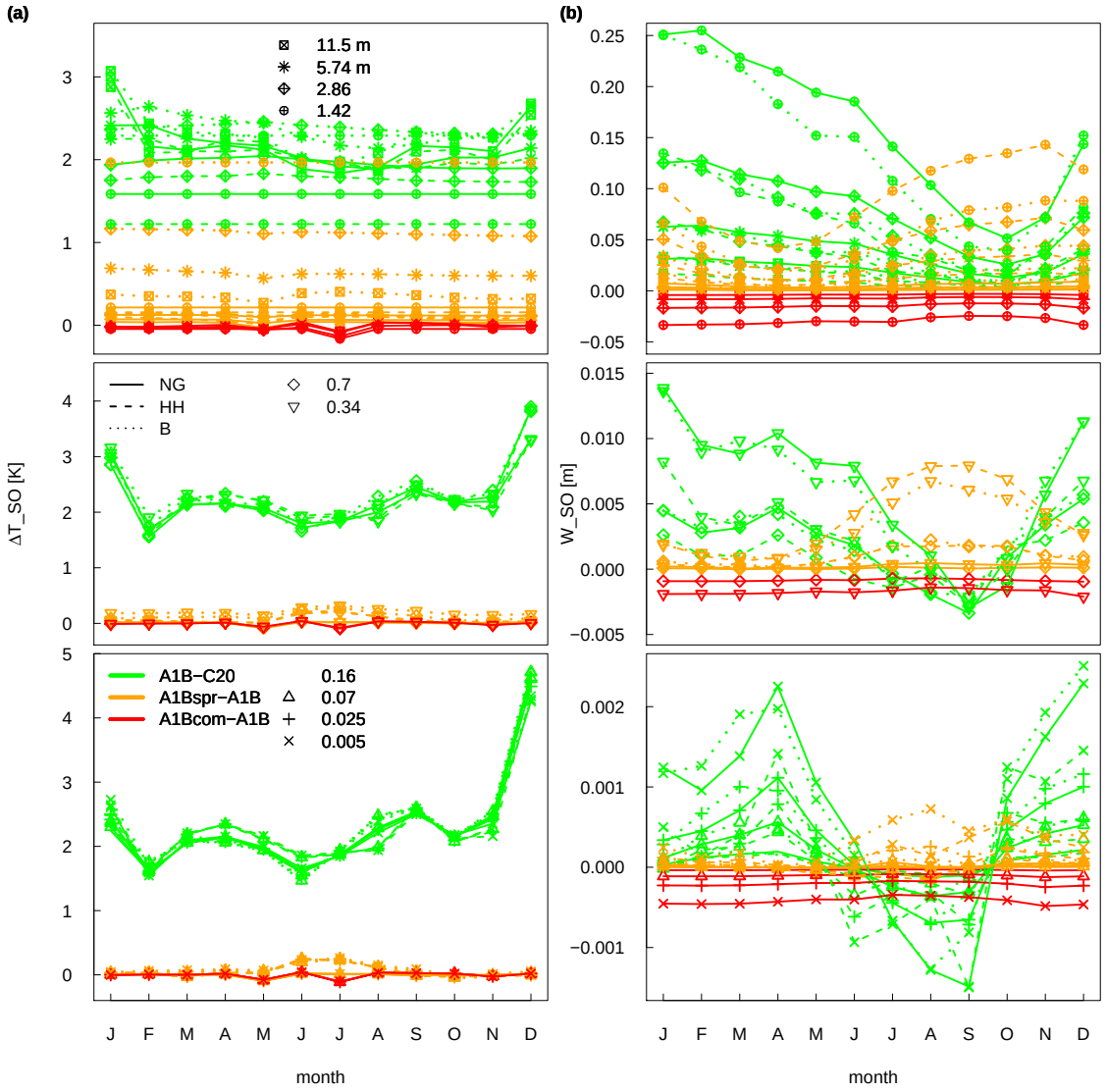

Figure 5.10.: a) Differences in the mean monthly soil temperature (T_{so}) in Kelvin (K) and b) differences in the soil water content (W_{SO}) in meters (m) for each soil layer of the long-term CCLM simulations. The layer depths indicate the vertical center of the soil layers (Fig. 3.1). The upper plot shows the results for the lower soil layers from 1.42 m up to 11.5 m depth. The plot in the middle illustrates the results of 0.34 to 0.7 m and the bottom plot shows the upper soil layers up to a depth of 0.16 m. This separation of the soil layers is conducted to allow to differentiate between the impacts of the land-cover scenarios.

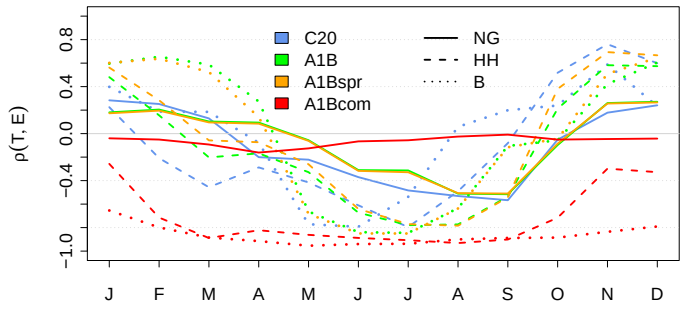

Figure 5.11.: Monthly correlation between the 2 m temperature and the surface evaporation for the domain of Northern Germany, Hamburg and Berlin excluding water bodies. In the correlations for the A1Bcom simulation for Berlin, the lines from November to April were cut since surface evaporation at this time goes to zero for this domain (Fig. 5.8).

scenario compared to the A1B scenario are larger than in the A1B simulation compared to the C20 simulation for most of the year.

The A1Bcom simulations leads to a decrease in W_{SO} for NG. This is caused by the sealed surfaces in this land-cover scenario. Sealed surfaces do not contain soil water in the model because water cannot be stored and evaporate from lower soil layers. Therefore, W_{SO} from the A1Bcom simulation for HH and B is not displayed in Fig. 5.10.

Soil moisture limitation

As done for the extreme cases in Chapter 4, Section 4.3.4, the role of soil moisture for the described climate impacts due to the A1B simulations are discussed. Here, the correlation of each grid-box in NG of the monthly mean 2 m temperature (T_{2m}) and the monthly surface evaporation (E) sum are computed. Grid boxes with water bodies are excluded from this analysis.

A moderate to high control of soil moisture upon evapotranspiration and temperature is illustrated for June to September in NG in all applied simulations. This becomes visible in terms of moderate negative correlations for these months (Fig. 5.11). In winter, weak to moderate positive correlations indicate strengthened atmospheric control to evaporation, again for all simulations. However, in January and February, the A1B scenario simulations show lower atmospheric control than the C20 simulation. In spring, the A1B scenario seems to strengthen the atmospheric control on evaporation, whereas in the C20 simulation, soil moisture seems to play a more important role. Nevertheless, the correlations between 2 m temperature and surface evaporation are weak at this time of the year.
For HH and B, the above discussed correlations between 2 m temperature and surface evaporation are stronger (Fig. 5.11). In HH, soil moisture turns earlier, already in March, to control the 2 m temperature than in B. In B, the atmospheric control is still dominant in March and April. From May beginning, also in B, the soil moisture control lasts a month longer to September.

For all three domains, the A1Bspr simulation shows curves similar to the A1B simulation. The effects of the A1Bcom scenario have to be analysed carefully, since parts of the domain, especially in HH and B are sealed. Sealed areas imply no soil moisture due to the soil texture rock. Therefore, correlations between 2 m temperature and surface evaporation are difficult or even invalid for this scenario.

5.3.4. Regional distribution of impacts by land-cover changes

The regional distribution of impacts due to the A1B, the A1Bspr and the A1Bcom scenario are examined in the following.

2 m temperature

Impacts on the 2 m temperature (T_{2m}) due to the A1B, A1Bspr and A1Bcom scenarios are shown as seasonal mean values (from left to right: MAM, JJA, SON and DJF) for the model domain in Fig. 5.12. On the one hand, the seasonal mean T_{2m} for NG as it is simulated by the C20 simulation (first row) is presented. On the other hand, the changes due to the applied scenarios are shown: The differences between the A1B and the C20 simulation (A1B-C20) for NG (2^{nd}), for HH (3^{rd} row) and for B (4^{th} row). In addition the impacts due to the A1Bspr and the A1Bcom scenario (A1Bspr-A1B, A1Bcom-A1B) compared to the A1B scenario are presented for HH and B.

It becomes visible that the A1B scenario introduces T_{2m} increases throughout the whole domain of NG (+1.6 to about +3.2 K). Therewith, also the North Sea and the Baltic Sea show clear increases in T_{2m} (+1.6 to about +2.8 K). In JJA and SON, an intensification of the T_{2m} increase is shown from the north to the south of the domain.
With the exception of MAM, the increase in T_{2m} due to the A1B scenario is slightly larger in B than in HH. Furthermore, in MAM and JJA, the T_{2m} increases are slightly larger in B than in the surroundings.

The A1Bspr scenario shows prominent higher increases where land-cover changes are applied and partly within the original built city in MAM (+0.1 to 0.3 K) and JJA (+0.3 to 0.8 K, Fig. 5.12). No impacts on T_{2m} due to the A1Bspr scenario are shown in SON or DJF.

Increases in T_{2m} due to the A1Bcom scenario are visible throughout the year- most pronounced in JJA (+0.2 up to more than +1.6 K). In MAM, JJA and SON, the A1Bcom scenario causes a wake with increased T_{2m} in the downwind area of HH and B. In MAM and SON, only neighbouring grid boxes are affected by a slight increase in T_{2m} by about 0.1 to 0.2 K. But in JJA, the wake of T_{2m} increase targets even distances of about 10 grid boxes- therefore, up to around 30 km for HH and up to 7 grid boxes (around 20 km) for B. In JJA, neighbouring grid boxes of the extended urban area in the A1Bcom scenario show even increases in T_{2m} of 0.2 to 0.3 K in mean. In MAM and JJA, the strongest T_{2m} increases appear in the north east of the sealed city core (Fig. 5.2) in the A1Bcom scenario (MAM: +1.2 K, JJA: +1.4 K). Whereas, in SON and DJF, the sealed city core itself, experiences the strongest temperature increases in the urban environment of the A1Bcom scenario (up to +0.5 K for DJF and +0.9 K in SON).

Fig. 5.12 shows finally that not only modified model grid boxes are affected by temperature impacts due to the land-cover scenarios but also adjacent areas. It is also shown that the degree of impacts on T_{2m} varies considerably.

Thermal extremes

Fig. 5.13 shows the spatial distribution of impacts of all simulations on extreme thermal events (summer days, hot days and tropical nights) in JJA. The number of hot periods and the number of consecutive hot days is not shown since the impacts are very low and independent on the urban areas.

Remarkably, because new compared to RCM simulations with usually coarser grids, an urban heat island (UHI) is illustrated for HH and B in terms of summer (SD) and hot days (HD) in the

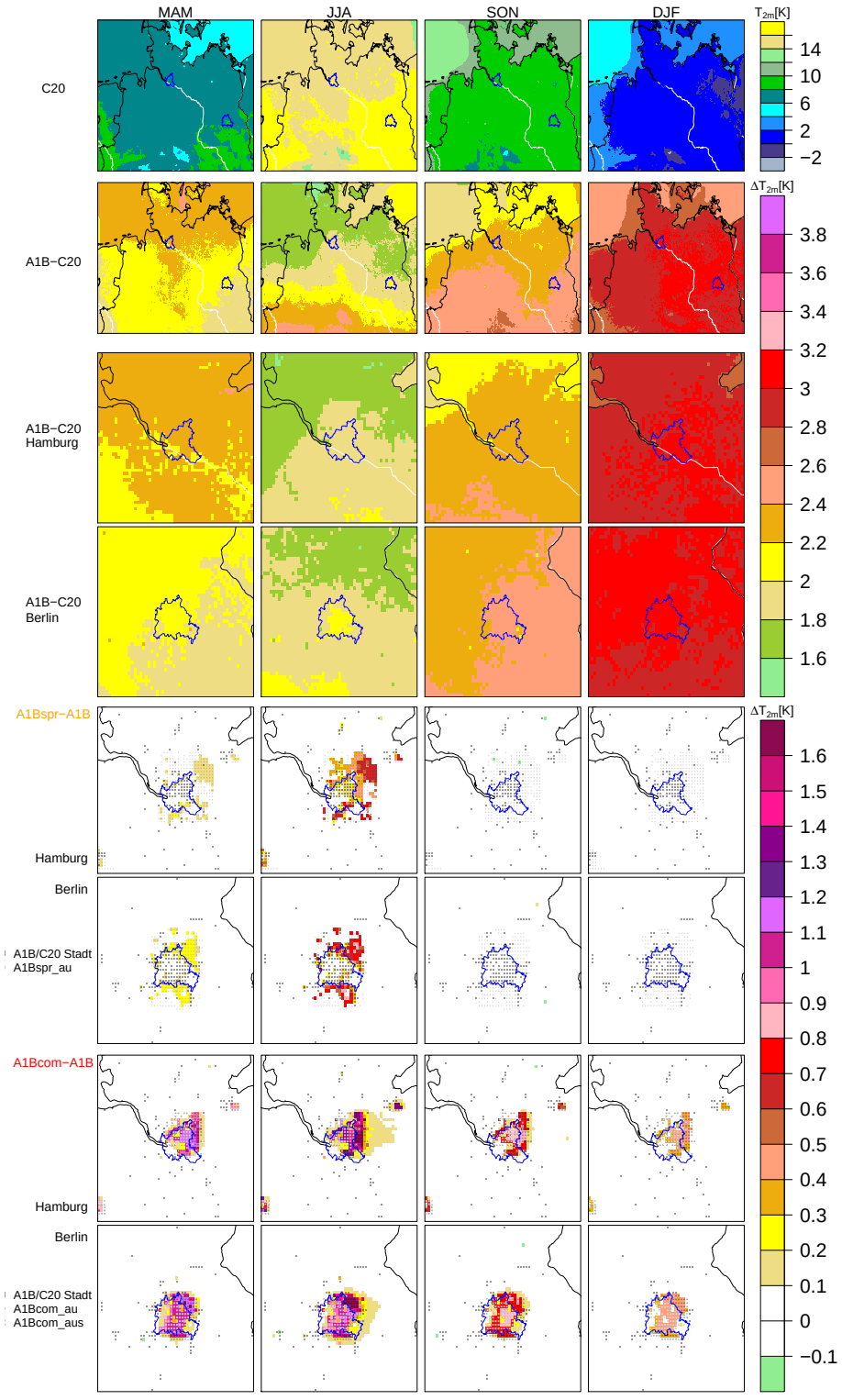

Figure 5.12.: Seasonal mean 2 m temperature in the C20 simulation (1st row) and changes due to the A1B scenario for NG (2nd row), HH (3rd row) and B (4th row), changes due to the A1Bspr scenario compared to the A1B scenario for HH and B (5th/6th row) and changes due to the A1Bcom scenario compared to the A1B scenario for HH and B (last two rows) for each season from left to right: MAM, JJA, SON and DJF. The urban shapes of the A1B/C20, the A1Bspr and the A1Bcom simulations are indicated by lightgrey points.

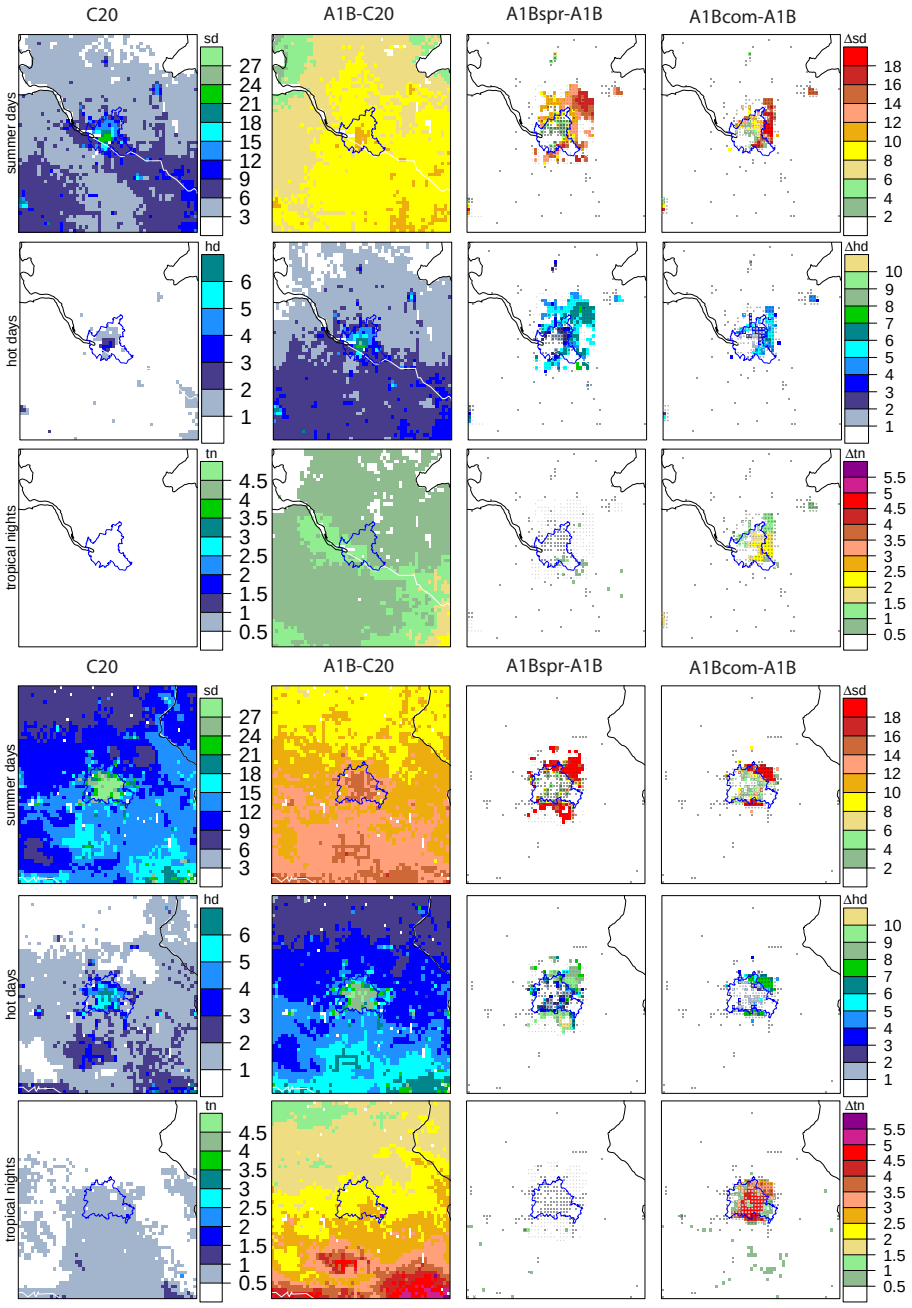

Figure 5.13.: Spatially distribution of thermal extremes in JJA for Hamburg (top) and Berlin (bottom): summer days (sd), hot days (hd) and tropical nights (tn, from top to bottom).

C20 simulation (Fig. 5.13). From the rural environment towards the city core, the number of SDs and HDs increases in both cities. The A1B scenario strengthens this effect as within the city the number of SDs (+10-12 days) and HDs is particularly increased (+ up to 8 days).

Both, the A1Bspr and the A1Bcom scenario lead to additional increases in the number of SDs and HDs in HH and B. Whereas, areas which are transformed from arable to urban land experience the strongest increases. Due to the A1Bspr scenario, there are up to 18 additional SDs in the north-east of the city core.

The regional distribution of tropical nights (TN) seems to be independent on the cities of HH and B in both, the C20 simulation and the A1B simulation. However, the A1B scenario leads to an increase in the number of TNs in the whole domain of HH (+1 day) and B (+2-3 days) and in the surroundings of the two cities. Here, noticeable differences are shown between the A1Bspr and the A1Bcom scenario. Whereas, there are no impacts on the number of tropical nights due to the A1Bspr scenario, there are considerable impacts due to the A1Bcom scenario: Especially within the two cities (+ 1.5 to 5 days) but also in the domain of transformed arable grid boxes (+1 to 3 days), the number of tropical nights increases more distinctly than due to the A1B scenario.

To summarize, in the A1Bspr simulation more SDs and HDs occur for a larger domain than in the A1Bcom scenario, but these high temperatures cool down at night such as nearly no TNs occur. Whereas, the A1Bcom scenario leads to less SDs and HDs for a smaller domain as due to the A1Bspr scenario but the thermal stress in the A1Bcom simulation is clearly higher, since high daytime temperatures do cool down less leading to a high number of TNs.

Wind speed in 10 m height

The spatial distribution of mean wind speeds in 10 m height (V_{10m}) in the C20 simulation shows low variation throughout the year (Fig. 5.14, first row). In general, highest V_{10m} is visible above the North and the Baltic Sea. In SON and DJF, V_{10m} above the North and Baltic Sea is higher than in MAM and JJA. Also the coasts are marked by higher V_{10m} than further inland as an effect of the increased surface roughness. The inland of NG shows V_{10m} between 3 to 5 m/s, whereas, HH and B are characterised by lower V_{10m} than their surroundings.

The A1B scenario leads to low impact on the land areas of NG in MAM, JJA, and SON (Fig. 5.14, 2nd to 4th row). Only in JJA diverging trends are shown, with low increases in V_{10m} near the coasts and low decreases in the south of NG. In SON, in the western part of NG's land masses low decreases of V_{10m} become apparent. Above the Baltic and the North Sea more pronounced impacts are illustrated. In MAM and SON, decreases of V_{10m} are shown. Whereas, in JJA, V_{10m} is increased in the A1B scenario above the Baltic Sea and particularly above the North Sea by up to 1 m/s.

As seen already in the annual cycle of V_{10m} (Fig. 5.7) there are increases in V_{10m} in January and February for NG. Here, it is illustrated that these increases in V_{10m} are spread throughout NG. Largest increases are drawn above the North Sea and the western part of NG. Further east, the increase in V_{10m} is lower. HH and B which have already a lower V_{10m} (shown in the C20 simulation) experience lower impacts in V_{10m} than their surroundings. This increases the difference in V_{10m} between HH and B and their surroundings.

While the impacts due to the change in the A1B simulation show seasonal dependent effects (Fig. 5.14), the effects on V_{10m} due to the land-cover scenarios (A1Bspr and A1Bcom) seem to be nearly independent from the season (Fig. 5.14). The reason is that the shapes and characteristics (Tab. 5.1) of the modified cities are nearly constant throughout the year and the roughness length (Z_0) and the roughness length of vegetation ($Z_{0(veg)}$) of A1Bspr varies only slightly and for the A1Bcom scenario even no variation occurs in the course of the year (Tab. 5.1). Impacts of the land-cover scenarios A1Bspr and A1Bcom on V_{10m} of HH and B show a comparable magnitude

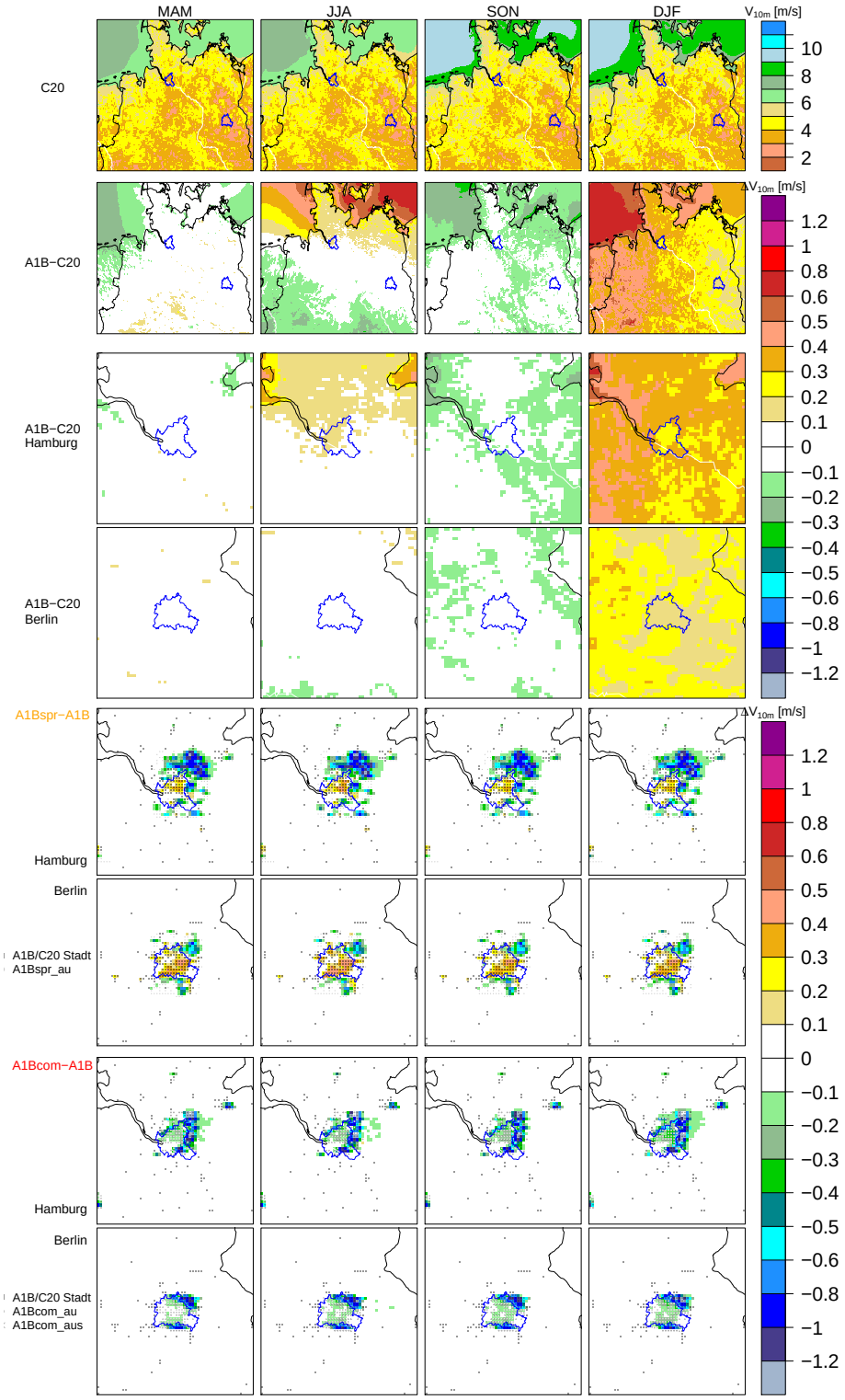

Figure 5.14.: Same as Fig. 5.12 but for seasonal mean wind speed in 10 m height.

as impacts due to the A1B scenario. Nevertheless, these impacts are clearly more limited in space.

A1Bspr causes increases in V_{10m} within the city borders of both cities, HH and B as shown in Fig. 5.14 (5th and 6th row). This increase is particularly pronounced in B by up to +0.5 m/s. In contrast, in the north-east of both cities, decreases in V_{10m} of more than 0.6 m/s occur- most prominent for HH. Especially for HH, the added urban grid boxes are affected by considerably lower V_{10m}. Most pronounced decreases in V_{10m} can be seen in the major downwind areas of both cities: in the north-east of HH (up to -1.4 m/s) and in the east of B (-0.7 m/s). Here, the V_{10m} reduction is at least partly caused by the increased roughness length of the arable to urban transformed grid boxes in this scenario. Also non modified land areas in the north-east of HH up to a distance of about 10 km experience slightly reduction in V_{10m} due to the A1Bspr scenario. But, this could also be an effect of the near location of the city Lübeck, which was also slightly modified due to the A1Bspr scenario.

In contrast, in the A1Bcom simulation, V_{10m} is slightly reduced within the borders of both cities by 0.1 to 0.4 m/s and clearly more pronounced for the added urban grid boxes in the downwind area of both cities (-1.4 m/s each, Fig. 5.14 (7th and 8th row)). As seen for the A1Bspr scenario, also the not modified surrounding in the downwind area of HH experiences wind speed reductions, especially in DJF, but also in MAM and JJA. Distances of more than 16 km experience a slight wind speed reduction due the the A1Bcom scenario in DJF. Nevertheless, the affected domain of impacts in terms of V_{10m} is clearly smaller in the A1Bcom scenario than in the A1Bspr scenario, and for B, the magnitude of change is clearly higher than in the A1Bspr scenario or in the A1B scenario compared to the C20 simulation.

Mean maximum Wind speed in 10 m height

The A1B scenario shows particularly two important impacts on the daily maximum wind speed $V_{10m(max)}$ on NG (Fig. 5.15). Firstly, $V_{10m(max)}$ is clearly increased above the Baltic Sea and also partly but with a lower amplitude above the North Sea in JJA. Secondly, in DJF, $V_{10m(max)}$ is considerably increased throughout the model domain - most pronounced above the North Sea and in the western part of the model domain (up to + 1.2 m/s). In MAM, JJA and SON $V_{10m(max)}$ above the land areas is mainly reduced - particularly in SON (-0.2 to -0.5 m/s).

As seen for V_{10m}, also impacts on $V_{10m(max)}$ appear to be lower or even negligible in the areas of HH and B. For HH, impacts due the A1B scenario are limited to SON and DJF. In SON and DJF, there are no differences detectable compared to the surrounding. For B, there are nearly no impacts on $V_{10m(max)}$ due to the A1B scenario - aside from the period DJF.

These results support the supposition that impacts on $V_{10m(max)}$ due to the A1B scenario are small within urban areas and even considerably damped therein. Only in DJF, the effects of the urban areas on $V_{10m(max)}$ vanishes (Fig. 5.15).

The map of changes in $V_{10m(max)}$ caused by the land-cover changes by the A1Bspr and the A1Bcom scenario shows clearly that the domain of HH and its surrounding is especially affected by impacts on $V_{10m(max)}$ (Fig. 5.15, 5th and 7th row). In the A1Bspr as well as in the A1Bcom simulation, there are far-reaching impacts on the surroundings in terms of the $V_{10m(max)}$ in the downwind area of HH. In both simulations, $V_{10m(max)}$ is reduced even outside the urban areas up to distances of about 60 km, touching Lübeck in DJF.

Impacts on B and its surrounding by the A1Bspr and A1Bcom scenario in terms of $V_{10m(max)}$ appear to be considerably smaller than for HH.

A1Bspr leads to an increase in $V_{10m(max)}$ within the political borders of HH and B (Fig. 5.15). In the area of added urban grid boxes both, increases and decreases of $V_{10m(max)}$ are visible.

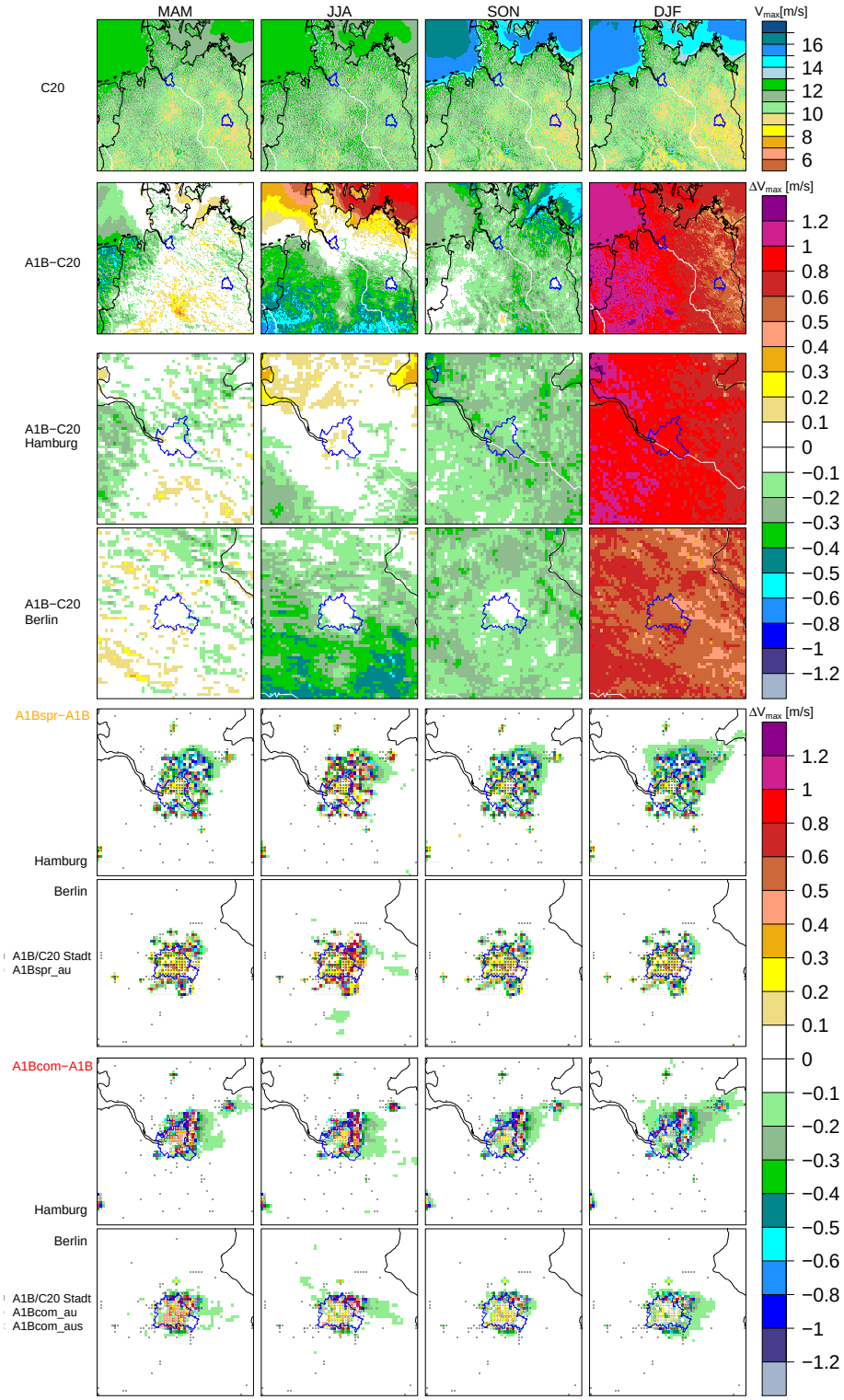

Figure 5.15.: Same as Fig. 5.12 but for seasonal mean maximum wind speed in 10 m height.

A1Bcom leads, same as A1Bspr, to increases in $V_{10m(max)}$ within the cities of HH and B but of a lower degree and limited to MAM, JJA and SON. In DJF, slight decreases of $V_{10m(max)}$ dominate above the cities. At the downwind side of the new city borders in the A1Bcom scenario most pronounced decreases in $V_{10m(max)}$ are located (about 0.5 up to more than 1.4 m/s lower than in the A1B simulation).

Wind directions and distribution of wind speed occurrences in 10 m height

The wind field (V_{10m}) of NG is mainly characterized by wind inflow from the west (W), west-south-west (WSW) and south-south-west (SSW) as shown in the C20 simulation in Fig. 5.16 (blue box). The A1B simulation leads to a change in the occurrence of wind directions and the distribution of wind speeds in dependence on the wind direction compared to the C20 simulation in NG (Fig 5.16, green box). In MAM, the percentage proportion of days with V_{10m} from the WSW is increased in the A1B simulation from about 14% to 20%. Particularly, wind speeds of more than 4 m/s occur more often for WSW-winds. However, the number of days with wind inflow from ENE and E is reduced in the A1B simulation in MAM (-4% for ENE and -2% for E). In JJA, the A1B simulations shows a higher percentage proportion of winds from the W, whereas mainly V_{10m} between 4 and 6 m/s occur more often than in the C20 simulation. Instead, V_{10m} from the SSW occurs less often in the A1B simulation. In SON, V_{10m} directions seem to be slightly rotated to southerly direction. The percentage proportion of V_{10m} from the W and WSW is reduced and the occurrence of V_{10m} from the south (S) and south-south-east (SSE) is increased. In DJF, less V_{10m} is shown from the W but the percentage proportion of V_{10m} from the WSW, SSW and S is increased in the A1B simulation compared to the C20 simulation. Therein, particularly strong V_{10m} of more than 8 m/s occur more often in the A1B simulation compared to the C20 simulation. For HH, the location to the coasts is also visible in the distribution of wind speeds of the A1B simulation. There are frequently higher V_{10m} in HH than in the further inland located B (Fig. 5.16, 3rd and 4th row).

Whereas V_{10m} and the direction of V_{10m} are hardly affected by the land-cover changes applied in the A1Bspr scenario (Fig. 5.16, orange box), the A1Bcom scenario leads to considerable impacts throughout the year (Fig. 5.16, red box). In HH, the percentage proportion of V_{10m} from the WSW is particularly increased in the A1Bcom simulation compared to the A1B simulation. Thereby, the proportion of wind speeds higher 4 m/s is reduced at the expense of lower wind speeds. In the A1Bcom simulation for HH, the occurrence of V_{10m} from the S is reduced in JJA, SON and DJF and of V_{10m} from the SSE is reduced throughout the year compared to the A1B simulation.

Also for B, the A1Bcom scenario leads to a decrease of the occurrence of high V_{10m} throughout the year. In JJA, SON and DJF, the percentage proportion of V_{10m} from the W is notably increased.

The relevance of changes in the wind field for citizen of affected areas

The wind speed reductions in the A1B scenario in JJA and SON would additionally exacerbate the effect of increasing temperatures and the occurrence of extreme thermal events linked to heat stress. The lower ventilation especially of urban areas might contribute to higher pollution loads.

The A1Bspr simulation provides for citizen of original urban grid boxes higher V_{10m}. This reduces the wind chill temperature level for this area.

Citizen of the enlarged parts of the compact cities of HH and B are due to the clearly lower wind speeds confronted by higher perceived temperatures.

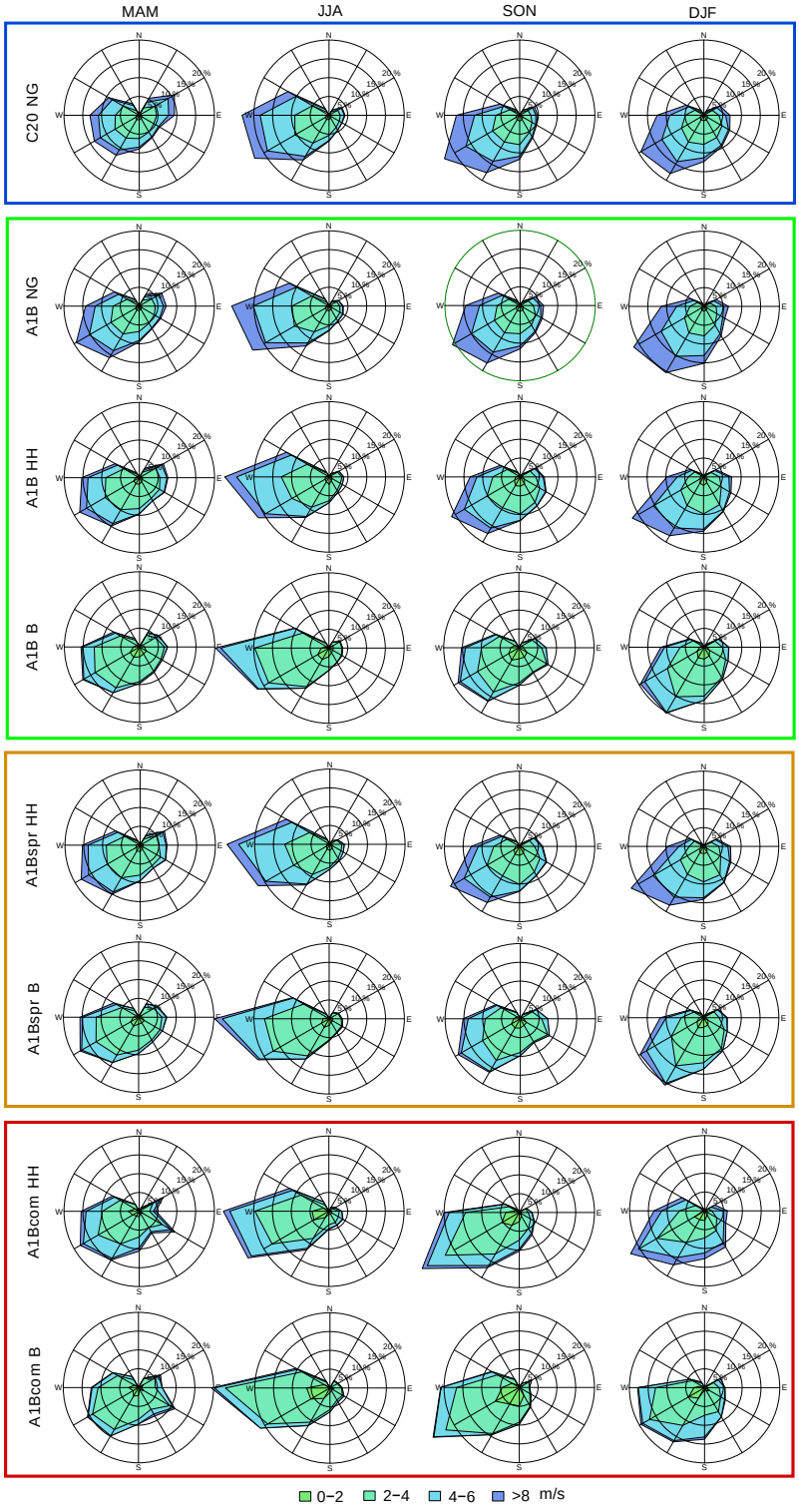

Figure 5.16.: Seasonal mean (MAM, JJA, SON, DJF from left to right) wind directions and wind speeds in 10 m height (V_{10m}) as simulated in the C20 (NG, blue box), the A1B (NG, HH, B, green box), the A1Bspr (HH, B, orange box) and the A1Bcom (HH, B, red box) simulation.

Total precipitation

The A1B scenario leads to increases in the monthly mean precipitation amount for nearly the whole domain of NG in MAM, SON and DJF (Fig. 5.17). This precipitation increase is particular marked above the North Sea in SON by an increase of more than 25 mm per month. The most pronounced precipitation increase above the land masses is visible by additional monthly mean precipitation sums of 10 to 25 mm for DJF. In JJA, NG is dominated by a decrease of the precipitation amount due to the A1B scenario. Only the North Sea and the Baltic Sea are covered by slight precipitation increases during that time.

Both, the A1Bspr as well as the A1Bcom scenario show overall slight increases in the total precipitation amount in the domains of HH and B (Fig. 5.17). Whereas, A1Bcom shows comparable effects on the precipitation pattern of HH and B throughout the year, there are differences in the effects on total precipitation due to the A1Bspr scenario for the two cities: In JJA, clear total precipitation decreases appear in the downwind domain of HH, whereas in and around B only increases in total precipitation are visible at the same time (Fig. 5.17). In MAM, A1Bspr leads to a precipitation increase in the upwind domain and above HH and a precipitation decrease above and in the upwind domain of B. Nevertheless, in the downwind area of both cities, in the east and north-east, clear precipitation increases due to the A1Bspr scenario become visible in MAN (+2-8 mm/month). Also, in SON and DJF, A1Bspr leads to a slight precipitation increase in the downwind areas of both cities, HH and B (+2-4 mm/month). Areas in a distance of up to about 20 km to 30 km are faced by a slight precipitation increase due to the A1Bspr scenario.

Again, in December the most pronounced impacts in terms of an increase in total precipitation of more than 25 mm per month occurs. During summer, the total precipitation amount decreases. The mean monthly precipitation sums are clearly reduced in the summer month June, July and August.

An increase in precipitation becomes visible in the urban district of HH, most pronounced in the north-east. Precipitation sums in the eastern part and in the downwind area of both cities are increased due to the A1Bcom scenario. This effect is most pronounced for HH (MAM: +2-7 mm/month, JJA: +2-10 mm/month, SON: +2-6 mm/month and DJF: +2-5 mm/month). For B, precipitation increases in the east, north-east of the city vary between 2 and 5 mm/month. The A1Bcom scenario causes in the downwind direction of HH in a distance of approximately 15 to 20 km an area of precipitation reduction of 2 up to 9 mm/month (in JJA). For B, there seems to be also an area of precipitation reduction in the distance of more than 30 km in the south-east of the city but less pronounced and less consistent for the different seasons.

In summary, as seen for the 2 m temperature and the wind speed, also the precipitation pattern are not only affected locally by the A1Bspr and the A1Bcom scenario but also the near surroundings and even areas in further distances of the city experience impacts.

Surface water budget

In Fig. 5.3.4, the seasonal mean surface budget is illustrated regionally. The regional distribution of the surface water budget in the C20 simulation shows in MAM a prominent west-east distribution: from a particular low towards a less low surface water budget. In JJA, HH and B are marked by a less low surface water budget whereas in the surroundings, clearly more water is transported to the atmosphere than absorbed at the surface (negative surface water budget). In SON and DJF, the total precipitation dominates over the other surface water budget components resulting in a positive surface water budget. From the coasts to the south-east of NG, the magnitude of the positive surface water budget increases. The regional maps of the surface water budget highlights the important role of the soil texture (Fig. 3.2) since structures of soil textures are mirrored in the

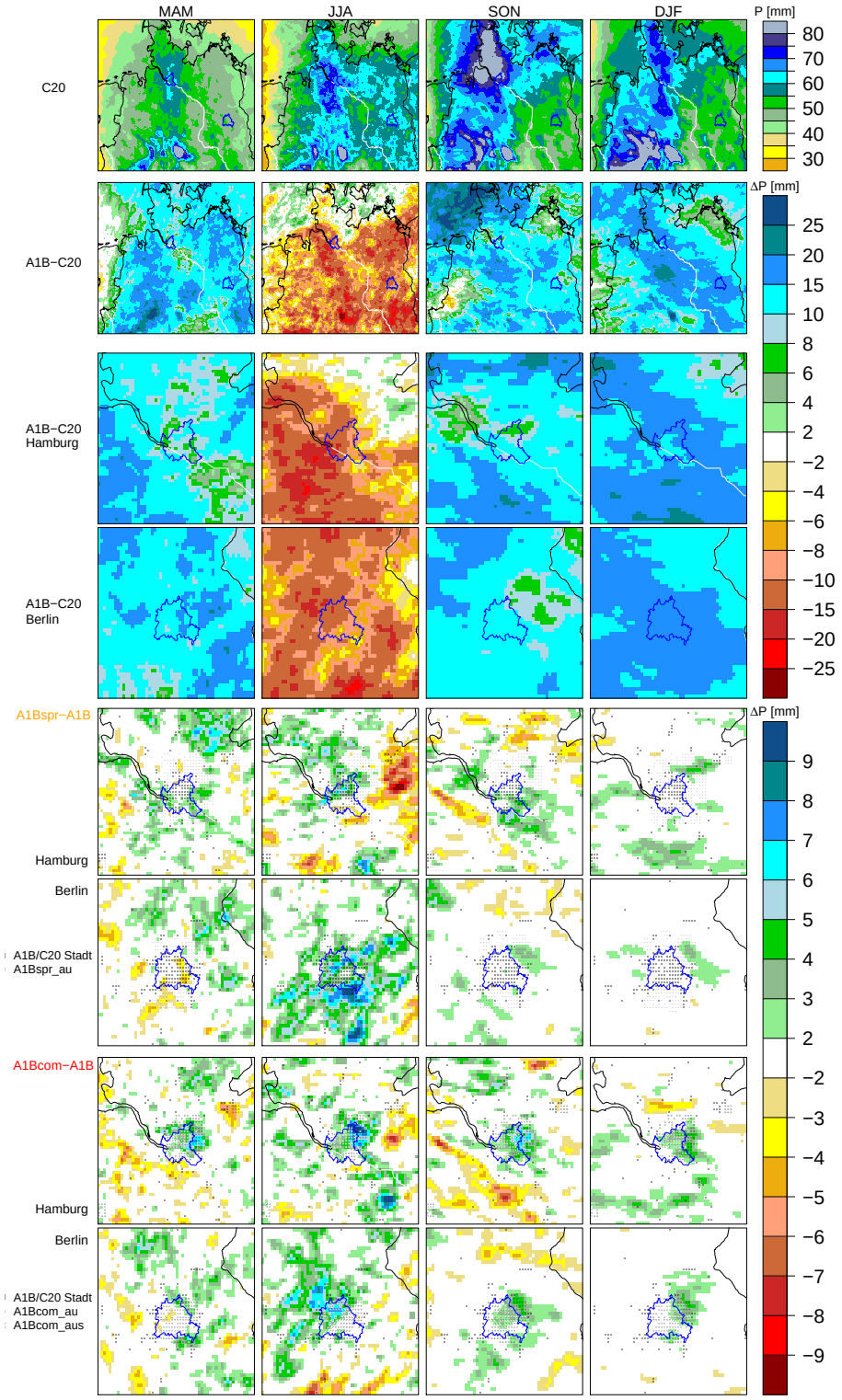

Figure 5.17.: Same as Fig. 5.12 but for monthly total precipitation sums in mm.

distribution of the level of the surface water budget.

As already discussed for the monthly spatial mean values of the surface water budget, the A1B leads to more water output in MAM and JJA and more water input in SON and DJF. It is illustrated that changes due to the A1B scenario look different for HH and B than in the surroundings. HH and B experience lower impacts due to the A1B scenario during all seasons. The domain of HH (Fig. 5.3.4, 3rd row, the distribution of the degree of change in the surface water budget is particularly marked by the influence of the soil texture.

Both land-cover scenarios, A1Bspr and A1Bcom counteract to the effects of the A1B scenario in terms of the surface water budget in MAM and SON. Impacts on the surface water budget are purely located above urban grid boxes. No effects on the surroundings are shown. The A1Bspr scenario shows for B more pronounced impacts than for HH for all seasons.

The A1Bcom scenario shows stronger impacts on the surface water budget than in the A1Bspr simulation but less grid boxes are affected by these changes.

Hydrological extremes

The number of consecutive dry days is particularly impacted for HH (Fig. 5.19, second row). The A1B scenario leads to a nearly doubling of the consecutive dry days particularly in the city core nearby the river Elbe. Both, the A1Bspr and the A1Bcom reduce this impact of the A1B scenario due to a reduction of the number of consecutive dry days also especially in the city core nearby the river Elbe. Also for B (Fig. 5.20, second row), the A1B scenario causes an increase in the number of consecutive dry days, nevertheless not urban specific. In the downwind area of B (north-east) a domain of reduced consecutive dry days is shown. The A1Bcom scenario leads to no visible impacts on B in terms of the number of consecutive dry days.

While the number of dry periods does not change due the A1B, A1Bspr or the A1Bcom scenario for HH (Fig. 5.19, first row), impacts are visible for B (Fig. 5.20, first row): On the one hand, the A1B leads to an increase of dry periods in the domain of B and around (therefore not urban specific), both the A1Bspr and the A1Bcom scenario reduce this climate change signal on the other hand by a reduction of dry periods compared to the A1B scenario for B.

The number of precipitation days decreases due to the A1B scenario area wide for HH and B with no urban specific pattern (Fig. 5.19, third row and Fig. 5.20, third row). For B, the A1Bspr and the A1Bcom scenario compensate this effect slightly due to a low increase of the number of precipitation days.

Only changes in the concentration of GHG in the A1B simulation lead to a decrease of wetperiods in DJF, MAM and SON in NG and an increase of wetperiods in JJA (Fig. 5.20). However, the applied land-cover changes in A1Bspr and A1Bcom dampen these effects of the A1B scenario.

In contrast to lower numbers of wet periods, the number of intense and heavy precipitation days is increased considerably by the A1B scenario in DJF, MAM and SON for 2090 to 2099 (Fig. 5.20 and Fig.5.20). Although, there can be seen an increase of precipitation events in MAM, the number of dry periods is increased by the A1B scenario at the same time (Fig. 5.20). Therefore, due to the A1B scenario, there will be more and heavier precipitation events in DJF at the end of the century. This can be explained by higher temperatures and higher integrated water vapor contents at the same time (Fig. 5.20).

5.3.5. Changes in the diurnal cycle

Impacts due to the A1B, A1Bspr and the A1Bcom scenario are analysed in terms of diurnal variations in the following.

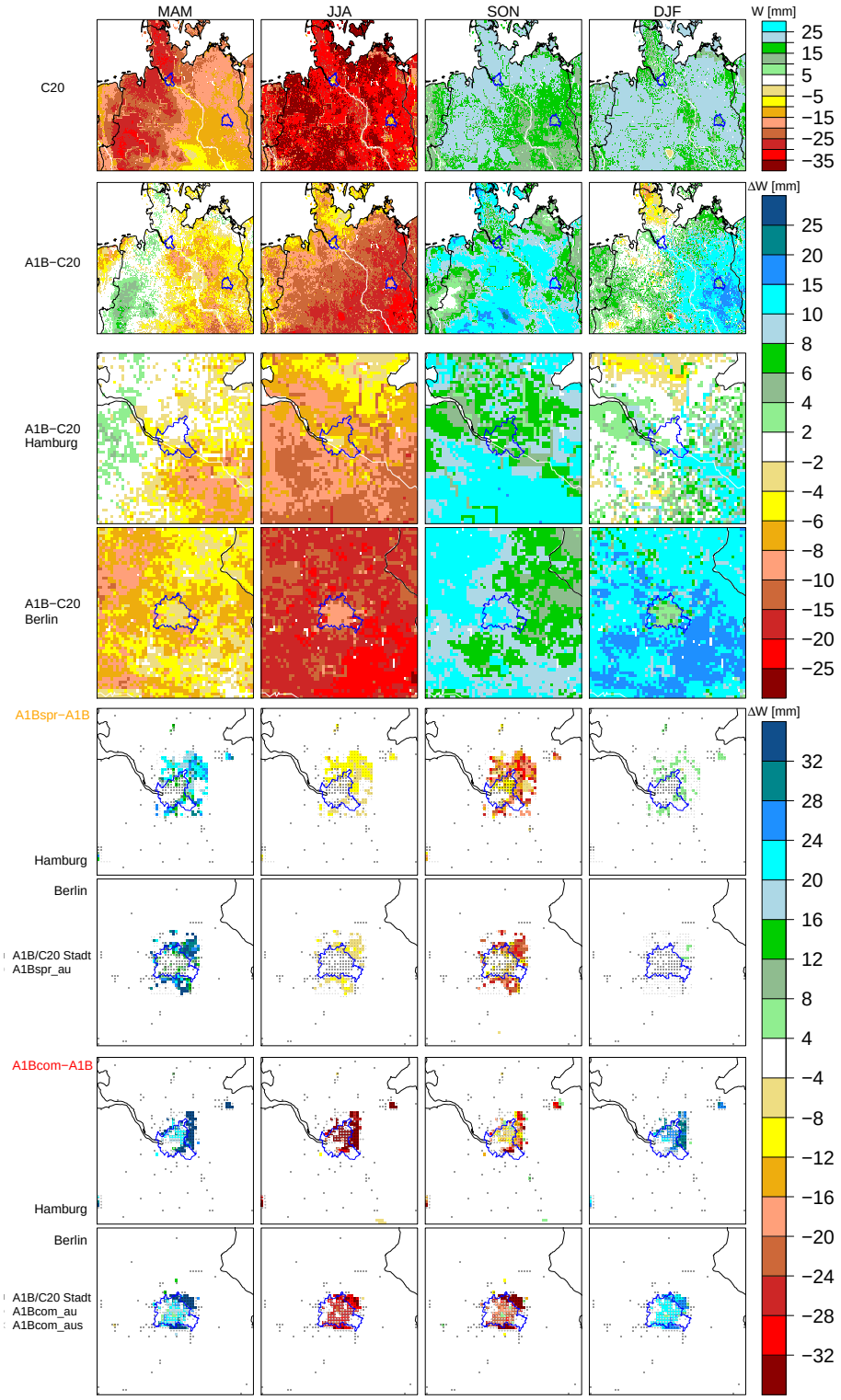

Figure 5.18.: Same as Fig. 5.12 but for the monthly surface water budget in mm.

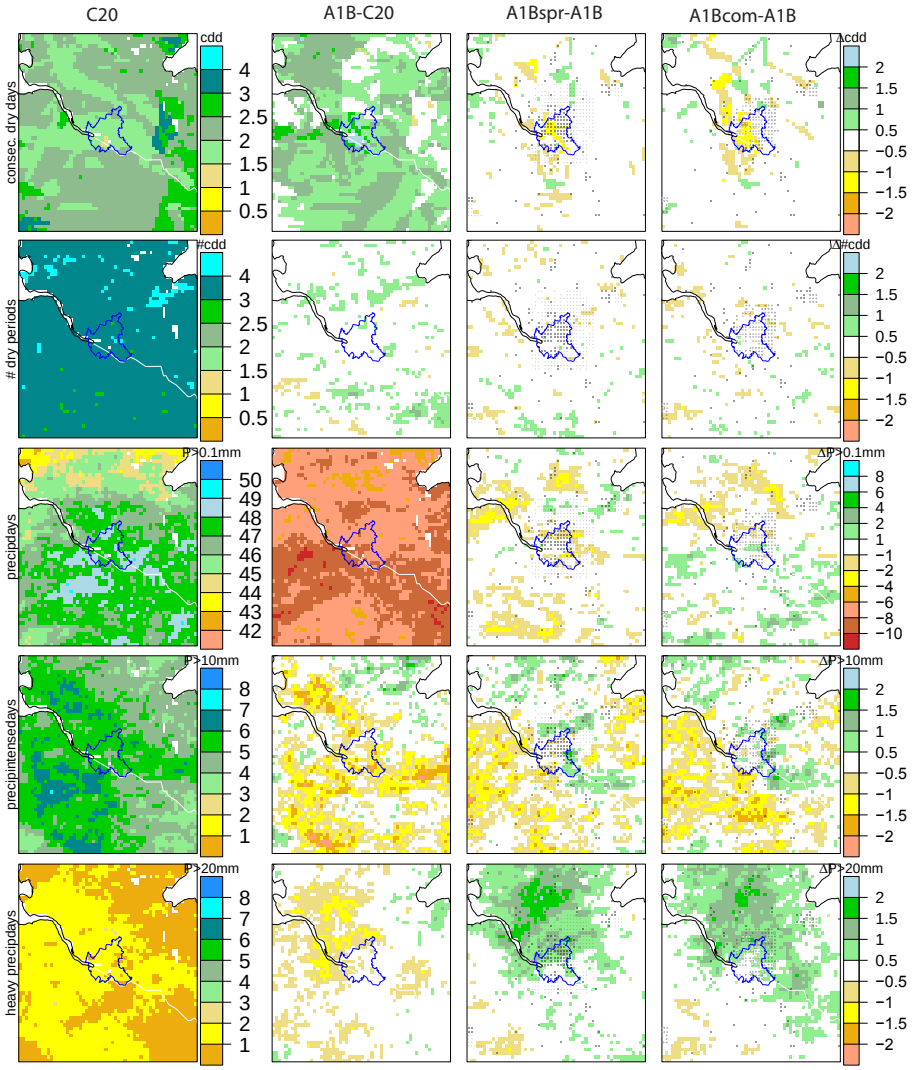

Figure 5.19.: Shown are hydrological (extreme) events for JJA for Hamburg: consecutive dry days, number of dry periods, precipitation days, intense precipitation days and heavy precipitation days (from top to bottom).

2 m temperature

In MAM, the C20 simulation shows that B reaches a higher daytime T_{2m} than NG and HH. HH shows slightly lower temperatures at night (Fig. 5.21). The A1B scenario leads to a clear reduction of the diurnal variation of T_{2m} for all domains. Overall, the T_{2m} increase throughout the diurnal cycle- especially at night by about 2.3 to roughly 2.5 K and for HH even more than 2.5 K. The lowest T_{2m} increase occurs around noon (+1.5 K for B and 1.7 K for NG and HH). Due to the A1Bspr scenario, the MAM daytime T_{2m} is increased by about 0.2 K at noon in HH and B. There are no impacts on the mean T_{2m} of NG by the A1Bspr scenario in MAM. A1Bcom leads to a T_{2m} increase throughout the diurnal variation of HH and B in MAM. Same as for A1Bspr, the mean diurnal cycle of NG is not affected. A1Bcom leads to a T_{2m} increase of 0.8 K at 14 UTC both, in HH and B. For HH, this T_{2m} increase weakens after the peak at 14 UTC to a minimum T_{2m} increase at 7 UTC (+0.3 K). For B, the maximum T_{2m} increase of 0.8 K persists until 20 UTC and

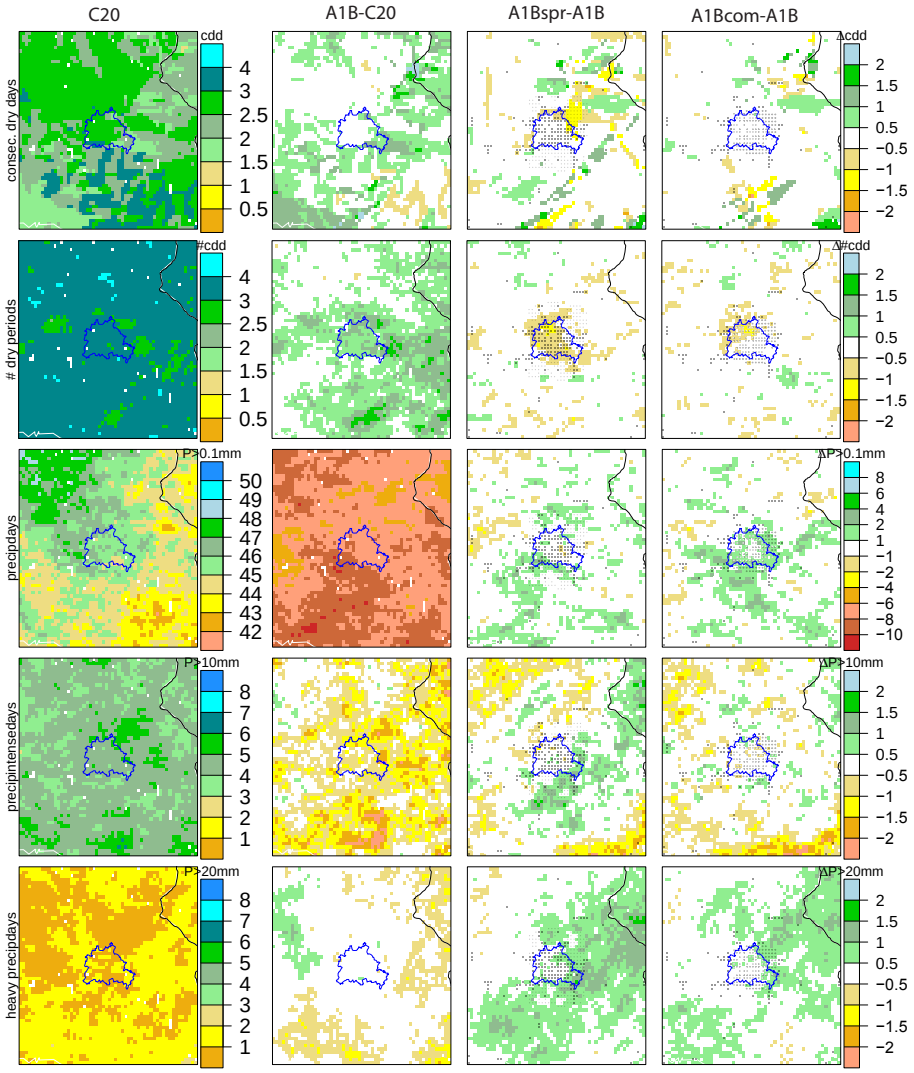

Figure 5.20.: Same as Fig. 5.19 but for Berlin.

finally weakens to an increase of 0.4 K at 7 UTC.

Smallest impacts on the diurnal cycle of T_{2m} by the A1B scenario occur in JJA. Same as in MAM, a T_{2m} increase throughout the diurnal variation occurs. Again, especially the night-time temperatures are increased (+2.1 K) in NG, B and HH. At daytime, there is an increase in T_{2m} of 1.8 K for the whole domain and B and a lower T_{2m} increase of 1.6 K for HH. However, the land-cover changes in A1Bspr and A1Bcom show largest impacts on the diurnal T_{2m} cycle in JJA. In the A1Bspr simulation the diurnal T_{2m} variation is strengthens with a maximum increase of about 0.3 K for HH and 0.4 K for B at 14 UTC. In the A1Bcom simulation impacts on T_{2m} are different in JJA for HH and B. T_{2m} of B is particularly increased at night-time by up to 0.9 K against midnight and lowest increased by about 0.4 K in the morning at 10 UTC. Whereas in HH, the A1Bcom scenario leads especially to a T_{2m} increase at daytime (+0.8 K at noon) and a lower T_{2m} increase at night (about 0.5 to 0.7).

In SON, the A1B scenario leads to an increase in T_{2m} throughout the day. Especially at night-

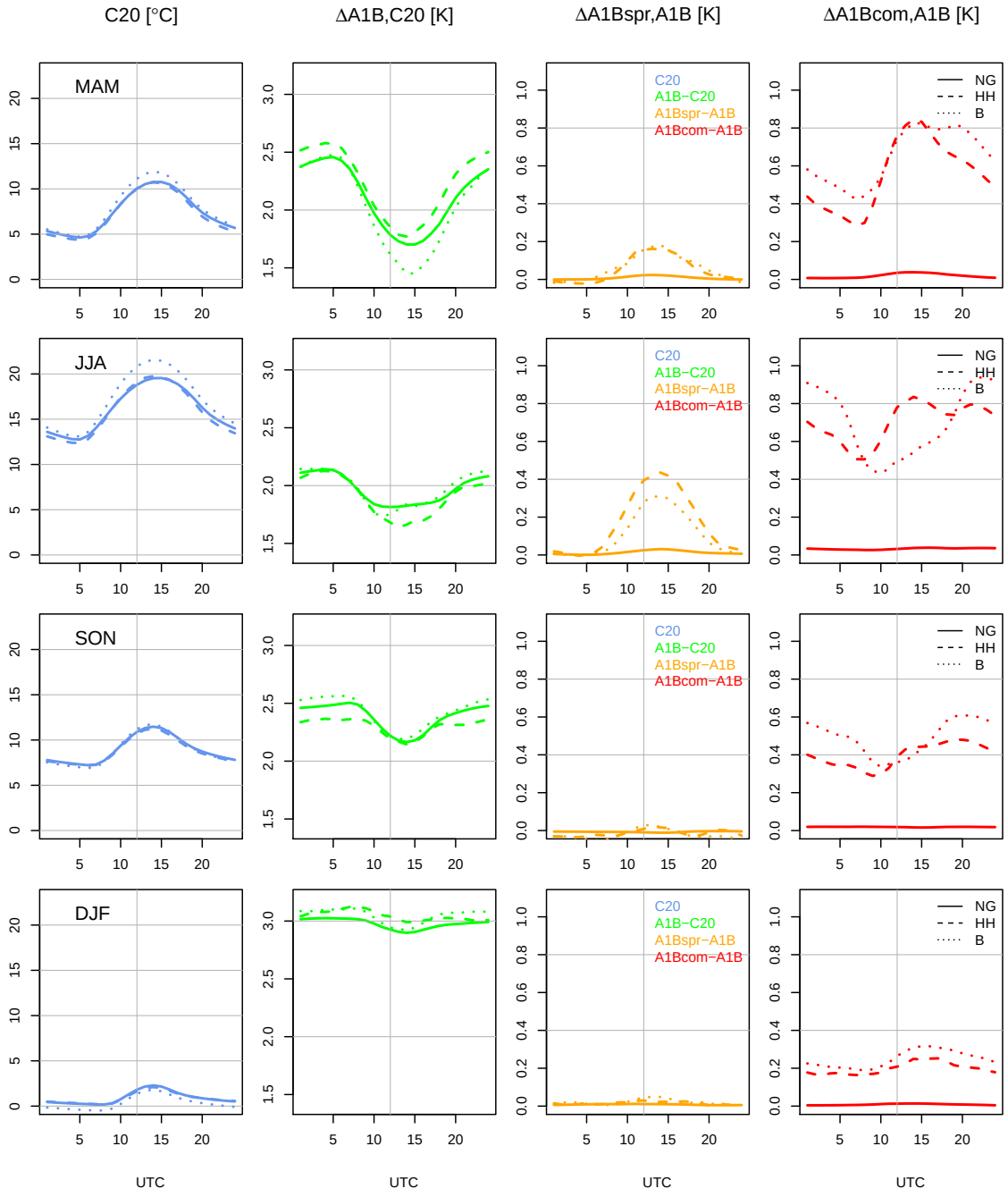

Figure 5.21.: Diurnal cycle of the 2 m temperature (T_{2m}) of the C20 simulation, and changes due to the A1B (A1B-C20), the A1Bspr (A1Bspr-A1B) and the A1Bcom (A1Bcom-A1B) scenario (from left to right). From top to bottom each season is shown: MAM, JJA, SON and DJF.

time (+2.5 K for NG and B, and +2.4 K for HH), T_{2m} is increased. At noon, the lowest increase of about 2.2 K occurs in T_{2m} (NG, B and HH). Impacts due to the A1Bspr scenario are very small in SON. There is a slight T_{2m} increase at noon and a slight T_{2m} decrease at nighttime for HH and B. In contrast, the A1Bcom simulation shows still particular impacts: For HH and B, T_{2m} is increased for the whole diurnal cycle (+0.3 to +0.5 for HH and 0.35 to 0.6 K for B). Same as for JJA, the A1Bcom scenario increases T_{2m} especially at night-time in B. In HH, impacts on T_{2m} are strongest in the afternoon.

The slightly lower T_{2m} of B compared to NG in DJF (Fig. 5.3) is visible throughout the day. Following the A1B scenario, T_{2m} of B will increase more than the mean monthly T_{2m} of NG at the end of the 21st century in DJF (Fig. 5.21, first two columns). This means, the difference in T_{2m} between B and NG might be reduced in DJF in future. Also for HH a larger increase in T_{2m} than for NG is illustrated. In general, the increase of the GHG concentration in the A1B scenario causes a T_{2m} increase of about 3 K throughout the diurnal cycle in DJF. Only at daytime, the T_{2m} increase is slightly lower.
A1Bspr leads to slightly higher T_{2m} in HH and B in DJF but there is no impact on the diurnal cycle of T_{2m} for NG. A1Bcom shows no impact on the mean diurnal cycle of NG, too. However, for HH and B an additional T_{2m} increase of more than 1.8 K occurs throughout the day. At late noon (15-16 UTC) the largest T_{2m} increase of the day due to the A1Bcom scenario can be seen (HH: +0.25 K, B: +0.3 K).

To conclude, while the A1B and the A1Bcom scenario lead to considerable impacts on the whole diurnal cycle of T_{2m}, the A1Bspr simulation shows only at daytime effects on T_{2m}. This can be explained by the issue that in the A1Bspr scenario no soil texture is changed and therefore the heat capacity is the same as in the A1B scenario. Whereas, the soil texture for the A1Bcom scenario is significantly different. The A1B scenario leads to lower T_{2m} variations throughout the day for all seasons. A1Bspr dampens this effect in MAM and JJA by an increased daytime T_{2m} and therefore a more pronounced diurnal cycle of T_{2m} is shown for HH and B. The A1Bcom scenario impacts different on the diurnal T_{2m} variation such as that only in DJF the daytime temperature is mostly increased in the course of the day. In SON, the diurnal variation in T_{2m} is additionally reduced due to the A1Bcom scenario. Here, same as in the A1B scenario alone, particularly night-time temperatures are increased. In MAM, the A1Bcom scenario causes increases in T_{2m} particularly at daytime in HH and B. In JJA, the effects of the A1Bcom scenario differ considerably for HH and B. Whereas for HH, day-time temperatures are mostly increased, the night-time temperatures are particularly increased in B.

Explanations for the diurnal variations of temperature changes

As seen for the changes in the annual T_{2m} cycle, also the changes in the diurnal T_{2m} cycle can be widely explained by another partitioning of λE and H as illustrated in Fig. 5.22.

As already formulated in Section 5.3.2, the increased T_{2m} in DJF could be at least partly a result of the increased λE flux at this time. Fig 5.22 (first row) shows an increase in λE at daytime, which underlines this assumption. In DJF, increased λE to the atmosphere could lead to an increase in cloud cover. This is usually followed by more evaporation of water and an increase of the IWV amount of the atmosphere which again leads to more heat in the atmosphere, and so on, in a positive feedback cycle.

In contrast, T_{2m} increases in the A1Bcom simulation are prominently caused by decreased λE fluxes. The increased T_{2m} results in increased H fluxes during all seasons for both cities. Only the diurnal variation and the amplitude of surface fluxes is slightly shifted for HH and B.

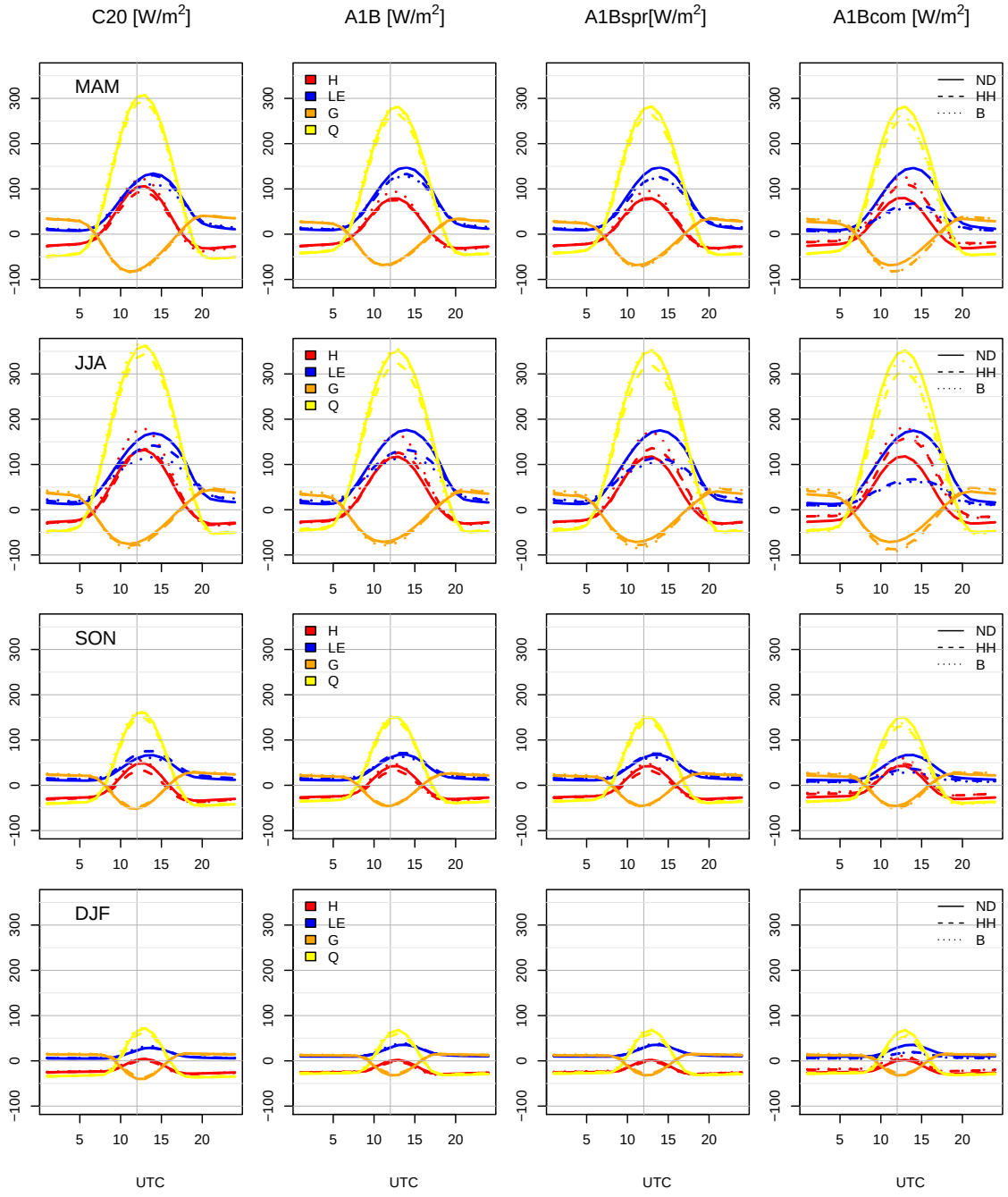

Figure 5.22.: Diurnal cycle of the surface energy budget: sensible heat flux (H), latent heat flux (λE), ground heat flux (G) and the net radiation budget (Q) for the C20 (first column), the A1B (second column), the A1Bspr (third column) and the A1Bcom (last column) simulation for each season: MAM, JJA, SON and DJF (from top to bottom).

Hydrological cycle

In Fig. 5.23 the diurnal variation of total precipitation (P), surface evaporation (E) and the surface and the subsurface run-off are shown. For NG, there are low variations in the daytime of P occurrences in the C20 simulation during all seasons in Fig. 5.23. Only in MAM and JJA, two small

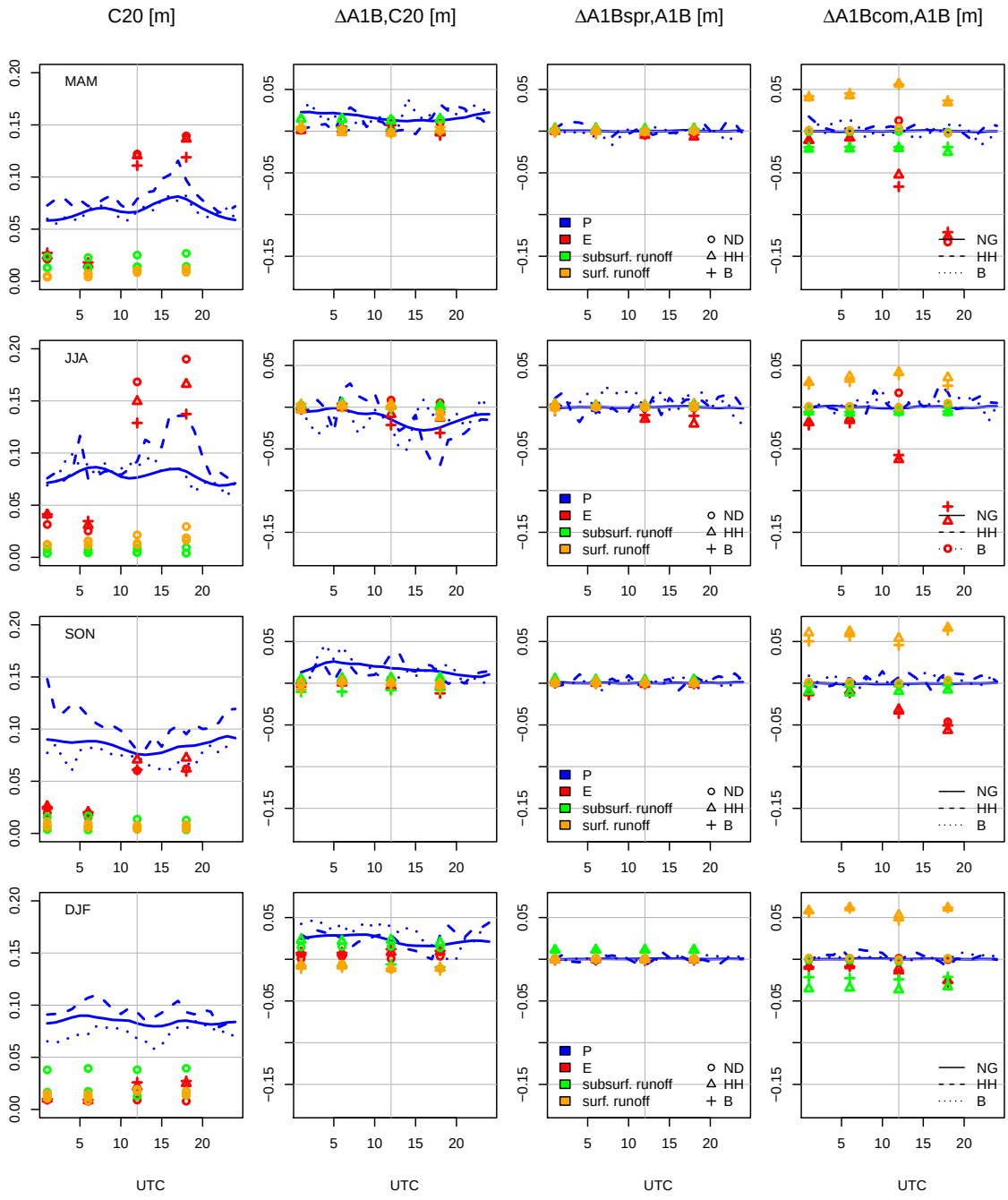

Figure 5.23.: Same as Fig. 5.21 but for total precipitation (P), surface evaporation (E), subsurface run-off and surface run-off.

peaks are shown: one in the early morning and one in the late afternoon. The distribution of P throughout the day is coupled to E. Highest E sums are shown in the afternoon in MAM and JJA. In MAM, JJA and also in SON, the E rate at night (0 UTC) is even slightly higher than at 6 UTC. This causes the small P peak in the early morning in the C20 simulation for MAM and JJA. In HH, higher P amounts in the course of the day occur throughout all seasons. In MAM and JJA, a clear P peak in the late afternoon is visible (0.11-0.13 mm/h) for HH. In B, lower P amounts throughout the day are shown in DJF and SON compared to HH.

The A1B scenario leads to an increase in P throughout the diurnal variation in DJF, MAM and SON for HH, B and NG, respectively. In DJF and MAM, more P occurs especially in the evening against 19 to 20 UTC in HH than in the mean for NG. In B, a large increase in P due to the A1B scenario is shown throughout the diurnal variation in DJF. However in JJA, P is more pronounced reduced in the afternoon for NG and HH in the A1B simulation. This could point to a decrease of convective precipitation. The decrease of P in the afternoon and also the illustrated increase of P in the morning means for HH that the main P amount is shifted from the afternoon to the morning. For B, several variations in the rate of change of P are illustrated in JJA. However, also here, P reductions dominate. The precipitation decreases for NG, HH and B are coupled to decreased E sums especially in the afternoon.

Both land-cover scenarios, A1Bspr and A1Bcom, lead to low P increases throughout the diurnal variation for HH and B in JJA. This effect counteracts to the climate change signal of the A1B scenario in JJA. In the rest of the year, impacts on the diurnal variation of P due to the A1Bspr and the A1Bcom scenario have no clear trend and are very low.

To conclude, impacts on the diurnal cycle of P are largest due to the A1B scenario. Whereas, impacts on E, surface and subsurface run-off are considerably higher for the A1Bcom simulation.

5.4. The relation between urbanized land and countryside

Impacts of the land-cover scenarios in the A1Bspr and the A1Bcom simulation are strongest, when changes from arable or rural land to urban land are applied as shown in Section 5.3.4. But also the unmodified adjacent areas are confronted with effects due to the modified urban areas as seen e.g. for the temperature (Fig. 5.12), for moisture (Fig. 5.17) and the wind speed (Fig. 5.14). This section aims at quantifying rural-urban differences which are caused by combined effects of land-cover and GHG concentration changes in terms of urban heat island effects (UHI) and urban impacts on precipitation (UIP). Additionally, effects in dependence on the position in the surrounding of the city core are addressed. As done in the previous section, the focus is put on Hamburg (HH) and Berlin (B).

To differentiate between urban and rural grid boxes with different characteristics, the domain is divided into four different zones as shown in Fig. 5.24.

The **"urban city core"** encompasses the urban grid boxes (from "today" as used in the C20/A1B simulation) within the political borders of HH and B respectively, which are not water bodies (size of the urban city core of HH: 51 grid boxes and the urban city core of B: 83 grid boxes). **"A1Bcom suburban"** describes the urban grid boxes which are added due to the A1Bcom scenario. Therefore, this domain can be viewed as suburban district of the A1Bcom scenario (HH: 67 grid boxes, B: 49 grid boxes). **"A1Bspr suburban"** declares the part of the added urban grid boxes following the A1Bspr scenario excluding the urban grid boxes of the A1Bcom scenario and water bodies (HH: 172 grid boxes, B: 107 grid boxes). The **"rural environment"** declares the area around the geographical centre of HH (53.5792°N and 10.0233°E) and B (52.5013°N and 13.4025°E) respectively within a maximum distance of 50 km, excluding urban grid boxes (from the A1B, the A1Bspr and the A1Bcom scenario) and water bodies (HH: 654 grid boxes, B: 647 grid boxes).

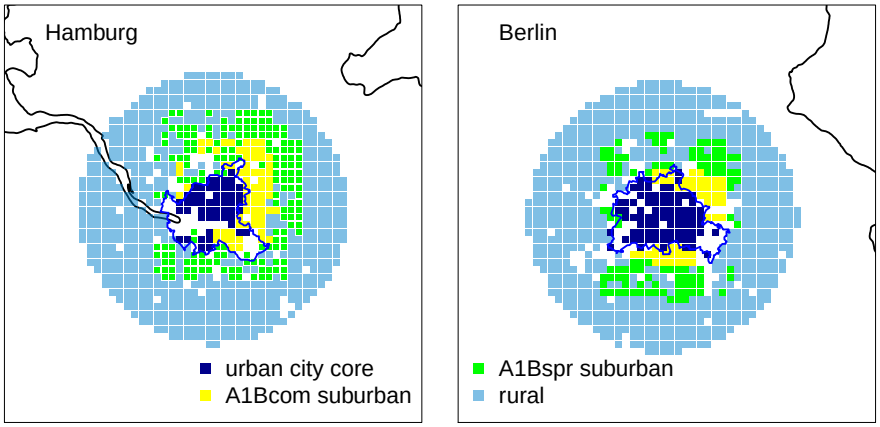

Figure 5.24.: Distinction between the urban city core, A1Bcom suburban, A1Bspr suburban and the rural environment for Hamburg (left) and Berlin (right).

The maximum distance of 50 km was chosen to avoid large impacts due to the North Sea and the Baltic Sea in respect to HH.

These subdivisions allow a more specific evaluation of urban-rural effects within the A1B, the A1Bspr and the A1Bcom scenarios.

5.4.1. Urban heat island effects

A prominent measure of urban-rural effects on weather and climate is the urban heat island (UHI) effect (Section 2.2.1). Although, this study does not account for e.g. anthropogenic heat terms and a specific heat storage in terms of e.g. urban materials, clear temperature differences between the urban city cores and the surrounded rural areas can be observed in the frame of simulation results (e.g. Fig. 5.12).

In order to quantify the UHI in the A1B, A1Bspr and A1Bcom simulation, the annual cycle of differences in the monthly mean T_{2m}, $T_{max(2m)}$ and $T_{min(2m)}$ between the urban city core and the rural environment (ΔT_{2m}, $\Delta T_{max(2m)}$ and $\Delta T_{min(2m)}$) are analysed for HH and B in Fig. 5.25. Although, there are no changes in the land-cover in the A1B scenario, ΔT_{2m} and $\Delta T_{max(2m)}$ increase compared to the C20 simulation in the warm month (April to September). During that time, the differences between the A1B and the C20 simulation are similar for both, ΔT_{2m} and $\Delta T_{max(2m)}$. The A1Bspr scenario leads to nearly no impacts on $\Delta T_{min(2m)}$ but visible effects on ΔT_{2m} and considerable effects on $\Delta T_{max(2m)}$ of up to 0.5 K are drawn (HH: May to August and B: May to September). The land-cover changes in the A1Bcom scenario show most pronounced impacts on the differences between the urban city core and the rural environment. Even ΔT_{2m} is increased by more than 1 K.

These results are contradictory to the actual characteristic of an UHIs. Usually, $\Delta T_{min(2m)}$ is assumed to represent the nocturnal UHI signal best by higher values than for ΔT_{2m} or $\Delta T_{max(2m)}$. Here, $\Delta T_{max(2m)}$ is larger than ΔT_{2m} and this again larger than $\Delta T_{min(2m)}$ (Fig. 5.25). This different effect of the A1Bspr and A1Bcom scenario on the ΔT_{2m} is basically the result of the not included anthropogenic heat and the not parametrized urban materials for large surfaces (if houses are taken into account separately). Usually the at daytime heated urban domain stores this heat for longer time-spans than the rural environment and leads therefore particularly in the late eventing to higher temperatures in the city than in the rural environment.

In the upper part, mean monthly values of the differences between the urban city core and the rural environment are evaluated. Nevertheless, studies have shown that temperature differences between urban and rural areas are clearly more pronounced under specific weather conditions (e.g Hoffmann et al., 2012). Low wind speeds and low cloud cover benefit the creation of an UHI. Therefore, both variables are used to select UHI favouring days as it was done by Arnds et al. (2015). Only days with a mean wind speed (V_{10m}) of less than 2 m/s and a total cloud cover (CLCT) of less than 50% are accounted for. To select UHI favouring dates, the rural environment was filtered based on these conditions. The rural environment is taken as reference to exclude urban impacts on V_{10m} and CLCT.

The ΔT_{2m} for UHI favouring dates is illustrated (Fig. 5.26 for HH (top) and B (bottom) for each season. Only UHI dates are selected which are valid for all simulations including the A1B GHG scenario: A1B, A1Bspr and A1Bcom. In general, there are clearly more often UHI favouring conditions for B (104) than for HH (48). Most of the UHI favouring conditions in both cities occur in JJA. Largest UHI effect occur usually in the late evening or rather at night. Therefore, in the following analysis, only mean ΔT_{2m} between 21 and 23 UTC are regarded.

In the A1B simulation, the urban city core shows slightly negative ΔT_{2m} in MAM, SON and DJF in the evening of UHI favourable days in HH (Fig. 5.26). Also in B ΔT_{2m} is negativ in SON and DJF. However, in MAM slightly positive ΔT_{2m} are shown for B. For both cities, the A1B scenario shows ΔT_{2m} of about 0.3 K during UHI conditions in JJA.

The A1Bspr simulations shows nearly similar results as for HH and for B in SON and DJF and for HH also in MAM. A clear increase in the mean ΔT_{2m} of HH and B occurs in JJA. The A1Bspr scenario strengthens the UHI effect by an additional ΔT_{2m} of about 0.3 K in HH and B resulting in a ΔT_{2m} of about 0.7 K between the urban city core and the rural environment.

It becomes evident that the A1Bcom scenario leads to clear higher ΔT_{2m} of both cities from

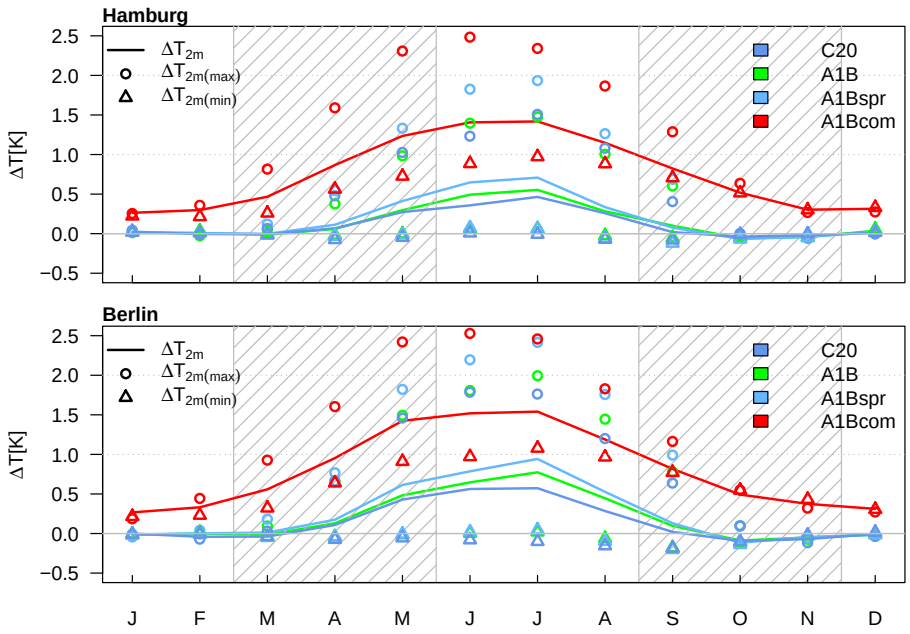

Figure 5.25.: Annual temperature cycle of the 2 m, 2 m maximum and 2 m minimum temperature differences between the urban city core and rural environment (as defined in Fig. 5.24) for Hamburg (top) and Berlin (bottom).

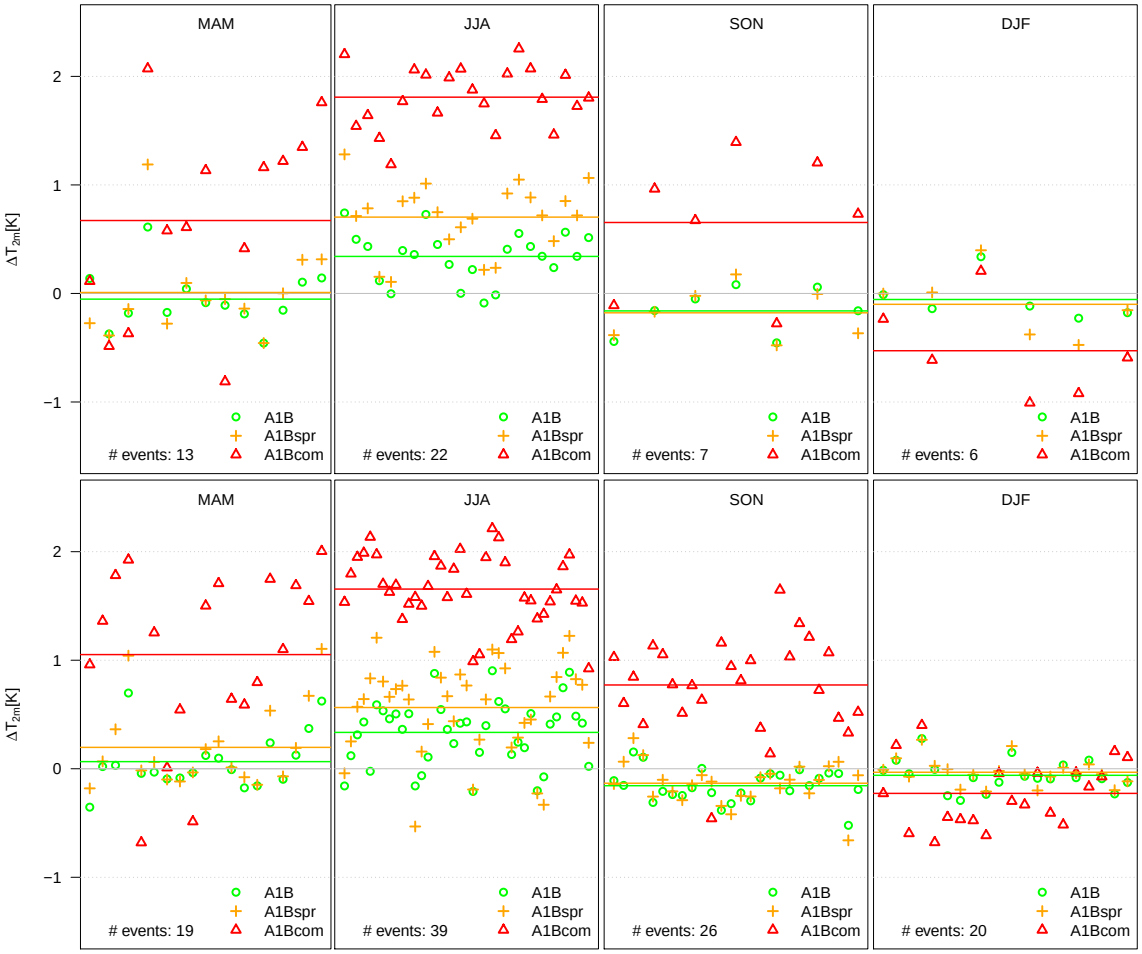

Figure 5.26.: 2 m temperature differences in the evening (21-23 UTC) between the urban city core and the rural environment for Hamburg (top) and Berlin (bottom) during favourable UHI conditions. Mean seasonal UHI values are indicated by solid horizontal lines in the corresponding colour of each scenario. The number of considered UHI days (# events) is presented in the left corner of each box.

March to November compared to the A1B or the A1Bspr scenario. Largest differences in ΔT_{2m} appear in JJA: +1.8 K in HH and +1.6 K in B. In DJF, same as in the A1B and the A1Bspr simulations, the A1Bcom scenario leads to lower ΔT_{2m} (-0.5 K for HH, -0.2 K for B). In contrast to the A1B and the A1Bspr simulation, the A1Bcom simulation shows also clear UHI effects in MAM and SON (ΔT_{2m} for HH: +0.7 K for MAM and SON, ΔT_{2m} for B: +1.1 K in MAM and 0.8 K in SON). While the UHI effect in the A1Bcom simulation is larger in HH than in B in JJA , the transitional seasons, MAM and SON show stronger UHI effects for B. Whereas in DJF, a more pronounced cool island effect is visible for HH compared to B. This differences might be attributed to the different soil textures in the rural environments of HH and B (Fig. 5.10).

UHI effects experienced by citizens of modified urban zones

Temperature impacts due to the different scenarios of this chapter as might be experienced by citizens of modified urban grid boxes are analysed in the following. This is done based on the assumption that citizen do not move to other grid boxes. People who originally lived in a rural

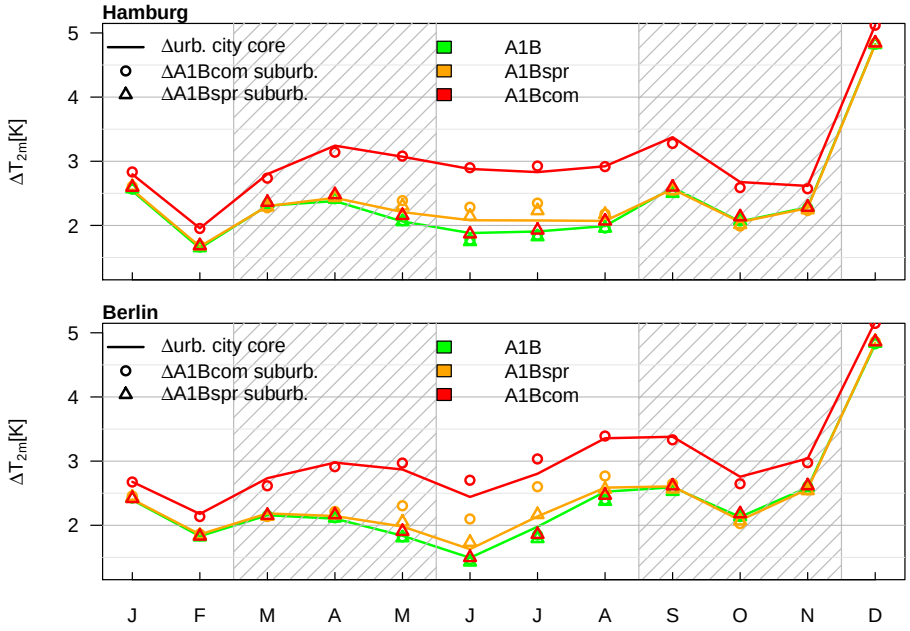

Figure 5.27.: Monthly mean 2 m temperature differences (ΔT_{2m}) of the city core, the A1Bcom suburban and the A1Bspr suburban zone in the A1B, A1Bspr and A1Bcom simulation compared to the corresponding zones in the C20 simulation for Hamburg (top) and Berlin (bottom).

environment seem to experience much larger climate effects than citizens of the original urban areas as suggested by the discussion of the regional distribution of impacts due the A1B, the A1Bspr and the A1Bcom scenario. Furthermore, the intention of this section is to figure out which people might have to deal with the most pronounced impacts due to the A1Bspr and the A1Bcom scenario.

Therefore, a more detailed analysis of subdivisions of HH and B is conducted in Fig. 5.27. It is differentiated between the urban city core, the suburban area of the A1Bcom (A1Bcom suburban) scenario and the suburban area of the A1Bspr scenario (A1Bspr suburban).

In Fig. 5.28 the monthly mean ΔT_{2m} values of the subdivisions of HH and B in the A1B, A1Bspr and A1Bcom simulation, are compared to the monthly mean ΔT_{2m} values of the corresponding domains in the C20 simulation.

It is shown that the A1B scenario causes nearly the same monthly mean ΔT_{2m} for the three defined subdivisions. Only the domain of "A1Bspr suburban" therefore the more distant rural surrounding shows a slightly lower ΔT_{2m} increase in JJA. Nevertheless, the ΔT_{2m} changes in the subdivisions are similar to the ΔT_{2m} changes for the whole city domain of HH and B shown in Fig. 5.3, a, right.

The A1Bspr scenario leads to the strongest ΔT_{2m} increases in the domain of "A1Bcom suburban" that means the extended city core which is framed by urban shapes and which was originally rural (HH: May to July, $\sim$ 2.2 K, in B: May to August, +2.1 up to 2.9 K). These additional increases in ΔT_{2m} are up to 0.5 K larger for HH and up to 1 K larger for B compared to the ΔT_{2m} in the A1B simulation. Also, the "A1Bspr suburban" zone is affected by a slightly higher increase in T_{2m} than the urban city core from May to July due to the A1Bspr scenario.

In the same domain ("A1Bspr suburban"), nearly no impacts due to the A1Bcom scenario are

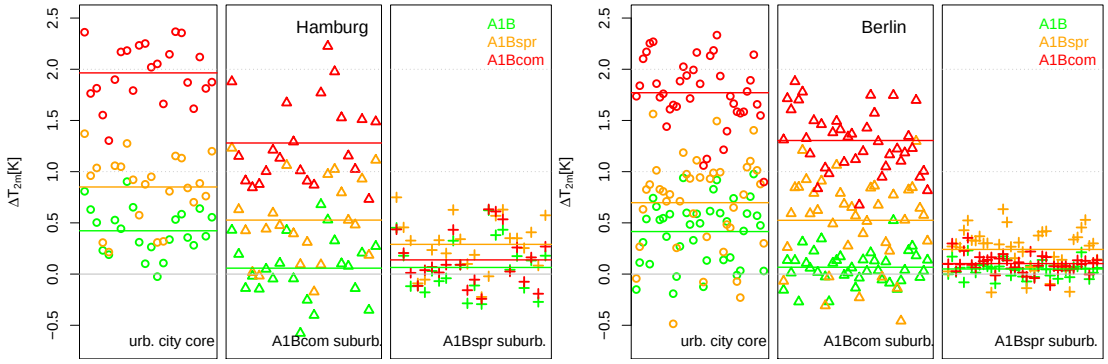

Figure 5.28.: Same as Fig. 5.26 but only for JJA differentiated for the urban city core, A1Bcom suburban and A1Bspr suburban for Hamburg (left) and Berlin (right).

detectable. However, strongest impacts on T_{2m} due to the A1Bcom scenario occur in the urban city core and in the A1Bcom suburban domain. For HH, only in July and for B from May to August, the A1Bcom suburban area experiences slightly stronger T_{2m} increases compared to the urban city core. During the rest of the year, the urban city core shows the largest T_{2m} increases. Compared to the A1Bspr simulations there are lower T_{2m} differences between the urban subdivisions in the A1Bcom simulation. However, due to the A1Bcom scenario, citizen of HH and B are faced by T_{2m} increases of up to 1.8 K compared to the A1B scenario.

5.4.2. Urban impacts on precipitation

To investigate the impacts of the modified urban structures on the occurrence of precipitation (P), daily P sums are separated according to wind directions in 850 hPa data from the rural environment (Fig. 5.24). For this, daily mean wind directions are computed in 850 hPa height for the rural environment of both, Hamburg and Berlin. The daily mean wind directions are sorted to the directions north (N, 338°-22°), north-east (NE, 23°-77°), east (E, 78°-112°), south-east (SE, 113°-157°), south (S, 158°-202°), south-west (SW, 203°-247°), west (W, 248°-292°), north-west (NW, 293°-337°). Corresponding to dates with wind directions from one direction, the mean daily precipitation sum is calculated for each wind direction (Fig. 5.4.2 and Fig. 5.30).

During winds from the N and NE lowest P for HH occurs as illustrated in Fig. 5.4.2. This low P under N-wind conditions is caused by the lee effect of the Scandinavian mountains (Lefebvre and Rosenhagen, 2008). Wind from the N also occurs very rarely. All scenarios (A1B, A1Bspr and A1Bcom) lead to an increase of P in this area during N-wind events. Also due to all scenarios, P in the NE and the SW of HH is particularly increased. The A1Bcom scenario causes lower P in the downwind area in the S of the city and in the SE than the A1B and the A1Bspr scenario during N-wind events. In general, the A1B and the A1Bspr scenario lead to more P under the condition of N-winds.

During NE-winds, the A1Bspr scenario leads to increases in P in the upwind area of HH. As shown in Fig. 5.14, here, the wind speed is especially reduced due to the land-cover changes in the A1Bspr scenario. The number of NE and E wind events is reduced by up to about 20% and more than 30% respectively. It is clearly illustrated that the large P also mainly associated with winds from the SW and the W. All scenarios lead to an increase in P in the N and the NW of HH for wind inflow from the W and SW. For wind inflow from the SW, the A1Bspr scenario intensifies P in the NW of HH. For winds from the W, the A1Bcom scenario leads to a clear increase in P in the

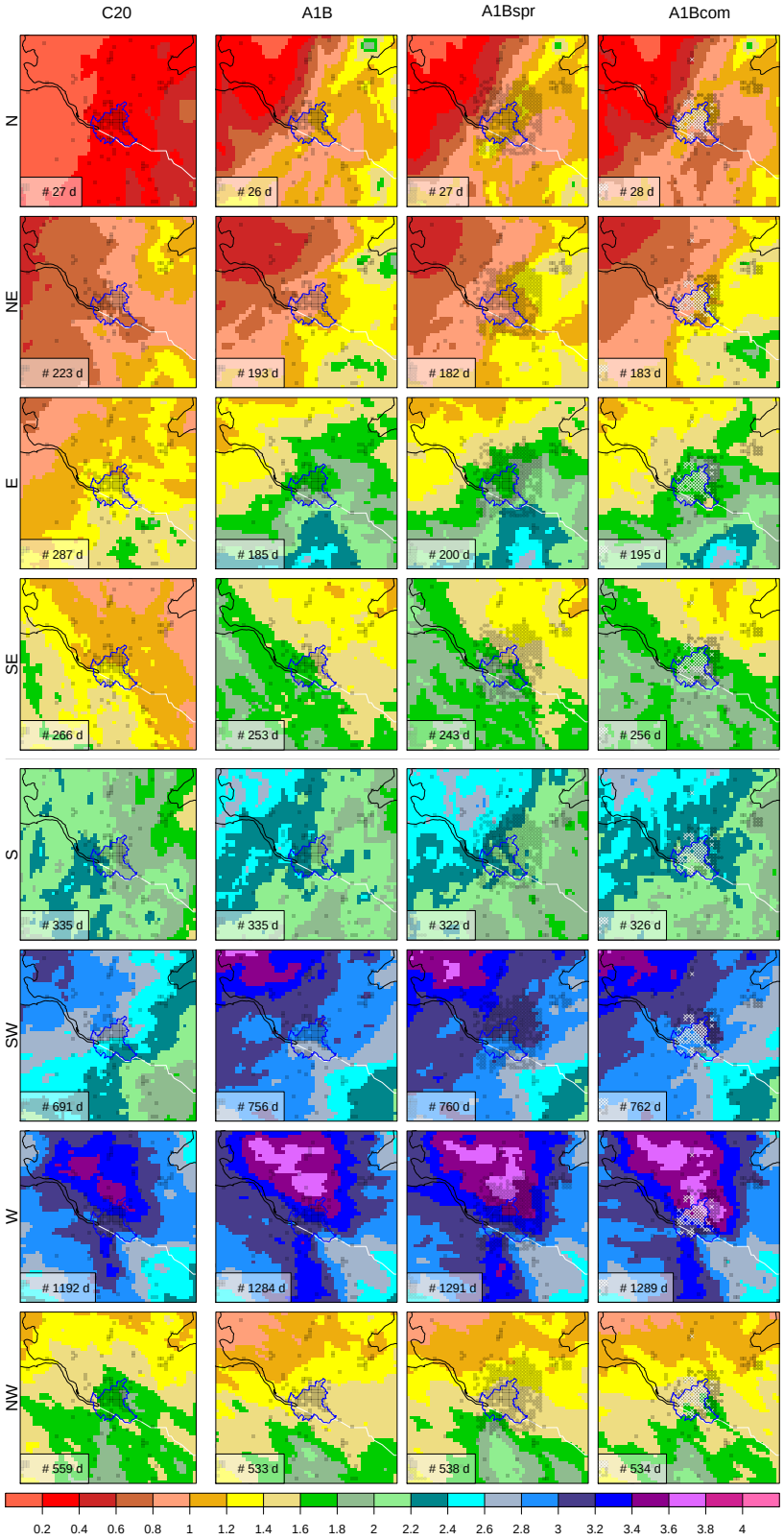

Figure 5.29.: Shown are the mean daily precipitation sums (P) in mm for different wind direction on the 850 hPa level in the rural environment of the city of Hamburg. In each row, the results of the A1B, the A1Bspr and and A1Bcom simulations are shown for wind directions from N (top) to NW (bottom). The boxes in the bottomleft corner of each plot indicate the number of days with the corresponding mean wind direction.

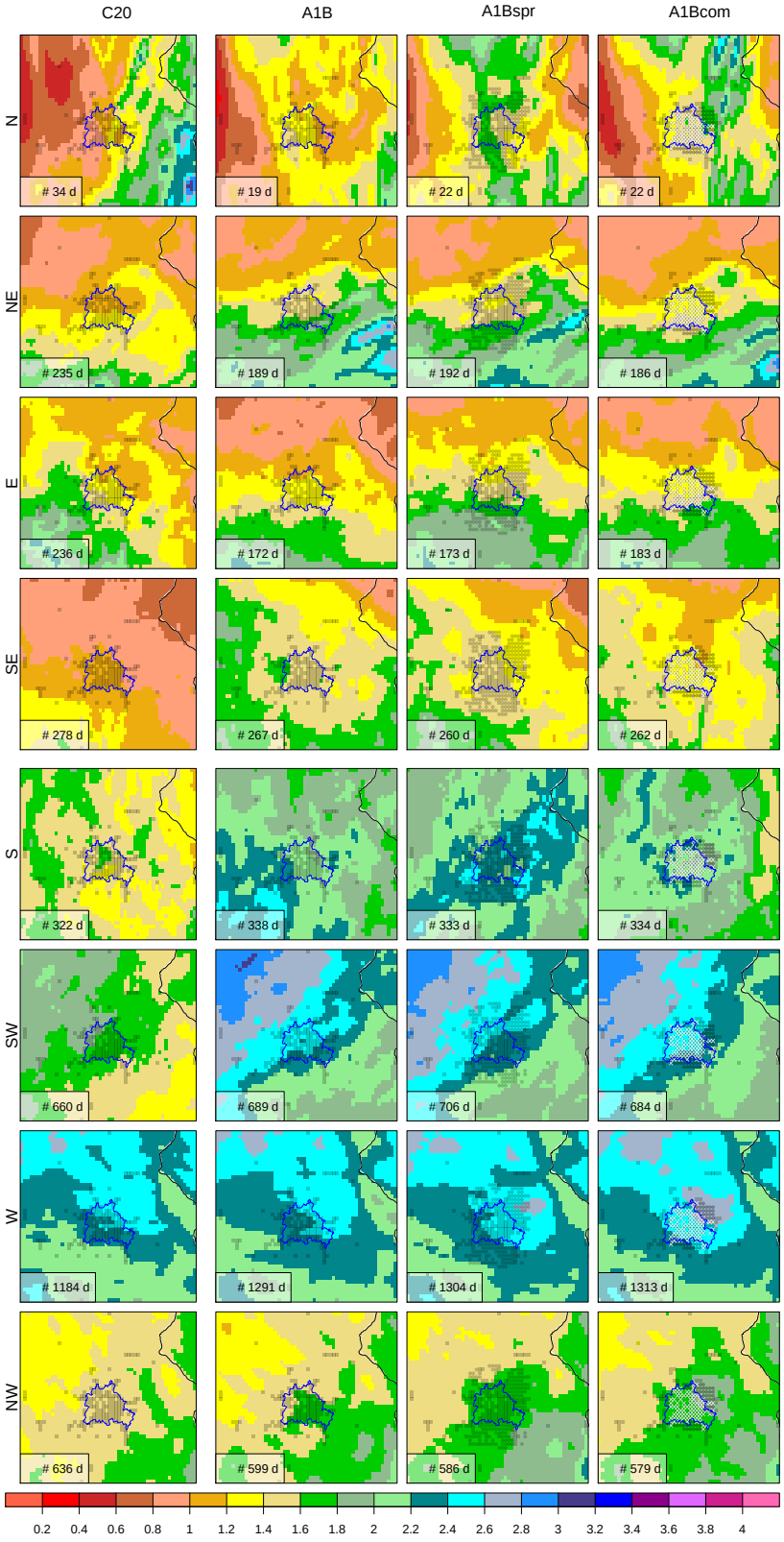

Figure 5.30.: Same as Fig. 5.4.2 but for Berlin

downwind area of HH- especially above the additional urban grid boxes in the E of the city and in the near surrounding.

Same as for HH, wind from the N occurs very rarely in B (Fig. 5.30). The A1B scenario leads to more P during N-wind conditions, the A1Bspr as well as the A1Bcom scenario lead to an additional increase of P during these conditions. For days with winds from the NW, an increase in P in the downwind area of B is visible due to the A1Bspr scenario and more pronounced due to the A1Bcom scenario.

5.5. Explaining factors of climate impacts due to land-cover changes

In this chapter various impacts due to the land-cover change scenarios are discussed. The degree of dependence of temperature changes and changes in different surface temperature affecting variables is going to be analysed in this section. The Kendall's rank correlation is computed for daily differences between variables of the land-cover change scenario simulations (A1Bspr and A1Bcom) and the A1B simulations to measure the strength of the relationship between the changes of two variables. This non-parametric and distribution-free measure of correlation tests the statistical associations of variables based on the rank of the data. The ranking of data is carried out on the variables that are separately put in order and are numbered. The calculation of the Kendall's rank coefficient (τ) is based on concordant and discordant pairs (Eq. 5.1). A concordant pair is when the rank of the second variable is greater than the rank of the former variable. Whereas, a discordant pair is when the rank is equal to or less than the rank of the first variable.

$$\tau = \frac{2 \cdot (no.of\,concordant\,pairs - no.of\,discordant\,pairs)}{n(n-1)}, \tag{5.1}$$

whereas n is the number of data points. Kendall's τ represents the difference between the probability that the considered data are in the same order versus the probability that the considered data are not in the same order.

The analysis is carried out for JJA because at this time both land-cover change scenarios, A1Bspr and A1Bcom, lead to considerably impacts on the 2 m (T_{2m}) and surface temperature (T_s).

It is notable that temperature changes in the A1Bcom scenario have a stronger relationship to influencing variables than in the A1Bspr simulation. This is shown both, for HH and B. This feature might be a result of the homogeneous character of A1Bcom. Herein, the soil texture "rock" dominates, which implies in this case no vegetation cover and no soil water. Due to the absence of additional heat storage components effects on T_{2m} and T_s show to be more linear than for the A1Bspr simulation.

Near surface temperature changes due to the A1Bspr scenario are mainly connected to changes in the latent heat flux, the sensible heat flux and the net long-wave radiation flux. Nevertheless, these correlations are weak ranging from 0.28 to 0.38 for HH and B.

The relationships between changes in the near surface temperature due to the A1Bcom scenario show differences between the two cities of HH and B. Whereas, there is a weak relationship between changes in the near surface temperature and the latent heat flux for HH, there is no relationship between these variables for B. Also, there is a moderate relationship between the changes of T_{2m} and α in B while no relationship is visible for these variables in HH. Changes in T_{2m} and T_s in the A1Bcom simulation show also a weak negative relationship to V_{10m}. The correlations point out that changes in various variables contribute to the described temperature changes in this chapter.

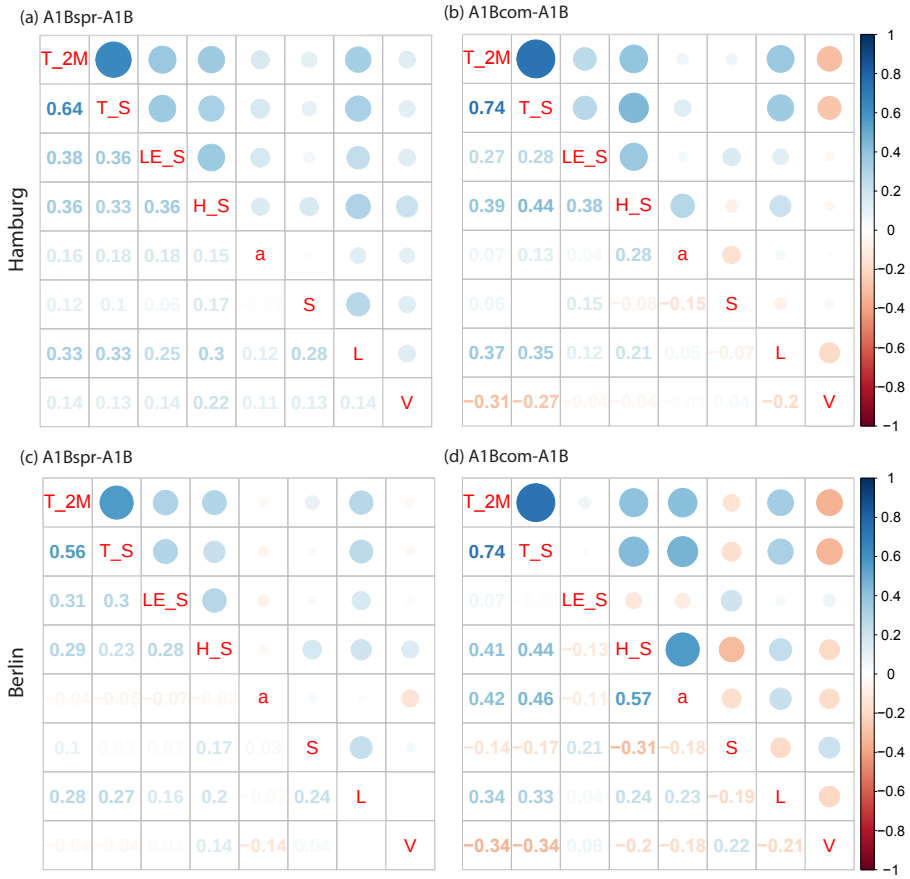

Figure 5.31.: Shown are the Kendall's correlations (τ) of daily differences between A1Bspr and A1B (a and c) and A1Bcom and A1B (b and d) of temperature affecting variables for Hamburg (a and b) and Berlin (c and d) in JJA. Correlations between the differences in the 2 m temperature (T_{2m}, here T_2M), the surface temperature (T_s, here: T_S), the latent heat flux (λE, here: LE_S), the sensible heat flux (H, here: H_S), the albedo (α, here: a), the net shortwave radiation (S_n), the net longwave radiation (L) and the wind speed in 10 m height (V_{10m}, here: V) are illustrated.

Correlations between hydrological components are not discussed at this point since precipitation impacts appeared not directly at modified land-cover grid boxes but rather in the surroundings. This issue makes it difficult to capture the relationships between precipitation influencing variables in the same way as done for the 2 m temperature.

5.6. Summary and discussion

The objective of this chapter is to explore impacts on the possible future climate of Northern Germany due to both, changed greenhouse-gas (GHG) concentrations and land-cover changes with special focus on the impact of both effects in combination.

The regional climate model COSMO-CLM is applied with a horizontal resolution of 2.8 km for climate simulations of two time slices: 1998-2007 and 2090-2099. Alongside a possible GHG

emission scenario (A1B), two land-cover change scenarios with a focus on urban growth are implemented. The first urban scenario is based on the assumption that urban areas increase especially horizontally in space, here called "urban sprawl". The second scenario assumes compact growing of cities ("compact city"). Cities are, in this case, partly enlarged but mainly the centre of these cities is made denser and higher buildings are constructed.

From a regional perspective, impacts due to the A1B scenario play the major role. However, on the local scale, land-cover changes have shown to be comparable and partly even more important. Not only changed grid boxes turn out to climatically affected by land-cover changes but also the surroundings up to a distance of about 60 km, and atmospheric levels up to a height of about 1 km and even deep the soil layers experience impacts.

The A1B scenario leads to a large temperature increase throughout the year. Most pronounced increases occur in winter and here, especially in December (+2.4 to +4.3 K). This higher temperature is a result of the increased amount of GHG in this scenario. Nevertheless, the particular strong temperature increase in December can be explained by a combination of factors. To begin with, a decreased surface albedo occurs during this period due to a lower snow cover height. Same as the near surface atmosphere, the Baltic and the North Sea experience higher temperatures throughout the year, therefore not only above the land masses but also especially above water bodies, the surface evaporation is increased, especially in December and January. This shows impacts on the total cloud coverage which is particularly increased in December. Also foggy conditions or a shift in thermal stratification might be potential reasons for the considerable increase in the temperature in December.

Also e.g. Riediger and Gratzki (2014) came to similar results for the future winter period of 2070 to 2099 in central Europe in terms of ensemble simulations based also on the A1B emission scenario. They found an ensemble mean winter temperature change of about +3 K. Highest temperature increases were obtained for south-east advection, with a anticyclonic (950 hPa level) and cyclonic (500 hPa level) cyclonality with its centre of action above the sea with upper air trough (Riediger and Gratzki, 2014).

Increased temperatures due to the A1B scenario play in summer in terms of extreme thermal events a fundamental role. Extreme thermal events are considerably increased which indicates a strengthens of the potential vulnerability of mankind. Riediger and Gratzki (2014) found strong increases in the occurrence of summer days for the period 2070-2099 compared to 1971-2000. As key contributor they could identify an increase of anticyclonic westerly circulations with an increase of 90 days (Riediger and Gratzki, 2014). In this chapter, also an increased occurrence of west-winds is illustrated.

Although, several numerical studies suggest that only high resolution simulations of at least 1 km horizontal grid mesh size are able to reproduce the UHI effect (e.g. Bohnenstengel et al., 2011; Grawe et al., 2013), in this chapter several UHI effects and UIP could be elaborated.

Next to temperature changes, the A1B scenario leads to increased precipitation amounts from October to May and decreased precipitation amounts from June to September. This feature is accompanied by higher integrated water vapor amounts in the atmosphere, as a result of higher evaporation rates nearly throughout the year. Also the soil water content shows this annual variations shifted in time in dependence on the depth of the soil layer. Particularly in December a pronounced increase in the soil water content is shown in the upper soil layers. This impact feedbacks on a high soil temperature in the same layers underlining the thesis of particularly increased heat stored and therefore heating the atmosphere.

Conclusions for the mitigation of Hamburg and Berlin for the future climate

Firstly, this chapter highlights that it is especially important to investigate climate change for cities individually. This study was able to detect specific climate impacts for Hamburg and Berlin. This is in line with e.g. Memon et al. (2011) who clearly stated that UHI effects vary from city to city. In the frame of "common" applied horizontal resolutions of regional climate models, these characteristics would have remained undetected. Even the A1B simulation without explicit land-cover changes leads to partly different climate impacts in the domains of the large cities Hamburg and Berlin than in the rural environment.

The two scenarios of urban growth, A1Bspr and A1Bcom, show next to similarities also large differences. Similar is the effect of reduced vegetation, leading to lower latent heat flux and surface evaporation and therefore to less cooling and increased surface temperatures particularly during the vegetation period. The increased surface heating contributes to an increase of the mean planetary boundary layer height. This again impacts on the wind field causing reduced wind speeds in the downwind area of the city where the mean precipitation amounts increase. These effects are more pronounced for the A1Bcom scenario than for the A1Bspr scenario. The dominant role of vegetation in urban domains was also shown in other studies (e.g. Fenner et al., 2014). Not only in terms of evaporation but also in respect to shadowing effects during hot days vegetation plays an important role by providing more comfortable living conditions during summer month.

Nevertheless, the results of the CCLM simulations with a horizontal resolution of 2.8 km are only suitable to indicate directions of the impacts of different urban shapes on climate. No specific recommendations concerning the future urban development can be derived from this study since buildings a far below the grid mesh size of the conducted CCLM simulations.

6. Synthesis and discussion

This study highlights the effects of both, land-cover changes and the combined effects of land-cover and GHG changes on the surface climate from different points of view. For different time-slices the impacts of current modifications of the land-cover of Northern Germany and in more detail for Hamburg and Berlin in comparison to the original land-cover are analyzed. Furthermore, extreme land-cover changes are discussed and finally the combined effects of land-cover and greenhouse gas changes are considered. The work presented in this thesis is based on model simulations with the regional climate model CCLM. The investigated horizontal resolution is 2.8 km grid-mesh size whereby CCLM is applied in a convection permitting mode. The CCLM simulations cover following time periods: 1998-2007, 2002/2003, 2007/2008 and 2090-2099. Even ten years have to be viewed as samples which are at any rate suitable to contribute to an overview. The following paragraphs will summarize the main findings as answers to fundamental questions in respect to the motivation of this thesis. The conclusions will be discussed in comparison to previous studies published in the literature.

What are the benefits of the applied model configuration in this thesis?

In this thesis the standard version of CCLM 4.8 with the Soil-Vegetation-Atmosphere Transfer (SVAT) scheme of moderate complexity, TERRA_ML is applied in a convection permitting mode at a horizontal resolution of 2.8 km grid mesh size. The advantage of this configuration is the consistency in the representation of resolved heterogeneous surface features throughout the annual cycle. This high horizontal resolution allows to capture urban areas which are normally beyond the model grid or only represented by few grid boxes.

This is an alternative approach to represent land-cover change impacts on climate. Usually, GCMs and RCMs with lower horizontal resolutions are combined with SVAT schemes with a higher complexity as given in TERRA_ML, such as TEB (e.g. Trusilova et al., 2009) or the Community Land Model (CLM, e.g. Davin et al., 2011). Or, case studies of short time-periods such as several seasons (Grossman-Clarke et al., 2016) or several days (e.g. Schubert and Grossman-Clarke, 2013, Hoffmann et al., 2016, in review or Boettcher et al., 2016, in review) are investigated. At present, it is computational too expensive to use a high complexity SVAT scheme at such a high horizontal resolution for long-term simulations of ten years as done in this thesis.

A further advantage of the applied model configuration is that deep convection is explicitly resolved in place of uncertain parametrizations in the evaluated CCLM simulations. Convection parametrization is a known source of uncertainties and errors in climate simulations (e.g. Brockhaus et al., 2008). As Prein et al. (2013) and Hohenegger et al. (2008) stated, the representation of summer temperatures is improved due to the convection permitting configuration. In addition, in Section 3.3.2 it is shown that the summer 2 m temperature bias is particularly low in the high resolved CCLM simulation.

In this thesis, the first long-term study of ten years with the CCLM is analyzed for a horizontal resolution of 2.8 km for the whole domain of Northern Germany. Usually smaller domains are investigated for comparable horizontal resolutions. The applied studies in this thesis allow a regional perspective of climate impacts and the classification of land-cover changes in the larger context.

The simulated impacts on the surface climate due to land-cover changes by CCLM simulations in this thesis are comparable to other studies. Key characteristics of land-cover change are repeated such as the changed portioning of surface fluxes depending on the vegetation amount. Moreover, many typical urban characteristics can be reproduced in this thesis, such as the increased sensible and decreased latent heat flux within the cities causing an urban heat island (UHI), shown in Section 4.3.2 or Section 5.3.2 which is in line with numerous other studies (e.g Grimmond and Oke, 1995; Jin et al., 2005). Also, the hydrological effects of sealed surfaces are reasonably captured by the model in this study. Due to low vegetation amounts and/or sealed surfaces, rain water is not stored at the surface or in the soil and high amounts of surface run-off occur. Therefore, there is only a small amount of water available to evaporate and to cool particularly during summer days the atmosphere. This leads to pronounced heating above the surfaces and the evolution of a higher planetary boundary layer. This effect becomes most apparent in the urban sprawl and the compact city scenario for Hamburg and Berlin. Increased turbulence above the cities causes impacts on the precipitation and the wind pattern above and nearby the cities. These described effects are in line with other studies dealing with the influence of urban areas on surface climate (e.g. Jin et al., 2005; Kueppers et al., 2007).

Which uncertainties have to be taken into account?

In the applied model configuration impacts of ecosystem dynamics and biogeochemical feedbacks on the climate system are not considered. Furthermore, there is no biochemical description of photosynthesis or stomata resistance - this was meanwhile introduced in newer CCLM versions. Additionally, no dynamic interactions between land surface and atmosphere are represented.

The representation of "urban areas" in this thesis has to be analyzed carefully as discussed in the Sections 3.2.2, 4.2, 4.2, 4.5 and 5.4.1. Some characteristics of real cities are introduced. But, as described in Chapter 2.2.1, cities are very complex. Due to the applied "sealing" in this thesis, a relatively high albedo is shown during dry periods. This issue has contributed to lower solar insolation and therefore damped the increase of the surface temperature. On one hand, this high albedo could represent a mitigation strategy to reduce the heating. On the other hand, it has to be kept in mind, that sealed areas have usually a lower albedo in urban areas which would strengthens the temperature increase. With a lower albedo, climate effects would be probably more intense. Another reason is that the anthropogenic heat is not taken into account in the frame of this thesis. Particularly for very dense built urban areas such as simulated in Chapter 4 by the urban sealed scenario or in Chapter 5 by the compact city scenario this heat term would very likely contribute to an intensification of the near surface temperature. In summer, air conditioning and in winter, the additional heating load would considerably impact on the anthropogenic heat term. But also, high traffic amounts occurring due to the sprawl city scenario in Section 5.2.2 would lead to a considerable amount of anthropogenic heat. Nevertheless, the largest values of anthropogenic heat occur in cities at high latitudes during winter due to the additional heating load (Taha, 1997). As all models also RCMs cannot represent the reality perfect and unavoidable uncertainties have to be taken into account as already contoured in Section 1.2. Several studies have shown the added value of RCM simulations (e.g. Feser, 2006). However, RCM simulations substantially depend on the boundary conditions. Uncertainties due to the boundary conditions, as given here by the GCM, are introduced. Grossman-Clarke et al. (2016) even concluded that the GCM determines the UHI characteristics in RCM simulations.

To what extend has the current land-cover of Northern Germany already contributed to climate modifications?

As stated in the motivation (Section 1.1) of this thesis, mankind modifies its surrounding throughout the ages. In Section 4.4 this anthropogenic impact by land-cover changes on Hamburg and Berlin is estimated for 2002 and 2003. The mean weather conditions with the present land-cover are compared to the mean weather conditions with the potential land-cover "mixed forest" which is comparable to the original wilderness, for 2002 and 2003. Higher temperatures in spring and summer (up to 1.5 K in June 2002 for Berlin) and in autumn and winter lower temperatures are shown for the current land-cover (up to -0.5 K in January 2002 for Berlin). The lower temperatures in January are in line with global impact studies which found a cooling effect due to the replacement of forest by arable land resulting in an increase in the surface albedo (e.g. Betts, 2005). Nevertheless, here, only two years are considered and the ERAinterim reanalyses data represent the current land-cover status. Furthermore, the current land-cover has led to increased total precipitation amounts in winter (<10 mm per month) and lower precipitation amounts in spring in the frame of this analysis. The increase in winter precipitation is also shown for the long-term simulations in Chapter 5. This might indicate that the effects of present land-cover on precipitation could be strengthened in future.

What climatic effects have land-cover changes on Northern Germany?

Which spectrum of meteorological variables is affected due to land-cover changes?

The surface energy balance as well as the hydrological cycle experience substantial impacts due to land-cover changes in the frame of this thesis. Well comprehensible is the impact on the surface temperature which is mainly caused by changed portioning of sensible and latent heat flux (Section 4.3.2 and Section 5.3.2). These temperature changes affect the soil layers in Chapter 5 for the A1Bspr scenario up to a mean depth of 2.86 m.

The planetary boundary layer (PBL) is influenced by land-cover changes. Turbulent fluxes are increased particularly above the sealed surfaces and rather the surfaces with increased surface roughness. Therefore, a higher PBL evolves which modifies the wind pattern (Section 5.3.2) and therewith the precipitation pattern in evidence (Section 5.4.2).

Impacts on the hydrological cycle are illustrated in terms of changed precipitation and evaporation amounts. The low-level cloud cover is affected only by large-scale land-cover changes in Chapter 4 but not by the urban scenarios A1Bspr or A1Bcom in Chapter 5. Due to the sealing, the soil characteristics below the sealed surface are completely cut off. No vegetation can be present. Thereby, not only the radiation budget is considerably influenced but also the hydrological cycle. This modification causes a fast heating of the surface and a prevention of evaporative cooling.

What effects have extreme land-cover changes on the regional climate under extreme climate conditions?

A high amount of sealed surfaces as given in the urban sealed scenario in Chapter 4 or in the compact city scenario in Chapter 5 leads to a strengthening of heat stress particularly during summer month. Considerably increased temperatures in combination with low or even no cooling effect due to evaporation lead to a fundamental increase in the vulnerability of citizen of these regions. Both, the urban sealed and the compact city scenario showed an intense increase in the number of tropical nights. This indicates especially heat stress and negative impacts on human comfort. Furthermore, the sealing of the surface leads to a rapid increase of the surface run-off which again can induce flooding and related damages.

What might be the maximum range of climate impacts due to land-cover changes in Northern Germany?

To answer this question with respect to changes in the 2 m temperatures (T_{2m}), daily summer (JJA) T_{2m} are compared for the current urban city cores (see Fig. 5.24) of Hamburg and Berlin under the conditions of all land-cover scenarios of this thesis (Fig. 6.1).

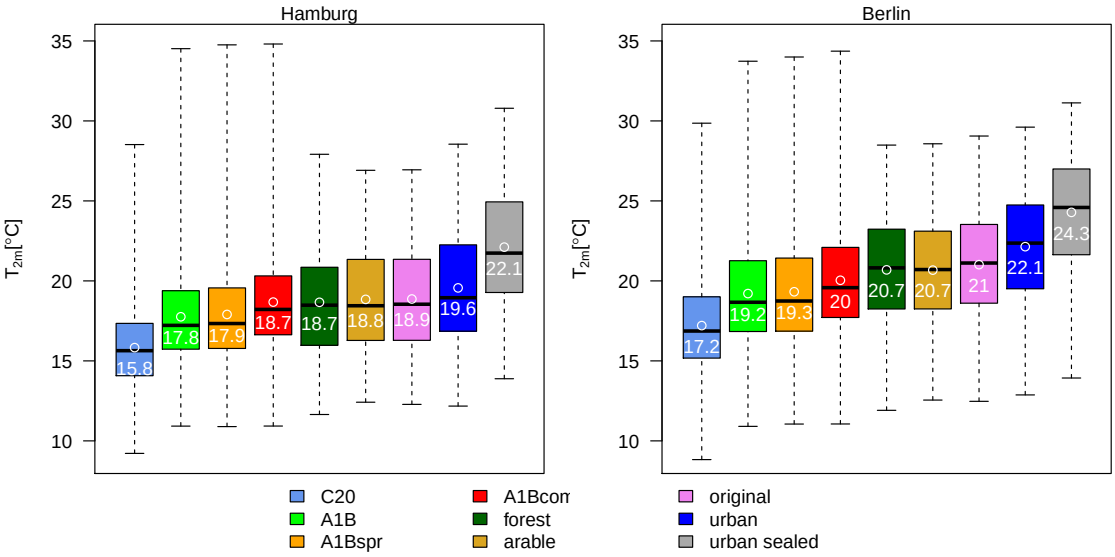

Figure 6.1.: Boxplots of daily JJA temperatures as given by the different CCLM simulations for Hamburg (left) and Berlin (right) for grid boxes as defined as "urban city core" in Fig. 5.24. White circles and corresponding white numbers within the boxes indicate the mean daily 2 m temperature.

Fig. 6.1 states clearly the generally higher temperature level of Berlin. This difference underlines the importance to analyze cities individually. For Hamburg, the range of mean daily JJA temperatures spans from 15.8 °C in the C20 simulation to 22 °C in the urban sealed scenario, that means a difference of 6.2 K. For Berlin, also the C20 simulation shows the lowest mean daily temperature of 17.2 °C and in the urban sealed simulation the highest value of 24 °C, therefore a range of 6.8 K. As already discussed, even higher temperature increases could be expected if the anthropogenic heat and lower albedo values would be taken into account. The A1B, the A1Bspr and the A1Bcom scenarios particular indicate by their large spread that extreme land-cover changes combined with GHG changes at the end of the 21st might lead to stronger impacts on the surface temperature than for the periods of 1998 to 2007.

In respect to land-cover impacts on the hydrological cycle, the considerably decrease of surface evaporation due to sealed surfaces is shown to play a major role. Large-scale sealing of Northern Germany in Section 4.3.3 leads not only to a "hot" atmosphere but also to a "dry" atmosphere due to fast run-off of precipitation, low surface evaporation and therewith low integrated water vapor of the atmosphere. This is followed by considerably decreases of the total cloud cover and the total precipitation amount. However, local-scale land-cover changes in terms of the A1Bspr and the A1Bcom scenario show also particular impacts on the surface evaporation but impacts on the integrated water vapor amount or the cloud cover could not be detected.

Where do we see the fingerprint of urban growth?

Land-cover changes effect not only the changed grid boxes but also the nearby surrounding. In Chapter 5, it is shown that the surrounding of modified grid boxes is also affected up to distances of 60 km. Especially the high roughness length in the compact city scenario causes a heat wake due to reduced wind speeds in the downwind area of the city. Also the precipitation pattern around the modified cities in Chapter 5 are influenced by the urban characteristics in the A1Bspr and the A1Bcom scenario (Section 5.4.2). Also this impact on precipitation is particularly caused by the increased roughness length above the cities. In addition, Bornstein and Lin (2000) or Thielen et al. (2000) have attributed impacts of cities on natural precipitation pattern to the surface roughness.

How could or should future land-cover of Northern Germany look like?

In this thesis, only a large-scale coverage with mixed forest and arable land and therefore a high degree of vegetation of Northern Germany is shown to at least partly reduce the magnitude of extreme weather events (e.g. Tab. 4.2). To mitigate climate impacts due to the A1B scenario, a high amount of vegetation cover could contribute to human comfort. The degree of sealed surfaces should be as low as possible for Northern Germany and especially in the cities since the sealing showed particularly negative impacts and increased the vulnerability of citizens. Also shown in this thesis but in more detail in other studies (Boettcher et al., 2016, in review), the albedo plays an important role. To reduce the urban heat island in cities, the usage of materials with a high albedo in urban areas is shown to be appropriate to reduce the surface temperatures. Schubert and Grossman-Clarke (2013) investigated the effect of increased albedo and vegetation cover for Berlin and indicated lower midday temperatures during heat waves due to both effects.

This thesis leads to the conclusion that urban growth should not happen in terms of simply densification of already built-up areas or the replacement of existing building stock by high skyscrapers as done in the A1Bcom scenario. On the contrary, urban growth should be considered thoroughly since effects of changed land-cover are not only connected to the location of change. Furthermore, the proportion of sealed surface should be as low as possible to prevent fast run-off of precipitation. Moreover, in respect to a slightly increased number of heavy precipitation days, as projected in the A1B simulation for 2090-2099 (Tab. 5.4), large proportions of land-cover with a high water absorption could avoid flooding caused by heavy precipitation events and provide a cooling effect due to evaporation of available water. As already stated above, urban material with high albedos could especially help to mitigate to increased temperatures. Vegetation plays an important role particularly in urban areas, e.g. the shadowing effect of trees and transpiration improve human comfort. However, during heat periods, trees have also shown to strengthen the surface temperature in this thesis. Nevertheless, as far as enough water is available through the root of the plants the cooling effects are dominant (Section 4.5).

All applied land-cover change scenarios in this study strengthen in mean the climate change signal in terms of increased summer temperatures. Whereas, the GHG induced impacts on the total precipitation amount are partly even reduced. But in general, these land-cover changes do not help to mitigate to GHG induced climate changes.

Where are the hot-spots of climate impacts due to combined effects of land-cover and GHG changes in Northern Germany at the end of the 21st century?

Even without land-cover changes, the climate of Northern Germany would face significant impacts on the surface climate following the A1B scenario. The city cores with already higher temperatures than in the rural environment experience additionally stronger temperature increases due to the A1B scenario than the rural environment. This depends on the dimension of land-cover changes.

The larger the modified domain and the stronger the applied changes are, the stronger is the impact on extreme climate events.

Citizen of the urban city core are currently confronted by strongest temperature extremes. And this will be strengthened by the A1B scenario for 2090 to 2099 (Fig. 5.13). However, citizen of originally arable domains which are transformed to urban areas experience the strongest change in the occurrence of thermal extremes such as hot or summer days.

What are interesting aspects for future work?

The ongoing increase of high performance computing for climate modelling will allow improved investigations of land-cover impacts on climate for horizontal scales of 2.8 km and lower in future. This will enable the application of several GHG and land-cover change scenarios for longer time-periods. Here, only one GHG emission scenario is applied. This is not representative for the wide range of existing GHG emission scenarios. Therefore, more different GHG respectively RCP scenarios should be taken into account to get a more complete overview for probable future impacts. Furthermore, ensemble simulations with different GCMs and RCMs combined with different SVAT schemes of different complexities would strengthen the reliability of impact studies.

The focus of this thesis is on the biogeophysical impacts, but in combination with the GHG emission scenarios, the biogeochemical cycle might change in combination with the land-cover scenarios. Currently, there is a lot of research in terms of alternative SVAT schemes- also for CCLM (Trusilova et al., 2016). Improved land-cover data sets could contribute to improved climate simulations of certain domains. More detailed land-use characteristics, as for instance, stomata resistance can improve the accuracy of surface-atmosphere dynamics (e.g. Ament, 2006). Changes in the land-cover, particularly in respect to the vegetation period, should be able to have a direct impact on the LAI and PLCOV. Until now these parameters are prescribed.

In the frame of this thesis, climate simulations with high horizontal resolutions have been produced. These data sets are suitable for further impact studies with respect to Northern Germany or domains therein. Further simulations nests with more sophisticated SVAT schemes could be e.g. implemented for more detailed analysis of UHI effects.

A. Supplementary material

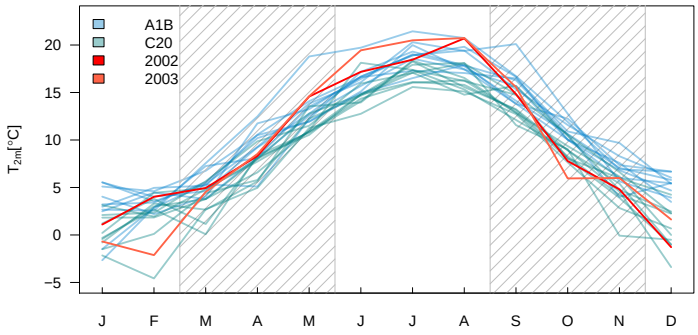

Figure A.1.: Annual cycle of the monthly mean spatially averaged 2 m temperature of NG illustrated for all simulations of this thesis including the original land cover.

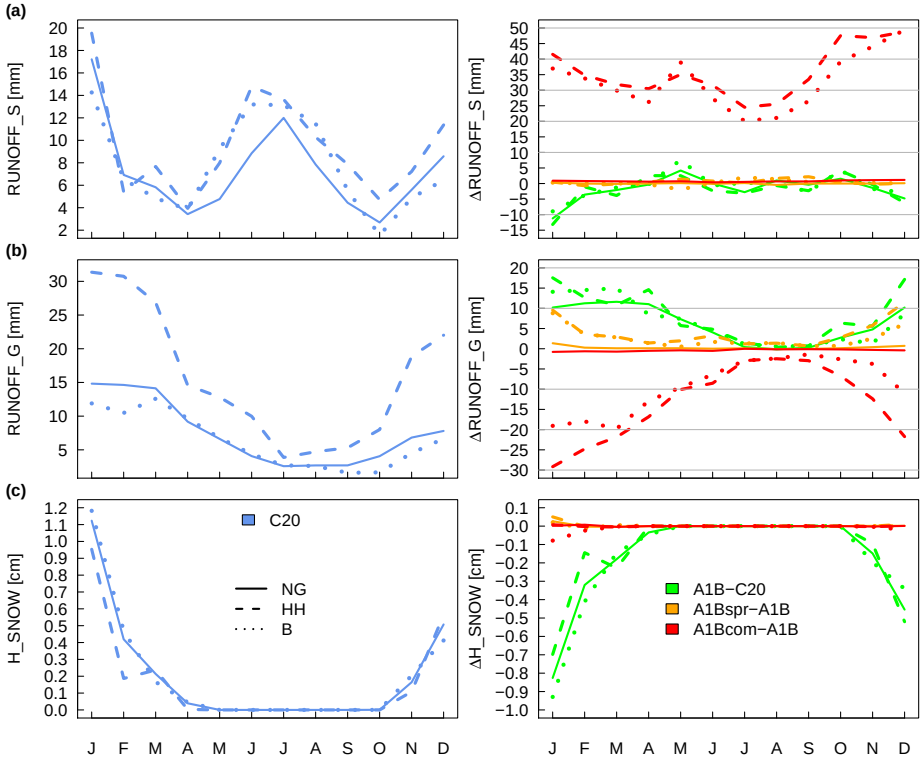

Figure A.2.: Same as Fig. 5.3 but for a) surface run-off, b) subsurface run-off and c) snow height.

Danksagung

Während meiner Doktorandenzeit habe ich Unterstützung von zahlreichen Personen bekommen, denen ich an dieser Stelle herzlich Danken möchte.

Zunächst möchte ich Frau Dr. Insa Meinke danken. Sie hat diese Doktorarbeit initiiert und in den Panel Meetings durch Ideen und Komentare stets hilfreiche Denkanstöße gegeben.

Bei Herrn Dr. Burkhardt Rockel möchte ich mich für die Betreuung und die Übernahme eines Gutachtens dieser Arbeit bedanken. Dank seiner Erfahrungen im Bereich der regionalen Klimamodellierung konnten insbesondere Probleme mit dem CCLM schnell behoben werden. Der mir gegebene große Freiraum hat mir ermöglicht meinen eigenen Weg in der Ausarbeitung dieser Arbeit zu finden.

Herrn Professor Hans von Storch gebührt mein Dank sowohl für die Übernahme des Gutachtens als auch für die hilfreichen Diskussionen zu dieser Arbeit.

Besonders möchte ich mich bei Herrn Prof. Felix Ament für die zahlreichen Anregungen, Diskussionen und Denkanstöße zu meiner Arbeit und vor allem auch die moralische Unterstützung bedanken.

Bei Frau Dr. Beate Geyer und ihren „Adleraugen“ möchte ich mich besonders bedanken. Selbst die kleinsten Fehler in Abbildungen oder Texten sind vor ihr nicht sicher und man findet bei ihr nicht nur in technischen Belangen, stets Unterstützung.

Mein Dank gilt weiterhin meinen Kollegen aus der Abteilung „Regionale Atmosphärenmodellierung“ und den Kollegen aus dem Institut für Küstenforschung. Sie alle haben zu einer angenehmen Arbeitsatmosphäre beigetragen, die den Rahmen zu dieser Arbeit gegeben hat.

In dieser Arbeit wurde das COMSO-CLM (COSMO model in Climate Mode) verwendet, das von der CLM-Community, einem internationalem Netzwerk von Wissenschaftlern, gepflegt und weiterentwickelt wird (www.clm-community.eu).

Dipl. Geogr. Sebastian Tuengerthal und Dipl. Geogr. Moritz Maneke möchte ich ganz herzlich für ihre Hilfe bei der Umwandlung der CORINE Daten und für die Erstellung der Sektorkarten mit GIS danken.

Dr. Peter Hoffmann, Dr. Karsten Peters, Dr. Beate Geyer, Dr. Katharina Klehmet und Dr. Janna Lindenberg möchte ich für die vielen hilfreichen Diskussionen und Kommentare zu dieser Arbeit danken.

An dieser Stelle möchte ich mich ganz herzlich bei meiner Familie bedanken. Nicht minder aufreibend waren die vergangenen Jahre für sie, die dieses Werk in allen Phasen mit jeder möglichen Unterstützung bedacht haben. Für meinen Mann André und mich umfasst meine Doktorandenzeit unseren wohl ereignisreichsten Lebensabschnitt, der von den Geburten von unseren Söhnen Simon und Erik gekrönt wurde. Ihr drei seid das wichtigste in meinem Leben und habt immer für den nötigen Ausgleich gesorgt. Danke André, dass du mich vor allem auch in den stressigsten Zeiten immer unterstützt hast.

Meine Eltern haben mich stark für mein Leben gemacht, mich stets unterstützt und waren immer für mich da, dafür möchte ich ganz herzlich Danke sagen.

I acknowledge the E-OBS dataset from the EU-FP6 project ENSEMBLES (http://ensembles-eu.metoffice.com) and the data providers in the ECA&D project (http://www.ecad.eu).

Bibliography

Adrian, G. (1996). Beschreibung der Wechselwirkung zwischen Erdboden und Atmosphaere in Regionalmodellen. *promet*, 25, 3:80–86.

Alcamo, J., Kok, K., Busch, G., Priess, J. A., Eickhout, B., Rounsevell, M., Rothman, D. S., and Heistermann, M. (2006). *Searching for the Future of Land: Scenarios from the Local to Global Scale*, pages 137–155. Springer Berlin Heidelberg, Berlin, Heidelberg.

Ament, F. (2006). *Energy and moisture exchange processes over heterogeneous land-surfaces in a weather prediction model*. PhD thesis, Rheinische Friedrich-Wilhelms-Universitaet Bonn.

Angel, S., Parent, J., Civco, D. L., Blei, A., and Potere, D. (2011). The dimensions of global urban expansion: Estimates and projections for all countries, 2000–2050. *Progress in Planning*, 75(2):53–107.

Arnds, D., Böhner, J., and Bechtel, B. (2015). Spatio-temporal variance and meteorological drivers of the urban heat island in a European city. *Theoretical and Applied Climatology*, pages 1–19.

Arnfield, A. J. (2003). Two decades of urban climate research: A review of turbulence, exchanges of energy and water, and the urban heat island. *International Journal of Climatology*, 23(1):1–26.

Arora, V. K. and Montenegro, A. (2011). Small temperature benefits provided by realistic afforestation efforts. *Nature Geoscience*, 4(8):514–518.

Avissar, R. (1998). Which type of soil-vegetation-atmosphere transfer scheme is needed for general circulation models: A proposal for a higher order scheme. *Journal of Hydrology*, 212-213(0):136–154.

Avissar, R. and Pielke, R. A. (1989). A parameterization of heterogeneous land surfaces for atmospheric numerical models and its impact on regional meteorology. *Mon. Wea. Rev.*, 117(10):2113–2136.

Avissar, R. and Werth, D. (2005). Global hydroclimatological teleconnections resulting from tropical deforestation. *Journal Of Hydrometeorology*, 6:134–145.

Bakker, M. M., Govers, G., Kosmas, C., Vanacker, V., van Oost, K., and Rounsevell, M. (2005). Soil erosion as a driver of land-use change. *Agriculture Ecosystems & Environment*, 105(3):467–481.

Bala, G., Caldeira, K., Wickett, M., Phillips, T. J., Lobell, D. B., Delire, C., and Mirin, A. (2007). Combined climate and carbon-cycle effects of large-scale deforestation. *Proceedings of the National Academy of Sciences of the United States of America*, 104(16):6550–6555.

Baldauf, M., Seifert, A., Förstner, J., Majewski, D., Raschendorfer, M., and Reinhardt, T. (2011). Operational Convective-Scale Numerical Weather Prediction with the COSMO Model: Description and Sensitivities. *Mon. Wea. Rev.*, 139(12):3887–3905.

BBSR (2016a). Anpassung an den Klimawandel in Stadt und Region. Technical report, Bundesinstitut für Bau-, Stadt- und Raumforschung.

BBSR (2016b). Querauswertung zentraler Verbundvorhaben des Bundes zur Anpassung an den Klimawandel mit Fokus Stadt- und Regionalentwicklung. Technical report, Bundesinstitut für Bau-, Stadt- und Raumforschung.

Bechtel, B. and Schmidt, K. (2011). Floristic mapping data as a proxy for the mean urban heat island. *Clim Res*, 49(1):45–58.

Beljaars, A. C. M. (1995). The parametrization of surface fluxes in large-scale models under free convection. *Q.J.R. Meteorol. Soc.*, 121(522):255–270.

Beniston, M. (2004). The 2003 heat wave in Europe: A shape of things to come? An analysis based on Swiss climatological data and model simulations. *Geophys. Res. Lett.*, 31(2):L02202–.

Betts, A. K. (2000). Idealized model for equilibrium boundary layer over land. *J. Hydrometeor*, 1(6):507–523.

Betts, A. K., Ball, J. H., Beljaars, A. C. M., Miller, M. J., and Viterbo, P. A. (1996). The land surface-atmosphere interaction: A review based on observational and global modeling perspectives. *Journal of Geophysical Research: Atmospheres*, 101(D3):7209–7225.

Betts, R. (2005). Integrated approaches to climate-crop modelling: Needs and challenges. *Philosophical Transactions of the Royal Society B: Biological Sciences*, 360(1463):2049–2065.

Betts, R. A. (2001). Biogeophysical impacts of land use on present-day climate: Near-surface temperature change and radiative forcing. *Atmospheric Science Letters*, 2(1-4):39–51.

Boettcher, M., Flagg, D., G., Grawe, D., Hoffmann, P., Petrik, R., Schlünzen, K. H., Schoetter, R., and Teichert, N. (2016, under review). Modelling impacts of urban development and climate adaption measures on summer climate of Hamburg. *Urban Climate*.

Bohnenstengel, S. I., Evans, S., Clark, P. A., and Belcher, S. E. (2011). Simulations of the London urban heat island. *QUARTERLY JOURNAL OF THE ROYAL METEOROLOGICAL SOCIETY*, 137(659, B):1625–1640.

Bonan, G. (1997). Effects of Land Use on the Climate of the United States. *Climatic Change*, 37(3):449–486.

Bonan, G. B. (1999). Frost followed the plow: Impacts of deforestation on the climate of the united states. *Ecological Applications*, 9(4):1305–1315.

Bonan, G. B. (2001). Observational Evidence for Reduction of Daily Maximum Temperature by Croplands in the Midwest United States. *J. Climate*, 14(11):2430–2442.

Bonan, G. B. (2008). Forests and climate change: Forcings, feedbacks, and the climate benefits of forests. *Science*, 320(5882):1444–1449.

Bornstein, R. and Lin, Q. (2000). Urban heat islands and summertime convective thunderstorms in Atlanta: Three case studies. *Atmospheric Environment*, 34(3):507–516.

Bosch, J. and Hewlett, J. (1982). A review of catchment experiments to determine the effect of vegetation changes on water yield and evapotranspiration. *Journal of Hydrology*, 55(1):3–23.

Bounoua, L., DeFries, R., Collatz, G. J., Sellers, P., and Khan, H. (2002). Effects of land cover conversion on surface climate. *Climatic Change*, 52(1-2):29–64.

Brisson, E., Demuzere, M., and van Lipzig, N. P. M. (2016). Modelling strategies for performing convection-permitting climate simulations. *METEOROLOGISCHE ZEITSCHRIFT*, 25(2):149–163.

Brockhaus, P., Lüthi, D., and Schär, C. (2008). Aspects of the diurnal cycle in a regional climate model. *Meteorologische Zeitschrift*, 17(4):433–443.

Brovkin, V., Boysen, L., Arora, V. K., Boisier, J. P., Cadule, P., Chini, L., Claußen, M., Friedlingstein, P., Gayler, V., van den Hurk, B. J. J. M., Hurtt, G. C., Jones, C. D., Kato, E., de Noblet-Ducoudre, N., Pacifico, F., Pongratz, J., and Weiss, M. (2013). Effect of anthropogenic land-use and land-cover changes on climate and land carbon storage in cmip5 projections for the twenty-first century. *Journal of Climate*, 26(18):6859–6881.

Brovkin, V., Ganopolski, A., Claußen, M., Kubatzki, C., and Petoukhov, V. (1999). Modelling climate response to historical land cover change. *Global Ecology And Biogeography*, 8(6):509–517.

Bundes-Ministerium für Umwelt, Natur-Schutz, B. u. R.-S. (2008). Deutsche Anpassungsstrategie an den Klimawandel.

Carraca, M. G. D. and Collier, C. G. (2007). Modelling the impact of high-rise buildings in urban areas on precipitation initiation. *Met. Apps*, 14(2):149–161.

Changnon, J. and Stanley, A. (1981). Metromex review and summary. *Meteor. Monogr.*, 40:181.

Changnon, S. (2001). Assessment of Historical Thunderstorm Data for Urban Effects: The Chicago Case. *Climatic Change*, 49(1-2):161–169.

Chase, T. N., Pielke, R. A., Kittel, T. G. F., Nemani, R. R., and Running, S. W. (2000). Simulated impacts of historical land cover changes on global climate in northern winter. *Climate Dynamics*, 16(2-3):93–105.

Chen, F., Mitchell, K., Schaake, J., Xue, Y., Pan, H.-L., Koren, V., Duan, Q. Y., Ek, M., and Betts, A. (1996). Modeling of land surface evaporation by four schemes and comparison with FIFE observations. *J. Geophys. Res.*, 101(D3):7251–7268.

Christensen, J., Hewitson, B., Busuioc, A., Chen, A., Gao, X., Held, R., Jones, R., Kolli, R., Kwon, W., Laprise, R., et al. (2007). Regional climate projections, Climate Change, 2007: The Physical Science Basis. Contribution of Working group I to the Fourth Assessment Report of the Intergovernmental Panel on Climate Change.

Christensen, J. H. and Christensen, O. B. (2003). Climate modelling: Severe summertime flooding in Europe. *Nature*, 421(6925):805–806.

Claußen, M., Brovkin, V., and Ganopolski, A. (2001). Biogeophysical versus biogeochemical feedbacks of large-scale land cover change. *Geophysical Research Letters*, 28(6):1011–1014.

Claußen, M., Cox, P. M., Zeng, X., Viterbo, P., Beljaars, A. C., Betts, R. A., Bolle, H.-J., Chase, T., and Koster, R. (2004). The global climate. In *Global Change: The IGBP Series*, pages 33–57–. Springer Berlin Heidelberg.

Cotton, W. R. and Pielke Sr, R. A. (2007). *Human impacts on weather and climate*. Cambridge University Press.

Couclelis, H. (2005). Where has the future gone? rethinking the role of integrated land-use models in spatial planning. *Environment and planning A*, 37(8):1353–1371.

Cramer, W., Bondeau, A., Woodward, F., Prentice, I., Betts, R., Brovkin, V., Cox, P., Fisher, V., Foley, J., Friend, A., Kucharik, C., Lomas, M., Ramankutty, N., Sitch, S., Smith, B., White, A., and Young-Molling, C. (2001). Global response of terrestrial ecosystem structure and function to CO_2 and climate change: results from six dynamic global vegetation models. *GLOBAL CHANGE BIOLOGY*, 7(4):357–373.

Crucifix, M., Betts, R. A., and Cox, P. M. (2005). Vegetation and climate variability: a gcm modelling study. *Climate Dynamics*, 24(5):457–467.

Crutzen, P. J. (2004). New Directions: The growing urban heat and pollution "island" effect – impact on chemistry and climate. *Atmospheric Environment*, 38:3539–3540.

Dai, A. G., Giorgi, F., and Trenberth, K. E. (1999). Observed and model-simulated diurnal cycles of precipitation over the contiguous United States. *Journal Of Geophysical Research-Atmospheres*, 104(D6):6377–6402.

Daneke, C. (2012). *Modellierung von Stadtentwicklungsprozessen am Fallbeispiel Hamburg : unter Berücksichtigung stadtklimatologischer Aspekte*. PhD thesis, University of Hamburg.

Davies, H. C. (1976). A lateral boundary formulation for multi-level prediction models. *Quarterly Journal of the Royal Meteorological Society*, 102(432):405–418.

Davin, E., Stöckli, R., Jaeger, E., Levis, S., and Seneviratne, S. (2011). COSMO-CLM^2: a new version of the COSMO-CLM model coupled to the Community Land Model. *Climate Dynamics*, pages 1–19. 10.1007/s00382-011-1019-z.

Davin, E. L. and Seneviratne, S. I. (2012). Role of land surface processes and diffuse/direct radiation partitioning in simulating the European climate. *Biogeosciences*, 9(5):1695–1707.

de Noblet-Ducoudré, N., Boisier, J.-P., Pitman, A., Bonan, G. B., Brovkin, V., Cruz, F., Delire, C., Gayler, V., van den Hurk, B. J. J. M., Lawrence, P. J., van der Molen, M. K., MÃijller, C., Reick, C. H., Strengers, B. J., and Voldoire, A. (2012). Determining Robust Impacts of Land-Use-Induced Land Cover Changes on Surface Climate over North America and Eurasia: Results from the First Set of LUCID Experiments. *J. Climate*, 25(9):3261–3281.

Deardorff, J. W. (1978). Efficient prediction of ground surface temperature and moisture, with inclusion of a layer of vegetation. *J. Geophys. Res*, 83(C4):1889–1903.

Dee, D., Uppala, S., Simmons, A., Berrisford, P., Poli, P., Kobayashi, S., Andrae, U., Balmaseda, M., Balsamo, G., and Bauer, P. (2011). The ERA-Interim reanalysis: Configuration and performance of the data assimilation system. *Quarterly Journal of the Royal Meteorological Society*, 137(656):553–597.

DeFries, R. S., Bounoua, L., and Collatz, G. J. (2002). Human modification of the landscape and surface climate in the next fifty years. *Global Change Biology*, 8(5):438–458.

DeFries, R. S., Foley, J. A., and Asner, G. P. (2004). Land-use choices: Balancing human needs and ecosystem function. *Frontiers In Ecology And The Environment*, 2(5):249–257.

Deggau, M. (2015). Siedlungs- und verkehrsfläche wächst täglich um 74 hektar. *Statistisches Bundesamt, Pressemitteilung Nr. vom 09.12.2015*.

Denman, K., Brasseur, G., Chidthaisong, A., Ciais, P., Cox, P., Dickinson, R., Hauglustaine, D., Heinze, C., Holland, E., Jacob, D., et al. (2007). *Couplings between changes in the climate system and biogeochemistry*. Cambridge University Press.

Dickinson, R. E. (1984). Modeling evapotranspiration for three-dimensional global climate models. In *Climate Processes and Climate Sensitivity*, pages 58–72. American Geophysical Union.

Diem, J. E. and Brown, D. P. (2003). Anthropogenic impacts on summer precipitation in central Arizona, USA. *The Professional Geographer*, 55(3):343–355.

Doms, G., Förstner, J., Heise, E., Herzog, H., Mironov, D., Raschendorfer, M., Reinhardt, T., Ritter, B., Schrodin, R., Schulz, J., et al. (2011). A description of the nonhydrostatic regional COSMO model. Part II: Physical Parameterization. *Consortium for Small-Scale Modelling, Deutscher Wetterdienst (DWD)*.

Dosch, F. and Beckmann, R. (2011). *Auf dem Weg, aber noch nicht am Ziel - Trends der Siedlungsflächenentwicklung* . Bundesinstitut für Bau-, Stadt-, und Raumforschung (BBSR) im Bundesamt für Bauwesen und Raumordnung (BBR).

Fan, H. and Sailor, D. J. (2005). Modeling the impacts of anthropogenic heating on the urban climate of Philadelphia: a comparison of implementations in two PBL schemes. *Atmospheric Environment*, 39(1):73–84.

FAO/UNESCO (1997). Soil map of the world , revised legend, with corrections and updates. Technical paper 20, isric, FAO, Wageningen.

Faroux, S., Masson, V., and Roujean, J. L. (2007). ECOCLIMAP-II: a climatologic global data base of ecosystems and land surface parameters at 1 km based on the analysis of time series of VEGETATION data.

Feddema, J. J., Oleson, K. W., Bonan, G. B., Mearns, L. O., Buja, L. E., Meehl, G. A., and Washington, W. M. (2005). The importance of land-cover change in simulating future climates. *Science*, 310(5754):1674–1678.

Fehrmann, P. (2009). Erster Bericht zum Klimawandel in Berlin: Auswirkungen und Anpassung. Available at `http://www.stadtentwicklung.berlin.de/umwelt/klimaschutz/klimawandel/download/klimawandel_bericht.pdf` , Accessed: 2016-02-20.

Fenner, D., Meier, F., Scherer, D., and Polze, A. (2014). Spatial and temporal air temperature variability in berlin, germany, during the years 2001Ã¢âĆňâĂIJ2010. *Urban Climate*, 10, Part 2:308 – 331. ICUC8: The 8th International Conference on Urban Climate and the 10th Symposium on the Urban Environment.

Feser, F. (2006). Enhanced detectability of added value in limited-area model results separated into different spatial scales. *Monthly Weather Review*, 134(8):2180–2190.

Findell, K. L., Shevliakova, E., Milly, P., and Stouffer, R. J. (2007). Modeled impact of anthropogenic land cover change on climate. *Journal of Climate*, 20(14):3621–3634.

Foley, J. A., DeFries, R., Asner, G. P., Barford, C., Bonan, G., Carpenter, S. R., Chapin, F. S., Coe, M. T., Daily, G. C., Gibbs, H. K., Helkowski, J. H., Holloway, T., Howard, E. A., Kucharik, C. J., Monfreda, C., Patz, J. A., Prentice, I. C., Ramankutty, N., and Snyder, P. K. (2005). Global consequences of land use. *Science*, 309(5734):570–574.

Frei, C., Christensen, J. H., Deque, M., Jacob, D., Jones, R. G., and Vidale, P. L. (2003). Daily precipitation statistics in regional climate models: Evaluation and intercomparison for the European Alps. *Journal Of Geophysical Research-Atmospheres*, 108(D3):4124.

Früh, B., Will, A., and Castro, C. L. (2016). Editorial: Recent developments in regional climate modelling with cosmo-clm. *Meteorologische Zeitschrift*, 25(2):119–120.

Gaillard, M.-J., Kleinen, T., Samuelsson, P., Nielsen, A. B., Bergh, J., Kaplan, J., Poska, A., Sandström, C., Strandberg, G., Trondman, A.-K., et al. (2015). Causes of regional change – land cover. In *Second Assessment of Climate Change for the Baltic Sea Basin*, pages 453–477. Springer.

Gálos, B., Mátyás, C., and Jacob, D. (2013). Regional characteristics of climate change altering effects of afforestation. *Environmental Research Letters*, 6(4):044010.

Geist, H., McConnell, W., Lambin, E. F., Moran, E., Alves, D., and Rudel, T. (2006). *Causes and Trajectories of Land-Use/Cover Change*, pages 41–70. Springer Berlin Heidelberg, Berlin, Heidelberg.

Geyer, B. (2013). High resolution atmospheric reconstruction for Europe 1948-2012: coastDat2. *Earth Syst. Sci. Data Discuss.*, 6(2):779–809.

Gibbard, S., Caldeira, K., Bala, G., Phillips, T. J., and Wickett, M. (2005). Climate effects of global land cover change. *Geophysical Research Letters*, 32(23):1–4.

Giorgi, F. (1990). Simulation of regional climate using a limited area model nested in a general circulation model. *J. Climate*, 3(9):941–963.

Giorgi, F. and Avissar, R. (1997). Representation of heterogeneity effects in earth system modeling: Experience from land surface modeling. *Rev. Geophys.*, 35(4):413–437.

Giorgi, F., Bi, X., and Pal, J. (2004). Mean, interannual variability and trends in a regional climate change experiment over Europe. II: climate change scenarios (2071-2100). *CLIMATE DYNAMICS*, 23(7-8):839–858.

Giorgi, F. and Mearns, L. O. (1999). Introduction to special section: Regional climate modeling revisited. *Journal Of Geophysical Research-Atmospheres*, 104(D6):6335–6352.

Goldewijk, K. K. (2001). Estimating global land use change over the past 300 years: the hyde database. *Global Biogeochem. Cycles*, 15:–.

Goodman, S. (1999). Urban climatology and air quality: Heat island. Available at `http://weather.msfc.nasa.gov/urban/urban_heat_island.html`, Accessed: 2016-05-20.

Govindasamy, B., Duffy, P. B., and Caldeira, K. (2001). Land use changes and northern hemisphere cooling. *Geophys. Res. Lett.*, 28(2):291–294.

Graßelt, R. (2010). *Validation of the COSMO: Land-surface Parameterization TERRA-ML with Discharge Measurements*. PhD thesis, Universitäts-und Landesbibliothek Bonn.

Grawe, D., Thompson, H. L., Salmond, J. A., Cai, X.-M., and Schluenzen, K. H. (2013). Modelling the impact of urbanisation on regional climate in the Greater London Area. *INTERNATIONAL JOURNAL OF CLIMATOLOGY*, 33(10):2388–2401.

Gregorio, A. D. and Jansen, L. J. (2000). Land cover classification system (lccs): Classification concepts and user manual. Technical report, Food and Agriculture Organization.

Grimmond, C. and Oke, T. R. (1995). Comparison of heat fluxes from summertime observations in the suburbs of four North American cities. *Journal of Applied Meteorology*, 34:873–889.

Grimmond, C. S. (2007). Urbanization and global environmental change: local effects of urban warming. *Geographical Journal*, 173(1):83–88.

Grossman-Clarke, S., Schubert, S., and Fenner, D. (2016). Urban effects on summertime air temperature in germany under climate change. *International Journal of Climatology*.

Grossman-Clarke, S., Zehnder, J. A., Loridan, T., and Grimmond, C. S. B. (2010). Contribution of land use changes to near-surface air temperatures during recent summer extreme heat events in the Phoenix metropolitan area. *Journal of Applied Meteorology and Climatology*, 49(8):1649–1664.

Han, J.-Y., Baik, J.-J., and Lee, H. (2014). Urban impacts on precipitation. *Asia-Pacific Journal of Atmospheric Sciences*, 50(1):17–30–.

Hanna, S., Marciotto, E., and Britter, R. (2011). Urban energy fluxes in built-up downtown areas and variations across the urban area, for use in dispersion models. *J. Appl. Meteor. Climatol.*, 50(6):1341–1353.

Hansen, J., Sato, M., Glascoe, J., and Ruedy, R. (1998). A common-sense climate index: Is climate changing noticeably? *Proceedings Of The National Academy Of Sciences Of The United States Of America*, 95(8):4113–4120.

Hartmann, D., Tank, A. K., Rusticucci, M., Alexander, L., Brönnimann, S., Charabi, Y., Dentener, F., Dlugokencky, E., Easterling, D., Kaplan, A., Soden, B., Thorne, P., Wild, M., and Zhai, P. (2013). Observations: Atmosphere and surface. *Climate Change 2013: The Physical Science Basis. Contribution of Working Group I to the Fifth Assessment Report of the Intergovernmental Panel on Climate Change*.

Haylock, M. R., Hofstra, N., Tank, A. M. G. K., Klok, E. J., Jones, P. D., and New, M. (2008). A european daily high-resolution gridded data set of surface temperature and precipitation for 1950?2006. *JOURNAL OF GEOPHYSICAL RESEARCH*, 113.

Hoffmann, P. (2009). Modifikation von Starkniederschlägen durch urbane Gebiete. Master's thesis, University of Hamburg.

Hoffmann, P., Krueger, O., and Schlünzen, K. H. (2012). A statistical model for the urban heat island and its application to a climate change scenario. *Int. J. Climatol.*, 32(8):1238–1248.

Hoffmann, P., Schoetter, R., and Schlünzen, K. H. (2016 in review). Statistical-dynamical downscaling of the urban heat island. *Meteorologische Zeitschrift*.

Hohenegger, C., Brockhaus, P., and Schar, C. (2008). Towards climate simulations at cloud-resolving scales. *Meteorologische Zeitschrift*, 17(4):383–394.

Hou, Y., Moorthi, S., and Campana, K. (2002). Parameterization of solar radiation transfer in the NCEP models. *NCEP office note*, 441:1–46.

Hoymann, J. and Goetzke, R. (2014). Die zukunft der landnutzung in deutschland–darstellung eines methodischen frameworks. *Raumforschung und Raumordnung*, 72(3):211–225.

Jaeger, E. and Seneviratne, S. (2011). Impact of soil moisture–atmosphere coupling on European climate extremes and trends in a regional climate model. *Climate Dynamics*, 36(9-10):1919–1939.

Jaeger, E. B., Anders, I., Luthi, D., Rockel, B., Schär, C., and Seneviratne, S. I. (2008). Analysis of ERA40-driven CLM simulations for Europe. *Meteorologische Zeitschrift*, 17(4):349–367.

Jin, M., Shepherd, J. M., and King, M. D. (2005). Urban aerosols and their variations with clouds and rainfall: A case study for new york and houston. *J. Geophys. Res.*, 110(D10):D10S20–.

Kalnay, E., Kanamitsu, M., Kistler, R., Collins, W., Deaven, D., Gandin, L., Iredell, M., Saha, S., White, G., Woollen, J., Zhu, Y., Chelliah, M., Ebisuzaki, W., Higgins, W., Janowiak, J., Mo, K. C., Ropelewski, C., Wang, J., Leetmaa, A., Reynolds, R., Jenne, R., and Joseph, D. (1996). The NCEP/NCAR 40-year reanalysis project. *Bulletin of the American Meteorological Society*, 77(3):437–471.

Keil, M., Bock, M., Esch, T., Metz, A., Nieland, S., and Pfitzner, A. (2010). Corine land cover aktualisierung 2006 für deutschland–abschlussbericht. *Deutsches Zentrum für Luft und Raumfahrt (DLR)/Deutsches Fernerkundungsdatenzentrum (DFD). http://www. corine. dfd. dlr. de/media/download/clc2006_endbericht_de. pdf (28.02. 2011)*.

Kjellström, E., Bärring, L., Jacob, D., Jones, R., Lenderink, G., and Schär, C. (2007). Modelling daily temperature extremes: recent climate and future changes over Europe. *Climatic Change*, 81(1):249–265.

Koster, R. D., Dirmeyer, P. A., Guo, Z., Bonan, G., Chan, E., Cox, P., Gordon, C. T., Kanae, S., Kowalczyk, E., Lawrence, D., Liu, P., Lu, C.-H., Malyshev, S., McAvaney, B., Mitchell, K., Mocko, D., Oki, T., Oleson, K., Pitman, A., Sud, Y. C., Taylor, C. M., Verseghy, D., Vasic, R., Xue, Y., and Yamada, T. (2004). Regions of strong coupling between soil moisture and precipitation. *Science*, 305(5687):1138–1140.

Koster, R. D., Guo, Z., Dirmeyer, P. A., Bonan, G., Chan, E., Cox, P., Davies, H., Gordon, C. T., Kanae, S., Kowalczyk, E., Lawrence, D., Liu, P., Lu, C.-H., Malyshev, S., McAvaney, B., Mitchell, K., Mocko, D., Oki, T., Oleson, K. W., Pitman, A., Sud, Y. C., Taylor, C. M., Verseghy, D., Vasic, R., Xue, Y., and Yamada, T. (2006). GLACE: The Global Land-Atmosphere Coupling Experiment. Part I: Overview. *JOURNAL OF HYDROMETEOROLOGY*, 7(4):590–610.

Koster, R. D. and Suarez, M. J. (1995). Relative contributions of land and ocean processes to precipitation variability. *Journal Of Geophysical Research-Atmospheres*, 100(D7):13775–13790.

Koster, R. D., Suarez, M. J., and Heiser, M. (2000). Variance and predictability of precipitation at seasonal-to-interannual timescales. *J. Hydrometeor*, 1(1):26–46.

Kotlarski, S., Keuler, K., Christensen, O. B., Colette, A., Déqué, M., Gobiet, A., Goergen, K., Jacob, D., Lüthi, D., van Meijgaard, E., Nikulin, G., Schär, C., Teichmann, C., Vautard, R., Warrach-Sagi, K., and Wulfmeyer, V. (2014). Regional climate modeling on european scales: a joint standard evaluation of the euro-cordex rcm ensemble. *Geoscientific Model Development*, 7(4):1297–1333.

Kruse, E., Zimmermann, T., Kittel, A., Dickhaut, W., Knieling, J., and Sörensen, C. (2014). Stadtentwicklung und klimaanpassung: Klimafolgen, anpassungskonzepte und bewusstseinsbildung beispielhaft dargestellt am einzugsgebiet der wandse, hamburg.

Kueppers, L. M., Snyder, M. A., and Sloan, L. C. (2007). Irrigation cooling effect: Regional climate forcing by land-use change. *Geophysical Research Letters*, 34(3):L03703.

Lambin, E., Geist, H., and Rindfuss, R. (2006). *Land-Use and Land-Cover Change: local processes and global impacts*. Springer-Verlag Berlin Heidelberg.

Lambin, E. F., Turner, B. L., Geist, H. J., Agbola, S. B., Angelsen, A., Bruce, J. W., Coomes, O. T., Dirzo, R., Fischer, G., Folke, C., George, P. S., Homewood, K., Imbernon, J., Leemans, R., Li, X. B., Moran, E. F., Mortimore, M., Ramakrishnan, P. S., Richards, J. F., Skanes, H., Steffen, W., Stone, G. D., Svedin, U., Veldkamp, T. A., Vogel, C., and Xu, J. C. (2001). The causes of land-use and land-cover change: moving beyond the myths. *Global Environmental Change-Human And Policy Dimensions*, 11(4):261–269.

Lamptey, B. L., Barron, E. J., and Pollard, D. (2005). Simulation of the relative impact of land cover and carbon dioxide to climate change from 1700 to 2100. *J. Geophys. Res.*, 110(D20):D20103–.

Landsberg, H. E. (1970). Man-made climatic changes: Man's activities have altered the climate of urbanized areas and may affect global climate in the future. *Science*, 170(3964):1265–1274.

Laprise, R. (2008). Regional climate modelling. *Journal of Computational Physics*, 227(7):3641–3666.

Lefebvre, C. and Rosenhagen, G. (2008). The climate in the north and baltic sea region. *Die Küste*, 74:45–59.

Lenderink, G., Ulden, A., Hurk, B., and Meijgaard, E. (2007). Summertime inter-annual temperature variability in an ensemble of regional model simulations: Analysis of the surface energy budget. *Climatic Change*, 81(1):233–247.

Leung, L. R. and Qian, Y. (2003). The sensitivity of precipitation and snowpack simulations to model resolution via nesting in regions of complex terrain. *J. Hydrometeor*, 4(6):1025–1043.

Levis, S. (2010). Modeling vegetation and land use in models of the earth system. *Wiley Interdisciplinary Reviews: Climate Change*, 1(6):840–856.

Liang, S., Kustas, W., Schaepman-Strub, G., and Li, X. (2010). Impacts of climate change and land use changes on land surface radiation and energy budgets. *IEEE Journal of Selected Topics in Applied Earth Observations and Remote Sensing*, 3(3):219–224.

Lubowski, R. N., Plantinga, A. J., and Stavins, R. N. (2008). What drives land-use change in the united states? a national analysis of landowner decisions. *Land Economics*, 84(4):529–550.

Luyssaert, S., Jammet, M., Stoy, P. C., Estel, S., Pongratz, J., Ceschia, E., Churkina, G., Don, A., Erb, K., Ferlicoq, M., Gielen, B., Grunwald, T., Houghton, R. A., Klumpp, K., Knohl, A., Kolb, T., Kuemmerle, T., Laurila, T., Lohila, A., Loustau, D., McGrath, M. J., Meyfroidt, P., Moors, E. J., Naudts, K., Novick, K., Otto, J., Pilegaard, K., Pio, C. A., Rambal, S., Rebmann, C., Ryder, J., Suyker, A. E., Varlagin, A., Wattenbach, M., and Dolman, A. J. (2014). Land management and land-cover change have impacts of similar magnitude on surface temperature. *Nature Clim. Change*, 4(5):389–393.

Mahmood, R., Pielke, R. A., Hubbard, K. G., Niyogi, D., Dirmeyer, P. A., McAlpine, C., Carleton, A. M., Hale, R., Gameda, S., Beltrán-Przekurat, A., Baker, B., McNider, R., Legates, D. R., Shepherd, M., Du, J., Blanken, P. D., Frauenfeld, O. W., Nair, U., and Fall, S. (2014). Land cover changes and their biogeophysical effects on climate. *Int. J. Climatol.*, 34(4):929–953.

Mahmood, R., Quintanar, A. I., Conner, G., Leeper, R., Dobler, S., Pielke, R. A., Beltran-Przekurat, A., Hubbard, K. G., Niyogi, D., Bonan, G., Lawrence, P., Chase, T., McNider, R., Wu, Y., McAlpine, C., Deo, R., Etter, A., Gameda, S., Qian, B., Carleton, A., Adegoke, J. O., Vezhapparambu, S., Asefi, S., Nair, U. S., Sertel, E., Legates, D. R., Hale, R., Frauenfeld, O. W., Watts, A., Shepherd, M., Mitra, C., Anantharaj, V. G., Fall, S., Chang, H.-I., Lund, R., Trevi, A., Blanken, P., Du, J., and Syktus, J. (2010). Impacts of land use/land cover change on climate and future research priorities. *Bull. Amer. Meteor. Soc.*, 91(1):37–46.

Manabe, S. and Bryan, K. (1969). Climate calculations with a combined ocean-atmosphere model. *J. Atmos. Sci.*, 26(4):786–789.

Martilli, A., Clappier, A., and Rotach, M. W. (2002). An urban surface exchange parameterisation for mesoscale models. *Boundary-layer Meteorology*, 104(2):261–304.

Matthews, H. D., Weaver, A. J., Meissner, K. J., Gillett, N. P., and Eby, M. (2004). Natural and anthropogenic climate change: incorporating historical land cover change, vegetation dynamics and the global carbon cycle. *Climate Dynamics*, 22(5):461–479.

Maynard, K. and Royer, J.-F. (2004). Sensitivity of a general circulation model to land surface parameters in African tropical deforestation experiments. *Climate Dynamics*, 22(6-7):555–572.

Meehl, G. A., Moss, R., Taylor, K. E., Eyring, V., Stouffer, R. J., Bony, S., and Stevens, B. (2014). Climate model intercomparisons: Preparing for the next phase. *Eos Trans. AGU*, 95(9):77–78.

Meehl, G. A. and Tebaldi, C. (2004). More intense, more frequent, and longer lasting heat waves in the 21st century. *Science*, 305(5686):994–997.

Mellor, G. L. and Yamada, T. (1982). Development of a turbulence closure model for geophysical fluid problems. *Reviews of Geophysics*, 20(4):851–875.

Memon, R. A., Leung, D. Y. C., Liu, C.-H., and Leung, M. K. H. (2011). Urban heat island and its effect on the cooling and heating demands in urban and suburban areas of hong kong. *Theoretical and Applied Climatology*, 103(3):441–450.

Mölders, N. and Olson, M. A. (2004). Impact of urban effects on precipitation in high latitudes. *J. Hydrometeor*, 5(3):409–429.

Molinari, J. and Dudek, M. (1992). Parameterization of convective precipitation in mesoscale numerical models: A critical review. *Mon. Wea. Rev.*, 120(2):326–344.

Moss, R. H., Babiker, M., Brinkman, S., Calvo, E., Carter, T., Edmonds, J. A., Elgizouli, I., Emori, S., Lin, E., Hibbard, K., et al. (2008). Towards new scenarios for analysis of emissions, climate change, impacts, and response strategies. *IPCC report*.

Moss, R. H., Edmonds, J. A., Hibbard, K. A., Manning, M. R., Rose, S. K., van Vuuren, D. P., Carter, T. R., Emori, S., Kainuma, M., Kram, T., Meehl, G. A., Mitchell, J. F. B., Nakicenovic, N., Riahi, K., Smith, S. J., Stouffer, R. J., Thomson, A. M., Weyant, J. P., and Wilbanks, T. J. (2010). The next generation of scenarios for climate change research and assessment. *Nature*, 463(7282):747–756.

Müller-Westermeier, G. and Riecke, W. (2003). Die Witterung in Deutschland. *DWD Klimastatusberichte*. Available at `http://www.dwd.de/bvbw/generator/DWDWWW/Content/Oeffentlichkeit/KU/KU2/KU21/ksb__beitraege/ksb__witterungdeutschland__2002,templateId=raw,property=publicationFile.pdf/ksb_witterungdeutschland_2002.pdf`, Accessed: 2012-10-20.

Müller-Westermeier, G. and Riecke, W. (2004). Die Witterung in Deutschland. *DWD Klimastatusberichte*. Available at `http://www.dwd.de/bvbw/generator/DWDWWW/Content/Oeffentlichkeit/KU/KU2/KU21/ksb__beitraege/ksb__witterungdeutschland__2003,templateId=raw,property=publicationFile.pdf/ksb_witterungdeutschland_2003.pdf`, Accessed: 2012-10-20.

Myhre, G., Shindell, D., Bréon, F., Collins, W., Fuglestvedt, J., Huang, J., Koch, D., Lamarque, J., Lee, D., Mendoza, B., et al. (2013). Climate change 2013: the physical science basis. contribution of working group i to the fifth assessment report of the intergovernmental panel on climate change. *K., Tignor, M., Allen, SK, Boschung, J., Nauels, A., Xia, Y., Bex, V., and Midgley, PM, Cambridge University Press Cambridge, United Kingdom and New York, NY, USA*.

Nakicenovic, N., Alcamo, J., Davis, G., de Vries, B., Fenhann, J., Gaffin, S., Gregory, K., Grubler, A., Jung, T., Kram, T., et al. (2000). Special report on emissions scenarios: a special report of Working Group III of the Intergovernmental Panel on Climate Change. Technical report, Pacific Northwest National Laboratory, Richland, WA (US), Environmental Molecular Sciences Laboratory (US).

Neunhäuserer, L., Fay, B., and Raschendorfer, M. (2007). Towards urbanisation of the non-hydrostatic numerical weather prediction model lokalmodell (lm). *Boundary-layer meteorology*, 124(1):81–97.

Nikulin, G., Kjellström, E., Hansson, U., Strandberg, G., and Ullerstig, A. (2010). Evaluation and future projections of temperature, precipitation and wind extremes over Europe in an ensemble of regional climate simulations. *Tellus A*, 63(1):41–55.

Oke, T. (1987). The surface energy budgets of urban areas. *Modeling the urban boundary layer. Boston: American Meteorological Society*.

Oke, T. R. (1982). The energetic basis of the urban heat island. *Quarterly Journal of the Royal Meteorological Society*, 108(455):1–24.

Oleson, K., Bonan, G., Levis, S., and Vertenstein, M. (2004). Effects of land use change on north american climate: impact of surface datasets and model biogeophysics. *Climate Dynamics*, 23(2):117–132–.

Oleson, K., Niu, G.-Y., Yang, Z.-L., Lawrence, D., Thornton, P., Lawrence, P., Stöckli, R., Dickinson, R., Bonan, G., Levis, S., et al. (2008). Improvements to the community land model and their impact on the hydrological cycle. *Journal of Geophysical Research: Biogeosciences*, 113(G1).

Pielke, R. (2005). Land use and climate change. *SCIENCE*, 310(5754):1625–1626.

Pielke, R. A. (2001). Influence of the spatial distribution of vegetation and soils on the prediction of cumulus convective rainfall. *Reviews of Geophysics*, 39(2):151–177.

Pielke, R. A., Liston, G. E., Eastman, J. L., Lu, L. X., and Coughenour, M. (1999). Seasonal weather prediction as an initial value problem. *Journal of Geophysical Research-atmospheres*, 104(D16):19463–19479.

Pielke, R. A., Marland, G., Betts, R. A., Chase, T. N., Eastman, J. L., Niles, J. O., Niyogi, D. D. S., and Running, S. W. (2002). The influence of land-use change and landscape dynamics on the climate system: relevance to climate-change policy beyond the radiative effect of greenhouse gases. *Philosophical Transactions Of The Royal Society Of London Series A-Mathematical Physical And Engineering Sciences*, 360(1797):1705–1719.

Pielke, R. A., Pitman, A., Niyogi, D., Mahmood, R., McAlpine, C., Hossain, F., Goldewijk, K. K., Nair, U., Betts, R., Fall, S., Reichstein, M., Kabat, P., and de Noblet, N. (2011). Land use/land cover changes and climate: modeling analysis and observational evidence. *Wiley Interdisciplinary Reviews-Climate Change*, 2(6):828–850.

Pielke, R. A., Sr, ., Avissar, R., Raupach, M., Dolman, A. J., Zeng, X., and Denning, A. S. (1998). Interactions between the atmosphere and terrestrial ecosystems: influence on weather and climate. *Global Change Biology*, 4(5):461–475.

Pitman, A., Narisma, G., Pielke Sr, R., and Holbrook, N. (2004). Impact of land cover change on the climate of southwest Western Australia. *J. Geophys. Res*, 109:D18109.

Pitman, A. J. (2003). The evolution of, and revolution in, land surface schemes designed for climate models. *International Journal Of Climatology*, 23(5):479–510.

Pitman, A. J., de Noblet-Ducoudre, N., Cruz, F. T., Davin, E. L., Bonan, G. B., Brovkin, V., Claussen, M., Delire, C., Ganzeveld, L., Gayler, V., van den Hurk, B. J. J. M., Lawrence, P. J., van der Molen, M. K., Muller, C., Reick, C. H., Seneviratne, S. I., Strengers, B. J., and Voldoire, A. (2009). Uncertainties in climate responses to past land cover change: First results from the LUCID intercomparison study. *Geophysical Research Letters*, 36:L14814.

Prein, A., Gobiet, A., Suklitsch, M., Truhetz, H., Awan, N., Keuler, K., and Georgievski, G. (2013). Added value of convection permitting seasonal simulations. *Climate Dynamics*, 41(9-10):2655–2677.

Ray, D., Nair, U., Welch, R., Han, Q., Zeng, J., Su, W., Kikuchi, T., and Lyons, T. (2003). Effects of land use in southwest australia: 1. observations of cumulus cloudiness and energy fluxes. *Journal of Geophysical Research D: Atmospheres*, 108(14):ACL 5–1.

Riecke, W. and Rosenhagen, G. (2010). Das Klima in Hamburg–Entwicklung des Klimas in Hamburg und der Metropolregion. *Berichte des DWD*, 234.

Riediger, U. and Gratzki, A. (2014). Future weather types and their influence on mean and extreme climate indices for precipitation and temperature in Central Europe. *Meteorologische Zeitschrift*, 23(3):231–252.

Ritter, B. and Geleyn, J. F. (1992). A comprehensive radiation scheme for numerical weather prediction models with potential applications in climate simulations. *Monthly Weather Review*, 120(2):303–325.

Rockel, B., Will, A., and Hense, A. (2008). The Regional Climate Model COSMO-CLM (CCLM). *Meteorologische Zeitschrift*, 17(4):347–348.

Roeckner, E., G., B., Bonaventura, L., Brokopf, R., Esch, M., Giorgetta, M., Hagemann, S., Kirchner, I., Kornblueh, L., Manzini, E., Rhodin, A., Schlese, U., Schulzweida, U., and Tompkins, A. (2003). The atmospheric general circulation model ECHAM5. *Part I: Model description. Max Planck Institute for Meteorology*, 349:127.

Rummukainen, M. (2010). State-of-the-art with regional climate models. *Wiley Interdisciplinary Reviews: Climate Change*, 1(1):82–96.

Sailor, D. J. and Fan, H. (2002). Modeling the diurnal variability of effective albedo for cities. *Atmospheric Environment*, 36(4):713 – 725.

Sanchez, E., Yague, C., and Gaertner, M. A. (2007). Planetary boundary layer energetics simulated from a regional climate model over Europe for present climate and climate change conditions. *Geophysical Research Letters*, 34(1):L01709.

Schär, C. and Jendritzky, G. (2004). Climate change: Hot news from summer 2003. *Nature*, 432(7017):559–560.

Schlünzen, K. H. (1990). Numerical studies on the inland penetration of sea breeze fronts at a coastline with tidally flooded mudflats. *Beitr. Phys. Atmos*, 63:243–256.

Schlünzen, K. H., Hoffmann, P., Rosenhagen, G., and Riecke, W. (2010). Long-term changes and regional differences in temperature and precipitation in the metropolitan area of Hamburg. *International Journal of Climatology*, 30(8):1121–1136.

Schoetter, R. (2013). *Can local adaptation measures compensate for regional climate change in Hamburg Metropolitan Region?* PhD thesis, Universität Hamburg.

Schrodin, R. and Heise, E. (2001). The multi-layer-version of the DWD soil model TERRA_ML. *Consortium for Small-Scale Modelling (COSMO) Tech. Rep*, 2:16.

Schubert, S. and Grossman-Clarke, S. (2013). The Influence of green areas and roof albedos on air temperatures during Extreme Heat Events in Berlin, Germany. *Meteorologische Zeitschrift*, 22(2):131–143.

Schubert, S., Grossman-Clarke, S., and Martilli, A. (2012). A double-canyon radiation scheme for multi-layer urban canopy models. *Boundary-Layer Meteorology*, 145(3):439–468.

Sellers, P., Dickinson, R., Randall, D., Betts, A., Hall, F., Berry, J., Collatz, G., Denning, A., Mooney, H., and Nobre, C. (1997). Modeling the exchanges of energy, water, and carbon between continents and the atmosphere. *Science*, 275(5299):502–509.

Seneviratne, S. I., Corti, T., Davin, E. L., Hirschi, M., Jaeger, E. B., Lehner, I., Orlowsky, B., and Teuling, A. J. (2010). Investigating soil moisture-climate interactions in a changing climate: A review. *Earth-Science Reviews*, 99(3-4):125–161.

Seneviratne, S. I., Luthi, D., Litschi, M., and Schär, C. (2006). Land-atmosphere coupling and climate change in Europe. *Nature*, 443(7108):205–209.

Seneviratne, S. I. and Stöckli, R. (2007). The role of land-atmosphere interactions for climate variability in Europe. In *Climate Variability and Extremes during the Past 100 Years*, pages 179–193. Springer.

Seto, K. and Dhakal, S. (2014). Chapter 12: Human settlements, infrastructure, and spatial planning. *Climate Change 2014: Mitigation of Climate Change. Contribution of Working Group III to the Fifth Assessment Report of the Intergovernmental Panel on Climate Change*, pages 67–76.

Seto, K. C., Sánchez-Rodríguez, R., and Fragkias, M. (2010). The new geography of contemporary urbanization and the environment. *Annual review of environment and resources*, 35:167–194.

Shepherd, J. M. (2005). A Review of Current Investigations of Urban-Induced Rainfall and Recommendations for the Future. *Earth Interact.*, 9(12):1–27.

Shepherd, J. M. and Burian, S. J. (2003). Detection of Urban-Induced Rainfall Anomalies in a Major Coastal City. *Earth Interact.*, 7(4):1–17.

Shepherd, J. M., Pierce, H., and Negri, A. J. (2002). Rainfall modification by major urban areas: Observations from spaceborne rain radar on the TRMM satellite. *Journal of Applied Meteorology*, 41(7):689–701.

Slater, A. G., Schlosser, C. A., Desborough, C. E., Pitman, A. J., Henderson-Sellers, A., Robock, A., Vinnikov, K. Y., Entin, J., Mitchell, K., Chen, F., Boone, A., Etchevers, P., Habets, F., Noilhan, J., Braden, H., Cox, P. M., de Rosnay, P., Dickinson, R. E., Yang, Z.-L., Dai, Y.-J., Zeng, Q., Duan, Q., Koren, V., Schaake, S., Gedney, N., Gusev, Y. M., Nasonova, O. N., Kim, J., Kowalczyk, E. A., Shmakin, A. B., Smirnova, T. G., Verseghy, D., Wetzel, P., and Xue, Y. (2001). The Representation of Snow in Land Surface Schemes: Results from PILPS 2(d). *J. Hydrometeor*, 2(1):7–25.

Smiatek, G., Rockel, B., and Schättler, U. (2008). Time invariant data preprocessor for the climate version of the COSMO model (COSMO-CLM). *Meteorologische Zeitschrift*, 17(4):395–405.

Spangmyr, M. (2010). Global effects of albdeo change due to urbanization. Master's thesis, Lund University, Department of Physical Geography and Ecosystems Science.

Steppeler, J., Doms, G., Schättler, U., Bitzer, H., Gassmann, A., Damrath, U., and Gregoric, G. (2003). Meso-gamma scale forecasts using the nonhydrostatic model LM. *Meteorology and Atmospheric Physics*, 82:75–96.

Strogies, M. and Gniffke, P. (2011). Berichterstattung unter der Klimarahmenkonvention der Vereinten Nationen und dem Kyoto-Protokoll 2011. Nationaler Inventarbericht zum Deutschen Treibhausgasinventar 1990 - 2009.

Stull, R. B. (1988). *An Introduction to Boundary Layer Meteorology*. Kluwer Academic Press.

Suklitsch, M., Gobiet, A., Truhetz, H., Awan, N. K., Goettel, H., and Jacob, D. (2011). Error characteristics of high resolution regional climate models over the Alpine area. *CLIMATE DYNAMICS*, 37(1-2):377–390.

Taha, H. (1997). Urban climates and heat islands: albedo, evapotranspiration, and anthropogenic heat. *Energy and Buildings*, 25(2):99 – 103.

Taylor, J. P., Edwards, J. M., Glew, M. D., Hignett, P., and Slingo, A. (1996). Studies with a flexible new radiation code. II: Comparisons with aircraft short-wave observations. *Q.J.R. Meteorol. Soc.*, 122(532):839–861.

Teuling, A. J., Seneviratne, S. I., Stockli, R., Reichstein, M., Moors, E., Ciais, P., Luyssaert, S., van den Hurk, B., Ammann, C., Bernhofer, C., Dellwik, E., Gianelle, D., Gielen, B., Grunwald, T., Klumpp, K., Montagnani, L., Moureaux, C., Sottocornola, M., and Wohlfahrt, G. (2010). Contrasting response of European forest and grassland energy exchange to heatwaves. *Nature Geoscience*, 3(10):722–727.

Thielen, J., Wobrock, W., Gadian, A., Mestayer, P., and Creutin, J.-D. (2000). The possible influence of urban surfaces on rainfall development: a sensitivity study in 2D in the meso-scale. *Atmospheric Research*, 54(1):15–39.

Tiedtke, M. (1989). A comprehensive mass flux scheme for cumulus parameterization in large-scale models. *Monthly Weather Review*, 117(8):1779–1800.

Trusilova, K., Jung, M., and Churkina, G. (2009). On climate impacts of a potential expansion of urban land in europe. *Journal Of Applied Meteorology And Climatology*, 48(9):1971–1980.

Trusilova, K., Jung, M., Churkina, G., Karstens, U., Heimann, M., and Claußen, M. (2008). Urbanization impacts on the climate in Europe: Numerical experiments by the PSU-NCAR Mesoscale Model (MM5). *Journal Of Applied Meteorology And Climatology*, 47(5):1442–1455.

Trusilova, K. and Riecke, W. (2015). Klimauntersuchung für die Metropolregion Hamburg zur Entwicklung verschiedener meteorologischer Parameter bis zum Jahr 2050. Technical report, Deutscher Wetterdienst.

Trusilova, K., Schubert, S., Wouters, H., Fruh, B., Grossman-Clarke, S., Demuzere, M., and Becker, P. (2016). The urban land use in the COSMO-CLM model: a comparison of three parameterizations for Berlin. *Meteorologische Zeitschrift*, 25(2):231–244.

United Nations (2011). Urban population, development and environment. Available at `http://www.un.org/esa/population/publications/2011UrbanPopDevEnv_Chart/urban_wallchart_2011-web-smaller.pdf`, Accessed: 2016-05-21.

Veldkamp, A. and Verburg, P. H. (2004). Modelling land use change and environmental impact. *Journal Of Environmental Management*, 72(1-2):1–3.

Verburg, P. H., Schot, P. P., Dijst, M. J., and Veldkamp, A. (2004). Land use change modelling: current practice and research priorities. *GeoJournal*, 61(4):309–324.

Vidale, P. L., Luthi, D., Wegmann, R., and Schar, C. (2007). European summer climate variability in a heterogeneous multi-model ensemble. *Climatic Change*, 81(1):193–208.

Vitousek, P. M., Mooney, H. A., Lubchenco, J., and Melillo, J. M. (1997). Human domination of Earth's ecosystems. *Science*, 277(5325):494–499.

von Storch, H. and Claußen, M. (2011). *Klimabericht für die Metropolregion Hamburg, Hamburg*. Springer-Verlag.

von Storch, H., Langenberg, H., and Feser, F. (2000). A spectral nudging technique for dynamical downscaling purposes. *Monthly Weather Review*, 128(10):3664–3673.

Warrach, K., Stieglitz, M., Mengelkamp, H.-T., and Raschke, E. (2002). Advantages of a topographically controlled runoff simulation in a soil-vegetation-atmosphere transfer model. *J. Hydrometeor*, 3(2):131–148.

Wiesner, S., Eschenbach, A., and Ament, F. (2014). Urban air temperature anomalies and their relation to soil moisture observed in the city of Hamburg. *Meteorologische Zeitschrift*, 23(2):143–157.

Zampieri, M., D'Andrea, F., Vautard, R., Ciais, P., de Noblet-Ducoudre, N., and Yiou, P. (2009). Hot European Summers and the Role of Soil Moisture in the Propagation of Mediterranean Drought. *Journal Of Climate*, 22(18):4747–4758.

List of figures

List of tables

List of symbols

α	Albedo.
ε	Surface emissivity.
λ	Latent heat of vaporization.
τ	Kendall rank coefficient.
ΔS	Water storage.
E_I	Evaporation from the interception store.
E_{bare}^{max}	Maximum bare soil evaporation rate.
E_{bare}	Bare soil evaporation.
E_s	Sublimation from the snow.
E_{trans}	Evapotranspiration of plants.
E	Evapotranspiration.
G	Ground heat flux.
H	Sensible heat flux.
I	Infiltration.
λE	Latent heat flux.
L_n	Thermal radiation budget or net longwave radiation.
P	Precipitation in mm.
Q	Run-off in mm.
RR20	Number of intense precipitation days with daily precipitation sums greater/equal 10 mm.
RR20	Number of very heavy precipitation days with daily precipitation sums greater/equal 20 mm.
R_n	Surface radiation budget.
$S_{dif\downarrow}$	Diffuse downward shortwave radiation.
S_n	Net shortwave radiation or solar radiation budget.
T_{2m}	2 m temperature.
$T_{max(2m)}$	2 m maximum temperature.
$T_{min(2m)}$	2 m minimum temperature.
T_{so}	Soil temperature.
T_s	Surface temperature.
$V_{10m(max)}$	Maximum wind speed in 10 m height.
V_{10m}	Wind speed in 10 m height.
W_{SO}	Soil water content.
W	Surface water budget.
$Z_{0(veg)}$	Vegetation roughness length.
Z_0	Roughness length.
f_I	Areal fraction covered by interception water.
f_s	Areal fraction covered by snow.
f_{veg}	Areal fraction covered by vegetation.

Acronyms

A1B	GHG emission scenario.
A1Bcom	Compact city scenario.
A1Bspr	Urban sprawl scenario.
B	Berlin.
BATS	Biosphere-Atmosphere Transfer Scheme.
BBSR	Bundesinstitut für Bau-, Stadt- und Raumforschung im Bundesamt für Bauwesen und Raumordnung.
BEP	Building Energy Parametrization.
CCLM	COSMO model in CLimate Mode.
CDD	Consecutive dry days.
CLCT	Total cloud cover amount.
CLM	Community Land Model.
CMIP5	Coupled Model Intercomparison Project Phase 5.
CMIP6	Coupled Model Intercomparison Project Phase 6.
CORINE	Coordinator of Information of the Environment.
CPCS	Convection permitting climate simulations.
CRU	Climate Research Unit.
DAS	Deutsche Anpassungsstrategie.
DCEP	Duoble Canyon Effect Parametrization.
DWD	Deutscher Wetterdienst, German National Meteorological Service.
ECOCLIMAP	An ecosystem classification and land surface parameter database.
ENSEMBLES	Research project: Climate change and its impacts at seasonal, decadal and centennial timescales.
ERAinterim	A global atmospheric reanalysis from 1979, continuously updated in real time.
FAO	Food and Agriculture Organisation.
FOR_D	Deciduous forest.
FOR_E	Evergreen forest.
GCM	General circulation model.
GHG	Greenhouse gases.
GLACE	Global Land-Atmosphere Climate Experiment.
HD	Hot days.

HH	Hamburg.
HP	Hot periods.
IWV	Integrated water vapour.
LAI	Leaf area index.
LSM	Land-surface model.
LSP	land-surface parametrization.
LUCID	Land-Use and Climate, IDentification of robust impacts.
LULC	Land-use and land-cover.
LULCC	Land-use and land-cover change.
MM5	PSU/NCAR mesoscale model.
NG	Northern Germany.
PBL	Planetary boundary layer.
PD	Number of precipitation days.
PLCOV	Plant cover.
RCM	Regional climate model.
ROOTDP	Root depth.
SD	Summer days.
SVAT	Soil-Vegetation-Atmosphere Transfer.
TEB	Town Energy Balance.
TERRA_ML	Multi-layer version of TERRA.
TN	Number of tropical nights.
UCM	Urban canopy model.
UHI	Urban heat island.
UIP	Urban impact on precipitation.

Declaration

(Eidesstattliche Erklärung)

Hiermit erkläre ich an Eides statt, dass ich die vorliegende Dissertationsschrift selbst verfasst und keine anderen als die angegebenen Quellen und Hilfsmittel benutzt habe.

Hamburg, den 4. Oktober 2016

Anja Hermans